A MECHANISTIC INVESTIGATION OF MIO-BASED AMINOMUTASES

By

Udayanga Wanninayake

A DISSERTATION

Submitted to Michigan State University in partial fulfillment of the requirements for the degree of

Chemistry-Doctor of Philosophy

2013

ABSTRACT

A MECHANISTIC INVESTIGATION OF MIO-BASED AMINOMUTASES

By

Udayanga Wanninayake

 β -Amino acids are biologically active compounds of interest in medicinal chemistry, which are used as precursors for the biosynthesis of several biologically active compounds such as taxol, andrimid, chondromides and C-1027. Also they are used as important precursors for the synthesis of β -lactams and β -peptides. A class I lyase-like family of aminomutases isomerizes (*S*)-α-arylalanines to the corresponding β -amino acids by exchange of the NH₂/H pair. This family uses a 3,5-dihydro-5-methylidene-4*H*-imidazol-4-one (MIO) group within the active site to initiate the reaction. The structures of a phenylalanine aminomutases from *Taxus canadensis* (*Tc*PAM) and from *Pantoea agglomerans* (*Pa*PAM) have been determined at 2.4 Å and 1.7 Å resolution, respectively.

TcPAM catalyzes the isomerization of (S)- α - to (R)- β -phenylalanine, making (E)-cinnamate (~10%) as a by-product at steady state. In contrast, when (S)-styryl- α -alanine is used as a substrate, TcPAM produces (2E,4E)-styrylacrylate as the major product (>99%) and (R)-styryl- β -alanine (<1%). Comparison of the rates of conversion of the natural substrate (S)- α -phenylalanine and (S)-styryl- α -alanine to their corresponding products (k_{cat} values of 0.053 \pm 0.001 and 0.082 \pm 0.002 s⁻¹, respectively) catalyzed by TcPAM suggests that the amino group resides in the active site longer than styrylacrylate. To demonstrate this principle, inhibition

constants ($K_{\rm I}$) for selected acrylates ranging from 0.6 to 106 μ M were obtained, and each had a lower $K_{\rm I}$ compared to that of (2E,4E)-styrylacrylate ($337 \pm 12 \mu$ M). Evaluation of the inhibition constants and the rates at which both the α/β -amino acids (between 7 and 80% yield) and styrylacrylate were made from a corresponding arylacrylate and styryl- α -alanine, respectively, by TcPAM catalysis revealed that the reaction progress was largely dependent on the $K_{\rm I}$ of the acrylate. Bicyclic amino donor substrates also transferred their amino groups to an arylacrylate, demonstrating for the first time that ring-fused amino acids are productive substrates in the TcPAM-catalyzed reaction.

Burst-phase kinetic analysis was used to evaluate the deamination rate of the aminated-methylidene imidazolone (NH₂-MIO) adduct of TcPAM. The kinetic parameters were interrogated by a non-natural substrate (S)-styryl- α -alanine that yielded a chromophoric styrylacrylate product upon deamination by the aminomutase. Transient inactivation of the enzyme by the NH₂-MIO adduct intermediate resulted in an initial burst of product, with reactivation by deamination of the adduct. This study validated the rate constants of a kinetic model, demonstrating that the NH₂-MIO adduct and cinnamate intermediate are sufficiently retained in the active site to catalyze the natural α - to β -phenylalanine isomerization.

| I dedicate this di | ssertation of my value | able graduate reseai | rch to my loving wife | Nadeesha for |
|--------------------|------------------------|----------------------|-----------------------|--------------|
| h | er wonderful support | and caring during i | my graduate career. | |
| | | | | |
| | | | | |
| | | | | |
| | | | | |

ACKNOWLEDGEMENTS

First, I should thank Prof. Kevin Walker for his valuable advice and academic guidance. He has a remarkable ability to point out weaknesses and emphasize my strengths that helped advanced me to the level of an outstanding scholar. His dedication and determination to be involved in science at all times was a benefit toward helping me achieve my goals. His scientific curiosity and inquiry have improved my cognitive and problem solving skills. Finally, I really appreciate our friendly relationship that eased our personality and culture differences, which in my opinion help us engage in valuable scientific discussions. Therefore, I acknowledge Prof. Walker for being the ideal mentor for me. I also thank Prof. Dana Spence for always believing in my potential as a graduate student and for always encouraging me to achieve the best. I really appreciate his friendly anecdotal discussions about life and his research in the hallways of the Chemistry building. I thank Prof. James Geiger for his collaboration, valuable insights, and contributions to my thesis research. It was a great opportunity to work side-by-side with him. I appreciate him recognizing the value of my contributions towards our productive collaboration. Further, I thank Dr Geiger's laboratory members for sharing their instruments for protein purification. I thank Prof. Babak Borhan for being a wonderful advisor from the beginning of my graduate career. His advice for finding the right path in graduate school helped me during my graduate tenure. I also appreciate him as a teacher, since my success in his courses was predicated on understanding scientific concepts. Furthermore, I appreciate the valuable insights he provided during my second year organic chemistry seminar (CEM 958), committee meetings, and second year oral exam. I appreciate the generous guidance offered by Dr. Ardeshir Azadnia towards me becoming an outstanding teacher. He always gave subtle clues that help improve my teaching. Furthermore, I appreciate him understanding the needs of international students to

travel home; he demonstrated this by adjusting the teaching assistant schedule to accommodate international travel itineraries. Because of his generosity, I was able go to my home country in the middle of the semester and get married. I always give special thanks to those mentioned above for writing recommendation letters on my behalf to help me find a suitable job. I thank Dr. Brad Cox for supervising and teaching me molecular biology and biotechnology techniques during my first year. He trained me how to conduct biochemical assays and other important methods needed for my graduate research. I thank Prof. Xuefei Huang for letting me sit in his lab in my first semester of graduate school. He seemingly always had a friendly demeanor, and thus it was wonderful to talk whenever we met. I thank Dr. Kathryn G. Severin for being a wonderful advisor during my first semester when I was working in the department of chemistry as a TE under her supervision. She was one of the friendliest and caring supervisors I ever met. She also helped me with the UV-VIS and IR spectrometers during my graduate career. I appreciate Dr. Chrysoula Vasileiou for helping me understand the Pymol software; this program became a centerpiece of my graduate studies. I thank Prof. Leslie Kuhn and Dr. Kaillathe (Pappan) Padmanabhan for their instructions on the use of the SLIDE software. I thank Mrs. Zeynep Altinsel for being an effective instructor in the English-speaking and listening class for international teaching assistants. My fluency in English improved because of her valuable guidance. I also thank the late Prof. Greg Baker for giving a lecture on "how to write a résumé," just before he passed away. This lecture helped me craft an effective résumé that, in part, enabled me to find a job before I graduated. Dr. Baker was a wonderful person to be around. In addition, Prof. Greg Baker's laboratory members graciously provided an H_2 reactor, distilled solvents, and H₂gas for my reactions. I take this opportunity to further acknowledge Prof. Honggao Yan in the Department of Biochemistry & Molecular Biology at MSU for allowing me to use his UV-VIS

stopped-flow spectrophotometer and lab space to conduct a burst-phase kinetics experiment. Access to this instrument enabled me to obtain valuable data for one of my Biochemistry manuscripts. I greatly appreciate the help from Dr. Daniel Holmes and Mr. Kermit Johnson, the NMR specialists, who helped me understand the principles of multinuclear NMR and execute NMR experiments. I extend thanks to Dr. Thomas P. Carter for the help he provided to print my posters and design publication quality graphics for my manuscripts. Dr. Richard Staples was also instrumental in obtaining crystal structure data for several compounds needed as supporting information for my publications. His insights on recrystallization techniques were impressive, and we successfully obtained suitable crystals for each of my compounds of interest. I extend my gratitude to Prof. Gavin Reid for providing exact mass data for my synthetic compounds. I also thank Prof. Gary Blanchard, Mrs. Joni Tucker, Mrs. Debbie Roper, and Mrs. Cherie Nelson for the wonderful guidance and advice to successfully complete the Ph.D. program as smoothly as possible. I thank the building engineer, Mr. Robert Rasico for his wonderful support and help to fix various apparati in the laboratory. I thank Mr. Bill Flick, Mr. Tom Geissinger, Dr. David Voss, Ms. Mellissa Parsons, and members of the Research Technology Support Facility (RTSF) at MSU for their technical help during my graduate career. My thank goes to Prof. Mitch Smith and his laboratory members for providing us equipment to fix our GC-MS instrument, and to the laboratory of Prof. Rob Maleczka for providing dry distilled THF. I thank Prof. Bill Wulff's laboratory members for providing a GC column, Prof. David Weliky's laboratory personnel for providing the NanodropTM instrument for protein quantification.

Most importantly, I thank my former lab mates: Dr. Danielle Nevarez, Dr. Irosha Nawarathne, Dr. Lei Feng, Dr. Mark Ondari, Dr. Susan Strom, Dr. Washington Mutatu, Mr. Yemane Mengistu, M.S., Dennis Quist, M.S., Getrude Dibo, M.S., and Sean Sullivan, M.S., and

undergraduates Joshua Bilsborrow, Ebony Love and Yvonne DePorre for their valuable instructions and contributions to my research. I also thank my current lab members, Chelsea Thornburg, Dilini Ratnayake, and Ruth Muchiri for their valuable advice during group meetings on my research projects. I acknowledge my colleagues Meisam Nosrati for helping me crystallize my enzyme, Amila Dissanayake, Heyi Hu, Iwan Setiwan, Kumar Ashtekar, Rahul Banerjee, Rosario Amado Sierra, and Quanxuan Zhang for their wonderful help during my graduate career. I thank Ajith Karunaratne, Lasantha Ratnayake, Salinda Wijeratne, Tharanga Wijetunga, and my roommate Damith Perera for their emotional support and friendship. I also thank my undergraduate supervisor Prof. Veranja Karunarathne, and my teachers, Prof. Gamini Rajapaksha, Prof. Namal Priyantha, and Prof. Rathnayake Bandara for their guidance, recommendation letters, and assistance to get me into a graduate school program in USA.

Lastly, I acknowledge my loving parents Mr. Piyasena Wanninayake and Mrs. Muthumenika Dissanayake for raising me, educating me, and giving me courage and strength to come to US for advanced professional training. I thank my loving parents Tikiribandara Rajapaksha and Chandra Rathnayake for wishing me good luck and being with me during happy and sad moments. I thank my loving sisters Iresha Rajapaksha, Ruvini Rajapaksha and Thejani Wanninayake for the wonderful support and care. Finally, but certainly not the least, I offer my sincere gratitude to my loving, patient, caring, kind and beautiful wife and life partner Nadeesha Rajapaksha ("The Trouble Maker") for providing courage, strength, and most importantly, love. My greatest achievements came after she entered into my life. I really appreciate her dedication and resolve during stressful moments of my day-to-day life as well as during the challenges of my graduate work.

TABLE OF CONTENTS

| LIST O | OF TABLES | xiii |
|---------|---|-------|
| LIST O | OF FIGURES | xiv |
| KEY T | O ABBREVIATIONS | xxiii |
| LIST O | OF SCHEMES | XXV |
| 1. | INTRODUCTION | 1 |
| 1.1. | β-Amino Acids as Important Precursors in Biologically Active Molecules | 1 |
| 1.2. | Synthesis of β-Amino Acids | 2 |
| 1.3. | Biosynthesis of β-Amino Acids | 4 |
| 1.3.1. | Biosynthesis of β-Amino Acids by Aminomutases | 4 |
| 1.4. | Aromatic Amino Acid MIO-dependent Aminomutases | 9 |
| 1.4.1. | 3,5-Dihydro-5-methylidene-4 <i>H</i> -imidazol-4-one (MIO) Prosthesis | 9 |
| 1.4.2. | Reaction Mechanism of MIO-Based Aminomutases | 11 |
| 1.4.3. | Stereochemistry of the Phenylalanine Aminomutase Catalysis | 14 |
| 2. | INSIGHTS INTO THE MECHANISM OF MIO-BASED | |
| | PHENYLALANINE AMINOMUTASE CATALYSIS | 22 |
| 2.1. | Introduction | 22 |
| 2.2. | Experimental | 25 |
| 2.2.1. | Chemicals | 25 |
| 2.2.2. | Expression and Purification of TcPAM | 25 |
| 2.2.3. | Expression and Purification of <i>PaPAM</i> . | 27 |
| 2.2.4. | PAM Activity Assays | 27 |
| 2.2.5. | GC/EIMS Analysis of PAM Catalyzed Products | 28 |
| 2.2.6. | Mutagenesis of <i>Tc</i> PAM cDNA for Expression of L104A Mutant. | 29 |
| 2.2.7. | Analysis of Kinetic Parameters of <i>Tc</i> PAM and PAMeLA_104 | 30 |
| 2.2.8. | Analysis of Products Formed from the Incubation of TcPAM with | |
| | [15N]Phenylalanine and [ring, β-C-2H ₆]- <i>trans</i> -Cinnamate Acid | 30 |
| 2.2.9. | Assessing the Product Distribution of <i>PaPAM</i> and <i>TcPAM</i> with 2'-Methyl-(S)- | |
| 2.2.>. | α-Phenylalanine | 31 |
| 2.2.10. | Conversion of Cinnamate to α - and β -Phenylalanine by $PaPAM$ | 31 |
| 2.3. | Results | 32 |
| 2.3.1. | X-ray Crystal Structure of <i>Tc</i> PAM | 32 |
| 2.3.2. | Site-Directed Mutation of an Active Site Leu of <i>Tc</i> PAM | 36 |
| 2.3.3. | Inter/Intramolecularity Analysis of the Tc PAM Reaction | 39 |
| 2.3.4. | X-ray Crystal Structure of <i>Pa</i> PAM | 40 |
| 2.3.5. | Distribution of Products in the Catalysis of 2'-Methyl-(S)- α -Phenylalanine by | 10 |
| 2.0.0. | TcPAM and $PaPAM$ | 42 |

| 2.3.6. | Formation of α - and β -Phenylalanines from Cinnamate and NH ₃ by $PaPAM$ | 43 |
|---------|---|------------|
| 2.4. | Discussion | 43 |
| 2.4.1. | Stereoselectivity of the Aminomutase Reaction | 52 |
| 2.4.2. | Effects of L104A Point Mutation on Enzymatic Activity of TcPAM | 54 |
| 2.5. | Conclusion | 57 |
| 3. | (S)-A-STYRYLALANINE USED TO PROBE THE INTERMOLECULAR MECHANISM OF AN INTRAMOLECULAR MIO-AMINOMUTASE | 59 |
| 3.1. | Introduction | 59 |
| 3.2. | Experimental | 63 |
| 3.2.1. | Chemicals | 63 |
| 3.2.2. | Instrumentation | 63 |
| 3.2.3. | Expression of the <i>tcpam</i> and Purification of <i>Tc</i> PAM | 64 |
| 3.2.4. | Identification of an Amine Donor Substrate | 64 |
| 3.2.5. | Assessing the Optimal Concentration of Amino Group Donor 6 | 65 |
| 3.2.6. | Calculation of the Inhibition Constants of Various Acrylates in the <i>Tc</i> PAM Reaction | 65 |
| 3.2.7. | Time Course Assays for Intermolecular Amino Group Transfer | 67 |
| 3.2.8. | Assessing the Absolute Stereochemistry of α - and β -Phenylalanine Product (8f) by the Tc PAM Transaminase Pathway | 67 |
| 3.2.9. | Assessing the Effects of Maintaining the Steady-State Conversion of 6 to 7 on the Production of 8f | 68 |
| 3.2.10. | Biosynthesis and Characterization of a 3,4-Dihydronaphthalene-2-carboxylic Acid (16-Acr) from 16 | 69 |
| 3.3. | Results | 70 |
| 3.3.1. | Overexpression of TcPAM | 70 |
| 3.3.2. | Calculation of K_{I} for Various Acrylates and Time Course Studies for Optimal Amino Transfer | 70 |
| 3.3.3. | Relationship between the Rates of Formation of 7 and 8 and the K_{I} values of 9– | 70 |
| 5.5.5. | • | 5 0 |
| 3.3.4. | 14 Titration of the Amino Group Donor 6 to Maintain Steady-State Conversion to 7 | 73 78 |
| 3.3.5. | Other Amino Donor Substrates | 79 |
| 3.4. | Discussion | 82 |
| 3.5. | Conclusion | 85 |
| 4. | ASSESSING THE DEAMINATION RATE OF NH ₂ -MIO ADDUCT BY BURST PHASE ANALYSIS | 87 |
| 4.1. | Introduction | 87 |
| 4.2. | Experimental | 91 |
| 4.2.1. | Chemicals | 91 |
| 4.2.2. | Enzyme Preparation | 92 |
| 4.2.3. | Quantification of Biosynthetic Styrylacrylate during Kinetic Progressions | 92 |
| 4.3. | Results | 93 |
| 4.4. | Discussion | 100 |
| 4.5. | Conclusion | 103 |

| 5. | A BACTERIAL TYROSINE AMINOMUTASE PROCEEDS THROUGH | |
|---|--|----------------|
| | RETENTION OR INVERSION OF STEREOCHEMISTRY TO | 105 |
| 5.1. | CATALYZE ITS ISOMERIZATION REACTION | 105 105 |
| 5.1. 5.2. | Introduction Experimental | 110 |
| 5.2.1. | Chemicals and Reagents | 110 |
| 5.2.2. | Instrumentation | 110 |
| 5.2.3. | Subcloning, Expression, and Purification of <i>Cc</i> TAM | 111 |
| 5.2.4. | Assessing the Activity and Stereochemistry of the <i>Cc</i> TAM Reaction | 112 |
| 5.2.5. | Synthesis of Authentic α - (1) and β -Tyrosine (2) and (<i>E</i>)-4-Hydroxycinnamic Acid Derivatives | 113 |
| 5.2.5.1. | 4'- <i>O</i> -Ethoxycarbonyl-(<i>E</i>)-coumaric Acid Methyl Ester (i.e., 4'- <i>O</i> -Ethylcarboxy-(E)-4'-Hydroxycinnamic Acid Methyl Ester) | 113 |
| 5.2.5.2. | The 4'- <i>O</i> ,2- <i>N</i> -Di(ethoxycarbonyl)-α-tyrosine Methyl Ester. | 114 |
| 5.2.5.3. | | 115 |
| 5.2.6. | Synthesis of [Rh(NBD) ₂]ClO ₄ Complex. | 116 |
| 5.2.7. | Synthesis of $[Rh(NBD)((R)-Prophos)]ClO_4$ Complex. | 116 |
| 5.2.8. | Synthesis of [² H]-Labeled (2S)-1 Isotopomers | 117 |
| 5.2.8.1. | Synthesis of (Z)-2-Benzamido-3-(4'-hydroxyphenyl)acrylic Acid | 117 |
| 5.2.8.2. | Synthesis of (<i>Z</i>)-2-Benzamido-[3- ² H]-3-(4'-hydroxyphenyl)acrylic Acid | 118 |
| 5.2.8.3. | Synthesis of $(2S,3S)$ - $[2,3-{}^{2}H_{2}]$ - and $(2S,3R)$ - $[3-{}^{2}H]$ -1 | 119 |
| 5.2.9. | Characterization of $(2S,3S)$ - $[2,3-{}^{2}H_{2}]$ - and $(2S,3R)$ - $[3-{}^{2}H]$ -1 | 120 |
| 5.2.10. | Synthesis of Authentic 4'- O ,3- N -Di((S)-2-methylbutanoyl) Methyl Esters of (R)- and (S)-2 | 121 |
| 5.2.11. | Assessing the Stereospecificity of the C _{\beta} -Hydrogen Abstraction Catalyzed by | |
| | CcTAM | 122 |
| 5.2.12. | Assessing the Stereospecificity of the Hydrogen Rebound at C_{α} Catalyzed by | |
| | CcTAM | 122 |
| 5.2.13. | Assessing the Intramolecular Proton Transfer Step of the <i>Cc</i> TAM Reaction | 123 |
| 5.2.14. | Assessing the Effect of pH on CcTAM Stereoselectivity | 124 |
| 5.2.15. | Synthesis of (R)-2 Methyl Ester | 124 |
| 5.3. 5.3.1. | Results CcTAM Activity and Stereochemistry | 125 125 |
| | | |
| 5.3.2.5.3.3. | Assignment of the Prochiral Hydrogens of (R)-2 by ¹ H-NMR Using NMR to Assess the Mechanism of the Hydrogen Transfer at C_{α} in the | 125 |
| | CcTAM Reaction | 128 |
| 5.3.4. | Assessing the Mode of the Amino Group Attachment at C_{β} by $CcTAM$. | 129 |
| 5.3.4.1. | Synthesis of $(2S,3S)$ - $[2,3-{}^{2}H_{2}]$ - and $(2S,3R)$ - $[3-{}^{2}H]$ - (S) -1 | 129 |
| 5.3.5. | Analysis of 2 Made by Cc TAM Catalysis from $(2S,3S)$ - $[2,3-{}^{2}H_{2}]$ - and $(2S,3R)$ - | |
| | $[3-^{2}H]-1$ | 129 |
| 5.3.6. | Assessing the D \rightarrow H Exchange Rate during Cc TAM Catalysis | 132 |

| REFER | RENCES | 201 |
|----------|---|-----|
| APPEN | DIX | 147 |
| 5.5. | Conclusion | 146 |
| 5.4.3. | Diastereomeric Product Ratio Catalyzed by CcTAM | 141 |
| 5.4.2. | Hydrogen Exchange during Migration | 139 |
| | | 136 |
| 5.4.1.1. | Amino Group Migration | 135 |
| | Reaction. | 135 |
| 5.4.1. | Retention of Configuration at the Migration Termini during the CcTAM | |
| 5.4. | Discussion | 135 |
| 5.3.8. | pH Effect on the Stereoselectivity of the Reaction Catalyzed by CcTAM | 134 |
| 5.3.7. | Re-evaluation of the Stereoisomeric Product Distribution Catalyzed by <i>Cc</i> TAM | 133 |

LIST OF TABLES

| Table 2.1 | Kinetic Parameters for TcPAM and PAMeLA_104 with Various Substrates | 37 |
|-----------|--|------|
| Table 2.2 | GC/EIMS Analysis: Diagnostic Ions of Biosynthetic [15N]-β-Phenylalanine ^a | 39 |
| Table 3.1 | Kinetic Parameters of Various Arylacrylates and Their Conversion to Aminoo Acids Using (S)-Styryl- α -alanine in the Tc PAM Reaction | 72 |
| Table 3.2 | Steady-State Rate of Formation of 7 from 6 and of 8 from an Acrylate-+NH ₂ - | |
| | MIO Complex in the Intermolecular <i>Tc</i> PAM Reaction. ^a | 74 |
| Table 3.3 | Relative Steady-State Rates of Transfer of an Amino Group from Non-Natural Amino Acids (6 and 15–17) to trans-3'-Methylcinnamate (14) by TcPAM Catalysis | 80 |
| Table 5.1 | | 1.00 |
| | Derivatives of Labeled and [² H]-Labeled Biosynthesized Isotopomers of 2 | 130 |

LIST OF FIGURES

| Figure 1.1 | $\beta\text{-amino}$ acids, found in some of the important bioactive compounds, are highlighted in red | 1 |
|------------|---|----|
| Figure 1.2 | a) 2,3-isomerization of the analogs of (S) - α -phenylalanine to corresponding analogs of (R) - β -phenylalanine by PAM. b) Ammonia addition to substituted <i>trans</i> -cinnamate analogs to form corresponding analogs of (S) - α -phenylalanine and (R) - β -phenylalanine by PAM. c) Ammonia addition to substituted <i>trans</i> -cinnamate analogs to | |
| | form corresponding (S)- α -phenylalanine analogs by PAL. ⁴⁴ | 5 |
| Figure 1.3 | Transaminase reaction of <i>Tc</i> PAM. | 7 |
| Figure 1.4 | Sequence homology model of <i>Tc</i> PAM, <i>Pa</i> PAM, <i>Sg</i> TAM, <i>Cc</i> TAM, PAL from <i>Petroselinum crispum</i> (<i>Pc</i> PAL), TAL from <i>Rhodobacter sphaeroides</i> (<i>Rs</i> TAL), and HAL from <i>Pseudomonas putida</i> (<i>Pp</i> HAL), showing conserved residues in shaded areas. | 8 |
| Figure 1.5 | The crystal structure of $SgTAM$ with a bound mechanism based inhibitor, a) 2,2-difluoro- $(3R)$ - β -tyrosine (PDB 2QVE) and b) $(3R)$ -amino-2,2-difluoro-3- $(4'$ -methoxyphenyl)propanoic acid (PDB 2RJS) | 13 |
| Figure 1.6 | a) Crystal structure of $TcPAM$ with bound cinnamic acid intermediate. b) The proposed orientation of the cinnamic acid intermediate which leads to the formation of (R) -phenylalanine with a retention of configuration at both migration termini, by Wu. et al. (Modeled using Pymol from PDB# 3NZ4) | 19 |
| Figure 2.1 | The Tc PAM active site-cinnamate complex (magenta) a) indicating the displacement of plane of the aromatic ring of the cinnamate relative to the π -bond plane of the propeonate carbon–carbon double bond, and (b) the topside view. The PAM active site residues are colored by atom as follows: C (green), O (red), and N (blue). | 33 |
| Figure 2.2 | (b) the 3'-methyl-(S)- α -phenylalanine substrate is modeled into the mutant PAMeLA_104 active site where the steric volume is increased through the mutation of Leu-104 to Ala; now, the closest distance between the bound substrate and residue 104 is estimated at ~ 4.4 Å, and The Tc PAM-cinnamate complex is used to approximate the trajectory of non-natural substrates. (a) The 3'-methylphenyl- α -alanine substrate is modeled into the active site of Tc PAM showing the distance (~2 Å) between the 3'-methyl group of the substrate and Leu-104. | 34 |

Figure 2.3 a) Electron density $(2F_o-F_c \text{ map, blue mesh})$ calculated at $1.0 \text{ }\sigma$ around the α - and β -phenylpropanoid that is covalently bound to the MIO found in monomer "B" $(C_\alpha \text{ and } C_\beta \text{ are indicated})$. Atoms are color-coded as C (green), O (red), N (blue). b) Active site of PaPAM in complex with a MIO-bound (S)- β -phenylalanine-type ligand (orange carbon atoms). Active site residues contributed by three monomers are colored accordingly (C: cyan, yellow, or green for each monomer; oxygen: red; nitrogen: blue).

41

48

50

75

- Figure 2.4 CLUSTAL 2.1 multiple sequence alignment ³⁸ of representative class I lyase-like PAL, PAM and TAM enzymes whose structures are known and five sequences highly homologous to *PaPAM* that were found in the GenBank database by BLAST search: *PaPAM*, PAM from *Pantoea agglomerans*; *V.bact*, possible PAM from *Vibrionales bacterium SWAT-3*; *S.marit*, PAL/PAM EncP from *Streptomyces maritimus*; *B.subtl*, possible PAM from *Bacillus Subtlis*; *K.pneu*, possible PAM from *Klebsiella pneumoniae 342*; *B.rhiz*, possible PAM from *Burkholderia rhizoxinica*; *SgTAM*, TAM from *Streptomyces globisporus*; *AvPAL* Phenylalanine ammonia lyase ³⁹ from *Anabaena variabilis*; *TcPAM*, PAM from *Taxus Canadensis*. Enzymes that have a concerved phenylalanine residue inside the active which correspond to F455 residue in *PaPAM*, produce (*S*)-β-phenylalanine (designated with asterisk (*)).
- Cinnamate diastereoisomers modeled into *Tc*PAM. a) A space-filled rendering and b) a skeletal structure of *cis*-cinnamate are modeled into *Tc*PAM by preserving the tight salt bridge with Arg325. The phenyl ring of the cinnamate is oriented toward the interior of the active site pocket. The collision distances between active site residues and the phenyl ring of the cisoid diastereoisomer are given: Asn231 0.8 Å, Leu227 2.7 Å, Phe371 2.7 Å, Asn355 (main chain) 2.7 Å. c) A space-filled rendering of *trans*-cinnamate is modeled into *Tc*PAM by orienting the carboxylate toward the salt bridge with Arg325; occlusions by active site residues on the transoid structure are absent. d) Shown is an overlay of the space-filled structures of (*cis*)- and *trans*-cinnamates modeled in the *Tc*PAM active site with the Arg325 salt bridge preserved.
- Figure 3.1 Ratio $[(v_0 \rightarrow 8)/(v_0 \rightarrow 7)]$ of the steady-state rates for the conversion of acrylates 9–14 to 8 and of the formation of the NH₂–MIO complex plotted vs $K_{I(A)}$ for 9–14 (shown in parentheses).
- Figure 3.2 (a) Time course assay. Amounts of (*S*)-styryl- α -alanine (\blacksquare , 6), (2*E*,4*E*)-styrylacrylate (\bullet , 7), (*S*)-3'-methyl- α and (*R*)-3'-methyl- β -phenylalanine (\bullet , 8f- α and 8f- β), and *trans*-3'-methylcinnamate (\blacktriangle , 14) in an aminotransferase reaction catalyzed by *Tc*PAM over 12 h. (b) Steady-state

| | α -alanine (6, \blacksquare), trans-3'-methylcinnamate (14, \spadesuit), and total of α - and β - isomers of 3'-methylphenylalanine (8f, \blacktriangle). | 77 |
|------------|---|-----|
| Figure 3.3 | Modeled in the Tc PAM active site are natural substrates (a) (S) - α -phenylalanine and (b) (R) - β -phenylalanine for reference, (c) (S) -styryl- α -alanine, (d) (S) - $2'$ -furyl- α -alanine, (e) $(3R)$ - 3 -aminotetralin- $(2R)$ - 2 -carboxylate, and (f) (S) - 2 -aminotetralin- 2 -carboxylate. PyMOL (Schrödinger LLC, Cambridge, MA) was used for the substrate modeling by preserving the key interactions with the active site residues. | 83 |
| Figure 4.1 | Evaluation of the kinetic model (Scheme 4.3, shaded inset) for $TcPAM$ burst kinetics (Eqn 4.1) was used to globally fit experimental progress curves (Kaleidagraph 4.0) spanning six different (S)-styryl- α -alanine concentrations incubated with $TcPAM$ (5.5 μ M). Release of (2 E ,4 E)-styrylacrylate was measured in a stopped-flow cell by A_{340} monitoring. Each time point is an average of three progression curves. | 94 |
| Figure 4.2 | Hanes-Woolf analysis of the steady-state rates. The progress curves (Figure 4.1) were individually fit to the burst equation (Eqn 4.1) to evaluate the steady-state velocities (A), for each concentration of styryl- α -alanine, of the Tc PAM burst kinetics. The average value for each data point A was used. The dependence $[S]_0/A$ on $[S]_0$ with S.D. for the triplicate measurements of A . Linear regression fit ($[S]_0/A = 554.7 + 5.309[S]_0$; $R^2 = 0.9913$) to the data (solid line). | 96 |
| Figure 4.3 | The progression curves (Figure 4.1) were individually fit to the burst equation (Eqn 4.1) to evaluate the steady-state velocity A and the burst amplitude B for the $TcPAM$ burst kinetics. The average value for each data point A was used. A^2 dependence on B with S.D. for the triplicate measurements. Linear regression fit ($A^2 = 0.001037 + 0.009153B$; $R^2 = 0.9914$) to the data (solid line). | 97 |
| Figure 4.4 | The progress curves (Figure 4.1) were individually fit to the burst equation (Eqn 4.1) to evaluate the steady-state velocity A and the burst amplitude B for the Tc PAM burst kinetics. The average value for each data point A was used. The dependence of A/B on $1/[S]_0$ with S.D. for the triplicate measurements. Linear regression fit ($A/B = 0.049558 + 6.88821/[S]_0$; $R^2 = 0.97933$) to the data (solid line). | 99 |
| Figure 5.1 | Partial 1 H-NMR profile of unlabeled 2 and the ${}^{3}J$ coupling constants for the ABX spin system of (R) -2. | 126 |

conversion of 6 to 7 of $8f/\alpha$ and $8f/\beta$ by transfer of an amino group from 6 to 14 (5 mg) by TcPAM catalysis: (2E,4E)-styrylacrylate $(7, \bullet)$, (S)-styryl-

| Figure 5.2 | a) ² H-NMR (after solvent exchange into CH ₃ OH); the relative area of the | |
|------------|---|-----|
| | peaks at δ 4.41 and 2.61 are shown and b) ¹ H-NMR (after solvent exchange into CD ₃ OD) of a mixture containing the remaining substrate | |
| | $(2S)$ - $[3,3-{}^{2}H_{2}]$ -1 and the biosynthetic $(2S,3R)$ - $[2,3-{}^{2}H_{2}]$ -2 after a Cc TAM- | |
| | catalyzed reaction. c) 1 H-NMR (in CD ₃ OD) of authentic (R)-2. The signals for the prochiral protons of authentic (R)-2 are aligned (boxes) with signals for the deuterium labeled product in the biosynthetic sample. | 128 |
| Figure 5.3 | Plotted are the D \rightarrow H exchange (×) and (2S)-[3,3- 2 H ₂]-1 (•), [2,3- 2 H ₂]-2 | |
| | (\blacktriangle), and [3- 2 H]-4'-hydroxycinnamic acid (\blacksquare) (as mol %) during the <i>Cc</i> TAM conversion of (2 <i>S</i>)-[3,3- 2 H ₂]-1 to labeled 2. | 133 |
| Figure 5.4 | Intramolecular salt-bridge between the ammonium ion and carboxylate group of (R)-2 in methanol. Dihedral angles (ϕ_1 and ϕ_2) between H_A and H_X and between H_B and H_X , respectively, in the pseudo six-membered ring formed by 2 are shown in Newman Projection. | 136 |
| Figure 5.5 | Analysis of the diastereomeric mixture of products catalyzed by Cc TAM. Plotted are mol % of (R) -2 (\bullet) and (S) -2 (\blacksquare) relative to amount of (S) -1 added. The amount of (R) -2 (as %) (\blacktriangle) relative to the total amount of (R) -and (S) -2 made at steady state. (Average of duplicate assays is plotted). | 138 |
| Figure 5.6 | (S)-2 (as % of total 2) measured after substrate (S)-1 was depleted by 13%, 35%, and 56% at pHs 7, 8, and 9 while incubated with <i>Cc</i> TAM. | 139 |
| Figure 5.7 | Comparison of the <i>Tc</i> PAM, <i>Pa</i> PAM, and <i>Sg</i> TAM active site structures co- crystallized with phenylpropanoid adducts or complexes and the <i>Cc</i> TAM active site with 4'-hydroxycinnamate was modeled on the <i>Tc</i> PAM crystal structure (PDB# 3NZ4). The orientation of phenylpropanoid (center of each diagram) relative to the Arg residue (at right of each diagram) is shown. Also shown are key non-catalytic residues involved in binding and positioning the substrate; the catalytic tyrosine residue is above the plane in each drawing and is not shown. | 142 |
| Figure A 1 | The linear relationship between the reciprocal of the steady-state rate $(1/v_0)$ and the concentrations of competitive inhibitors ([I] ₀ in eq. 4 above): Top Left) <i>trans</i> -4'-Chloro- (9), Top Right) <i>trans</i> -4'-Methyl- (10), Middle Left) <i>trans</i> -4'-Fluorocinnamate (11), Middle Right) <i>trans</i> -Cinnamate (12). | 148 |
| Figure A 2 | Double Reciprocal Plots of the Rate of Conversion of 8b/α to 8b/β and Concentration of Substrate (S)-4'-Methyl-α-phenylalanine (S)- S 0 in | |

| | <i>Tc</i> PAM Reactions Containing (2 <i>E</i> ,4 <i>E</i>)-Styrylacrylate (7) at 0 (\bullet), 50 (\blacksquare), 100 (\bullet), 200 (\blacktriangle) μ M to Assess the $K_{\rm I}$ of 7. | 150 |
|-------------|---|-----|
| Figure A 3 | a) 1 H-NMR spectrum ((500 MHz, CDCl ₃) δ : 7.68 (s, 1 H), 7.32 - 7.17 (m, 4 H), 2.91 (t, $J = 8.4$ Hz, 2 H), 2.64 (dt, $J = 1.5$, 8.5 Hz, 2 H))of and the b) 13 C-NMR spectrum ((126 MHz, CDCl ₃) δ : 172.2, 138.7, 137.2, 132.3, 129.9, 128.8, 128.4, 127.7, 126.8, 27.5, 21.9) of 16-Acr | 151 |
| Figure A 4 | Overlay of gas chromatography profiles of; a) N -[(1'S)-camphanoyl] methyl esters of (2S)- α -4'-fluorophenylalanine (13.72 min) derived from intermolecular amino group transfer | 152 |
| Figure A 5 | GC EI/MS fragments of a) N -[(1'S)-camphanoyl] methyl ester of (2S)- α -4'- fluorophenylalanine and b) N -[(1'S)-camphanoyl] methyl ester of (3 R)- β -4'-fluorophenylalanine | 154 |
| Figure A 6 | EI-MS fragmentation of 4'- <i>O</i> -(ethoxycarbonyl) methyl ester derivative of authentic 4'-hydroxycinnamic acid. Diagnostic fragment ions are m/z 178 and 147. | 155 |
| Figure A 7 | a) 1 H NMR of 4'- O -(ethoxycarbonyl) methyl ester of 4'-hydroxycinnamic acid 1 H NMR (500 MHz, CDCl ₃) δ : 7.68 (d, J = 16.1 Hz, 1 H), 7.55 (d, J = 8.3 Hz, 2 H), 7.22 (d, J = 8.3 Hz, 1 H), 6.41 (d, J = 16.1 Hz, 1 H), 6.41 (d, J = 16.1 Hz, 1 H), 4.34 (q, J = 7.3 Hz, 2 H), 3.82 (s, 3 H), 1.41 (t, J = 7.3 Hz, 3 H) | 156 |
| Figure A 8 | a) ¹³ C NMR of 4'- <i>O</i> -(ethoxycarbonyl) methyl ester of 4'-hydroxycinnamic acid ¹³ C NMR (126 MHz, CDCl ₃) δ: 167.2, 153.2, 152.4, 143.6, 132.2, 129.2, 121.6, 118.1, 65.1, 51.7, 14.2 | 157 |
| Figure A 9 | EI-MS fragmentation of 4'- O ,3- N -di(ethoxycarbonyl) methyl ester derivatives of unlabeled (S)-1. Diagnostic fragment ions are m/z 250, 178, and 107. | 158 |
| Figure A 10 | a) 1 H NMR of 4'- O ,2- N -di(ethoxycarbonyl) methyl ester of α -tyrosine. 1 H NMR (500 MHz, CDCl3) δ = 7.21 - 6.98 (m, 4 H), 5.10 (d, J = 7.3 Hz, 1 H), 4.67 - 4.55 (m, 1 H), 4.28 (q, J = 7.1 Hz, 2 H), 4.08 (q, J = 6.7 Hz, 2 H), 3.69 (s, 3 H), 3.10 (dd, J = 6.1, 14.0 Hz, 1 H), 3.05 (dd, J = 6.1, 14.0 Hz, 1 H), 1.36 (t, J = 7.0 Hz, 3 H), 1.20 (t, J = 6.7 Hz, 3 H). | 159 |
| Figure A 11 | a) 13 C NMR of 4'- <i>O</i> ,2- <i>N</i> -di(ethoxycarbonyl) methyl ester of α -tyrosine. 13 C NMR (126 MHz, CDCl3) δ = 171.9, 155.8, 153.5, 150.2, 133.6, 130.3, 121.0, 64.8, 61.2, 54.5, 52.3, 37.6, 14.4, 14.1 | 160 |

| Figure A 12 | ¹ H NMR of 4'- <i>O</i> ,2- <i>N</i> -di(ethoxycarbonyl) ethyl ester of α-tyrosine. ¹ H NMR (500 MHz, CDCl3) δ = 7.17 (d, J = 8.6 Hz, 2 H), 7.14 - 7.11 (m, J = 8.6 Hz, 2 H), 5.14 (d, J = 7.8 Hz, 1 H), 4.63 (dd, J = 5.6, 13.4 Hz, 1 H), 4.33 (q, J = 7.1 Hz, 2 H), 4.17 (q, J = 7.2 Hz, 2 H), 4.12 (q, J = 7.1 Hz, 2 H), 3.11 (d, J = 5.1 Hz, 2 H), 1.40 (t, J = 7.1 Hz, 3 H), 1.25 (t, J = 7.3 Hz, 3 H), 1.24 (t, J = 7.2 Hz, 3 H) | 161 |
|-------------|---|-----|
| Figure A 13 | ¹³ C NMR of 4'- <i>O</i> ,2- <i>N</i> -di(ethoxycarbonyl) ethyl ester of α-tyrosine. ¹³ C NMR (126 MHz, CHCl ₃) δ: 171.7, 156.1, 153.8, 150.4, 133.9, 130.6, 121.3, 65.1, 61.8, 61.4, 54.9, 38.0, 14.7, 14.4, 14.3 | 162 |
| Figure A 14 | a) GC profile of derivatized $\beta\text{-tyrosine}$ (with ethylchloroformate and CH_2N_2 | 163 |
| Figure A 15 | EI-MS fragmentation of 4'- O ,3- N -di(ethoxycarbonyl) ethyl ester derivatives of authentic (R)-2. Diagnostic fragment ions are m/z 280, 266, and 194. | 165 |
| Figure A 16 | a) ¹ H NMR of 4'- O ,3- N -di(ethoxycarbonyl) ethyl ester of β-tyrosine. ¹ H NMR (500 MHz, CDCl ₃) δ: 7.34 (d, J = 8.5 Hz, 2 H), 7.16 (d, J = 8.8 Hz, 2 H), 4.33 (q, J = 7.3 Hz, 2 H), 4.12 (q, J = 7.1 Hz, 2 H), 4.09 (q, J = 7.3 Hz, 2 H), 2.92 - 2.78 (m, 2 H), 1.40 (t, J = 7.3 Hz, 3 H), 1.24 (t, J = 7.2 Hz, 3 H), 1.19 (t, J = 7.3 Hz, 3 H) | 166 |
| Figure A 17 | a) ¹³ C NMR of 4'- <i>O</i> , 3- <i>N</i> -di(ethoxycarbonyl) ethyl ester of β-tyrosine. ¹³ C NMR (126 MHz, CDCl ₃) δ: 170.7, 155.8, 153.5, 150.3, 138.8, 127.4, 121.3, 64.8, 61.0, 60.7, 51.0, 40.6, 14.5, 14.1, 14.0 | 167 |
| Figure A 18 | ¹ H NMR of 4'- <i>O</i> ,3- <i>N</i> -di(ethoxycarbonyl) methyl ester of β-tyrosine. ¹ H NMR (500 MHz, CDCl ₃) δ = 7.29 (d, J = 8.5 Hz, 2 H), 7.12 (d, J = 8.5 Hz, 1 H), 5.66 (br. s., 1 H), 5.17 - 5.07 (m, 1 H), 4.28 (q, J = 6.9 Hz, 2 H), 4.08 (q, J = 7.3 Hz, 2 H), 3.60 (s, 3 H), 2.90 - 2.73 (m, 2 H), 1.36 (t, J = 7.3 Hz, 3 H), 1.20 (t, J = 7.0 Hz, 3 H) | 168 |
| Figure A 19 | ¹³ C NMR of 4'- <i>O</i> ,3- <i>N</i> -di(ethoxycarbonyl) methyl ester of β-tyrosine. ¹³ C NMR (126 MHz, CD ₃ COCD ₃) δ: 170.7, 155.9, 153.4, 150.5, 140.3, 128.4, 121.7, 65.0, 64.4, 60.0, 51.0, 40.2, 14.1, 13.6 | 169 |
| Figure A 20 | Crystal structure of a) (<i>Z</i>)-2-benzamido-[3- ² H]-3-(4'-hydroxyphenyl) acrylic acid and Color coding: Carbon (black), Hydrogen (Cyan), Deuterium (green) Oxygen (red), and Nitrogen (blue), | 170 |

| Figure A 21 | ¹ H NMR spectrum of (<i>Z</i>)-2-Benzamido-[3- ² H]-3-(4'-hydroxyphenyl)acrylic Acid. ¹ H NMR (500 MHz, DMSO-d ₆) δ: 12.49 (br. s., 1 H), 9.91 (s, 1 H), 9.77 (s, 1 H), 7.99 (d, $J = 7.1$ Hz, 2 H), 7.59 (t, $J = 7.6$ Hz, 1 H), 7.56 - 7.49 (m, 4 H), 6.77 (d, $J = 8.3$ Hz, 2 H) | 172 |
|-------------|--|-----|
| Figure A 22 | ¹³ C NMR spectrum of (<i>Z</i>)-2-Benzamido-[3- ² H]-3-(4'-hydroxyphenyl)acrylic Acid. ¹³ C NMR (126 MHz, DMSO-d ₆) δ: 166.6, 165.9, 158.8, 133.7, 133.4, 131.9, 131.8, 128.5, 128.3, 127.7, 127.5, 124.6, 123.9, 115.5, 115.4 | 173 |
| Figure A 23 | ¹ H NMR spectrum of (<i>Z</i>)-2-Benzamido-3-(4'-hydroxyphenyl)acrylic Acid. ¹ H NMR (500 MHz, DMSO-d ₆) δ: 12.49 (br. s., 1 H), 9.91 (br. s., 1 H), 9.82 - 9.72 (m, 1 H), 7.99 (d, $J = 7.3$ Hz, 2 H), 7.59 (t, $J = 7.1$ Hz, 1 H), 7.56 - 7.47 (m, 4 H), 7.41 (s, 1 H), 6.77 (d, $J = 8.3$ Hz, 2 H) | 174 |
| Figure A 24 | ¹³ C NMR spectrum of (<i>Z</i>)-2-Benzamido-3-(4'-hydroxyphenyl)acrylic Acid. ¹³ C NMR (126 MHz, DMSO-d ₆) δ: 166.6, 165.9, 158.8, 134.0, 133.8, 131.9, 131.8, 128.5, 128.4, 127.7, 127.5, 124.6, 124.0, 115.5, 115.4 | 175 |
| Figure A 25 | ¹ H NMR spectrum of [Rh(NBD) ₂]ClO ₄ . ¹ H NMR (500 MHz, CDCl ₃) δ: 5.20 (q, $J = 2.2$ Hz, 8 H), 4.15 - 4.11 (m, 4 H), 1.51 (t, $J = 1.6$ Hz, 4 H) | 176 |
| Figure A 26 | ¹ H NMR spectrum of [Rh(NBD)(R)-Prophos]ClO ₄ •0.5 CH ₂ Cl ₂ . Trace amounts of THF, H ₂ O, and silicon grease are present as impurities. ¹ H NMR (500 MHz, CDCl ₃) δ = 7.79 - 7.73 (m, 2 H), 7.72 - 7.67 (m, 3 H), 7.65 - 7.61 (m, 2 H), 7.61 - 7.58 (m, 6 H), 7.58 - 7.55 (m, 6 H), 7.47 - 7.41 (m, 2 H), 7.35 - 7.29 (m, 2 H), 5.42 (br. s., 2 H), 5.31 (s, 1 H), 4.87 (br. s., 1 H), 4.28 (br. s., 1 H), 4.16 (br. s., 1 H), 2.71 - 2.59 (m, 2 H), 2.04 (td, J = 7.4, 12.5 Hz, 1 H), 1.84 - 1.76 (m, 2 H), 1.21 (dd, J = 6.5, 12.5 Hz, 3 H) | 177 |
| Figure A 27 | ¹³ C NMR spectrum of [Rh(NBD)(R)-Prophos]ClO ₄ •0.5 CH ₂ Cl ₂ . Trace amounts of THF, is present as impurities. ¹³ C NMR (126 MHz, DMSO-d ₆) δ = 143.1, 135.1, 135.1, 134.8, 134.5, 134.1, 133.9, 132.8, 132.7, 132.0, 131.9, 131.7, 131.1, 131.0, 130.9, 130.1, 129.3, 129.3, 128.9, 128.8, 128.8, 128.6, 128.5, 128.2, 127.8, 125.9, 125.5, 63.4, 48.2, 34.2, 33.0, 14.7 | 178 |
| Figure A 28 | EI-MS fragmentation of 4'- O ,2- N -di(ethoxycarbonyl) methyl ester derivatives of (2 S ,3 S)-[2,3- 2 H ₂]-1. Diagnostic fragment ions are m/z 252, 180, and 108. | 180 |

| Figure A 29 | EI-MS fragmentation of 4'- O ,2- N -di(ethoxycarbonyl) methyl ester derivatives of $(2S,3R)$ - $[3^{-2}H]$ -1. Diagnostic fragment ions are m/z 251, 179, and 108. | 181 |
|-------------|--|-----|
| Figure A 30 | EI-MS fragmentation of 4'- O ,2- N -di(ethoxycarbonyl) methyl ester derivatives of (2 S)-[3,3- 2 H ₂]-1. Diagnostic fragment ions are m/z 251, 179, and 109. | 182 |
| Figure A 31 | Partial NMR spectra of isotopomers of (<i>S</i>)-1. | 183 |
| Figure A 32 | ¹ H NMR spectrum of α-tyrosine. ¹ H NMR (500 MHz, D ₂ O) δ: 7.22 (d, J = 8.5 Hz, 2 H), 6.92 (d, J = 8.5 Hz, 2 H), 3.96 (dd, J = 5.1, 7.8 Hz, 1 H), 3.23 (dd, J = 5.0, 14.8 Hz, 1 H), 3.08 (dd, J = 7.8, 14.6 Hz, 1 H) | 185 |
| Figure A 33 | a) 1 H NMR spectrum of $(2S,3S)$ - $[2,3^{-2}H_{2}]$ - α -tyrosine. 1 H NMR (500 MHz, D ₂ O) δ : 7.22 (d, J = 8.5 Hz, 2 H), 6.92 (d, J = 8.5 Hz, 2 H), 3.08 (s, 1 H). b) 2 H NMR spectrum of $(2S,3S)$ - $[2,3^{-2}H_{2}]$ - α -tyrosine. 2 H NMR (77 MHz, H ₂ O) δ : 3.97 (bs, 1 2 H) 3.22 (bs, 1 2 H). | 186 |
| Figure A 34 | a) 1 H NMR spectrum of $(2S,3R)$ - $[3^{-2}$ H]- α -tyrosine. 1 H NMR (500 MHz, D ₂ O) δ : 7.22 (d, J = 8.5 Hz, 2 H), 6.92 (d, J = 8.5 Hz, 2 H), 3.97 (d, J = 5.0 Hz, 1 H), 3.22 (d, J = 5.0 Hz, 1 H) b) 2 H NMR spectrum of $(2S,3R)$ - $[3^{-2}$ H]- α -tyrosine. 2 H NMR (77 MHz, H ₂ O) δ : 3.08 (bs, 1 2 H). | 187 |
| Figure A 35 | ¹ H NMR spectrum of β-tyrosine. ¹ H NMR (500 MHz, CD ₃ OD) δ: 7.25 (d, $J = 8.8$ Hz, 2 H), 6.81 (d, $J = 8.8$ Hz, 2 H), 4.41 (dd, $J = 4.2$, 10.0 Hz, 1 H), 2.73 (dd, $J = 10.0$, 16.6 Hz, 1 H), 2.61 (dd, $J = 4.2$, 16.6 Hz, 1 H) | 188 |
| Figure A 36 | a) 1 H NMR and b) 2 H NMR spectra of the reaction mixture of biosynthesized products catalyzed by <i>Cc</i> TAM from (2 <i>S</i>)-[3,3- 2 H ₂]- α -tyrosine. | 189 |
| Figure A 37 | ¹ H NMR spectrum of β-tyrosine methyl ester. ¹ H NMR (500 MHz, CD ₃ OD) δ: 7.29 (td, $J = 2.2$, 8.5 Hz, 2 H), 6.85 (td, $J = 2.2$, 8.5 Hz, 2 H), 4.63 (dd, $J = 6.3$, 7.8 Hz, 1 H), 3.09 (dd, $J = 7.8$, 16.6 Hz, 1 H), 2.98 (dd, $J = 6.3$, 16.7 Hz, 1 H) | 190 |
| Figure A 38 | GC trace of 4'- O ,3- N -di((S)-2-methylbutanoyl) methyl ester derivatives of authentic (S)-2 (18.68 min) and (R)-2 (19.06 min) (a). EI-MS fragmentation of 4'- O ,3- N -di((S)-2-methylbutanoyl) methyl ester derivatives of authentic (R)-2. Diagnostic fragment ions are m/z 278 and 194. | 191 |

| Figure A 39 | GC trace of 4'- O ,3- N -di((S)-2-methylbutanoyl) methyl ester derivatives of (S)-2 (18.68 min) and (R)-2 (19.06 min) (a) and EI-MS fragmentation of 4'- O ,3- N -di((S)-2-methylbutanoyl) methyl ester derivatives of (R)-2 biosynthesized by Cc TAM from unlabeled (S)-1. | 193 |
|-------------|---|-----|
| Figure A 40 | EI-MS fragmentation of 4'- <i>O</i> -(ethoxycarbonyl) methyl ester derivative of 4'-hydroxycinnamic acid biosynthesized by <i>Cc</i> TAM from unlabeled (<i>S</i>)-1. | 194 |
| Figure A 41 | EI-MS fragmentation of 4'- O ,3- N -di(ethoxycarbonyl) ethyl ester derivatives of 2 biosynthesized by Cc TAM from unlabeled (S)-1. Diagnostic fragment ions F1, F2, and F3 (m/z 280, 266, and 194) are highlighted. | 196 |
| Figure A 42 | EI-MS fragmentation of 4'- O ,3- N -di(ethoxycarbonyl) ethyl ester derivatives of isotopomers of 2 biosynthesized by Cc TAM from (2 S ,3 S)-[2,3- 2 H ₂]-1. Diagnostic fragment ions F1, F2, and F3 (m/z 282, 266, and 194) are highlighted. | 197 |
| Figure A 43 | EI-MS fragmentation of 4'- O ,3- N -di(ethoxycarbonyl) ethyl ester derivatives of isotopomers of 2 biosynthesized by Cc TAM from (2 S ,3 R)-[3- 2 H]-1. Diagnostic fragment ions F1, F2, and F3 (m/z 281, 267, and 195) are highlighted. | 198 |
| Figure A 44 | EI-MS fragmentation of 4'- O ,3- N -di(ethoxycarbonyl) ethyl ester derivatives of isotopomers of 2 biosynthesized by Cc TAM from (2 S)-[3,3- 2 H ₂]-1. Diagnostic fragment ions F1, F2, and F3 (m/z 282, 267, and 195) are highlighted. | 199 |
| Figure A 45 | EI-MS fragmentation of 4'- <i>O</i> -(ethoxycarbonyl) methyl ester derivative of biosynthesized [3- ² H]-4'-hydroxycinnamic acid biosynthesized by <i>Cc</i> TAM from (2 <i>S</i>)-[3,3- ² H ₂]-1. Diagnostic fragment ions are m/z 179 and 148. | 200 |

KEY TO ABBREVIATIONS

4'-HOCinn 4'-hydroxycinnamic acid

AA1 Hypothetical amino acid that serves as an amino group donor in the double-

displacement reaction catalyzed by TcPAM

AA2 Hypothetical amino acid derived from the amination of an exogenously supplied

arylacrylate in the double-displacement reaction catalyzed by TcPAM

AC1 Hypothetical arylacrylate derived from an amino acid after elimination of

ammonia in the double-displacement reaction catalyzed by TcPAM

AC2 Hypothetical exogenously supplied arylacrylate in the double-displacement

reaction catalyzed by TcPAM

Acr Any Arylacrylic acid

AMs Aminomutases

AvPAL Phenylalanine ammonia lyase from Anabaena variabilis

B.rhiz PAM from Burkholderia rhizoxinica

B.subtl PAM from Bacillus subtlis

CcTAM Tyrosine aminomutase from Chondromyces crocatus

(R)-β-Dopa 3,4-dihydroxy-β-phenylalanine

Eqn Equation

E. coli Escherichia coli

GC-EIMS Gas Chromatography Electron Impact Mass Spectrometer

HALs Histidine ammonia lyases

K.pneu PAM from Klebsiella pneumoniae 342

MIO 3,5-dihydro-5-methylidene-4*H*-imidazol-4-one

MWCO Molecular weight cutoff filters

NBD Norbornadiene (Bicyclo[2.2.1]hepta-2,5-diene)

Ni-NTA Nickel nitrilotriacetic acid

PALs Phenylalanine ammonia lyases

PAM Phenylalanine aminomutase

PAMeLA104 Phenylalanine aminomutase exchange Leu→Ala104

PaPAM Phenylalanine aminomutase from Pantoea agglomerans

PcPAL Phenylalanine ammonia lyases from Petroselinum crispum

PDB Protein Data Bank

PpHAL Histidine ammonia lyases from Pseudomonas putida

RgPAL Phenylalanine ammonia lyases from Rhodotorula glutinis

RsTAL Tyrosine ammonia lyases from Rhodobacter sphaeroides

SDS-PAGE Sodium dodecyl sulfate polyacrylamide gel electrophoresis

SgTAM Tyrosine aminomutase from Streptomyces globisporus

S.marit PAL/PAM EncP from Streptomyces maritimus

TALs Tyrosine ammonia lyases

TAM Tyrosine aminomutase

TcPAM Phenylalanine aminomutase from Taxus canadensis

TMSCH₂N₂ (Trymethylsilyl) diazomethane

V. bact PAM from Vibrionales bacterium SWAT-3

LIST OF SCHEMES

| Scheme 1.1 | Synthesis of β-Amino Acids. ¹⁴ (a) Michael addition of ammonia to 3- | |
|------------|--|----|
| | methylbut-2-enoic acid derivatives. (b) Hydrolysis of 6,6-disubstituted | |
| | dihydrouracils. (c) Three component Mannich reaction of a ketone, NH ₃ , and a malonic acid derivative. (d) Ritter transformation of 3- | |
| | hydroxycarboxylates with nitriles in the presence of conc. H_2SO_4 . (e) Cycloaddition of chlorosulfonyl isocyanate with allenes to give an alkylidene β -lactam. (f) Reaction of substituted cyclopropanes with chlorosulfonyl isocyanate to yield β -lactams. (g) Cycloaddition of disubstituted alkenes and chlorosulfonyl isocyanate, reductive cleavage of the chlorosulfonyl group. (h) Indium-mediated reaction of enamines with methyl bromoacetate in the presence of acid. 14 | 3 |
| Scheme 1.2 | a) Formation of MIO, and b) The Structure of the Chromophore of Green Fluoroscence Protein. | 10 |
| Scheme 1.3 | Two Proposed Mechanisms for the Conversion of Substrate to Product in a Generic Aminomutase: a) Amino-group Alkylation Pathway and b) Friedel–Crafts Aryl-Alkylation Pathway. | 12 |
| Scheme 1.4 | Stereochemistry of the Migrating Amino Group and the Proton of the Substrate and the Product during the Catalysis of a) Tc PAM and (The Configurations at both C_{α} and C_{β} Positions are Retained) b) Pa PAM (The Configurations at both C_{α} and C_{β} Positions are Inverted) is Shown.* | 15 |
| Scheme 2.1 | The Proposed Mechanism of the Aminomutase Catalysis. Tyr is the Presumed Catalytic Base, Situated "Above" the Intermediate, and the NH ₂ -MIO Complex is Shown "Below" the Intermediate. In $SgTAM$ and $PaPAM$, After the Initial E ₂ -Type Elimination to Form the Intermediate, the Amino Group is Rebound at the C _{\beta} Position from the Si Face (Same Face), of the Intermediate while in $CcTAM$ and $TcPAM$, the Intermediate Under Go 180° Rotation About the C ₁ -C _{\alpha} and C _{\beta} -C _{\text{ipso}} Bonds in order | |
| | for the Amino Group to Attack at the C_{β} Position from the Re Face (Opposite Face) of the Intermediate. | 53 |
| Scheme 3.1 | Mechanism of the Transaminase Reaction Catalyzed by <i>Tc</i> PAM with Its Natural Substrate | 61 |
| Scheme 4.1 | Mechanism of MIO-Dependent Aminomutases | 88 |

| Scheme 4.2 | a) Intermolecular Amino Group Transfer from [15 N]- α -Phenylalanine to [2 H ₆]-Cinnamate by Tc PAM Catalysis. b) Predominantly Ammonia Lyase | |
|------------|---|-----|
| | Behavior of Tc PAM with (S)-styryl- α -alanine. | 90 |
| Scheme 4.3 | Kinetic Model for Transaminase Reaction Catalyzed by TcPAM ^a | 91 |
| Scheme 4.4 | Kinetic Model for the Proposed Mechanism of the Tc PAM-Catalyzed Conversion of α - to β -Phenylalanine | 102 |
| Scheme 5.1 | General MIO-dependent Aminomutase Mechanism | 107 |
| Scheme 5.2 | The CcTAM Reaction on the Chondramides A-D Pathway | 108 |
| Scheme 5.3 | Inversion and Retention of Configuration Pathways Catalyzed by $CcTAM^a$ | 141 |

1. INTRODUCTION

1.1. β -Amino Acids as Important Precursors in Biologically Active Molecules

Aryl-β-Amino acids belong to an important class of compounds that are present in medicinally and pharmaceutically important natural products (Figure 1.1).

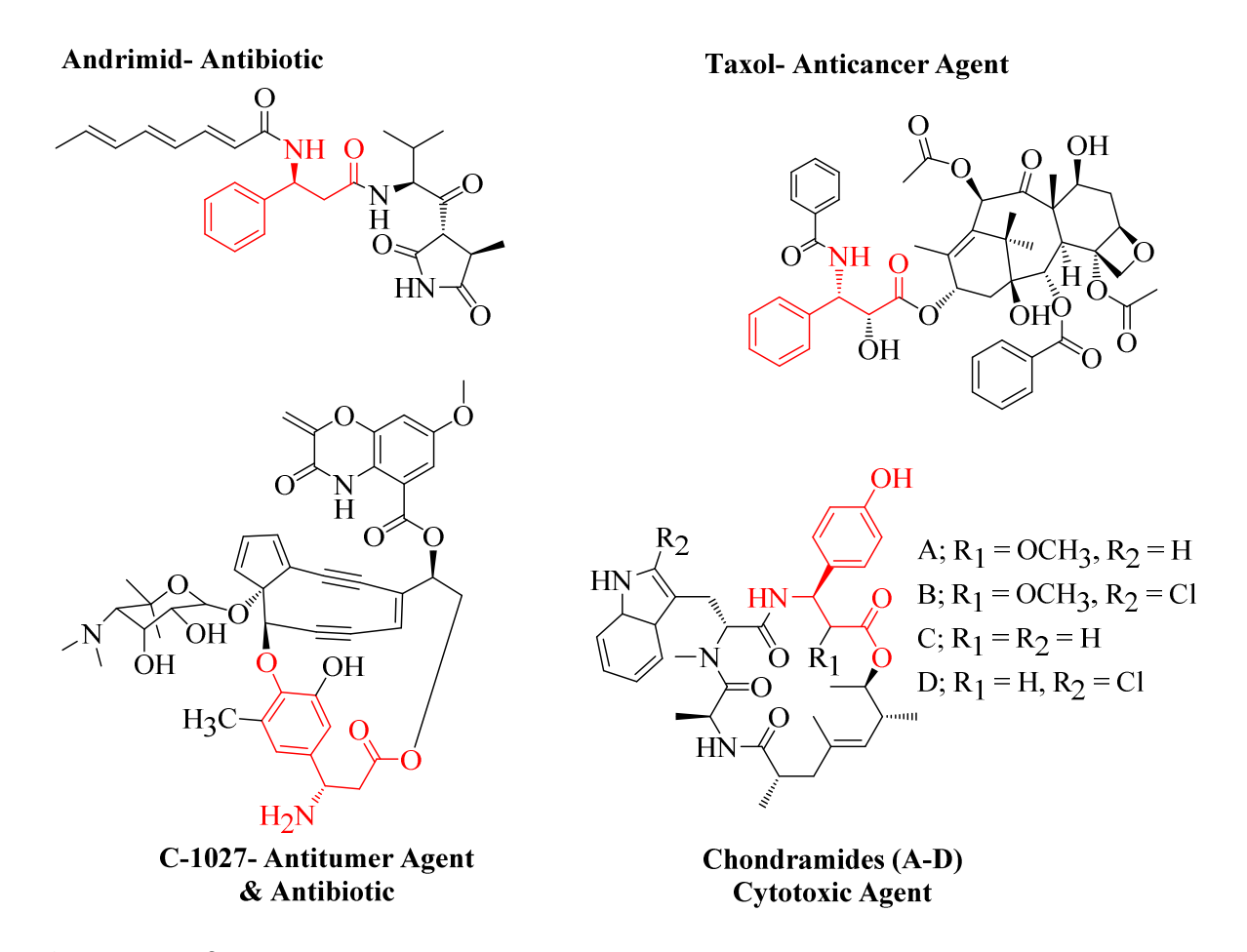


Figure 1.1. β -amino acids, found in some of the important bioactive compounds, are highlighted colored (red). (For interpretation of the references to color in this and all other figures, the reader is referred to the electronic version of this dissertation)

Some examples are the antineoplastic agent Taxol, from plant Taxus sp., the pigment,

Fe(III)-catecol complex ((R)-β-dopa (3,4-dihydroxy-β-phenylalanine)) from mushroom *Cortinarius* sp., ² the antifungal agent Jasplakinolide from marine sponge *Jaspis* sp., ³ antibiotic enediyne C-1027 from bacteria *Streptomyces gloibisporus*., ⁴ the cytotoxic agents Chondramides from bacteria *Chondromyces crocatus*., ⁵ and the antibiotic Andrimid from bacteria *Pantoea agglomerans*. ⁶ Other amino acids have been used as building blocks toward the synthesis of complex bioactive molecules, including β-lactams, ⁷ and β-peptides as mimics of α-peptide hormones and as antimicrobial compounds. ⁸ β-peptides demonstrate an increased metabolic stability, ⁹ a higher structural diversity, ¹⁰ and well-defined formation of secondary structure, ¹¹ compared to their α-analogues.

1.2. Synthesis of β-Amino Acids

An increasing demand for β -amino acids has resulted in the development of various synthetic routes to synthesize β -amino acids. ¹²⁻¹⁶ Such as Arndt-Eistert homologation, ¹⁷ Stereoselective synthesis of β -amino acids starting from aspartic acid, ¹⁸ asparagine, and derivatives, ¹⁹ Curtius rearrangement, ²⁰ through the intermediary preparation of perhydropyrimidin-4-ones, ²¹ conjugate addition to α,β -unsaturated esters and imides, ²² hydrogenation, ²³ reductive amination, ²⁴ amino hydroxylation, ²⁵ and through asymmetric β -lactam synthesis. ²⁶ The resolution of enantiomers from racemic mixtures is performed by synthesizing the diastereomers with chiral bases, such as (-)-ephedrine. ¹⁵

Scheme 1.1. Synthesis of β -Amino Acids. ¹⁴(a) Michael addition of ammonia to 3-methylbut-2-enoic acid derivatives. (b) Hydrolysis of 6,6-disubstituted dihydrouracils. (c) Three component Mannich reaction of a ketone, NH3, and a malonic acid derivative. (d) Ritter transformation of 3-hydroxycarboxylates with nitriles in the presence of conc. H₂SO₄. (e) Cycloaddition of chlorosulfonyl isocyanate with allenes to give an alkylidene β -lactam. (f) Reaction of substituted cyclopropanes with chlorosulfonyl isocyanate to yield β -lactams. (g) Cycloaddition of disubstituted alkenes and chlorosulfonyl isocyanate, reductive cleavage of the chlorosulfonyl group. (h) Indium-mediated reaction of enamines with methyl bromoacetate in the presence of acid. ¹⁴

However, these approaches have their inherent drawbacks; involvement of multistep synthesis schemes (**Scheme 1.1**), use of less greener chemicals, and production of by-products.

Due to the difficulty of resolving β -amino acid enantiomers, kinetic resolution of racemic β -amino acid derivatives or precursors (such as esters, nitriles, amides, β -lactams, and dihydrouracils) are performed using enzymatic resolution, employing such enzymes as aspartases ²⁷ and aminotransferases. ²⁸

1.3. Biosynthesis of β -Amino Acids

Due to the inherent drawbacks of chemical synthesis and semi-synthesis of enantiopure β-amino acids, greener, novel, biocatalytic asymmetric approaches, with fewer steps were introduced. Therefore, *in vivo* biocatalysts using enzymes expressed in host cells like *E. coli*, and yeast have been investigated. Aminomutases expressed in *E. coli*, utilized for the asymmetric synthesis of enantiopure β-amino acids, can potentially function as a biocatalytic system. Semi-synthesis of chiral amino acids uses hydrolytic enzymes such as lipases, acylases and hydantoinases. In addition, new methods have been developed, which are based upon asymmetric transformations, such as resolution of racemic amines using amine oxidases, and also transaminases. $^{35, 36}$

1.3.1. Biosynthesis of β -Amino Acids by Aminomutases

A phenylalanine aminomutase from *Taxus canadensis* (*Tc*PAM) catalyzes the 2,3-isomerization of (*S*)- α -phenylalanine to (*R*)- β -phenylalanine. The *Tc*PAM reaction also has broad substrate specificity (**Figure 1.2**a). In addition to catalyzing its forward reaction, *Tc*PAM catalyzes an amination reaction in the presence of NH₃ and substituted analogs of *trans*-

cinnamate (**Figure 1.2**b) to form enantiomerically pure (S)- α -arylalanine and (R)- β -arylalanine. ⁴⁰ In an independent studied by another group, this "reverse" reaction was further modified through mutation (Q319M) to increase the β -regioselectivity. ⁴¹

c
$$R = H, F \text{ and } Cl$$

$$PAL / NH_3 \qquad R = \frac{O}{NH_3}$$

Figure 1.2. a) 2,3-isomerization of the analogs of (*S*)-α-phenylalanine to corresponding analogs of (*R*)-β-phenylalanine by PAM. ^{38, 39, 42} b) Ammonia addition to substituted *trans*-cinnamate analogs to form corresponding analogs of (*S*)-α-phenylalanine and (*R*)-β-phenylalanine by PAM. ⁴⁰ c) Ammonia addition to substituted *trans*-cinnamate analogs to form corresponding (*S*)-α-phenylalanine analogs by PAL. ⁴⁴

Furthermore, a phenylalanine aminomutase (also known as AdmH) from Pantoea agglomerans (PaPAM) produces (S)-β-phenylalanine from (S)-α-phenylalanine. ^{6,42} Therefore, phenylalanine aminomutases are efficient catalysts for the enantiopure synthesis of β-amino acids. Also, phenylalanine ammonia lyase from Rhodotorula glutinis (RgPAL) was reported to catalyze the production of (S)- α -phenylalanine, in the presence of *trans*-cinnamate analogs and high concentrations (8M) of NH₃. This ammonia addition reaction has broad substrate specificity (**Figure 1.2**c). These α -phenylalanine analogs are further isomerized to β phenylalanine analogs by phenylalanine aminomutase at >99% ee. 39 In addition, tyrosine SgcC4 from Streptomyces globisporus (SgTAM),⁴ and CmdF from aminomutases Chondromyces crocatus $(CcTAM)^5$ are also known to produce β -tyrosine from α -tyrosine. Furthermore, we recently found that TcPAM can act as a transaminase enzyme in the presence of an amino group donor (substrates showing predominant lyase activity) and an amino group acceptor (cinnamate analog) to form enantiomerically pure α - and β -arylalanines. Several amino group donors, including bicyclo compounds, along with several amine group acceptors were found to be functional in the transaminase reaction catalyzed by TcPAM (**Figure 1.3**). ³⁵ A more detailed explanation will be found in the Chapter 3 of this thesis.

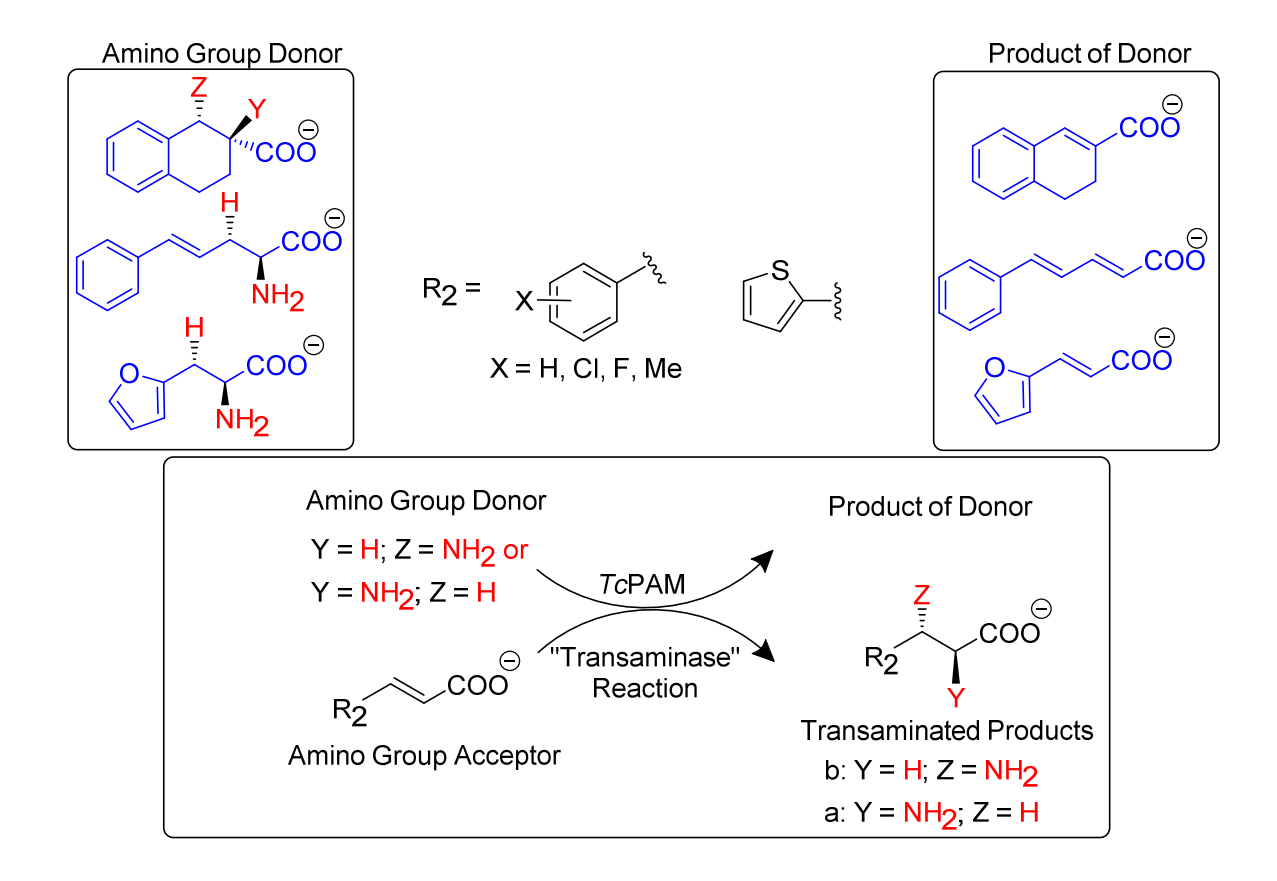


Figure 1.3. Transaminase reaction of *Tc*PAM.

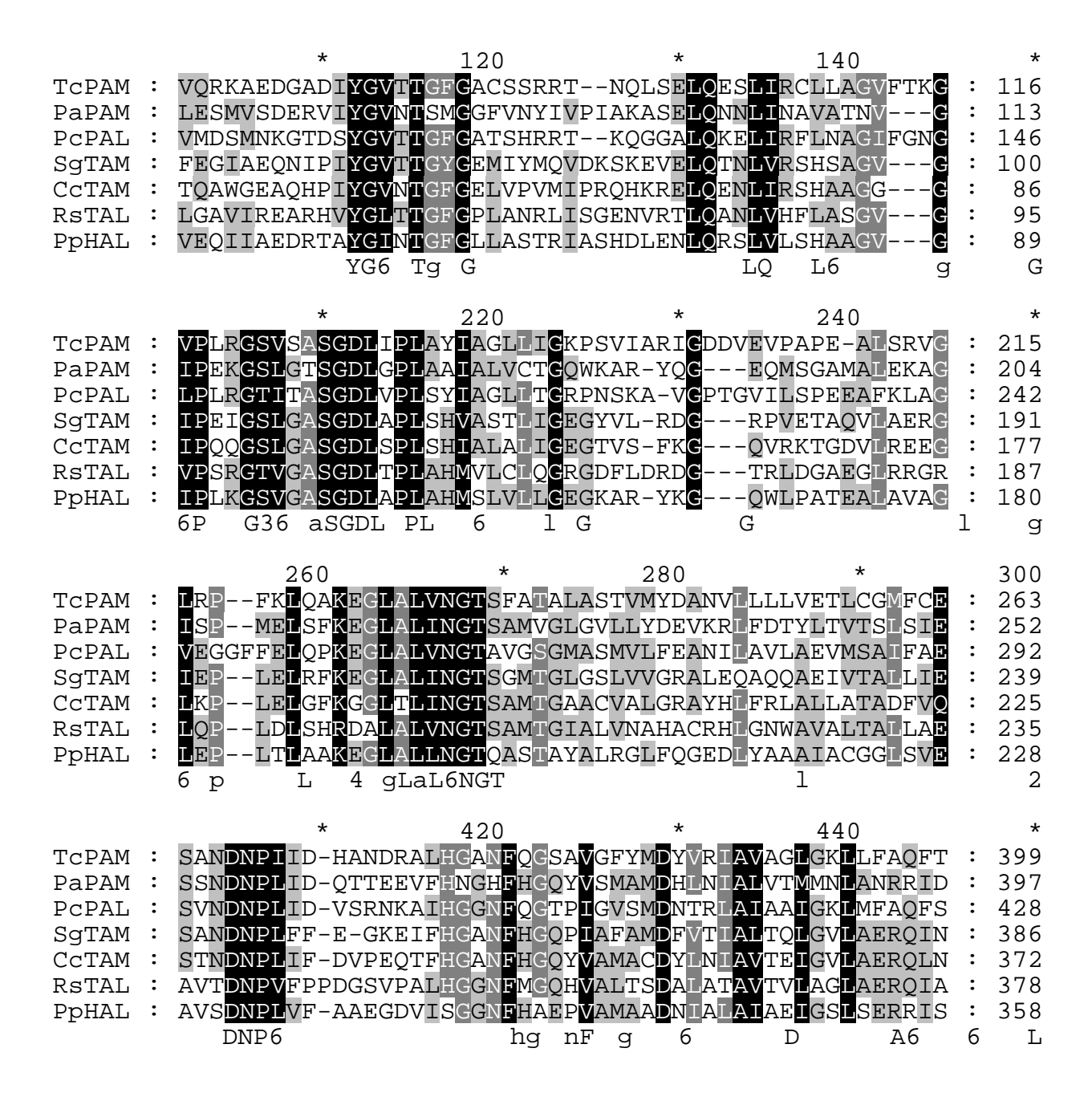


Figure 1.4. Sequence homology model of *Tc*PAM, *Pa*PAM, *Sg*TAM, *Cc*TAM, PAL from *Petroselinum crispum* (*Pc*PAL), TAL from *Rhodobacter sphaeroides* (*Rs*TAL), and HAL from *Pseudomonas putida* (*PpHAL*), showing conserved residues in shaded areas.

1.4. Aromatic Amino Acid MIO-dependent Aminomutases

Phenylalanine- and tyrosine aminomutases (PAMs⁶, ⁴⁵ and TAMs,⁴, ⁴⁶ respectively) catalyze the 2,3-isomerization of (*S*)-α-arylalanine to (*R*)- or (*S*)-β-arylalanine. These aminomutases (AMs) are members of the class I lyase-like family and show high sequence homology with its members: phenylalanine ammonia lyases (PALs),⁴⁷ tyrosine ammonia lyases (TALs),⁴⁸ and histidine ammonia lyases (HALs) (Figure 1.4).⁴⁹ PALs, TALs, and HALs produce aryl acrylates from the corresponding amino-acid substrate by the elimination of ammonia.

1.4.1. 3,5-Dihydro-5-methylidene-4*H*-imidazol-4-one (MIO) Prosthesis

By analogy, PALs, HALs, and TALs, aminomutases, SgTAM, 4 CcTAM, 46 TcPAM, 45 and PaPAM all use an electrophilic prosthetic group 3,5-dihydro-5-methylidene-4H-imidazol-4-one (MIO), which initiates the reaction. However, early studies suggested that the active site prosthesis was a dehydroalanine, which was thought to derive by dehydration of a conserved Ser residue in the histidine ammonia lyase from $Pseudomonas\ putida\ (PpHAL)$. When the ammonia lyase was treated with of NaB 3 H₄, and the enzyme was cleaved hydrolytically, [3 H]-labeled alanine was recovered. This evidence strongly suggested the identity of a dehydroalanine group in the active site of the enzyme. Further support that the dehydroalanine served as an active site moiety came from a substrate-shielding experiment; preincubation of the HAL with histidine prevented the NaB 3 H₄ reduction. 51

It was not until the crystal structure of PpHAL was solved that the MIO group was first characterized. The MIO group is proposed to form post-translationally by a tandem of active site residues, typically Ala-Ser-Gly (**Scheme 1.2a**). The amide nitrogen of the Gly residue presumably attacks the carbonyl carbon of Ala to create the five membered imidazolidin-4-one ring precursor, followed by two dehydration steps to form the MIO moiety. The first dehydration step resembles that found for the formation of the chromophore in the green fluorescent protein (**Scheme 1.2b**), 53 yet the overall mechanism of formation is slightly different from that of the MIO.

Scheme 1.2: a) Formation of MIO, and b) The Structure of the Chromophore of Green Fluoroscence Protein.

$$\begin{array}{c} \text{Alia} \\ \text{HO} \\ \text{H} \\ \text{H} \\ \text{O} \\ \text{H} \\ \text{H} \\ \text{O} \\ \text{O} \\ \text{H} \\ \text{O} \\ \text{O}$$

The MIO is believed to function as an electrophilic α/β -unsaturated keto functional group (i.e., a 1,4-Michael acceptor). The nucleophile amino group of the substrate purportedly attacks

the exocyclic methylidene carbon of MIO moiety. This addition reaction is proposed to be driven by the aromatization of the MIO to an imidazole ring system (**Figure 1.2**). ^{50, 52, 54}

1.4.2. Reaction Mechanism of MIO-Based Aminomutases

Two mechanisms for MIO-based aminomutase were proposed in early reports and the debates continued until 2010. ³⁸ In one mechanism, the amino group of the amino acid substrate acts as a nucleophile and attacks the methylidene of the MIO through conjugate addition, forming an N-alkyl adduct. ⁵⁵ The N-alkyl group is subsequently expelled from substrate through α/β -elimination to form an acrylate reaction intermediate. Notably, in MIO-dependent ammonia lyase reactions, this acrylate intermediate is released as the product (Figure 1.2a). ⁵⁶ However, in the MIO-aminomutase reactions the acrylate remains in the active site for amino group rebound to form the β -amino acid product. ^{38, 57} A second proposed mechanism suggests that π -electrons of the phenyl ring of the substrate attack the MIO, by Friedel–Crafts-like activation, to form a σ -complex through the *ortho*-carbon of the substrate (Figure 1.2b). ^{47, 58, 59} The second process was principally assigned to ammonia lyase reactions, ^{47, 49, 58} but was extended to include the aminomutase reactions. ⁶⁰

Scheme 1.3: Two Proposed Mechanisms for the Conversion of Substrate to Product in a Generic Aminomutase: a) Amino-group Alkylation Pathway and b) Friedel-Crafts Aryl-Alkylation Pathway.

It should be noted that TcPAM and PaPAM enzymes catalyze residual ammonia lyase activity and produce trans-cinnamic acid as a minor product during steady-state catalysis. ^{38, 45, 61} Likewise, the SgTAM and CcTAM enzyme show similar relictual chemistry, producing trans-coumarate and β -tyrosine. ^{46, 62}

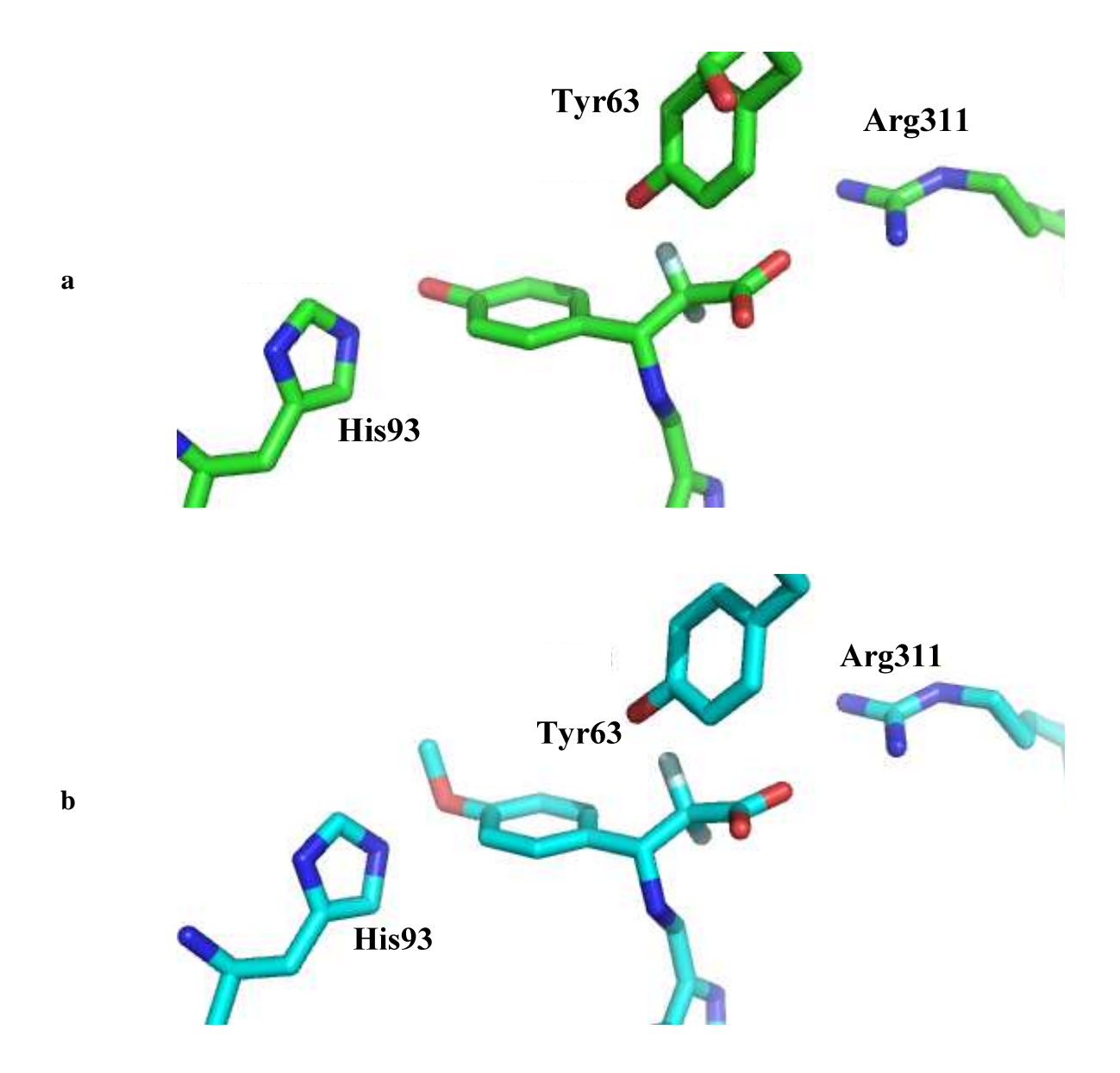


Figure 1.5. The crystal structure of SgTAM with a bound mechanism based inhibitor, a) 2,2-difluoro-(3R)-β-tyrosine (PDB 2QVE) and b) (3R)-amino-2,2-difluoro-3-(4'-methoxyphenyl)propanoic acid (PDB 2RJS)

The mechanism by which these enzymes catalyze their reactions remained ambiguous until now. Two SgTAM, crystal structures were resolved with separately bound mechanism-based inhibitors, 2,2-difluoro-(3R)- β -tyrosine (PDB 2QVE), and (3R)-amino-2,2-difluoro-3-(4')-

methoxyphenyl)propanoic acid (PDB 2RJS), ⁶³ where the amino group of the inhibitor was bound to the MIO group (**Figure 1.5**).

However, in the present study described in this thesis, in collaboration with crystallographer Prof. James Geiger, we resolved the crystal structure of PaPAM forming a covalent adduct partially with both (S)-α-phenylalanine and (S)-β-phenylalanine (PDB 3NUV). Both ligands were attached to the MIO group by the amine group (cf. chapter 2), which showed definitively that the MIO formed a covalent adduct during the catalysis of MIO-dependent aminomutases (**Figure 1.2**a). The deamination rate of the NH₂-MIO formed after removal of NH₃ from the substrate was determined for the first time, for any MIO-dependent enzyme, in this study. Burst phase kinetic analysis of TcPAM catalyzing the lyase reaction on (S)-α-styrylalanine was used to calculate the residence time of the NH₂-MIO adduct. This study is explained in further detail in Chapter 4.

1.4.3. Stereochemistry of the Phenylalanine Aminomutase Catalysis

Due to their dependence on the MIO moiety, ALs and MIO-based AMs likely follow similar mechanistic courses. Thus, *trans*-stereoisomers of cinnamate and coumarate represent intermediates on the reaction pathway of the phenylalanine and tyrosine aminomutases, respectively. However, SgTAM and PaPAM produce predominantly the corresponding (S)- β -amino acids with stereochemistry opposite to that of the (R)- β -amino acids products made by TcPAM and CcTAM. However, the mechanism by which these enzymes control their stereoselectivity was further elucidated and validated for the first time in this thesis work. To provide detailed mechanistic information, the stereochemistry of the migrating NH_2/H pair upon

reattachment to the phenylpropanoid skeleton to form the β -amino acid isomer was conducted for two PAM enzymes, TcPAM, ⁶⁶ and PaPAM. ⁶¹ The studies showed that both PAMs initiate the catalysis by abstracting pro-(3S) proton and eliminating the NH₂ of the substrate to form a trans-cinnamic acid intermediate. ⁶¹, ⁶⁶

Scheme 1.4: Stereochemistry of the Migrating Amino Group and the Proton of the Substrate and the Product during the Catalysis of a) TcPAM and (The Configurations at both C_{α} and C_{β} Positions are Retained) b) PaPAM (The Configurations at both C_{α} and C_{β} Positions are Inverted) is Shown.*

* Color Coding of the Protons: Pro (3S) Proton (Red), Pro (3R) Proton (Blue) and C_{α} Proton.

The abstracted proton and the amino group, dwelling momentarily in the active site, exchange positions and are rebounded to C_{α} and C_{β} positions respectively to form the final β -phenylalanine product. Stereospecific deuterium labeling studies revealed that Tc PAM proceeds

through retention of configuration at both C_{α} and C_{β} (Scheme 1.4a), whereas PaPAM through an inversion of configuration at both terminal carbons (Scheme 1.4b). ⁶¹ Even though the stereochemical studies reveal the different modes (retention or inversion of configuration) of the stereochemical reattachment of the NH₂/H pair, we also provided preliminary data showing how these enzymes create a microenvironment that can influences the mode of retention or inversion of configuration. We propose that the si or re face selectivity of the intermediate trans-cinnamic acid governs the observed stereochemistries during catalysis of all MIO dependent aminomutases. After the initial E2-type anti elimination step, the resultant intermediate can reattach at C_{β} to the amino group bound by the MIO amino group on the same face or the opposite face. If the rebound approaches on the same (si) face, (S)- β -stereochemistry results from inversion of configuration at C_{α} and C_{β} of PaPAM and SgTAM. Alternatively, if rebound approaches from the opposite (re) face, the observed (R)- β - stereochemistry results from retention of configuration at both migration termini of TcPAM and CcTAM. 38, 61, 64, 67

There is a debate over how the TcPAM and CcTAM present the opposite face of the intermediate to the MIO-bound NH₂ group. Wu et al., in a separate account, proposed (by inference from empirical data from our group) that after the initial E2-type *anti* elimination step in the TcPAM reaction sequence, a 180° rotation of the C_{β} – C_{ipso} bond of the cinnamate intermediate, in complex through a strong bidentate salt bridge with Arg325 and H-bonding with surrounding residues, is preferred. This rotation is purported to re-orient the carboxylate of the cinnamate, after breaking the salt bridge, into a favorable trajectory to form a monodentate interaction and H-bonding network with Arg325 and further H-bond interactions with Gln319,

Asn355, and Asn231 (**Figure 1.6**). It should be noted that during this proposed re-orientation, to place the C_{β} at the correct geometry for the amino group attack, the phenyl ring is forced into a sterically crowded active-site pocket that is electronically unfavorable (Glu455, Lys427, and Ile431) for binding an aromatic ring. Therefore, rotation about the C_{β} – C_{ipso} bond alone followed by lateral translation of the phenylpropanoid skeleton into a proper trajectory seems relatively unlikely as a mechanism to present the *re* face of the cinnamate intermediate to the NH₂-MIO adduct.

The authors of the independent study with TcPAM continue and suggest that the loss of bidentate salt bridge and the formation of H-bonds lower the energy of the LUMO of the carboxylate to promote the conjugate addition of the NH_2 bound to the MIO at C_{β} . Thus, the Q319M mutant made Wu et al. should lose an H-bonding partner, and thus increase the LUMO of the carboxylate group compared to the wild type enzyme. Accordingly, the preference for conjugate addition should decrease, based on the authors' explanation. Interestingly, the Q319M mutant shows higher β-regioselectivity, compared to the wild type TcPAM during the catalyzed addition of NH₃ to cinnamic acid, used in this case as a substrate. The authors continue to suggest that interactions between cinnamic acid and the residues in the Q319M mutant oriented the cinnamate at a trajectory that disfavored the formation of α -phenylalanine (**Figure 1.6**). ⁴¹ The latter observation seems paradoxical; the Q319M mutant, with one less H-bonding interaction, should likely favor rotation of the cinnamate back to the stronger bidentate salt bridge interaction with Arg325, and thus preferentially make α-phenylalanine. Also, the authors investigate an Arg325K mutant, showing increased β-regioselectivity. Lysine, like arginine, is

known to form strong electrostatic interactions (point charges) and H-bond interactions with counter-charged carboxylate anions. In our view, this electrostatic complex would increase the LUMO energy level of the cinnamate carboxylate group and should therefore dissuade conjugate addition of the amino group at C_{β} of the α/β -unsaturated carboxylate in the PAM reaction. Furthermore, the authors argue that the carboxylate group of the cinnamate intermediate is an electron sink. They conclude that during the conjugate addition, the π -bond electrons between $C_{\alpha}-C_{\beta}$, shift to form a π -bond between $C_{\alpha}-C_{1}$, placing a negative charge on both of the carboxylate oxygens. They continue to surmise that the migratory pro-(3S) proton (which is partially exchanged with solvent protons as dissected in our laboratory) could transfer to one of the carboxylate oxygens, which then would be vulnerable for exchange with protons within the enzyme. If this mechanistic consideration is evaluated across all PAM enzymes, then the PaPAM reaction mechanism should proceed similarly. However, 100% of the migratory pro-(3S) proton transfers from C_{β} to C_{α} in the PaPAM-catalyzed isomerization reaction, ⁶¹ an observation that contradicts the one posited by the other research group. An additional piece of evidence shows that PaPAM and SgTAM, which form the (S)- β -amino acid isomers, do not form a bidentate salt bridge with the Arg residue positioned analogously as that found in TcPAM and CcTAM. 63, 64 Instead, PaPAM and SgTAM lock their substrates in a monodentate interaction through sterics and/or electrostatics. These trajectories are analogous to those proposed by Wu, et al. for TcPAM after the enzyme rotates the cinnamate intermediate into a favorable position for amino group attack at C_B. Thus, PaPAM and SgTAM, according to the rationale posited by Wu, et al., regarding the cinnamate trajectory (above), should catalyze the addition of NH₃ to the

cinnamate substrate in the "reverse" and produce predominantly the β -amino acid isomer. However, our group showed that the "reverse" reaction catalyzed by PaPAM produces a 50:50 distribution of α - and β -phenylalanine products.

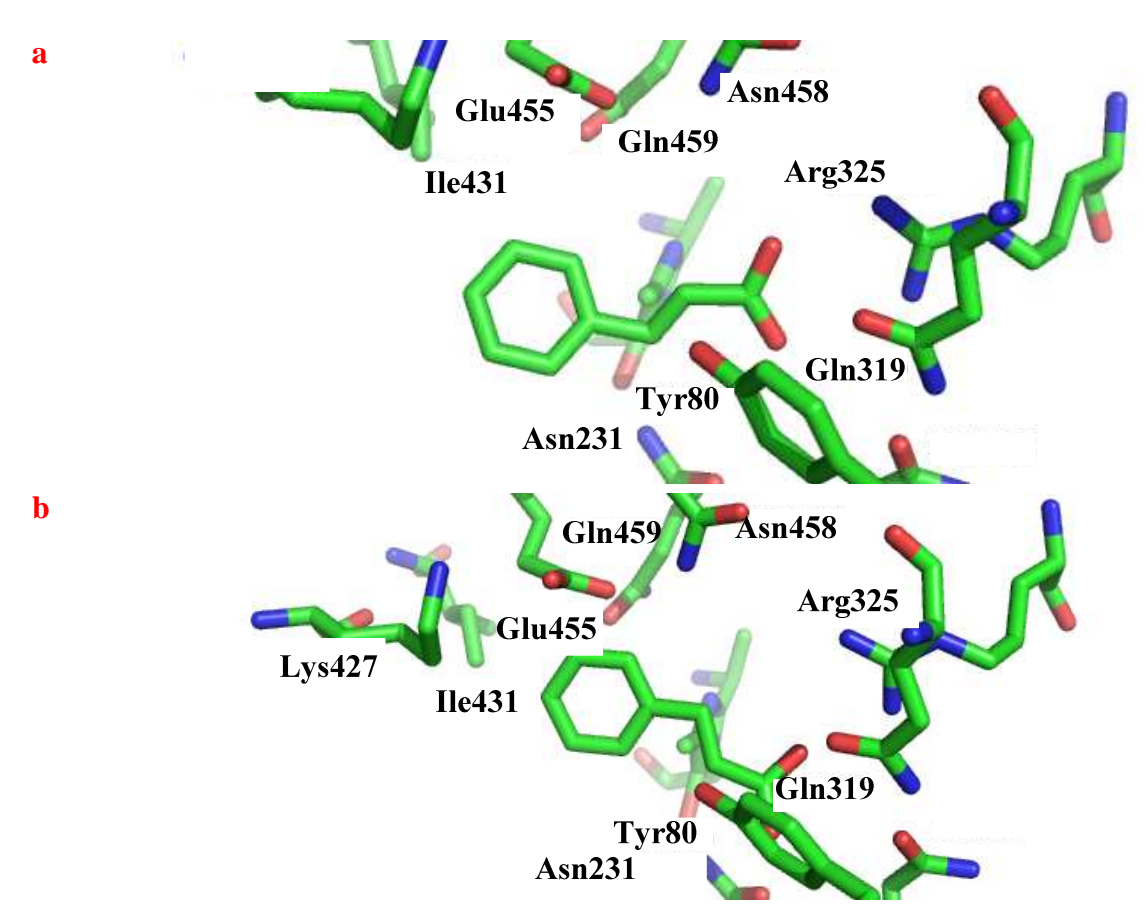


Figure 1.6. a) Crystal structure of TcPAM with bound cinnamic acid intermediate. b) The proposed orientation of the cinnamic acid intermediate which leads to the formation of (R)-β-phenylalanine with a retention of configuration at both migration termini, by Wu. et al. (Modeled using Pymol from PDB# 3NZ4)

After consideration of our empirical data and the theoretical speculations offered by Wu, et al., we support a mechanism for aminomutase that make (R)- β -amino acid isomers that proceed via 180° rotation of the transient cinnamate intermediate about the C_1 - C_{α} and C_{β} - C_{ipso} bonds.

In view of a molecular model, this crankshaft rotation results in minimal translational displacement of the phenyl ring, the rotating carbons, and the carboxylate group. Also, this model keeps the bidentate salt bridge intact between the carboxylate and active site arginine. This rotation mode also minimizes unfavorable steric and electronic interactions between the phenyl ring and active site residues. Chapter 2 provides details on the monodentate salt bridge between the (S)- β -amino acid ligands in PaPAM and SgTAM, formed without rotation of the cinnamate intermediate. The adducts shown in the crystal structures of these enzymes are contrasted to the bidentate salt bridge interactions between the ligand found in TcPAM and purported to reside in CcTAM. 38 , 61 , 64

Prior to the work studied in this body of work, only the stereochemistry of the PAM reactions was known. This thesis explores the complete direct stereochemical analysis for a TAM enzyme. The stereochemistry of SgTAM was indirectly explored using an epoxide ((2S,3R)-3-(4-fluorophenyl)oxirane-2-carboxyate) as suicide substrate. The epoxide analog formed a covalent interaction with the MIO through the epoxide oxygen followed by an epoxide ring opening by a water molecule. Inversion at C_3 of the substrate in the active site resulted in a single diastereomer (2R,3S)-2,3-dihydroxy-3-(4-fluorophenyl)propanoic acid observed in the crystal structure. The observed diol was proposed to be generated either through an S_N1 or S_N2 -type mechanism, yet with net inversion of configuration at C_3 .

While this was an elegant inference of the reaction stereochemistry of SgTAM, we sought to understand the complete stereochemistry of a homologous MIO-dependent tyrosine aminomutase (CcTAM). So far, five MIO-dependent aminomutases are known to isomerize either (S)- α -phenylalanine (EncP from $Streptomyces\ maritimus$, 68 AdmH (PaPAM) from

Pantoea agglomerans, $^{6, 61}$ and $^{6, 61}$ an

2. INSIGHTS INTO THE MECHANISM OF MIO-BASED PHENYLALANINE AMINOMUTASE CATALYSIS

Reproduced in part with permission from [Feng, L.; Wanninayake, U.; Strom, S.; Geiger, J.; Walker, K. D., Mechanistic, mutational, and structural evaluation of a *Taxus* phenylalanine aminomutase. *Biochemistry* **2011**, 50, (14), 2919-2930], and from [Ratnayake, N. D.; Wanninayake, U.; Geiger, J. H.; Walker, K. D., Stereochemistry and mechanism of a microbial phenylalanine aminomutase. *J. Am. Chem. Soc.* **2011**, 133, (22), 8531-8533] Copyright © 2011 American Chemical Society.

Reproduced in part with permission from [Strom, S.; Wanninayake, U.; Ratnayake, N. D.; Walker, K. D.; Geiger, J. H., Insights into the mechanistic pathway of the *Pantoea agglomerans* phenylalanine aminomutase. *Angew. Chem., Int. Ed. Engl.* **2012**, 51, 11-17] Copyright © 2012 WILEY-VCH Verlag GmbH & Co. KGaA, Weinheim.

2.1. Introduction

As described in Chapter 1 of this thesis, methylidene imidazolone (MIO)-dependent aminomutases (AMs)⁴⁻⁶⁻⁴⁵⁻⁴⁶ and ammonia lyases⁴⁷⁻⁴⁹ are members of the class I lyase-like family and use phenylalanine, tyrosine, and histidine amino acids as substrates. The ALs produce arylacrylates from the corresponding amino acid substrate by the elimination of ammonia, $^{47-49}$ while the AMs isomerize the α -amino acid substrates to their β -amino acids. $^{4-6-45-46}$ These enzymes use an active site prosthesis MIO to catalyze their reactions. In one proposed mechanism for this group of enzymes, the amino group of the amino acid substrate acts as a nucleophile 55 and in the second, the π -electrons at the *ortho*-carbon atom of the phenyl ring of

the substrate attack the Lewis acidic MIO by Friedel–Crafts-like activation (see Scheme 1.3).⁴⁷, ⁵⁸, ⁵⁹ Production of *trans*-cinnamate analogs as a result of residual ammonia lyase activity of the MIO-dependent aminomutases during steady-state catalysis, ³⁸, ⁴⁶, ⁶¹, ⁶² suggests that the lyases and aminomutases follow analogous mechanistic courses and that *trans*-cinnamate analogues represent intermediates on the reaction pathway of the aminomutases.

The structures of several enzymes of the MIO-dependent family were characterized in earlier reports.⁵⁰ The structure of Rhodobacter sphaeroides tyrosine ammonia lyase (RsTAL) in complex with the competitive inhibitor 2-aminoindan-2-phosphonic acid, which is covalently bound by its amino group to the MIO in the active site (PDB 207E) was determined. 70 Yet. despite acquiring the structure, neither MIO-based mechanism was discussed for the RsTAL reaction. 70 Also available are structures of the tyrosine aminomutase from Streptomyces globisporus (SgTAM) in complex with inhibitors 2,2-difluoro-(S)-β-tyrosine (PDB 2QVE) and separately with (3S)-amino-2,2-difluoro-3-(4'-methoxyphenyl)propanoic acid (PDB 2RJS) (see Chapter 1).⁶³ These β-amino acids were alkylated at their amine groups by the MIO, which is consistent with the aminoalkyl mechanism that involves the elimination of an alkylamine (see Chapter 1). However, automated docking and molecular dynamics simulation studies of phenylalanine ammonia lyase from Petroselinum crispum (PcPAL, PDB 1W27)⁷¹ suggested that the Friedel-Crafts mechanism is nevertheless used by both PAL and PAM enzymes. 60 A debate about the mechanism used by these MIO-based enzymes remained open. In addition, the crystal structure SgTAM in complex with (S)-α-tyrosine (PDB 3KDZ) showed that Y63 was in close proximity to the geminal protons of the substrate. A non-functional Y63F mutant suggested the

important catalytic function of the highly conserved tyrosine residue towards abstracting the C_{β} proton during the α,β -elimination step of the aminomutase reaction.⁵⁴ In addition to acquiring crystal structure data to inform on the mechanism of the PAM reactions, experiments were conducted to assess whether the isomerization occurred inter- or intramolecularly. Earlier studies on the TcPAM mechanism using cell free assays of Taxus cambial bark³⁷ and recombinantly expressed TcPAM66 inferred that the amino group of the (S)-α-phenylalanine substrate was transferred to C_{β} intramolecularly, while the proton was reciprocally transferred partially intramolecularly. It was clear from these earlier studies that the migratory amino group and hydrogen reattached to the phenylpropanoid skeleton with retention of configuration at C_{α} and C_B. It should be noted, that assays with the purified, recombinant TcPAM contained a cleaner metabolite background with fewer contaminating enzymes than the assays derived from the crude cell free extracts of Taxus bark.³⁷ While this early study elucidated the mode of the NH₂group transfer, the influence of cinnamate and other cinnamate modifying enzymes in the crude plant enzyme extract on the NH2-transfer process was not considered. Therefore, in the current study, the intramolecular mode of NH2-transfer was re-examined by incubating purified, recombinant TcPAM with a mixture of [ring, β -C- ${}^{2}H_{6}$]-trans-cinnamate and [${}^{15}N$]phenylalanine. This confirmatory study was important since a purified, recombinantly expressed Taxus PAM was recently shown to catalyze the formation of β -phenylalanine from cinnamate and ammonia co-substrates.⁷² In this scenario, it could be imagined that cinnamate molecules could bind and de-bind the *holo* (NH₂-MIO) form of *Tc*PAM before the NH₂-rebound step.

To provide further information on the mechanism of this class of catalysts, the X-ray crystal structures of $PaPAM^{64}$ and $TcPAM^{38}$ were determined. The TcPAM structure along with modeled-in substrates also showed that the 3'-carbon of the aromatic ring of the bound cinnamate intermediate/substrate is proximate to and makes a direct hydrophobic interaction with Leu104. This residue and several other distal hydrophobic interactions between the aromatic ring of cinnamate and Leu179, Leu227, and Val230 likely contribute to substrate binding and to defining the topology of the active site. In addition, the mechanism and stereochemistry of how (inter- or intramolecularly) the migratory groups attach at their receiving carbon centers (with retention or inversion of stereochemistry) during the reaction was evaluated.

2.2. Experimental

2.2.1. Chemicals

(*S*)-α-Amino acids (*R*)/(*S*)-β-amino acids were commercially available from PepTech Corporation (Burlington, MA), except for styryl-(*R*)-β-alanine, which was synthesized by modification of a described procedure.⁷³ 5-Phenyl-(2*E*,4*E*)-pentadienoic acid ((*E*,*E*)-styrylacrylate) was purchased from Alfa Aesar (Ward Hill, MA). [ring, β-C- 2 H₆]-*trans*-cinnamic acid and *trans*-2/methylcinnamic acid were obtained from Sigma-Aldrich (St. Louis, MO), and 15 Nlphenylalanine was obtained from Cambridge Isotope Laboratories (Andover, MA).

2.2.2. Expression and Purification of *Tc*PAM

Codon-optimized wild-type⁷⁴ or a mutant *Tc*PAM derived from the optimized clone was overexpressed in *Escherichia coli* BL21 (DE3) cells. The cells (six 1-L cultures) were grown in Luria–Bertani medium supplemented with kanamycin (50 µg/mL), induced for expression with

isopropyl- β -D-thiogalactopyranoside (100 μ M) at 16 °C, and, after 16 h, were harvested by centrifugation (4,000g for 20 min). To the cell pellet was added 100 mL of resuspension buffer (50 mM sodium phosphate containing 10 mM imidazole, 5% (v/v) glycerol, and 300 mM NaCl, pH 8.5), the suspension was lysed by sonication, and the cellular debris and light membranes were removed by centrifugation at 9,700g (45 min) then at 102,000g (1 h), respectively. The resultant crude aminomutase in the soluble fraction was purified by nickel-nitrilotriacetic acid affinity chromatography according to the protocol described by the manufacturer (Qiagen, Valencia, CA); TcPAM was eluted in 250 mM imidazole (3 mL total volume, at >90% purity by SDS-PAGE with Coomassie Blue staining).

The fraction of protein that eluted from the nickel-nitrilotriacetic acid affinity column containing active *Tc*PAM (76 kDa) was exchanged with elution buffer (20 mM Tris-HCl, pH 7.5, 50 mM NaCl, and 5% glycerol) through several concentration/dilution cycles using a Centriprep centrifugal filter (30,000 MWCO, Millipore) to remove the 250 mM imidazole. The protein, concentrated to 1 mL, was loaded onto a pre-calibrated gel filtration chromatography column (Superdex 200 prep grade, GE Healthcare Life Sciences) connected to a Pharmacia FPLC system (comprising a Biotech Recorder 102, Pharmacia Pump P-500, and Liquid Chromatograph Controller LCC-500). *Tc*PAM was eluted at 1 mL/min with elution buffer and was isolated in two peaks, one with an elution volume consistent with that of a 150 kDa MW standard, considered to be a dimer, and a larger peak consistent with protein >300 kDa, likely a multimeric aggregate.

2.2.3. Expression and Purification of *PaPAM*.

PaPAM was expressed according to a previously described procedure, and is described briefly here. 61 E. coli cells (twelve 1-L cultures) were grown in Luria-Bertani medium supplemented with kanamycin (50 µg/mL), induced for expression with isopropyl-β-Dthiogalactopyranoside (100 µM) at 16 °C and harvested by centrifugation after 16 h. To the cell pellet was added 125 mL of resuspension buffer (50 mM sodium phosphate containing 5% (v/v) glycerol, 300 mM NaCl and 10 mM imidazole, pH 8.0), the cells were lysed by sonication, and the cellular debris and light membranes were removed by centrifugation. The resultant crude aminomutase in the soluble fraction was purified by nickel-nitrilotriacetic acid affinity chromatography according to the protocol described by the manufacturer (Qiagen, Valencia, CA); PaPAM eluted in 250 mM imidazole. Fractions containing active soluble PaPAM (59 kDa) were combined, and the buffer was exchanged with 50 mM sodium phosphate buffer (pH 8.0) containing 5% (v/v) glycerol through several concentration/dilution cycles using a Centriprep centrifugal filter (30,000 MWCO, Millipore) to a final concentration of 7 mg/mL (calculated by the Bradford protein assay). The purity of the concentrated enzyme was assessed at >95% by SDS-PAGE with Coomassie Blue staining.

2.2.4. PAM Activity Assays

An aliquot (50 μ L) of the fraction containing TcPAM ($\sim 80 \mu g$) from the nickel-nitrilotriacetic acid affinity column elusions was added to 50 mM phosphate buffer solution (1 mL final volume, pH 8.5) containing 5% glycerol and (S)- α -phenylalanine (100 μ M), and the solution was incubated at 31 °C for 1 h. This procedure was repeated for PaPAM.

Equimolar amounts of protein from each fraction (40 μ g of the 150 kDa fraction and 80 μ g of the >300 kDa fraction) from the gel extraction chromatography were separately incubated with (*S*)- α -phenylalanine (100 μ M) at 31 °C for 1 h. Products were analyzed using GC/EIMS (described in section 2.2.5). The aminomutase in the 150 kDa fraction had 3-fold higher activity than in the >300 kDa fraction; therefore, the fraction containing the dimer was used for the crystallographic study, loaded into a size-selective centrifugal filtration unit (30,000 MWCO), and concentrated to 10 mg/mL. The purity (>95%) of the concentrated enzyme was assessed by SDS–PAGE with Coomassie Blue staining, and the quantity was determined by the Bradford protein assay.

2.2.5. GC/EIMS Analysis of PAM Catalyzed Products

The reactions were quenched with 6 N HCl, the pH was adjusted to pH 2, and then internal standards 3'-fluoro-(R)- β -phenylalanine (at 20 μ M) and *trans*-2'-methylcinnamic acid (at 20 μ M) were added. The cinnamic acids were extracted into diethyl ether, the organic solvent was evaporated *in vacuo*, the residue was dissolved in ethyl acetate/methanol (3:1, v/v) (200 μ L), and the solution was treated with a TMS-diazomethane dissolved in ether (\sim 5 μ L) to convert the acids to their methyl esters. Each sample was separately analyzed by GC/EIMS and quantified by linear regression analysis. The remaining aqueous fraction was adjusted to pH >10 with 6 N NaOH, and the amino acids were derivatized to their N-di(ethoxycarbonyl) esters, as before. Each sample was separately analyzed/quantified by GC/EIMS; in brief, the relative amounts of the α - or β -amino acid were determined by linear regression analysis of the area of the base peak ion of the derivatized α - and β -amino acids generated in the EIMS. The peak area was converted to concentration by solving the corresponding linear equation, derived by plotting the area of the

base peak ion (produced by the corresponding authentic standard) against concentration ranging from 0 to 1.5 mM.

2.2.6. Mutagenesis of TcPAM cDNA for Expression of L104A Mutant.

Point mutations of TcPAM were performed using the QuikChange II XL Site-Directed Mutagenesis Kit (Stratagene, La Jolla, CA). The oligonucleotide primers used to exchange residue L104 to alanine (Ala) in the mutagenesis reactions were as follows: L104A (forward primer): 5'-GCAGGAGAGCGCCATCCGCTGTC-3' (mutations are bold and underlined). The corresponding reverse complement primer (5'-GACAGCGGATGGCGCTCTCCTGC-3') was paired with the respective forward primer. Expression vector pET-28a(+) containing the wildtype tcpam cDNA (10 ng) was used as the DNA template in the PCR reactions, the corresponding forward and reverse primers (150 ng each), dNTP mix (1 µL), 10X reaction buffer (5 μL), QuickSolution reagent (3 μL), PfuUltra HF DNA polymerase (1 μL at 2.5 U/μL) and ddH2O to bring the volume to 50 µL. The PCR program conditions were as follows: initial denaturing at 95 °C for 2 min followed by 30 cycles at 95 °C for 50 s, 55 °C for 50 s, and 68 °C for 7 min, and finally, the reactions were held at 68 °C for 7 min. The reactions were place on ice, to each was added restriction enzyme DpnI (1 µL at 10 U/µL), and the reactions were incubated at 37 °C for 1 h to digest the template DNA. An aliquot (2 µL) of the plasmid solution from each PCR reaction was used to transform XL10-Gold ultracompetent cells (provided in the QuikChange II XL Site-Directed Mutagenesis Kit). The resultant plasmids encoding the L104A mutation in the tcpam cDNA (designated as PAMeLA_104: phenylalanine aminomutase exchange Leu—Ala_104) were confirmed by sequencing the corresponding tcpam104A cDNA. The mutant gene was expressed as described for the wild-type.

2.2.7. Analysis of Kinetic Parameters of TcPAM and PAMeLA_104

The substrates (S)- α -phenylalanine, 3'- and 4'-methyl-(S)- α -phenylalanine, and styryl-(S)- α -alanine were incubated separately with wild-type TcPAM and PAMeLA_104 to establish steady-state conditions with respect to a fixed protein concentration and time at 31 °C. Under steady-state conditions, each substrate at 10, 20, 40, 80, 150, 300, 500, and 750 μ M was separately incubated with TcPAM or PAMeLA_104 in triplicate, single stopped-time assays. Each of the products in the reaction mixture was derivatized to their N-(ethoxycarbonyl) methyl ester and then quantified by GC/EIMS analysis, as described previously. The kinetic parameters ($K_{\rm M}$ and $k_{\rm cat}$) were determined from the Hanes-Woolf plot (R^2 was typically >0.98), and the stereochemistry of enzyme-catalyzed products was assessed by chiral GC/EIMS analysis (Chirasil-D-Val column, Varian).

2.2.8. Analysis of Products Formed from the Incubation of $\mathit{Tc}PAM$ with [^{15}N]Phenylalanine and [ring, β -C- 2H_6]- trans -Cinnamate Acid

Purified TcPAM (100 µg) was incubated with a mixture of [^{15}N]-phenylalanine and [ring, β - $C^{-2}H_6$]-trans-cinnamate acid (10 mmol of each) for 1 h. The α - and β -phenylalanine isotopomers were derivatized to their N-(ethoxycarbonyl) methyl esters, and cinnamic acid was converted to its methyl ester and analyzed by GC/EIMS.

2.2.9. Assessing the Product Distribution of PaPAM and TcPAM with 2'-Methyl-(S)- α -Phenylalanine

*Pa*PAM and *Tc*PAM, each at 20 μg/mL in separate 1-mL assays, were incubated with 2'-methyl-(S)-α-phenylalanine (at 1 mM) at 31 °C for 1 h. Internal standards 3'-fluoro-(R)-β-phenylalanine and *trans*-cinnamic acid (each at 20 μM) were added. The reactions were acidified (pH 2, 6 N HCl) and the cinnamic acid analogues were separately extracted (3 × 1 mL) into ethyl acetate. An aliquot of a TMS-diazomethane solution was added to convert the acids to their methyl esters. The remaining amino acids were derivatized to their ethoxycarbonyl methyl esters according to a previously described method separately analyzed by GC/EIMS, and the analytes were quantified by comparison against a standard curve.

2.2.10. Conversion of Cinnamate to α - and β -Phenylalanine by PaPAM

*Pa*PAM (7 mg/mL) was incubated for 48 h at 31°C with cinnamic acid (1.25 mM) in phosphate buffer (pH 8.5) containing 60 μM of ammonia in triplicate 1-mL assays. The reactions were quenched with 6 M NaOH and 3'-fluoro-(R)-β-phenylalanine (20 nmol) was added as the internal standard. To each assay was added ethyl chloroformate (100 μL) to N-carbonylate the amino acids. The assay solutions were acidified (6 N HCl) to pH 2 on ice, the putative, derivatized amino acids were extracted with ethyl acetate (3 × 1 mL), and TMS-diazomethane dissolved in methanol was added drop wise to the organic fractions until the yellow color of diazomethane persisted. The organic solvent was removed, and the residue from each sample was re-dissolved in 3:1 (v/v) ethyl acetate:methanol (200 μL) and analyzed by GC/EIMS, and the base peak ions were evaluated. The amount of the derivatized α - and β -amino acid was quantified as follows. Ratio 1 (abundance of the base peak ion of the internal standard at 20 μM:

abundance of the base peak ion of the analyte) was used to calculate product concentration. The abundance of the base peak ion produced by the corresponding authentic standard at varying concentrations in a dilution series was plotted against the abundance of the base peak ion produced by the internal standard (at $20~\mu M$). The linear equation derived from this plot was used to convert Ratio 1 to analyte (i.e., product) concentration.

2.3. Results

2.3.1. X-ray Crystal Structure of TcPAM

In the TcPAM structure (PDB 3NZ4), A trans-cinnamate molecule is bound in the active site, lying above the MIO and under a loop region that includes residues 80–97, which define the top of the active site (**Figure 2.1a**). The trans-cinnamate molecule lies about 3.4 Å above the methylidene carbon of the MIO moiety. The carboxylate of the cinnamate makes a salt bridge interaction with a strongly conserved Arg325, which serves to position the product in the active site. The plane of the aromatic ring of the cinnamate was observed to be displaced ~ 40° relative to the π -bond plane of the propeonate C=C double bond (**Figure 2.1a**). The aromatic ring is bound relatively loosely in the active site, making only one direct hydrophobic interaction with Leu-104 (3.3 Å, not shown). The only other close contact between cinnamate and an active site residue is a 2.9 Å interaction between the hydroxyl of Tyr80 and C_{α} of the cinnamate (**Figure 2.1b**).³⁸

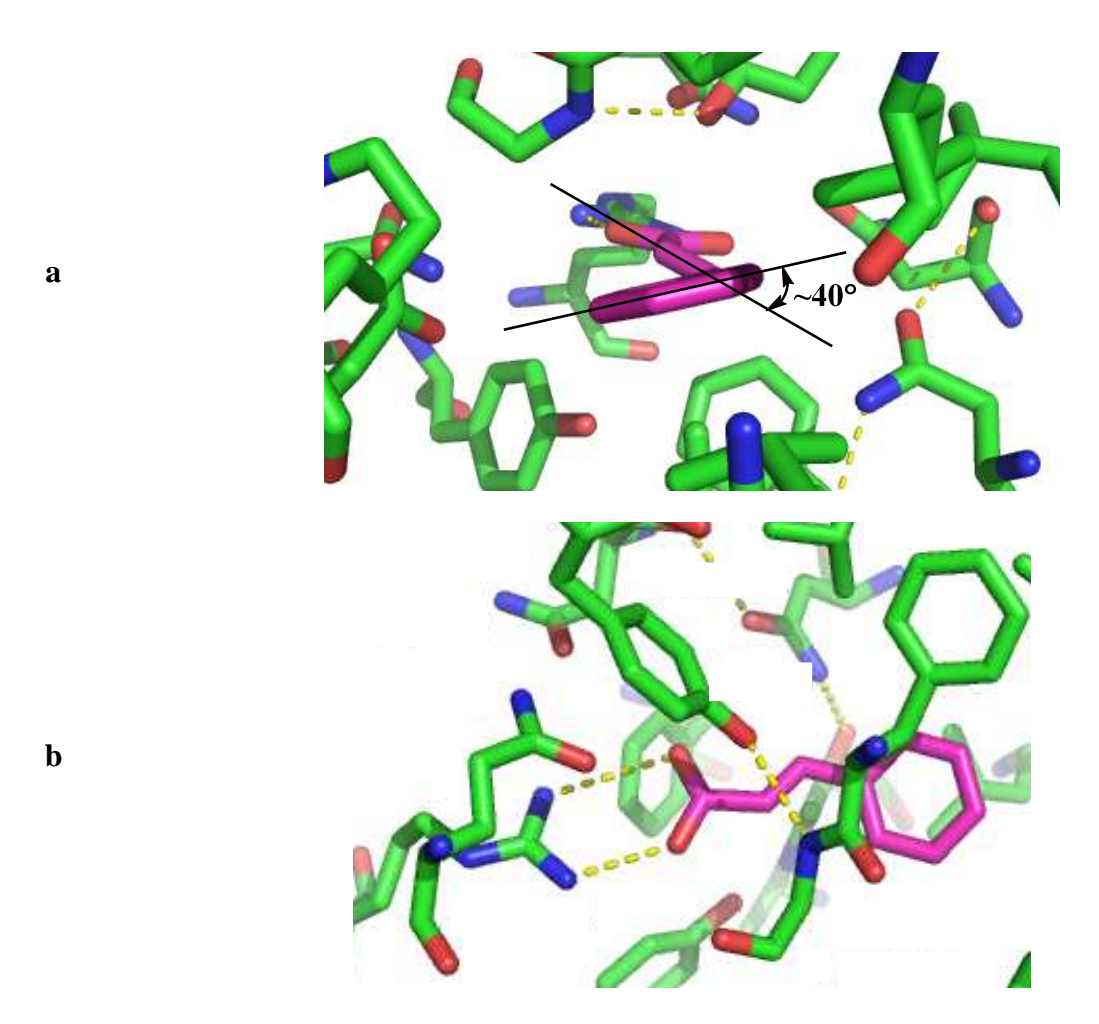


Figure 2.1. The TcPAM active site-cinnamate complex (magenta) a) indicating the displacement of plane of the aromatic ring of the cinnamate relative to the π -bond plane of the propeonate carbon–carbon double bond, and (b) the topside view. The PAM active site residues are colored by atom as follows: C (green), O (red), and N (blue).

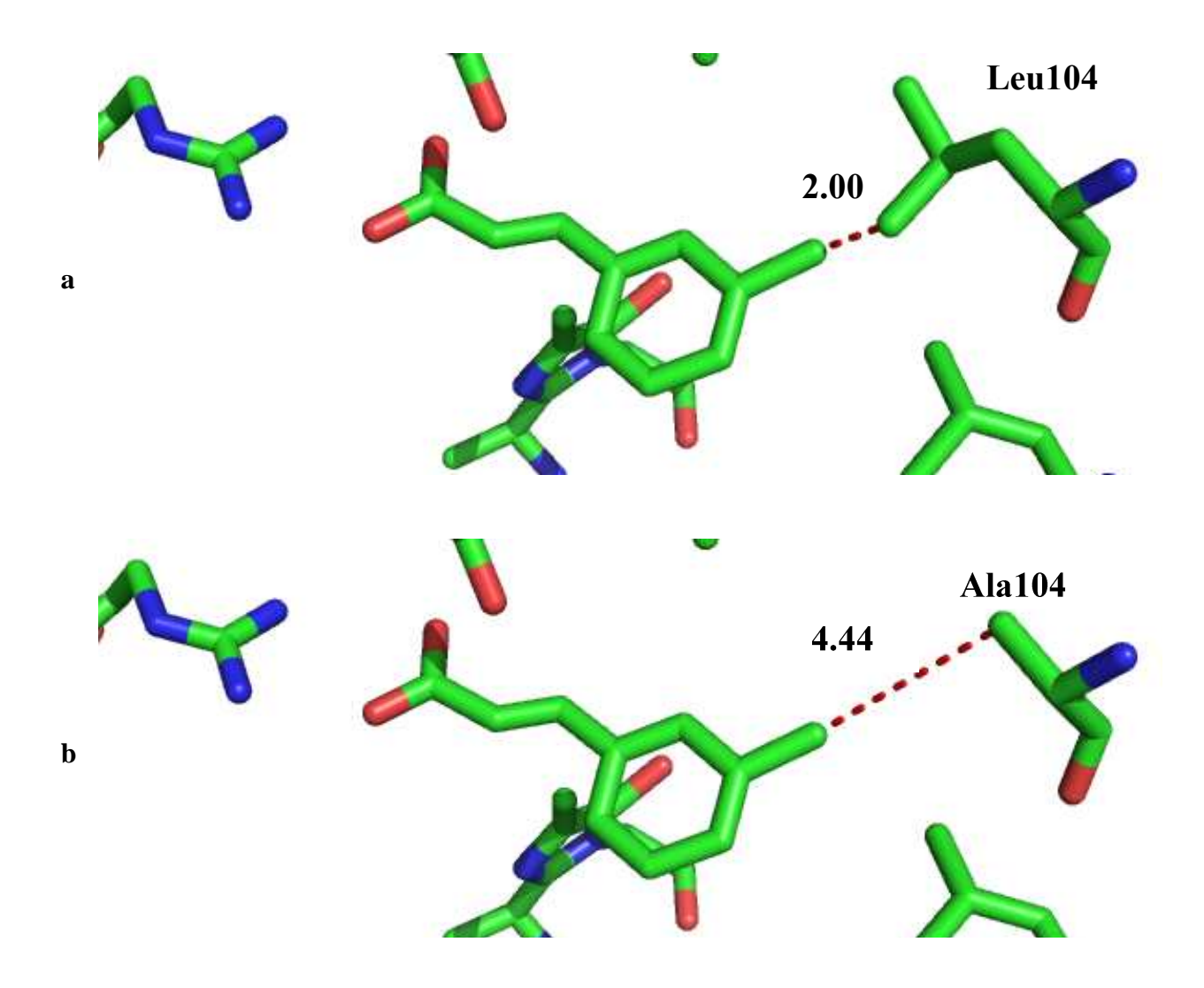
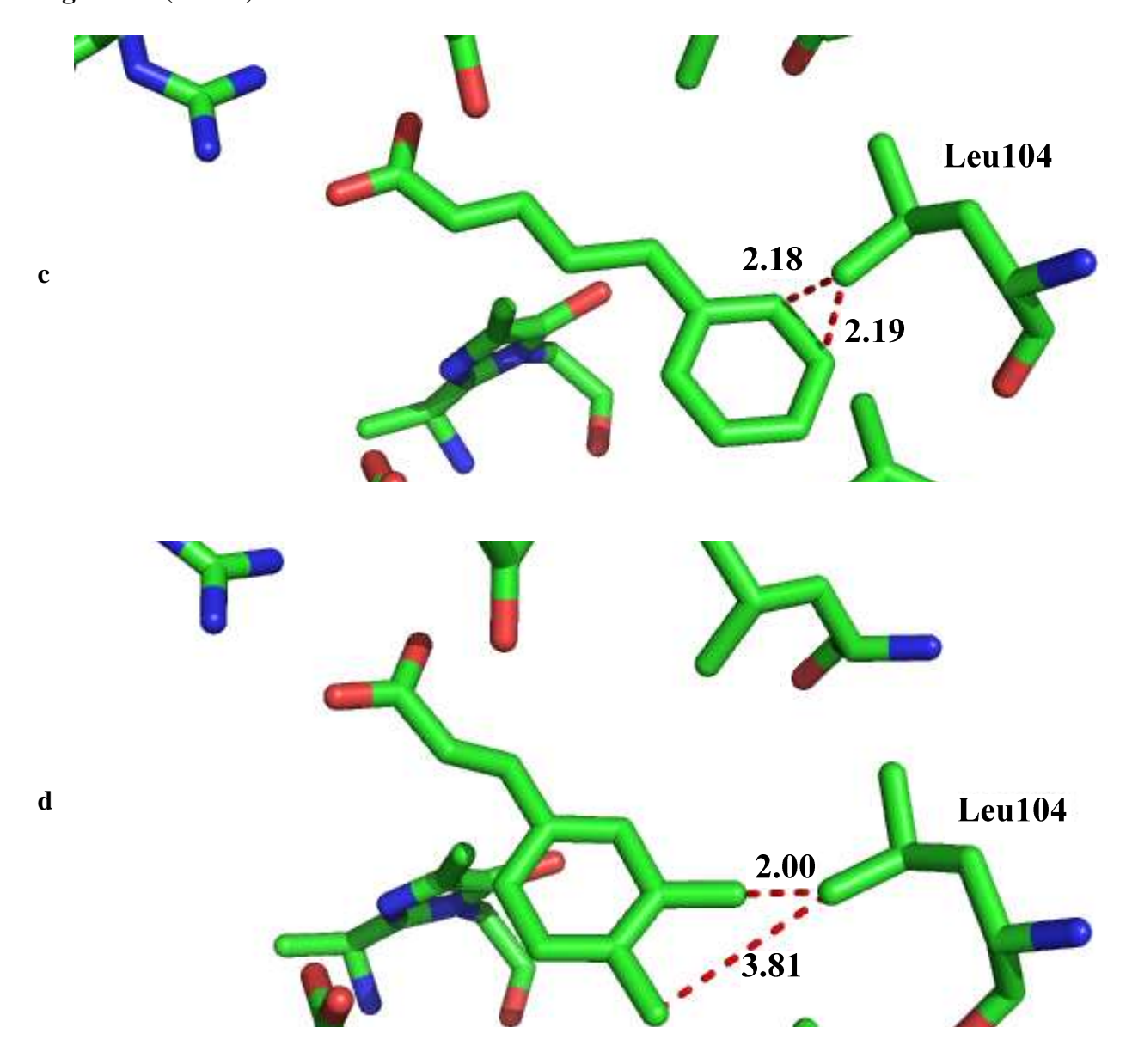


Figure 2.2. (b) the 3'-methyl-(S)-α-phenylalanine substrate is modeled into the mutant PAMeLA_104 active site where the steric volume is increased through the mutation of Leu-104 to Ala; now, the closest distance between the bound substrate and residue 104 is estimated at \sim 4.4 Å, and The *Tc*PAM-cinnamate complex is used to approximate the trajectory of non-natural substrates. (a) The 3'-methylphenyl-α-alanine substrate is modeled into the active site of *Tc*PAM showing the distance (\sim 2 Å) between the 3'-methyl group of the substrate and Leu-104.

Figure 2.2 (cont'd).



c) styryl-(S)- α -alanine modeled in the TcPAM active site showing the hydrophobic interaction with Leu 104 at a distance of ~ 2.2 Å. . (d) 3'- and 4'-methyl-(S)- α -phenylalanine are superimposed and modeled in the TcPAM active site. The relative positions of the methyl substituents on the phenyl ring of each substrate to Leu-104 are shown along with the distances (~ 2 and ~ 3.8 Å, respectively) between the C $_{\delta}$ of Leu-104 and 3'-methyl and 4'-methyl.

2.3.2. Site-Directed Mutation of an Active Site Leu of TcPAM

As noted earlier, the TcPAM-cinnamate complex shows that the 3'-carbon of the bound intermediate is close to residue L104, likely involved in a van der Waals interaction with the substrate (**Figure 2.2**). L104 of TcPAM was changed to an A104 mutant (designated as PAMeLA_104) to assess how this would affect the aminomutase reaction with sterically demanding non-natural substrates compared to the reaction with the wild-type enzyme. The kinetic parameters were obtained separately for TcPAM with substrates 3'-methyl-(S)- α -phenylalanine, styryl-(S)- α -alanine, and 4'-methyl-(S)- α -phenylalanine and compared to those obtained for PAMeLA_104 in parallel enzyme assays with the same substrates (**Table 2.1**).

Notably, (R)- β -arylalanines and the various *trans*-cinnamate (**Table 2.1**) are products of the TcPAM reaction when (S)- α -arylalanines are used as substrates; ⁴⁵ therefore, the sum of their production rates at steady-state was used to calculate the turnover rate (k_{cat}) (**Table 2.1**). The catalytic efficiency (k_{cat}/K_M) of TcPAM and $PAMeLA_104$ for the natural substrate (S)- α -phenylalanine **1** is 1100 M^{-1} ·s⁻¹ and 560 M^{-1} ·s⁻¹, respectively. The product distribution of the TcPAM reaction, after 30 min, was dominated by (R)- β -phenylalanine, made at 0.053 s⁻¹, and cinnamate was made more slowly at 0.012 s⁻¹. Reciprocally, the product pool of the $PAMeLA_104$ reaction with **1** principally contained cinnamate, which was made at a rate of 0.073 s⁻¹, while the β -amino acid was made fractionally at 0.003 s⁻¹.

Table 2.1. Kinetic Parameters for TcPAM and PAMeLA_104 with Various Substrates

| | Substrate | Enzyme | $K_{\rm M}$ (M) × 10^3 | $^{\beta}k_{\mathrm{cat}}(\mathrm{s}^{-1})^{\mathrm{a}}$ | $\frac{\sin_{k_{\text{cat}}}}{(s^{-1})^{a}}$ | $k_{\text{cat}}/K_{\text{M}}$ $(\text{M}^{-1} \cdot \text{s}^{-1})$ |
|---|----------------------|--------|--------------------------|--|--|---|
| 1 | O NH ₃ | TcPAM | 0.057 (±0.004) | 0.053 (±0.001) | 0.012 (±0.002) | 1100 (±100) |
| | | PAMeLA | 0.136 (±0.002) | 0.003 (<±0.001) | 0.073 (±0.003) | 560 (±10) |
| 2 | O NH ₃ | TcPAM | 0.397 (±0.030) | 0.022 (±0.002) | 0.017 (±0.002) | 100 (±20) |
| | | PAMeLA | 0.083 (±0.008) | 0.028 (±0.003) | 0.032 (±0.003) | 720 (±20) |
| 3 | O NH ₃ | TcPAM | 0.091 (±0.005) | 0.030 (±0.002) | 0.005 (±0.002) | 380 (±20) |
| | | PAMeLA | 0.073 (±0.005) | 0.020 (±0.002) | 0.017 (±0.002) | 510 (±10) |
| 4 | O NH ₃ | TcPAM | 0.250 (±0.004) | <0.0002 | 0.082 (±0.002) | 330 (±10) |
| | | PAMeLA | 0.120 (±0.004) | 0.003 (±0.002) | 0.12 (<±0.01) | 1030 (±20) |

a. The terms ${}^{\beta}k_{cat}$ and ${}^{cin}k_{cat}$ represent the kinetic constants for the formation of the β -arylalanines and trans-arylacrylates, respectively.

b. The kinetic constant $k_{cat} = {}^{\beta}k_{cat} + {}^{cin}k_{cat}$. (S)- α -Phenylalanine (1), 3'-methyl-(S)- α -phenylalanine (2), 4'-methyl-(S)- α -phenylalanine (3), and styryl-(S)- α -alanine (4) at steady-state. Standard errors are in parentheses.

The catalytic efficiency of TcPAM and $PAMeLA_104$ for 3'-methyl-(S)- α -phenylalanine (2) is 48 $M^{-1} \cdot s^{-1}$ and 720 $M^{-1} \cdot s^{-1}$, respectively. The increase in catalytic efficiency for substrate 2 is due largely to the ~ 5-fold decrease in $K_{\rm M}$ of PAMeLA_104 (83 $\mu{\rm M}$) compared to the $K_{\rm M}$ of TcPAM (397 μM). The distribution of the 3'-methyl-(R)-β-phenylalanine and 3'methylcinnamate was at ~1:1 for both PAMeLA 104 and TcPAM catalysis; however, the combined rate of formation of both 3'-methyl-(R)-phenylalanine and 3'-methylcinnamate by PAMeLA_104 (0.060 s⁻¹) is slightly increased compared to the rate of the same reaction by TcPAM (0.039 s⁻¹) (**Table 2.1**). Interestingly, both TcPAM ($k_{cat} = 0.035 \text{ s}^{-1}$) and PAMeLA_104 $(k_{cst} = 0.037 \text{ s}^{-1})$ were kinetically similar when 4'-methyl-(S)- α -phenylalanine (3) was used as the substrate, and their K_{M} values, 91 $\mu\mathrm{M}$ and 73 $\mu\mathrm{M}$, respectively, were comparable as well as their catalytic efficiency values (380 M⁻¹·s⁻¹ and 510 M⁻¹·s⁻¹ (**Table 2.1**)). However, the rates of formation of the 4'-methyl-(R)- β -phenylalanine and 4'-methylcinnamate products (0.030 s⁻¹ and 0.005 s^{-1} , respectively) catalyzed by TcPAM from 3 were significantly different from the respective distribution catalyzed by PAMeLA 104 (0.020 s⁻¹ and 0.017 s⁻¹). TcPAM was incubated with styryl- α -alanine (4) and rapidly catalyzed the exclusive conversion of 4 to the corresponding 5-phenyl-(2E,4E)-pentadienoate (i.e., (E,E)-styrylacrylate) at $0.082~{\rm s}^{-1}$ and styryl-(R)- β -alanine at <0.0002 s⁻¹ (**Table 2.1**). Comparatively, PAMeLA_104 converted **4** to the corresponding (E,E)-styrylacrylate faster, at 0.12 s⁻¹; however, styryl-(R)- β -alanine was produced significantly faster by PAMeLA_104 than by TcPAM, yet still at a slow rate of 0.003 $\rm s^{-1}$. It is worth noting that the Michaelis constants for both $\it Tc$ PAM and PAMeLA_104 are 250 μM and 120 μM, respectively, for the styryl-(S)-α-alanine substrate, suggesting that the L104A

mutation is able to enhance the binding affinity for **4** and thus contributes toward increasing the overall catalytic efficiency from 330 $M^{-1} \cdot s^{-1}$ for TcPAM to 1000 $M^{-1} \cdot s^{-1}$ for $PAMeLA_104$.

2.3.3. Inter/Intramolecularity Analysis of the TcPAM Reaction

Table 2.2. GC/EIMS Analysis: Diagnostic Ions of Biosynthetic [15N]-β-Phenylalanine^a

Authentic standards of *N*-(ethoxycarbonyl)-β-phenylalanine methyl ester eluted from the GC column at 9.87 min. The mass spectrum of the derivatized biosynthetic (R)-β-phenylalanine (~ 200 nmol) isolated from the incubation allowed for quantitative analysis of the isotope enrichment and distribution. A molecular ion (M^+) of m/z = 252 indicated that the biocatalyzed product contained one extra mass unit compared to the mass of the unlabeled isotopomer (m/z = 251). The molecular ion and diagnostic fragment ions (base peak [$M - CH_3CH_2CO_2$]⁺ = 179, and lesser abundant ions m/z = 192 [$M - HC(O)OCH_3$]⁺ and m/z = 163 [m/z 192 – CH_3CH_2]⁺ (Table 2.2)) indicated that the additional mass unit was derived from the ¹⁵N-atom. In addition, the ratio (10:1) of the ion abundance for the base peak m/z = 178 and m/z = 179 for authentic N-(ethoxycarbonyl)-β-phenylalanine methyl ester is identical to the calculated ratio of the base peak m/z = 179 and m/z = 180 of the N-(ethoxycarbonyl) methyl ester of the biosynthesized [¹⁵N]-(R)-β-phenylalanine made after the incubation of TcPAM with [¹⁵N]-(S)-α-phenylalanine

and [ring, β -C- 2 H₆]-trans-cinnamate acid. This suggested a 15 N enrichment of 98% and that no unlabeled (R)- β -phenylalanine derivative was present. A small percentage (3%) of the biosynthetically derived (R)- β -phenylalanine contained seven additional mass units, according to a base peak fragment ion m/z = 185; the [15 N]-(R)- β -phenylalanine derivative was present at 97%. The isotopomer containing seven additional mass units was derived from the [ring, β -C- 2 H₆]-trans</sub>-cinnamate acid in the mixed substrate assay with TcPAM and was not present in control assays where the labeled cinnamate acid was left out.

2.3.4. X-ray Crystal Structure of PaPAM

PaPAM has similar architecture to the class of MIO-dependent aminomutases and ammonia lyases.³⁸⁻⁵⁰⁻⁶⁹⁷¹ The monomer consists of mostly α helices that run parallel to one another and form a four helix bundle at the center. The catalytically relevant species is a dimer of dimers, in which the two monomers in the asymmetric unit are related by a crystallographic twofold axis to the other two monomers that comprise the catalytically functional PaPAM tetramer, and each subunit contains an active site.⁶⁴ At the end of this bundle is the active site, which resides at the interfaces between three of the monomers in the tetramer, and includes residues from all three protomers. PaPAM, similar to other bacterially derived members of this family whose structures are known, lacks the C-terminal capping domain that is present in the related plant enzymes, such as TcPAM.³⁸ The inner-loop region, which rests just above the active site, is packed tighter towards MIO than that of TcPAM, and is well ordered. However, the PaPAM MIO is made autocatalytically from an amino acid tandem T-S-G⁶⁴ instead of from the common A-S-G sequence.

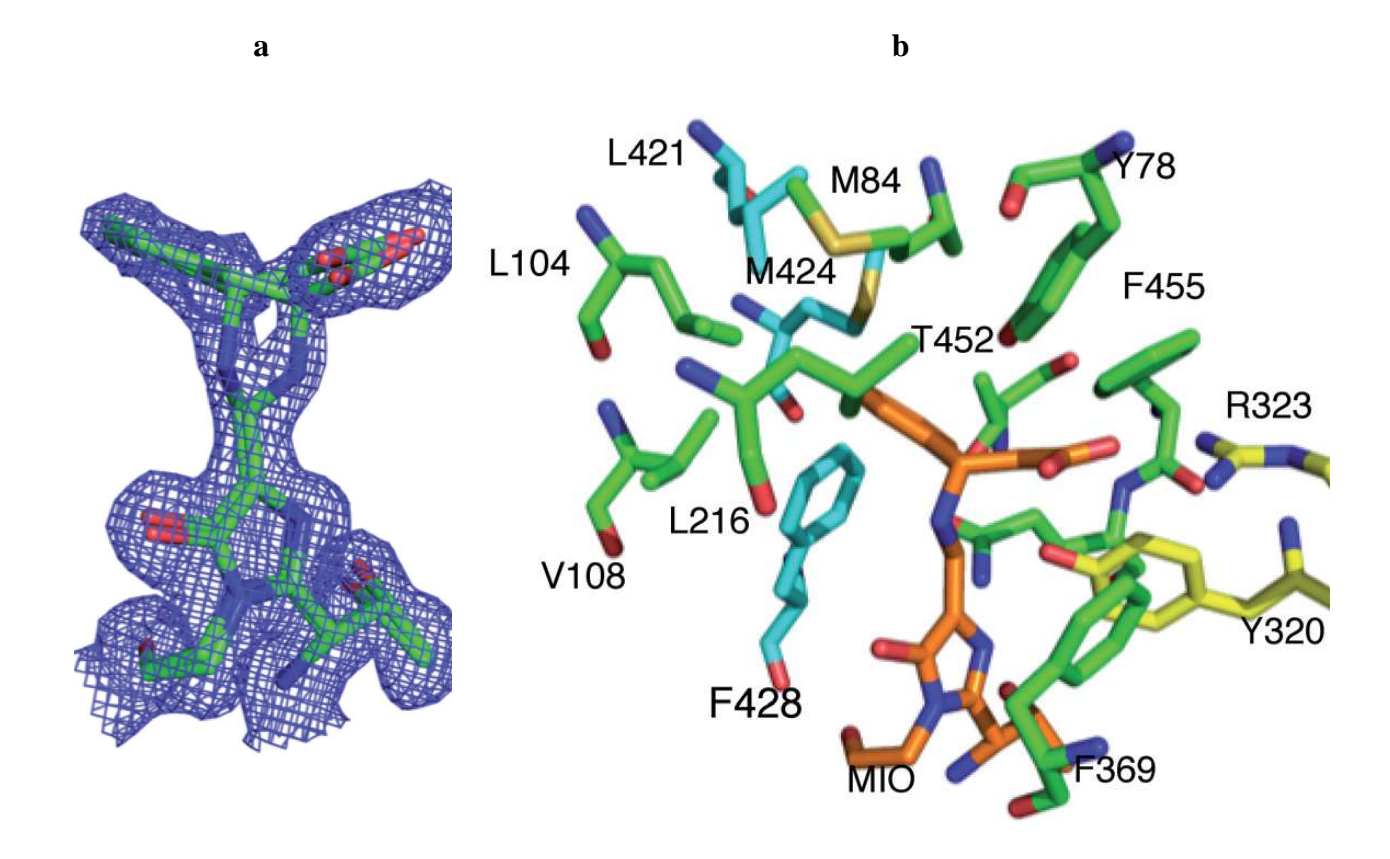


Figure 2.3. a) Electron density $(2F_0-F_c \text{ map}, \text{ blue mesh})$ calculated at 1.0 σ around the α- and β-phenylpropanoid that is covalently bound to the MIO found in monomer "B" (C_α and C_β are indicated). Atoms are color-coded as C (green), O (red), N (blue). b) Active site of *PaPAM* in complex with a MIO-bound (*S*)-β-phenylalanine-type ligand (orange carbon atoms). Active site residues contributed by three monomers are colored accordingly (C: cyan, yellow, or green for each monomer; oxygen: red; nitrogen: blue).

The active sites of the two monomeric structures in the asymmetric unit differ in what is bound to them. In monomer "A", a molecule that is indistinguishable (by electron density) from (R)- β -phenylalanine is found covalently attached by its amino group to the methylidene carbon atom of MIO. This complex is consistent with an enzyme-bound (R)- β -phenylalanine-type

intermediate along the conjugate amino-addition pathway (cf. **Scheme 1.3a**) In contrast, the electron density of monomer "B" suggests partial occupancy of two ligand types. The electron density for a (S)- β -phenylalanine-type complex is evident, as seen in monomer "A". However, electron density shows a structural feature consistent with a (S)- α -phenylalanine molecule covalently attached by its amino group to the methylidene carbon atom of MIO (**Figure 2.3a**). These complexes are, to our knowledge, the first structural identification of naturally occurring pathway intermediates from an unmodified MIO-dependent enzyme, and provide additional evidence that reactions catalyzed by *PaPAM* do not proceed through a Friedel–Crafts pathway, as recently proposed. 60

2.3.5. Distribution of Products in the Catalysis of 2'-Methyl-(S)- α -Phenylalanine by TcPAM and PaPAM

Evidence to support the proposed pathways for the PaPAM and TcPAM reactions was provided by incubating 2'-methyl-(S)-\$\alpha\$-phenylalanine (1 mM) at 31 °C for 1 h separately with each enzyme. The distribution of 2'-methyl-(S)-\$\beta\$-phenylalanine and trans-2'-methylcinnamate made from 2'-methyl-(S)-\$\alpha\$-phenylalanine by PaPAM catalysis was 98:2, while a reciprocal distribution (~1:99) was observed for TcPAM catalysis. Comparison of the kinetic parameters for PaPAM ($k_{cat} = 0.061 \text{ s}^{-1}$, \$\beta\$-amino acid production; $K_{M} = 0.05 \text{ mM}$) and TcPAM ($k_{cat} = 0.002 \text{ s}^{-1}$, cinnamate production; $K_{M} = 0.01 \text{ mM}$) with 2'-methyl-(S)-\$\alpha\$-phenylalanine showed that the catalytic efficiency ($k_{cat}/K_{M} = 1.2 \text{ s}^{-1} \text{ mM}^{-1}$) of PaPAM was 6-fold greater than the efficiency of TcPAM, due largely to the superior k_{cat}

2.3.6. Formation of α- and β-Phenylalanines from Cinnamate and NH₃ by PaPAM

Presumably, the α - and β -phenylalanines were formed by the reaction of a cinnamate ion with the covalent amino-MIO adduct, which was made when the recombinant protein was expressed in E. coli and retained during protein purification. Notably, the Luria-Bertani⁷⁶ media (pH 7.3) that was used to grow the bacteria for this crystallography study was estimated to contain ammonium salts at a concentration of 2.4 mM, as assessed in an earlier study. 76 Therefore, LB media was a practical source of ammonia that could bind to the MIO of PaPAM that was overexpressed in E. coli. To assess whether PaPAM could transfer the amino group to the cinnamate ions that were added to the crystallization buffer, in a manner similar to that of other MIO-dependent enzymes, ⁷⁷ PaPAM (7 mg in 1 mL assay), cinnamic acid (1.25 mM), and ammonia (60 µM) were incubated together for 48 h at 31 °C. Analysis of the products showed that (S)- α -phenylalanine (6.6 \pm 0.9 nmol) and (R)- β -phenylalanine (8.7 \pm 0.9 nmol) were produced. These results indicate that a concentration as low as 60 µM of ammonia in the bulk media was sufficient to aminate the MIO of PaPAM and to catalyze the reverse reaction. Similarly, MIO adducts of either amino^{56 70} or hydroxy⁵⁰ groups of MIO were detected in previous crystallographic studies of enzymes in this class.

2.4. Discussion

Structures have been determined for several members of this lyase class I-like family, including *PpHAL*, ⁵⁰ *RsTAL*, ⁷⁰ PALs from *Anabaena variabilis*, ⁷⁸ *Nostoc punctiforme*, ⁷⁸ *Rhodosporidium toruloides*, ⁵⁶ and *Petroselinum crispum*, ⁷¹ respectively, and *SgTAM* from *Streptomyces globisporus*. ⁶⁹ All have very similar overall folds, contain MIOs imbedded in an

active site of similar overall architecture, and exist as homotetramers. In most structures, two of the subunits significantly contribute active site residues, and a third subunit encapsulates one side of the active site, while in SgTAM, this third subunit contributes a Tyr residue that interacts with the 4'-hydroxy group of the substrate. In recent studies, α - and/or β -tyrosine mimics were covalently trapped in the active sites of SgTAM, 63 and RsTAL, 70 and their structures were determined, demonstrating that the amino group of the substrate attacks the MIO of this aminomutase. The SgTAM structures bound to the substrate or product mimics show that a nucleophile at either C_{α} or C_{β} will attack the MIO moiety. 57 , 63 These results have shed considerable light on the mechanism of the MIO-based catalysts, countering previous work inferring that the MIO couples as an electrophile to the aromatic ring of the substrate to activate catalysis. 79

In earlier studies, the stereochemical evaluation of the ammonia lyase reactions included an assessment of the stereoselectivity, showing universally that the *trans*-isomer of the acrylate product is made exclusively upon elimination of ammonia⁸⁰ and that one prochiral hydrogen at C_{β} is stereospecifically removed from the substrate during the process.^{81,82} S_g TAM and PaPAM of bacterial origin, and TcPAM of plant origin are the only aminomutases in the class I ammonia lyase-like family whose structures are known, and the reaction stereochemistry of the aminomutases have been evaluated. The SgTAM and PaPAM reactions were found to make (S)- β -amino acids; the mode of transfer for SgTAM (inversion or retention of configuration and intra- or intermolecular group transfer) was not evaluated.^{57,69} However, evaluation of the cryptic components of the TcPAM and PaPAM reactions has shown that the amino group and hydrogen are removed from the substrate, their positions exchanged, and then both are reattached

intramolecularly to the original carbon skeleton with retention of configuration in $TcPAM^{66}$ and with inversion of configuration in PaPAM. The results of the mixed substrate assay containing [ring, β -C- 2H_6]-trans-cinnamate and [^{15}N]-(S)- α -phenylalanine indicate that the nitrogen migrates quantitatively from the α - to the β -carbon with negligible exchange to exogenously supplied cinnamate molecules at a concentration (10 mM) likely much higher than physiological levels. TcPAM maintains high fidelity with the natural phenylalanine substrate through tight binding of the substrate and reaction intermediate, at the exclusion of competitive substrates, in order to achieve the observed reaction efficiency.

Despite the wealth of structural data collected on this family of enzymes with overall very similar active site architecture, none sheds any light to explain how the stereochemistry of the TcPAM reaction proceeds with retention of configuration and makes the (3R)-β-phenylalanine isomer, which is opposite to the (3S)-stereochemistry found in the product of the SgTAM and PaPAM reaction. Therefore, a favorable binding conformation of the trans-cinnamate substrate in the TcPAM-cinnamate complex (**Figure 2.1a**) and PaPAM-α/β-amino acid complex (**Figure 2.3a**) were used as basis to understand how these aminomutases control product stereoselectivity. The aminomutase reaction is proposed to be made from an arylalanine via a concerted Hoffmanlike elimination reaction during the reaction cycle. The catalytic base Tyr is situated above the C_{α} - C_{β} bond of the bound phenylalanine substrate (in a staggered conformation), with the pro-(3S) hydrogen closest to Tyr (**Figure 2.3b**); the MIO moiety is positioned below the C_{α} - C_{β} bond of the substrate, with the amino group proximate to the methylidene of the MIO. The formation of the transoid acrylate product supports the stereoselective removal of the pro-(3S) proton by an anti elimination. Furthermore, evaluation of the α - and β -phenylalanine complexes of monomer

"B" (**Figure 2.3a**) suggests that during the course of the amino group isomerization catalyzed by PaPAM, the phenylpropanoid carbon backbone remains mostly stationary above the amino group that is attached to the MIO moiety. These configurations are consistent with the mechanism of stereoselectivity for this enzyme that proceeds with inversion of configuration at each migration terminus. ⁶¹

However, for the production of (R)-β-phenylalanine, the mechanism of catalysis must adhere to an intramolecular amino group transfer, where the amino group does not exchange with that from another substrate molecule. In addition, the stereochemistry must account for the retention of configuration at the migration termini. These data suggest that the amino group and hydrogen displaced from the (2S)- α -phenylalanine substrate must rebind, respectively, at C_{β} and C_{α} of the *trans*-cinnamate before it diffuses from the active site. The constraints of the intramolecularity and stereochemistry of the TcPAM reaction present a challenge because the amino group must attach to the cinnamate on the side facing opposite to that of the NH₂-MIO intermediate (cf. **Figure 2.1a**) to produce the (R)-product. Since this stereochemistry is opposite to the (S)- β -phenylalanine product made by PaPAM, the covalent intermediate derived by reacting PaPAM with a product analog having the configuration at C_{β} as the natural (S)- β -product is not a valid representation of the TcPAM reaction stereochemistry.

The PaPAM active site contains key catalytic residues that are found in other structurally characterized enzymes in the class I lyase-like family (**Figure 2.3b**). Tyr78 (Tyr80 in TcPAM and Tyr63 in SgTAM) is positioned above and within 3.5 Å of both the α - and β -carbon atoms of the phenylalanine complexes, and is poised to de- and re-protonate the intermediate phenylalanine complexes at both the α and β positions. Tyr320 (Tyr322 in TcPAM and Tyr308

in SgTAM) is only 2.6 Å from the amino group of the MIO-bound (S)- α -phenylalanine, and is thought to facilitate proton transfers when the amino group is removed from the (S)- α phenylalanine substrate and added to MIO. In contrast, differences in the residues near the active site of PaPAM are notable when compared with those of other MIO-dependent catalysts (Figure **2.4**). For example, Phe455 (Asn458 in TcPAM) is a glutamine or an asparagine in almost all other enzymes in the family. When the TcPAM-cinnamate structure³⁸ is overlaid onto the PaPAM-phenylalanine structure, the TcPAM-cinnamate ligand clashes with the sterically bulkier Phe455. In the PaPAM structure, however, the covalently-bound α - and β -phenylalanine ligands avoid the steric clash with Phe455 by altering their trajectory through the active site, which avoids the collision ((Figure 1.5a). The new trajectory results in a weaker mono dentate salt bridge with Arg323 (versus the bi dentate salt bridge that is present in TcPAM) and is almost identical to the trajectory of tyrosine in the SgTAM structure. This similar alignment of ligands is reinforced by the superimposition of the bridging atoms (likely nitrogen) of the α - and β phenylpropanoid–MIO adducts in PaPAM and the nitrogen and oxygen atoms, respectively, of the α-difluoro-β-tyrosine and 2,3-dihydroxycoumarate inhibitor–MIO adducts in the two SgTAM structures (**Figure 1.5b**).^{57, 63}

| PaPAM | SNGLPPFLCAE-NAGLRLGLMGGQ F MTASITAESRASCMPMSIQSLS | 450 |
|----------|---|-----|
| *V.bact | $\verb SNGLPAFLCAE-NAGLRLGLMGGQFMTASITAESRASCMPMSIQSLS $ | 450 |
| *S.marit | ${\tt SNGLPAFLCRE-DPGLRLGLMGGQ} \textbf{\textit{F}} {\tt MTASITAETRTLTIPMSVQSLT}$ | 426 |
| *B.subtl | ${\tt SNGLPAFLTKE-NPGLRLGLMGGQ} \textbf{\textit{F}} {\tt MSTSLTAENRSLCTPLSIQTLT}$ | 432 |
| *K.pneu | ${\tt SNGLPSFLCAE-NGGLRFGLMGGQ\textbf{\textit{F}}MSSSVTAENRSLATPVSIQTLT}$ | 438 |
| *B.rhiz | ${\tt SNGLPPFLCAN-EQGIRLGLMGGQ} \textbf{\textit{F}} {\tt MSASLASENRSLCVPVSIHSLP}$ | 429 |
| SgTAM | SYGLPEFLVSG-DPGLHSGFAGAQYPATALVAENRTIG-PASTQSVP | 438 |
| AvPAL | ${\tt SNGLPPSLLGNRERKVNMGLKGLQICGNSIMPLLTFYGNSIADRFPT}$ | 445 |
| TCPAM | SNGLPGNLSLGPDLSVDYGLKGLDIAMAAYSSELQYLANPVTTHVHS | 453 |

Figure 2.4. CLUSTAL 2.1 multiple sequence alignment ³⁸ of representative class I lyase-like PAL, PAM and TAM enzymes whose structures are known and five sequences highly homologous to *PaPAM* that were found in the GenBank database by BLAST search: *PaPAM*, PAM from *Pantoea agglomerans*; *V.bact*, possible PAM from *Vibrionales bacterium SWAT-3*; *S.marit*, PAL/PAM EncP from *Streptomyces maritimus*; *B.subtl*, possible PAM from *Bacillus Subtlis*; *K.pneu*, possible PAM from *Klebsiella pneumoniae 342*; *B.rhiz*, possible PAM from *Burkholderia rhizoxinica*; *Sg*TAM, TAM from *Streptomyces globisporus*; *Av*PAL Phenylalanine ammonia lyase ³⁹ from *Anabaena variabilis*; *Tc*PAM, PAM from *Taxus Canadensis*. Enzymes that have a concerved phenylalanine residue inside the active which correspond to F455 residue in *Pa*PAM, produce (*S*)-β-phenylalanine (designated with asterisk (*)).

SgTAM, however, contains a nonconserved His93 (Val108 in PaPAM) that forms a hydrogen bond with the hydroxy group of the tyrosine substrate. ⁵⁴ This hydrogen-bonding interaction, which is absent in PaPAM, enforces the trajectory of tyrosine in the SgTAM active site. Thus, SgTAM and PaPAM catalyze equivalent stereochemistries, presumably by orienting their

substrates identically in their active sites, but use a distinct set of enzyme–substrate interactions to accomplish this. PaPAM mutants F455A and F455N (F455N is analogous to N458 of TcPAM) each form the same products, but at approximately 2% of the rate of PaPAM, in a 40:60 ratio, where trans-cinnamate prevails. These data are consistent with the hypothesis that Phe455 is important for the proper trajectory of the substrate in the active site for transfer of the amino group from the α to the β position. 64

Intrigued by the possibility that other class I lyase-like enzymes that catalyze the formation of the same (S)- β -phenylalanine produced by PaPAM may exist, a BLAST⁸⁵ search was performed, and five other MIO-dependent enzymes, each from a distinct organism, were found to have a Phe residue that is equivalent to Phe 455 (**Figure 2.4**). In each case, all of the other residues in the vicinity of the active site were also identical to those of PaPAM. Of these enzymes, EncP from $Streptomyces\ maritimus$, was characterized as a slow phenylalanine ammonia lyase (k_{cat} =0.0061 s⁻¹) that is required for the biosynthesis of the antibiotic enterocin in this organism. ⁷⁸ ⁸⁶ ⁸⁷ Subsequent studies, however, showed that this enzyme has much higher phenylalanine aminomutase activity (with (S)- β -phenylalanine as the product) than lyase activity below 50 °C. ⁸⁸ Furthermore, another organism ($Vibrionales\ bacterium\ SWAT-3$) identified by the BLAST search produces andrimid, which contains an amino acid moiety that is derived from (S)- β -phenylalanine. ⁸⁹

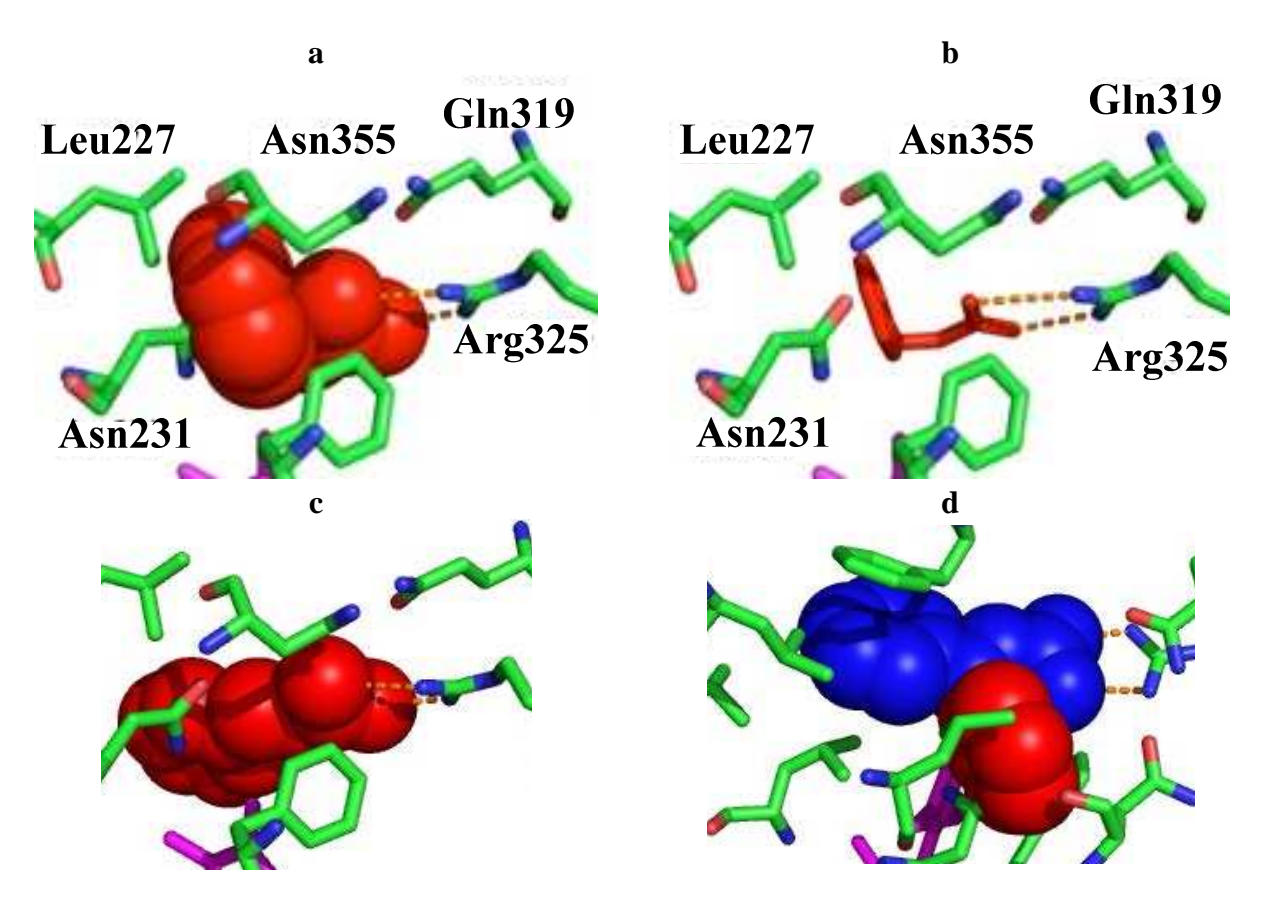


Figure 2.5. Cinnamate diastereoisomers modeled into *Tc*PAM. a) A space-filled rendering and b) a skeletal structure of *cis*-cinnamate are modeled into *Tc*PAM by preserving the tight salt bridge with Arg325. The phenyl ring of the cinnamate is oriented toward the interior of the active site pocket. The collision distances between active site residues and the phenyl ring of the cisoid diastereoisomer are given: Asn231 - 0.8 Å, Leu227 - 2.7 Å, Phe371 - 2.7 Å, Asn355 (main chain) - 2.7 Å. c) A space-filled rendering of *trans*-cinnamate is modeled into *Tc*PAM by orienting the carboxylate toward the salt bridge with Arg325; occlusions by active site residues on the transoid structure are absent. d) Shown is an overlay of the space-filled structures of (*cis*)-and *trans*-cinnamates modeled in the *Tc*PAM active site with the Arg325 salt bridge preserved.

The trajectory of the (S)- α -amino acid in the active site of TcPAM is determined by the direction of the carboxylate group when it forms a salt bridge with the δ -guanidinium group of a proximate Arg325, as in the TcPAM-cinnamate complex and all other bound structures of enzymes from the lyase-like family. 50° 56° 69°71° 78 In previous investigations, assessing the stereochemical course of the TcPAM reaction in the absence of structural data, it was suggested that the differences in the stereochemistry of the TcPAM reaction compared to that of the PaPAM reaction resulted from fundamental differences in the active sites of these isomerases. The substrate was hypothesized to bind the TcPAM active site with the carboxylate and phenyl ring in a syn-periplanar trajectory to position the migrating H and NH₂ groups of the (S)phenylalanine on the same side of the molecule to account for the retention of configuration at the reaction termini. 66 Shown herein, however, the active site of TcPAM is arranged similar to the other MIO-dependent enzymes, where the catalytic base and MIO (amino group acceptor) are antipodal with respect to the substrate; thus, the migration of the H and NH2 groups must also occur on opposite sides. Consequently, a syn-periplanar trajectory or cis-cinnamate configuration of a reactive intermediate would confound the observed retention of stereochemical configuration of the TcPAM reaction. More importantly, a cisoid phenylpropanoid (either as Scis-phenylalanine or cis-cinnamate) in a modeled complex with TcPAM would be sterically occluded by several active site residues (Figure 2.5). Further, electron density consistent with a trans-cinnamate is clearly observed in the TcPAM structure and provides good evidence that the reaction proceeds via a transoid intermediate.³⁸

2.4.1. Stereoselectivity of the Aminomutase Reaction

In the PaPAM and SgTAM reactions, the amino group can migrate from C_{α} to C_{β} across the same face (Si face) of the arylacrylic acid intermediate to isomerize (S)- α - to (S)- β -arylalanine (Scheme 2.1). In contrast, for the TcPAM reaction, and possibly for the CcTAM reaction the C_{α} amino group must be removed from the Si-face (using C_{β} of the arylacrylic acid intermediate as reference), then reattach at C_B on the Re face. A possible explanation involves approximately 180° rotations of the already-bound arylacrylate intermediate about both the C_1 – C_{α} and C_{β} – C_{ipso} bonds prior to rebound of the amino group to C_B by the NH₂-MIO, without breaking the salt bridge to Arg-325, and with minor displacement of the aromatic ring from its original position (Scheme 2.1). This rotamer positions C_{β} for nucleophilic attack by the NH₂-MIO moiety to form the enzyme/product covalent intermediate. Catalytic Tyr residue is in position on the opposite side to reprotonate the phenylpropanoid at C_{α} , resulting in overall retention of configuration in the product. The nitrogen linking the MIO to the product is likely protonated by Tyr-322 that initiates the departure of the product from the MIO. Concomitant rotation about the C_1 - C_α and C_{eta} - C_{ipso} bonds does not result in any steric clashes in the active site, nor in breaking direct interactions between enzyme and substrate. The foregoing proposed mechanism is consistent with all of the stereochemical and mechanistic findings for TcPAM. In addition, the $K_{eq} = 1$ for TcPAMreaction⁶⁶ suggests that the rotamers energetically equivalent. the are

Scheme 2.1: The Proposed Mechanism of the Aminomutase Catalysis. Tyr is the Presumed Catalytic Base, Situated "Above" the Intermediate, and the NH₂-MIO Complex is Shown "Below" the Intermediate. In SgTAM and PaPAM, After the Initial E₂-Type Elimination to Form the Intermediate, the Amino Group is Rebound at the C_{β} Position from the Si Face (Same Face), of the Intermediate while in CcTAM and TcPAM, the Intermediate Under Go 180° Rotation About the C_1-C_{α} and $C_{\beta}-C_{ipso}$ Bonds in order for the Amino Group to Attack at the C_{β} Position from the Re Face (Opposite Face) of the Intermediate.

To further confirm the above phenomena the product distribution of the catalysis of 2'methyl-(S)- α -phenylalanine by TcPAM and PaPAM was analyzed. The 2'-methyl substituent at ortho position of the cinnamic acid likely affected the rotation of the intermediate to access Re face, and thus only trans-2'-methylcinnamate was made by TcPAM. In contrast, PaPAM presumably utilized a single 2'-methylcinnamate rotamer (Si face) to make 2'-methyl-(S)-αphenylalanine without encountering the torsional barrier⁶¹. The difference in product distribution between the two enzymes supports a model consistent with steric and torsional strain between the 2'-methyl substituent and the C_q -hydrogen of the intermediary trans-2'-methylcinnamate in the TcPAM reaction. Notably, alternative or additive steric interactions between the 2'-methyl substrate and active-site residues can also prevent interchange between si and re face and abort the TcPAM reaction (Scheme 2.1). Conversely, it can be imagined that the single rotamer si face on the PaPAM pathway need not encounter the same active-site interactions to proceed from 2'methyl-(S)- α - to 2'-methyl-(S)- β -phenylalanine. The underlying mechanism responsible for the proposed rotational dynamics of PaPAM and TcPAM is not fully understood and is intriguing since the positions of most of the catalytic amino acids, the presumed H-bonding residues, and van der Waals interactions in each active site are conserved.

2.4.2. Effects of L104A Point Mutation on Enzymatic Activity of TcPAM

In this study, the effect of a targeted point mutation on substrate selectivity and enzymatic reactivity were investigated for the *Taxus* phenylalanine aminomutase. The structure of *Tc*PAM revealed that Leu-104 makes a direct hydrophobic interaction with the aromatic ring (nearest the 3'-carbon) of the presumed reaction intermediate cinnamate. Mutation of this Leu-104 to a sterically smaller alanine residue was proposed to increase the active site volume, reduce a steric

interaction between the substrate and the active site, and thus increase the catalytic efficiency of the catalyst for arylalanine substrates bearing a substituent on the 3'-carbon of the ring. For proof of principle, sterically demanding substrates 3'-methyl-(S)- α -phenyl-, 4'-methyl-(S)- α -phenyl-, and styryl-(S)- α -alanine were chosen to evaluate the effects of the L104A mutation in TcPAM (PAMeLA_104).

In a previous investigation, TcPAM was found to generally isomerize α -arylalanines to their corresponding β -arylalanines; however, the catalytic efficiency of TcPAM decreased markedly with increasing steric bulk on the α -amino acid substrate.³⁹ Thus, the steric hindrance of the active site seemingly limited its catalytic efficiency. Kinetic parameters of the PAMeLA_104 enzyme with non-natural aryl amino acids were compared to the TcPAM catalyst, demonstrating that Leu-104 has significant influence on substrate binding (approximated by $K_{\rm M}$), product distribution, and k_{cat} Notably, the K_{M} of PAMeLA_104 increases over 2-fold with the phenylalanine substrate (1) compared to the $K_{\rm M}$ of ${\it Tc}{\rm PAM}$, suggesting that Arg-325 and Leu-104 participate in substrate docking via a salt bridge and hydrophobic interaction, respectively. PAMeLA_104 released total product ((R)- β -phenylalanine and trans-cinnamate) at a rate (k_{cat} = $0.076~\mathrm{s^{-1}})$ comparable to that of $Tc\mathrm{PAM}$ ($k_{\mathrm{cat}} = 0.065~\mathrm{s^{-1}}$) but produced (~ 6-fold) more cinnamate than β-phenylalanine (cf. Table 2.1). Likely, an accessible trajectory of phenylalanine in the mutant causes the reaction to stall after the first reaction step and release the acrylate product. Apparently, this trajectory is not achievable in TcPAM, which preferentially makes βphenylalanine. In contrast, the $K_{\rm M}$ of PAMeLA_104 was nearly 5-fold lower with 3'-methyl-(S)- α -phenylalanine (2) compared to the K_{M} of Tc PAM, suggesting that the 3'-methyl substituent of the substrate enhanced substrate binding in the mutant. While the Leu-Ala exchange likely

reduced unfavorable steric strain (cf **Figure 2.2a**), the smaller alanine residue, however, could still make a constructive hydrophobic interaction with the 3'-methyl group of **2** (cf. **Figure 2.2b**). Remarkably, the catalytic efficiency of PAMeLA_104 for **2** increased \sim 7-fold compared to TcPAM catalysis, which is primarily a reflection of the considerable (5-fold) reduction in $K_{\rm M}$ (i.e., better binding) of PAMeLA_104 compared to that of TcPAM.

While TcPAM and PAMeLA_104 displayed dramatic differences in their kinetic parameters with α -phenylalanine and 3'-methyl-(S)- α -phenylalanine, they did not display significant differences with 4'-methyl- α -phenylalanine (3). The K_{M} of Tc PAM with substrate 3 was 1.6-fold higher than that for TcPAM with its natural substrate 1, suggesting that the 4'-methyl group of the substrate only modestly affected binding. Interestingly, the $K_{\rm M}$ of PAMeLA_104 for 3 was slightly lower than that of TcPAM, suggesting that the Leu \rightarrow Ala replacement likely enabled the 4'-methylphenyl functional group to adopt a suitable conformation to interact favorably with other distal hydrophobic residues (Leu-179, Leu-227, and Val-230) of the active site pocket (cf. Figure 2.2d). Moreover, the structural data for TcPAM shows no active site residues proximate to the 4'-carbon of the natural substrate that would interfere sterically with a 4'-alkyl substituent of 3. TcPAM converted styryl- α -alanine (4) almost exclusively to (2E,4E)-styrylacrylate, while PAMeLA_104 made the corresponding β-amino acid from 4, albeit slowly, at about 3% of the styrylacrylate production rate at 0.12 s⁻¹. The wild-type and mutant enzymes made the styrylacrylate product from 4 faster than they were able to convert any of the other aryl amino acid substrates to their corresponding β -amino acids and acrylate products combined (cf. **Table** 2.1). These data suggest that the ammonia lyase function of both enzymes remains largely efficient with 4. The stability of the conjugated π -bonds and the larger steric volume of the product, likely affected the rapid release of the intermediate, reducing the residence time needed

to isomerize the α - to β -amino acid. PAMeLA_104 noticeably made more styryl-(R)- β -alanine than does TcPAM under steady-state conditions, indicating that the mutation likely increased the residence time of the substrate and ensuing intermediate in the active site. The 2-fold lower $K_{\rm M}$ of PAMeLA_104 compared to that of TcPAM for substrate 4 demonstrates that the mutant can accommodate 4 better. (cf. **Figure 2.2c**). Clearly, the hydrophobic region of the TcPAM active site surrounding the aromatic ring of the purported reaction intermediate (cinnamate) plays a major, but mechanistically unknown, role in substrate selectivity and in governing the distribution of the intermediate acrylic acid that is released and is converted to the β -amino acid.

2.5. Conclusion

The structure of PaPAM was solved as α - and β -phenylpropanoid adducts, presumably with (S)- α - and (S)- β -phenylalanine. These intermediates provide strong evidence that PaPAM reacts by an alkylamine elimination pathway (such as a Hoffmann-type or E2-type elimination process), which involves covalent attachment between the amino group of the substrate and the product as well as the MIO cofactor, as demonstrated previously for SgTAM. The results indicate that the carbon skeleton of the (S)-phenylalanine substrate remains in one rotameric conformation (Si face) while the exocyclic C-N bond of the NH₂-MIO adduct rotates into position below the α - and β -carbon atoms to complete the isomerization reaction (**Figure 2.3a**). Thus, the structure also confirms the inversion of configuration at each migration terminus during the isomerization of the α -amino acid substrate into its β -isomer. The structure of the phenylalanine aminomutase on the Taxol biosynthetic pathway has been presented. The TcPAM active site was observed to be arranged similar to that of other members of the MIO-dependent family of enzymes. The (S)-product stereochemistry catalyzed by the bacterial

SgTAM and $PaPAM^4$ 6 is opposite to the (R)-product stereochemistry catalyzed by TcPAM of plant origin and CcTAM of bacterial origin. Conceptually, the stereochemistry of the TcPAM and CcTAM reaction can be achieved by rotation of the intermediate cinnamate in the active site by approximately 180° about the C_1 – C_0 / C_{ipso} – C_β bonds prior to rebinding of the amino group at the β -position on the trans-cinnamate intermediate. Comparing the active sites of TcPAM, PaPAM and SgTAM showed subtle structural differences that may account for the significant changes in the trajectory of the substrate, possibly causing stereodifferentiation.

On the basis of the TcPAM crystal structure complex, the PAMeLA_104 mutant was constructed and demonstrated superior catalytic efficiencies for substrates 3'-methyl-(S)- α -phenylalanine and styryl- α -alanine possessing larger molecular steric volume. The L104A mutation likely reduced unfavorable steric clash that conceivably created an altered alignment of the substrate and/or the ensuing acrylate intermediate within the active site that changed the kinetic parameters of PAMeLA_104 compared to the wild-type TcPAM.

3. (S)-α-STYRYLALANINE USED TO PROBE THE INTERMOLECULAR MECHANISM OF AN INTRAMOLECULAR MIO-AMINOMUTASE

Reproduced with permission from [Wanninayake, U.; DePorre, Y.; Ondari, M.; Walker, K. D., (S)-Styryl-a-alanine used to probe the intermolecular mechanism of an intramolecular MIO-aminomutase. *Biochemistry* **2011**, 50, (46), 10082-10090] Copyright © 2011 American Chemical Society

3.1. Introduction

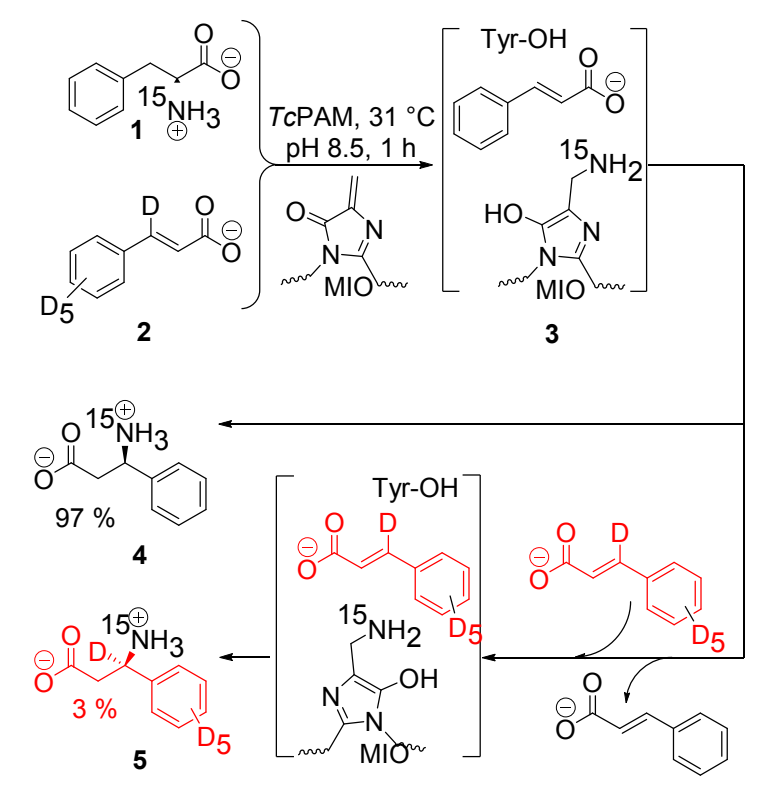
A *Taxus canadensis* phenylalanine aminomutase (TcPAM) requires no cofactors to intramolecularly transfer the amino group of (S)- α -phenylalanine to form (R)- β -phenylalanine, utilizing the same carbon skeleton. This aminomutase activates the amino group of the substrate as an alkylammonium leaving group via ligation with a 3,5-dihydro-5-methylidene-4H-imidazol-4-one (MIO) prosthetic group, formed by autocatalytic post-translational condensation of active site residues (Ala-Ser-Gly). This MIO purportedly serves as an electrophilic sink (a 1,4-Michael acceptor) and is nucleophilically attacked by the amino group of the substrate to form the alkylammonium complex to facilitate Hofmann-like elimination. He pro-3pro-3pro4 hydrogen and an alkylamine are transiently eliminated to form a cinnamate intermediate and then rebound to interchanged positions on the phenylpropenoid skeleton. Under steady-state reaction conditions, pro4 Catalyzes the production of a significant proportion of (pro6-phenylalanine compared to pro6 times slower.

A recent study showed that when TcPAM was co-incubated with both [^{15}N]-(S)- α -phenylalanine (1) and [ring,3- $^{2}H_{6}$]-trans-cinnamate (2) (each at 10 mM), the [^{15}N]-amino group incorporated (97%) intramolecularly into (R)- β -phenylalanine. However, slight intermolecular amino group transfer occurred, as well. Analysis of the isolated β -phenylalanine revealed a crossover reaction, in which the amino group of 1 was incorporated partially into precursor 2 to form [^{15}N , $^{2}H_{6}$]- β -phenylalanine (5) in ~ 3% yield (Scheme 3.1). 38 Thus, the unlabeled cinnamate intermediate 3 derived from [^{15}N]- α -phenylalanine did not appreciably dissociate from the active site or exchange with exogenous ^{2}H -labeled cinnamate (only a 3% occurrence), before the amino group of the $^{15}NH_{2}$ -MIO complex rebounded. A few labeled cinnamate molecules did, however, competitively bind the active site, accounting for the dearth of doubly labeled β -amino acid product observed.

The foregoing intermolecular data are supported by an earlier study demonstrating that a tyrosine aminomutase (TAM) transferred the amino group from 3'-chlorotyrosine to 4-hydroxycinnamate to form 3'-chloro-4'-hydroxycinnamate and a mixture of α - and - β -tyrosine. The results of the latter intermolecular process were paradoxically used to explain that the TAM reaction proceeds intramolecularly. This argument was further thought to be supported by the faster transfer of the amino group in the cross reaction compared to the rate when exogenous NH₄⁺ was used as the amino group source. Notably, the high molar concentrations of ammonia used in the catalysis of the reverse reaction likely approached conditions typically used to precipitate and denature proteins, ⁹² and thus affected the catalytic efficiency of the ammonia transfer reaction. In this earlier study, it also remained unclear whether the amino group removed

from α -tyrosine was then transferred intramolecularly to the same 4'-hydroxycinnamate reaction intermediate en route to β -tyrosine, on the natural reaction pathway.⁶²

Scheme 3.1: Mechanism of the Transaminase Reaction Catalyzed by *Tc*PAM with Its Natural Substrate (Exogenously supplied cinnamate is color coded in red)



2 exchanges with 3 in TcPAM active site

Moreover, a homologous phenylalanine aminomutase (PAM) isolated from *Taxus chinensis*, in an earlier study, was incubated with an exogenous supply of 6 M NH_4^+ salts (pH 10) to provide ammonia to the reaction. The ensuing NH_2 –MIO complex (or other amine complex) likely formed, and the hydrogen and amino group (from the MIO complex) were transferred to various *trans*-arylacrylates to form a mixture of the corresponding enantiopure α - and β -amino

acids in the reverse reaction. 40,93 This latter study was identical in technique to another earlier work demonstrating that mechanistically similar MIO-dependent enzymes also catalyzed their reverse reactions. This earlier compendium of work includes a description of how a phenylalanine ammonia lyase added a hydrogen/amino group pair from 6 M NH₄⁺ salts (pH 10) to trans-arylacrylates to produce non-natural (S)- α -amino acids, ⁹⁴ while a tyrosine aminomutase analogously added the same pair from NH_4^+ salts to 4-hydroxycinnamate to form a mixture of α and β -tyrosine. ⁶² Furthermore, while TcPAM converts (S)- α -phenylalanine principally to (R)- β phenylalanine at a rate of $0.053 \pm 0.001 \text{ s}^{-1}$, it also converts (S)-styryl- α -alanine to (2E,4E)styrylacrylate as the major product (99%) at approximately the same rate (0.082 \pm 0.002 s^{-1}). 38 Consequently, the styrylacrylate is released from the active site before the amino group can rebound appreciably to form styryl-β-alanine. These kinetic data along with the proposed MIOdependent mechanism suggest that when (S)-styryl- α -alanine is converted to (2E,4E)styrylacrylate, the transient amino group remains as the $\mathrm{NH}_2 ext{-}\mathrm{MIO}$ complex, likely for the same duration as the α - β -phenylalanine isomerization reaction.

A hypothesis emerged from the aforementioned intra- and intermolecular mechanistic evaluations³⁸ and observations.⁴⁰ ⁶² ⁹⁴ Conceptually, a weakly binding acrylate (AC1) intermediate derived from an amino acid (AA1) in the TcPAM reaction was replaced in the active site with a tighter binding, competitive acrylate (AC2). The amino group removed from AA1, but now in complex with the enzyme, could rebind to AC2 and form α - and β -amino acids (AA2) different from those derived from AA1. Thus, guided by the partial intermolecular process observed for $TcPAM^{38}$ and by the details of the kinetic parameters described herein, we explored four non-natural amino acids as amino group donor substrates. The amino group of

these donor substrates was transferred intermolecularly to another arylacrylate skeleton by TcPAM catalysis to form an α - and β -arylalanine mixture.

3.2. Experimental

3.2.1. Chemicals

(R)-β-Phenylalanine, 3'-methyl-(S)-α-, 3'-methyl-(R)-β-, 4'-methyl-(S)-α-, 4'-methyl-(R)-β-, 4'-fluoro-(S)-α-, 4'-fluoro-(R)-β-, and 3'-fluoro-(R)-β-phenylalanine and (S)-styryl-α-, (S)-2'-thienyl-α-, (R)-2'-thienyl-β-, and (S)-2'-furyl-α-alanine were purchased from Peptech Inc. (Burlington, MA). (1'S)-Camphanoyl chloride, (S)-α-phenylalanine, (S)-2-aminotetralin-2-carboxylic acid, (3R)-3-aminotetralin-(2R)-2-carboxylic acid, (3R)-3-aminotetralin-(3R)-3-aminotetralin-(3R)-3-aminotetralin-(3R)-3-aminotetralin-(3R)-3-aminotetralin-(3R)-3-aminotetralin-(3R)-3-aminotetralin-(3R)-3-aminotetralin-(3R)-3-aminotetralin-(3R)-3-aminotetralin-(3R)-3-aminotetralin-(3R)-3-aminotetralin-(3R)-3-aminotetralin-(3R)-3-aminotetralin-(3R)-3-aminotetralin-(3R)-3-aminotetralin-(3R)-3-aminotetralin-(3R)-3-aminot

3.2.2. Instrumentation

The GC oven (Agilent, model 6890N) conditions were as follows. The column temperature was programmed from 70 to 250 °C at a rate of 10 °C/min (18 min total run time); splitless injection was selected, and helium was used as the carrier gas (1.2 mL/min). The GC oven was coupled to a mass selective detector (Agilent, model 5973 *inert*) in ion scan mode from 100 to 300 atomic mass units at a 70 eV ionization voltage.

3.2.3. Expression of the tcpam and Purification of TcPAM

Codon-optimized *tcpam* cDNA was previously ligated into expression vector pET28a(+), and the recombinant plasmid encoded an N-terminal His₆ tag.⁷⁴ The *tcpam* clone was overexpressed in six 1 L cultures of *Escherichia coli* BL21(DE3) cells by induction with isopropyl β-D-thiogalactopyranoside. The overproduced protein was isolated from the bacteria and purified to 95% by Ni affinity chromatography to yield 5 mg of protein, as described previously.⁷⁴ Routine assays for assessing enzyme function were conducted with (*S*)-α-phenylalanine at saturation (1 mM) and *Tc*PAM (100 μg, 1.3 nmol) in 50 mM phosphate buffer (pH 8.5) in 1 mL assays.

3.2.4. Identification of an Amine Donor Substrate

(*S*)-Styryl-α-alanine (**6**), 2'-furyl-(*S*)-α-alanine (**15**), (3*R*)-aminotetralin-(2*R*)-carboxylic acid (**16**), and (*S*)-2-aminotetralin-2-carboxylic acid (**17**) (each at 1 mM) were incubated separately with TcPAM (250 μg, 3.3 nmol) and 3'-methylcinnamate (**14**) (1 mM) in 5 mL assays at 31 °C. To calculate the initial steady-state rates, aliquots (1 mL) were withdrawn at 10, 20, 30, and 40 min from the reaction mixture containing **6**, at 15, 30, 45, and 60 min from the reaction mixture containing **15**, and at 1, 2, 3, and 4 h from the reaction mixture containing **16** or **17**. An internal standard (*R*)-3'-fluoro-β-phenylalanine (20 nmol) was added; the reactions were quenched by increasing the pH to 10 (6 N NaOH), and the amino acids were immediately *N*-carbonylated by adding ethyl chloroformate (100 μL). After 10 min, the reaction mixtures were acidified to pH 2 (6 N HCl), the derivatives were extracted with diethyl ether (2 × 1 mL), and the solvent was removed in vacuo. To the remaining residue was added a (trimethylsilyl) diazomethane solution dissolved in an ethyl acetate/methanol mixture (3:1, v/v) (methanol was used to liberate the

diazomethane), until the yellow color of diazomethane persisted, to convert the *N*-acyl amino acids to their methyl esters.

3.2.5. Assessing the Optimal Concentration of Amino Group Donor 6

After compound **6** had been identified as an amino group donor, **6** was incubated at 400, 600, 800, 1000, 2000, and 3000 μ M in the presence of TcPAM (50 μ g, 0.7 nmol) in 1 mL reaction mixtures for 30 min at 31 °C. An aliquot (1 mL) was withdrawn from the reaction mixture and added to a 1.5 mL polystyrene cuvette (General Laboratory Supply, Pasadena, TX) and analyzed by UV–visible spectroscopy (Beckmann DU 640, Beckmann Coulter, Brea, CA) with A_{305} monitoring of the sample to quantify the product (2E,4E)-styrylacrylate (**7**). The absorbance values obtained from the samples were compared against those of a concentration series (ranging from 0.3 to 80 μ M) made from authentic (2E,4E)-styrylacrylate dissolved in 50 mM phosphate buffer (pH 8.5), analyzed by the same method. A sample blank of **6** (λ_{max} = 275 nm; A_{305} = 0.007 at 0.1 mM) was used to subtract the background absorbance. A nonlinear regression plot of the steady-state production rate of **7** versus the concentration of **6** was used to calculate the maximal steady-state velocity (V_{max}) and to assess which concentrations of **6** were at V_{max} .

3.2.6. Calculation of the Inhibition Constants of Various Acrylates in the TcPAM Reaction

Kinetic parameters and inhibition constants for various substrates and inhibitors in the TcPAM reaction were acquired by first establishing the linearity of enzyme activity with respect to both time and protein concentration for the substrate without inhibitor. (2E,4E)-Styrylacrylate (at 50, 100, and 200 μM) (inhibitor) was incubated with TcPAM (30 μg, 0.4 nmol) containing 4′-methyl-(S)-α-phenylalanine as the substrate at 10, 20, 40, 80, 150, 300, 500, 750, and 1000 μM

(in separate dilution series) in 50 mM phosphate buffer (pH 8.5, 1 mL) for 30 min. To each reaction mixture were added 3'-fluoro-(R)-β-phenylalanine and trans-2'-methylcinnamic acid (at final concentrations of 20 µM) as internal standards at 0 °C. The reaction mixtures were basified to pH 10 (6 N NaOH). Ethyl chloroformate (100 µL) was added. After 5 min, the pH of the samples was readjusted to 10. A second batch of ethyl chloroformate (100 µL) was added, and the solution was mixed for 5 min. The samples were acidified to pH 2 (6 N HCl), and the arylacrylic acids and N-(ethoxycarbonyl) amino acids were extracted into diethyl ether (2×1) mL). The organic fractions were combined, and the solvent was removed in vacuo. To the remaining residue was added a (trimethylsilyl) diazomethane solution dissolved in an ethyl acetate/methanol mixture until the yellow color of diazomethane persisted to produce the methyl esters of the N-(ethoxycarbonyl) amino acids and arylacrylates. The derivatized samples were quantified by GC/EIMS, wherein the relative abundances of the base peak fragment ions of the amino acid derivatives present in the samples were compared to those of authentic standards at various concentrations. From the Lineweaver-Burk plots of the data, the Michaelis-Menten constants, inhibition constants, and rates were calculated.

trans-Cinnamate (3), trans-4'-chloro-, trans-4'-methyl-, trans-4'-fluoro-, and trans-3'-methyl-cinnamate (9–11 and 14, respectively), and trans-2'-thienylacrylate (13) (each at 50, 100, 150, 300, 500, 1000, and 2000 μM in separate dilution series) were incubated with *Tc*PAM (50 μg, 0.7 nmol) containing 6 (1 mM) as a cosubstrate in 50 mM phosphate buffer (pH 8.5, 1 mL) for 30 min. The reaction mixtures in each series were placed on ice and acidified to pH 2 (6 N HCl); trans-2'-methylcinnamic acid (at a final concentration of 20 μM) was added to each as an internal standard, and the carboxylic acids were extracted into diethyl ether (2 × 1 mL). The organic fractions were combined, and the solvent was removed in vacuo. To the remaining

residue was added a (trimethylsilyl) diazomethane solution dissolved in an ethyl acetate/methanol mixture until the yellow color of diazomethane persisted to produce the methyl esters of the acrylate. The derivatized samples were quantified by GC/EIMS, wherein the relative abundances of the base peak fragment ions of methyl styrylacrylate in the samples were compared to those of an authentic standard (see Appendix) at various concentrations. From the Lineweaver–Burk plots of these data, the Michaelis–Menten constants and rates were calculated.

3.2.7. Time Course Assays for Intermolecular Amino Group Transfer

TcPAM (300 μg, 3.9 nmol) was incubated separately with various acrylates at 50, 100, 150, 300, 500, 1000, and 2000 μM and 6 (1 mM) in 6 mL assays in 50 mM phosphate buffer (pH 8.5). Aliquots (1 mL) were withdrawn from each reaction mixture at 0.5 h intervals over 1 h, and then at 2, 4, 8, and 12 h. Internal standards *trans*-2′-methylcinnamic acid and 3′-fluoro-(R)-β-phenylalanine (each at 20 μM) were added to each aliquot, and the reactions were quenched by increasing the pH to 10 (6 N NaOH). The amino acids and acrylates were derivatized, as described earlier, and quantified by GC/EIMS.

3.2.8. Assessing the Absolute Stereochemistry of α - and β -Phenylalanine Product (8f) by the TcPAM Transaminase Pathway

trans-4'-Fluorocinnamate (500 μM) was incubated with TcPAM (200 μg, 2.6 nmol) and 6 (1 mM) in 1 mL assays in 50 mM phosphate buffer (pH 8.5) at 31 °C. After 3 h, the amino acids were derivatized to their N-[(1'S)-camphanoyl] methyl esters. The derivatized α - and β -amino acids were identified by GC/EIMS analysis and compared against the retention time and mass spectrometry fragmentation of authentic N-[(1'S)-camphanoyl]-4'-fluoro-(2S)- α - and -4'-fluoro-(3R)- β -phenylalanine methyl esters (Figure A 4 & Figure A 5 in Appendix).

3.2.9. Assessing the Effects of Maintaining the Steady-State Conversion of 6 to 7 on the Production of 8f

To a solution of **6** (31 µmol) in 50 mM phosphate buffer (pH 8.5, 30 mL) were added *trans*-3'-methylcinnamic acid (**14**) (31 µmol) and TcPAM (1.5 mg, 20 nmol) at 31 °C. The reaction mixture was shaken slowly in a water bath. An aliquot (20 µL) was withdrawn from the reaction flask every hour and diluted to 200 µL in 50 mM phosphate buffer. The entire sample was added to a 450 µL cuvette (Quartz, Hellma GmbH & Co. KG, Müllheim, Germany) and analyzed by UV–visible spectroscopy (Beckmann DU 640, Beckmann Coulter) with A_{305} monitoring of the sample to quantify the product (2E,4E)-styrylacrylate (**7**) by comparison against a concentration series (ranging from 1 to 100 µM) made from authentic (2E,4E)-styrylacrylate dissolved in 50 mM phosphate buffer (pH 8.5), analyzed by the same method. A sample blank of **6** (λ_{max} = 275 nm; A_{305} = 0.007 at 0.1 mM) was used to subtract the background absorbance. Every hour, amino group donor **6** was added in an amount equal to that of **7** produced, to keep **6** at a concentration of ~1 mM during reaction.

Aliquots (100 μ L) were withdrawn at 0, 4, 7, 10, 15, and 20 h, and to each were added internal standards 2'-methylcinnamate and 3'-fluoro-(R)- β -phenylalanine (100 nmol of each) and 6 N HCl, until the pH was 2. The samples were extracted with diethyl ether (2 \times 1 mL). The organic fractions were combined. The solvent was evaporated, and the remaining residue was treated with a dilute diazomethane solution to convert the acrylic acids to their methyl esters. Methyl esters of the biosynthetically derived 7 and the unused acrylates 14 in the reaction mixture were quantified by GC/EIMS. The abundances of their base peak fragment ions were compared to those of the same fragment ions generated from authentic samples of the methyl

esters of **7** and **14**, analyzed by an identical method. The remaining aqueous fraction was basified to pH 10 (6 N NaOH), and the amino acids were derivatized to their *N*-(ethoxycarbonyl) methyl ester analogues by reaction with ethyl chloroformate and subsequently with a dilute diazomethane solution, as described before. The esters were quantified by GC/EIMS analysis where the abundance of the base peak fragment ion derived from each ester was compared to that of the same ion generated by identically analyzed authentic samples of *N*-acyl 3'-methyl-(*S*)- α -and (*R*)- β -phenylalanine methyl esters at concentrations between 1 and 100 μ M.

3.2.10. Biosynthesis and Characterization of a 3,4-Dihydronaphthalene-2-carboxylic Acid (16-Acr) from 16

(1*R*)-1-Amino-1,2,3,4-tetrahydronaphthalene-2-carboxylic acid (16) (5 mM) was incubated with TcPAM (1 mg, 13 nmol) in 50 mM phosphate buffer (20 mL, pH 8.5) at 31 °C. After 3 days, the reaction mixture was acidified to pH 2 (6 N HCl), and the acrylate derived by deamination of 16 (designated 16-Acr) was extracted into diethyl ether (3 × 20 mL). The ether layer was dried (NaSO₄) and evaporated to dryness. The residue (~ 10 mg) was recrystallized with a 0.1 M HCl/ethanol mixture (10:1, v/v), and the solvent was decanted and removed in vacuo. The resulting crystals were characterized by 1 H and 13 C NMR and GC/EIMS analyses. The exact mass was assessed on a Q-TOF Altima API mass spectrometer (Waters, Milford, MA): 1 H NMR (500 MHz, CDCl₃) δ : 7.65 (bs, 1H, H–C=C, olefin), 7.22 (m, 4H, aromatic-H), 2.88 (t, 2H, $^{3}J_{HH}$ = 8.5 Hz, CH₂, benzylic), 2.61 (dt, 2H, $^{3}J_{HH}$ = 8.5 Hz, $^{4}J_{HH}$ = 1.0 Hz, CH₂, allylic); 13 C NMR (125 MHz, CDCl₃) δ : 172 (C=O), 138.8 (H–C=C–CO₂H), 126.8 (H–*C*=C–CO₂H), 137.2, 132.3, 129.9, 128.8, 128.4, 127.7 (aromatic-C), 27.5 (CH₂ benzylic), 21.8 (CH₂).

allylic); exact mass [M – H]⁻observed 173.0599, calculated 173.0603 for $C_{11}H_9O_2$ (see **Figure A** 3).

3.3. Results

3.3.1. Overexpression of *Tc*PAM

Codon-optimized *tcpam* was overexpressed from a pET vector by induction with isopropyl β-D-thiogalactopyranoside in six 1 L cultures of *E. coli* BL21(DE3) cells engineered to express *tcpam*. The overproduced *Tc*PAM was isolated from the bacteria as an N-terminal His₆ fusion, purified to ~95% by nickel affinity chromatography, as described previously.⁷⁴ A 1 mL stock of this enzyme at 5 mg/mL was used as the source of *Tc*PAM in the assays described herein.

3.3.2. Calculation of $K_{\rm I}$ for Various Acrylates and Time Course Studies for Optimal Amino Transfer

Preliminary guidelines were established to examine the intermolecular transfer of the amino group from (S)-styryl- α -alanine (6) to an arylacrylate catalyzed by TcPAM. First, under steady-state conditions and in the absence of an inhibitor, 6 was optimally converted to 7 at V_{max} when the concentration of 6 was 1 mM, but conversely, the rate plummeted when the concentration of 6 exceeded 1 mM (data not shown), likely because of substrate inhibition by a so far unknown mechanism. Therefore, 1 mM 6 was used in reaction mixtures with TcPAM to assess the dynamics of the transamination reaction in the presence of various arylacrylates at varying concentrations. Next, arylacrylates (9–14) were each separately incubated with TcPAM during the catalysis of 6 to 7 to calculate the competitive dissociation constants $[K_{I(A)}]$ of 9–14. A

relationship between $1/v_0$ vs $[I_0]$ was derived from **Eqn 3.1** and $K_{I(A)}$ was extracted from the slope (m) of the linear regression curves shown in figure A1 (See also **Eqn 3.2**, **Eqn 3.3**, and **Eqn 3.4**).

$$v_0 = \frac{[E]_0 [S]_0 k_{cat}}{[S]_0 + K_M \left(1 + \frac{I_0}{K_I}\right)}$$
 Eqn 3.1

$$\frac{1}{v_0} = \left(\frac{[S]_0 + K_M}{[E]_0 [S]_0 k_{cat}}\right) + \frac{K_M}{[E]_0 [S]_0 k_{cat} K_I} [I_0]$$
 Eqn 3.2

$$m = \frac{K_M}{[E]_0^{[S]} 0^k cat^{K_I}}$$
 Eqn 3.3

$$K_{I} = \frac{K_{M}}{m([E]_{0}[S]_{0}^{k}_{cat})}$$
 Eqn 3.4

The $K_{\rm I(A)}$ values were lower for arylacrylate inhibitors **9–14** (Table 3.1 and Figure A1 of the Appendix) than for (2*E*,4*E*)-styrylacrylate (7) ($K_{\rm I}$ = 337 ± 12 μ M) (Figure A 2 of the Appendix), suggesting that in the amine exchange reactions, **9–14** would bind *Tc*PAM better than the styrylacrylate product **7**, derived from **6**. Amino donor substrate **6** at 1 mM (initial concentration) was incubated with each acrylate (**9–14**) between 50 and 2000 μ M and co-incubated with *Tc*PAM (50 μ g, 0.7 nmol) to evaluate the steady-state rate parameters and to assess the point at which **6** could out compete **9–14** for the active site.

Table 3.1. Kinetic Parameters of Various Arylacrylates and Their Conversion to Aminoo Acids Using (S)-Styryl- α -alanine in the TcPAM Reaction

| | COO NH ₂ | 7cPAM 4-9 | R | X Z | ,coo ⊙ | 1 2^a |
|---|---------------------|---|--|-------------------|--------------------|-----------|
| | • | | α : Y = H; Z = NH ₂ β : Y = NH ₂ ; Z = H | | 2 | |
| | Arylacrylate | $K_{\mathrm{I(A)}}\left(\mu\mathrm{M}\right)^{b}$ | nmol ^c | 2 (nmol) | 2 (%) ^d | 2(α:β) |
| 3 | CI COO | 0.60 (± 0.04) | 150 | 72 (2a) | 48 (2a) | 49:51 |
| 4 | coo | 1.70 (± 0.05) | 150 | 120 (2b) | 80 (2b) | 17:83 |
| 5 | COO O | 12.0 (± 0.5) | 150 (8 h) | 120 (2c) | 80 (2c) | 33:67 |
| 6 | COO | 23.0 (± 0.7) | 300 | 170 (2d) | 57 (2d) | 41:59 |
| 7 | coo | 47.0 (± 2.6) | 1000 | 73 (2e) | 7.3 (2e) | 75:25 |
| 8 | coo | 106 (± 8) | 1000 | 200 (2f) | 20 (2f) | 25:75 |

 ${}^{a}R$ - Substituents are inferred from structures. ${}^{b}TcPAM$ catalyzed reaction converting 8b/a to $8b/\beta$ was inhibited for the calculation of K_{I} values. ${}^{c}Initial$ concentration of acrylate in the 12 h transamination assays containing TcPAM (0.1 mg/mL). ${}^{d}Yield$ is with respect to the arylacrylate substrate. The standard deviations are shown and were calculated from triplicate

The production of arylalanines (8a-f) for each reaction was measured over time, and the yield was found to be maximal at ~12 h, typically when the corresponding arylacrylate precursor was between 150 and 1000 μ M (Table 3.1). Then 8a-f were converted to their *N*-(ethoxycarbonyl) methyl ester derivatives and verified by GC/EIMS analysis. The stereochemistry of 8c was assessed, as an example, by converting the amino acids to their *N*-[(1'S)-camphanoyl] methyl ester derivatives. The retention times and mass spectrometry fragment ions determined by GC/EIMS analysis of the derivatized biosynthetic amino acid diastereomers were compared to those of diastereomerically pure authentic compounds; the stereochemistries of the biosynthetic α - and β -amino acids were identified as 2S and 3R, respectively. These stereochemical data supported earlier findings reported elsewhere for the *Tc*PAM reaction.³⁹⁻⁷⁴

3.3.3. Relationship between the Rates of Formation of 7 and 8 and the $K_{\rm I}$ values of 9–14

The approximate steady-state production rate of 8a-f (designated as $v_0\rightarrow 8$), reflecting the overall reaction flux after 1 h, was compared to that of the formation of the NH₂-MIO complex, estimated by the observed rate at which 6 (at 1 mM) was converted to 7 (designated as $v_0\rightarrow 7$) (Table 3.2). The $(v_0\rightarrow 8)/(v_0\rightarrow 7)$ ratio was charted versus the inhibition constants for each acrylate (9–14) $[K_{I(A)}]$, yielding a logarithmic relationship (Figure 3.1) (Eqn 3.5). This set of arylacrylates 9–14 was selected for this study because the dissociation constants (0.6–106 μ M) of these inhibitors were wide-ranging, thus allowing the logarithmic dependence between K_I and reaction rates to be observed (Figure 3.1).

The regression fit of the ratio of the steady state rates for the formation of **8** from acrylates **9** – **14** and of the NH₂-MIO complex $(v_0 \rightarrow 8)/(v_0 \rightarrow 7)$ plotted against $K_{I(A)}$ for each compound **9** – **14**

is defined by the following **Eqn 3.5**. Theoretically, if $K_{I(A)}$ were increased to 438 μ M, the $(v_0 \rightarrow 8)/(v_0 \rightarrow 7)$ ratio would approach zero as $v_0 \rightarrow 8$ was slowed because of the poor binding acrylate (amine acceptor). Meanwhile, $v_0 \rightarrow 7$ would effectively approach the maximum rate at which **6** can be converted to **7**; i.e., the conditions could resemble those as if the acrylate were absent. By contrast, as $K_{I(A)}$ hypothetically approached 0 μ M (**Figure 3.1**) (representative of an irreversibly bound acrylate), the $(v_0 \rightarrow 8)/(v_0 \rightarrow 7)$ ratio mathematically approached a maximum of ~ 3.8 under steady-state conditions (**Eqn 3.5**). Thus, an amine acceptor that bound tightly and nonproductively to TcPAM yet also bound productively to the acryl- $^+$ NH₂-E complex (Scheme 3.1) would theoretically increase the overall reaction rate $(v_0 \rightarrow 8) \sim 3.8$ -fold relative to $v_0 \rightarrow 7$.

Table 3.2: Steady-State Rate of Formation of 7 from 6 and of 8 from an Acrylate-+NH₂-MIO Complex in the Intermolecular *Tc*PAM Reaction.^a

| Arylacrylate | $K_{\mathrm{I(A)}}$ | $v_0 \rightarrow 8 \times 10^4 \mathrm{s}^{-1}$ | $v_0 \rightarrow 7 \times 10^4 \mathrm{s}^{-1}$ |
|--------------|---------------------|---|---|
| 9 | 0.60 (± 0.04) | 8a: 1.7 (± 0.1) | 1.7 (± 0.1) |
| 10 | $1.70~(\pm~0.05)$ | 8b: 3.5 (± 0.1) | 4.4 (± 0.3) |
| 11 | $12.0~(\pm~0.5)$ | 8c: 18 (± 1) | 29 (± 3) |
| 12 | 23.0 (± 0.7) | 8d: 26 (± 2) | 60 (± 5) |
| 13 | 47.0 (± 2.6) | 8e: 46 (± 6) | 150 (± 3) |
| 14 | 106 (± 8) | 8f: 140 (± 13) | 650 (± 20) |

^a The steady-state rate for the conversion of **6** to **7** (0.082 (\pm 0.002) s⁻¹) and the K_I (337 μ M) of **7** in the TcPAM reaction are provided for comparison.

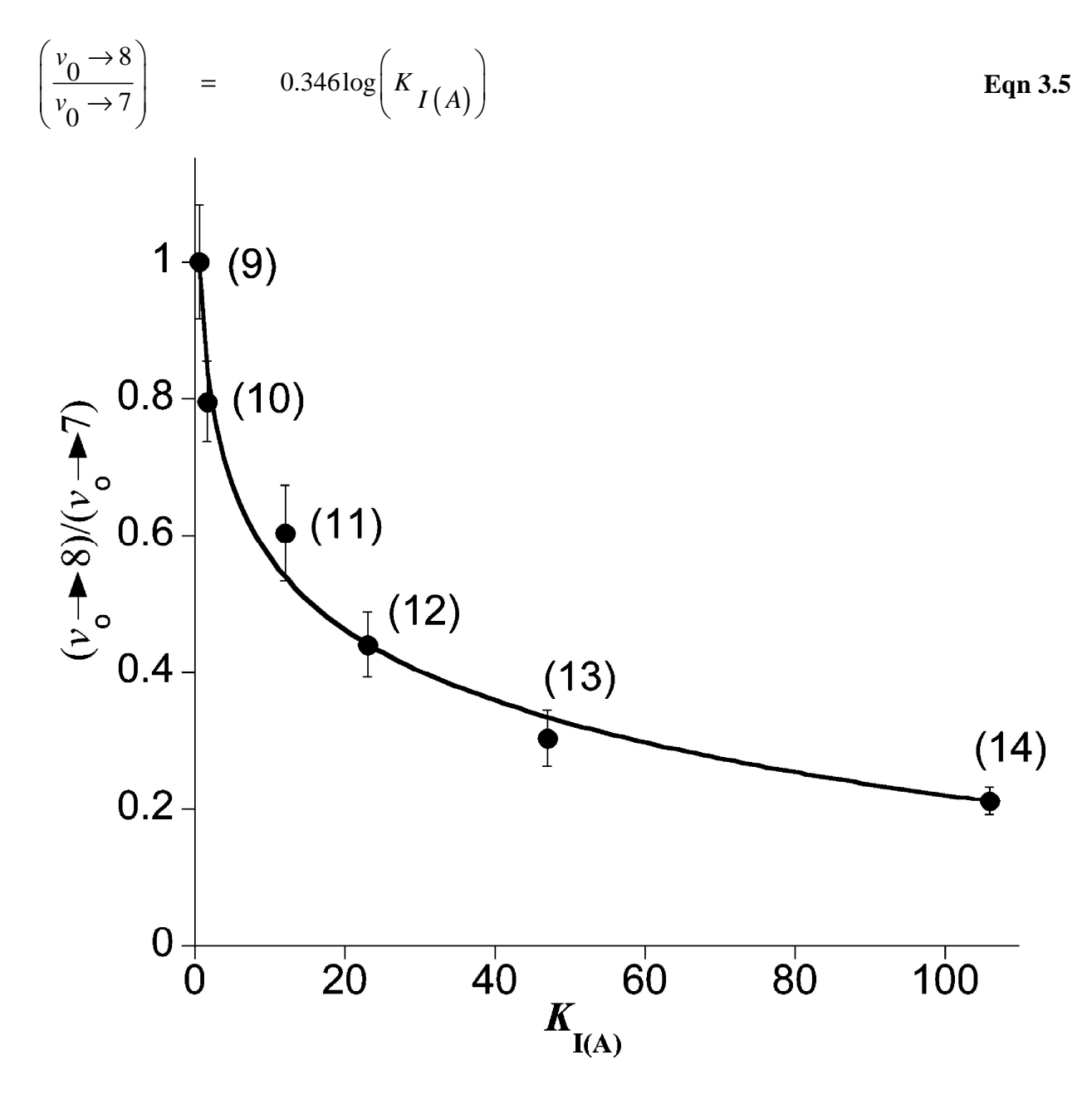


Figure 3.1. Ratio $[(v_0 \rightarrow 8)/(v_0 \rightarrow 7)]$ of the steady-state rates for the conversion of acrylates 9–14 to 8 and of the formation of the NH₂-MIO complex plotted vs $K_{I(A)}$ for 9–14 (shown in parentheses).

Understandably, the rate of production of 8a-f cannot exceed the rate at which the amine complex is formed in TcPAM (estimated by $v_0 \rightarrow 7$). Therefore, $v_0 \rightarrow 8$ can never exceed $v_0 \rightarrow 7$, and consequently, $(v_0 \rightarrow 8)/(v_0 \rightarrow 7)$ approaches 1 as the $K_{I(A)}$ approaches 0 μM (Figure 3.1) in the ping-pong-like reaction mechanism (Scheme 3.1). This was evident when the steady-state production rate of 8a $[v_0 \rightarrow 8a = (1.7 \pm 0.1) \times 10^{-4} \text{ s}^{-1}]$ was compared to that of 7 $[v_0 \rightarrow 7 = (1.7 \pm 0.1) \times 10^{-4} \text{ s}^{-1}]$ $0.1) \times 10^{-4} \ s^{-1}$] (Table 3.2). These data indicated that the rate of transfer of an amino group to acrylate 9, producing 8a, matched the amination rate for formation of the NH2-E complex (Scheme 3.1), suggesting that 100% of the amino group was transferred from the enzyme to the acrylate. Further evaluation of the steady-state rates demonstrated that the amino group was likely lost from the NH2-MIO complex as an inherent process of the reaction. To illustrate, the steady-state production rate of **8f** [$v_0 \rightarrow \mathbf{8f} = (140 \pm 13) \times 10^{-4} \, \mathrm{s}^{-1}$] was compared to that of **7** $[v_0 \rightarrow 7 = (650 \pm 20) \times 10^{-4} \text{ s}^{-1}]$ in a separate transamination reaction (Table 3.2). The comparison indicated that the rate of transfer of the amino from the enzyme to acrylate 14, producing 8f, was 4.6-fold slower than the rate of amination to form the modified enzyme (NH2-E complex of TcPAM (Scheme 3.1)) suggesting that only ~ 20% of the amino group was productively transferred from the enzyme to the acrylate. The remaining NH2-E complex must revert to free enzyme trans (Scheme 3.1) by competitive loss of NH₃ to keep the conversion of 6 to 7 at steady state, as observed.

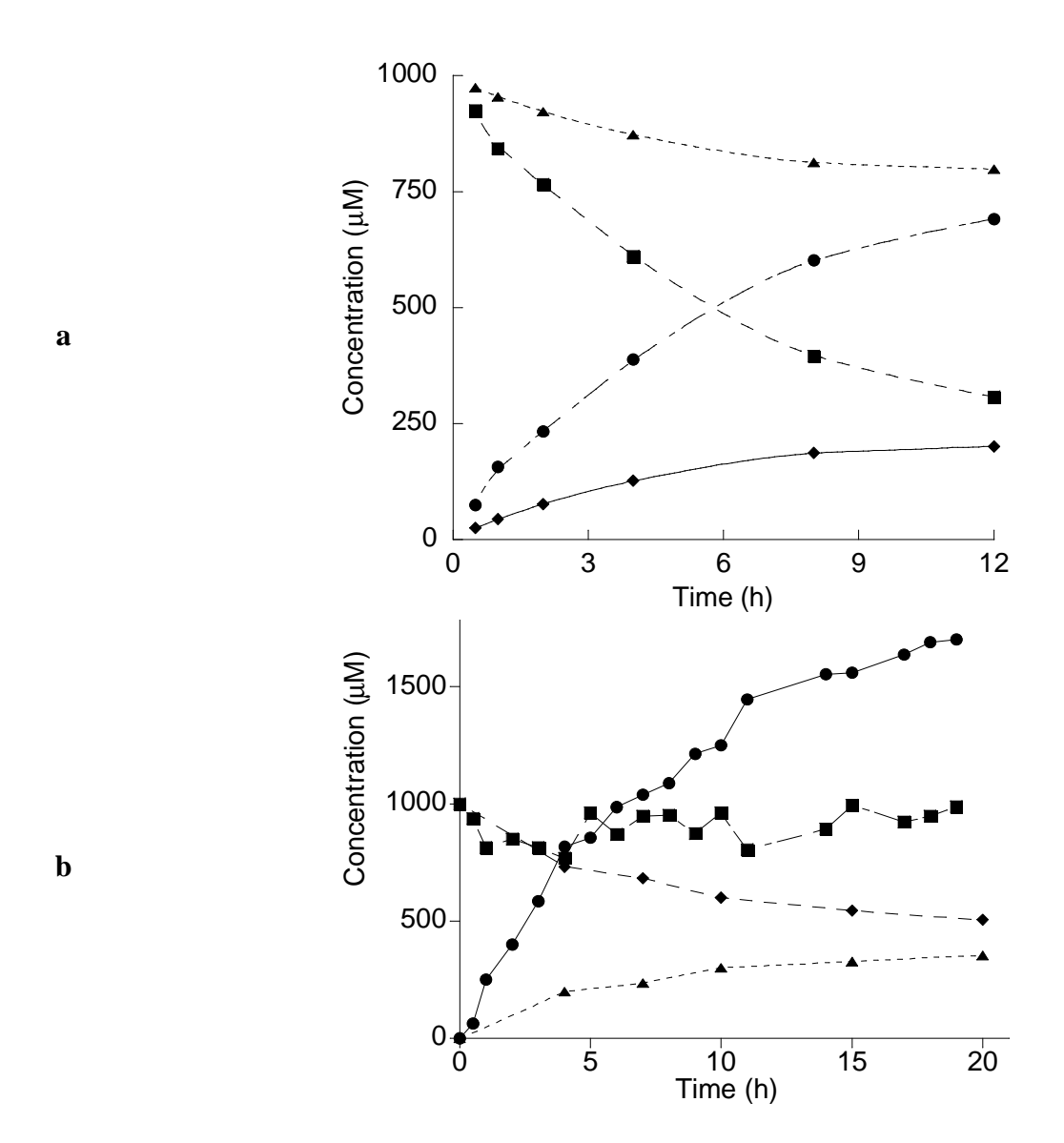


Figure 3.2. (a) Time course assay. Amounts of (*S*)-styryl-α-alanine (\blacksquare , 6), (2*E*,4*E*)-styrylacrylate (\bullet , 7), (*S*)-3'-methyl-α- and (*R*)-3'-methyl-β-phenylalanine (\bullet , 8f-α and 8f-β), and *trans*-3'-methylcinnamate (\blacktriangle , 14) in an aminotransferase reaction catalyzed by *Tc*PAM over 12 h. (b) Steady-state conversion of 6 to 7 of 8f/α and 8f/β by transfer of an amino group from 6 to 14 (5 mg) by *Tc*PAM catalysis: (2*E*,4*E*)-styrylacrylate (7, \bullet), (*S*)-styryl-α-alanine (6, \blacksquare), *trans*-3'-methylcinnamate (14, \bullet), and total of α- and β-isomers of 3'-methylphenylalanine (8f, \blacktriangle).

3.3.4. Titration of the Amino Group Donor 6 to Maintain Steady-State Conversion to 7

Also observed during the time course study, when a mixture of **6** and **14** (each at 1 mM) and TcPAM (300 µg, 3.9 nmol in 6 mL of buffer) were incubated (12 h), the production of **8f** was maximal at ~ 20% converted yield (36 ng). Beyond 12 h, **6** was depleted, and consequently, the rate of production of **8f** rapidly approached equilibrium (**Figure 3.2a**). Thus, as an alternative, the conversion of **6** to **7** was monitored by UV spectroscopy at A_{305} during the reaction, and **6** was added accordingly to maintain its concentration at 1 mM in the presence of **14** (5 mg, 31 µmol) and TcPAM (1.5 mg, 20 nmol). The production of **8f** was measured over 20 h and was obtained at 42% converted yield (2.3 mg, 13 µmol) with respect to **14** (**Figure 3.2b**).

Therefore, when the reaction mixture was titrated with 6, $v_o \rightarrow 7$ was apparently kept at the steady-state rate over a longer time frame, resulting in the greater production yields of 8f. As mentioned previously, 6 M ammonium salts were used in previous studies⁷⁷ to provide a hydrogen/amino group pair that was added across the double bond of an acrylate substrate in reverse reactions catalyzed by various MIO-dependent enzymes. These reverse reactions were typically conducted at pH 10 at high ammonium salt concentrations, which likely affected the catalytic activity. In this study, the metered addition of the amino group donor 6 likely allowed the pH of the reaction to remain optimal at 8.5 and, more importantly, prevented an excessive surplus of ammonium ions from accumulating in the reaction mixture that could potentially affect the rate of catalysis.

3.3.5. Other Amino Donor Substrates

Non-natural amino acids, (S)-2'-furyl- α -alanine ($\mathbf{15}$), (3R)-aminotetralin-(2R)-carboxylic acid ($\mathbf{16}$), and (S)-2-aminotetralin-2-carboxylic acid ($\mathbf{17}$), were incubated in separate assays to assess their utility as amino group donors. These amino acids were chosen because, like $\mathbf{6}$, they were nearly exclusively converted by TcPAM to their corresponding acrylates with only minor (<10%), if any, isomeric amino acid made (Table 3.3). This suggested that the acrylates from $\mathbf{15}$ - $\mathbf{17}$ were likely derived by a route mechanistically similar to that of $\mathbf{7}$ (i.e., the acrylates dissociate from TcPAM and leave the NH₂-MIO enzyme complex behind). Compounds $\mathbf{15}$ - $\mathbf{17}$ indeed transferred their amino group to $\mathbf{14}$, but $\mathbf{6}$ did so faster (0.56 \pm 0.02 nmol/min) (Table 3.3).

Table 3.3. Relative Steady-State Rates of Transfer of an Amino Group from Non-Natural Amino Acids (6 and 15–17) to trans-3'-Methylcinnamate (14) by TcPAM Catalysis

| | Donor Substrate | $K_{\mathbf{M}} \left(\mu \mathbf{M}\right)^{a}$ | $k_{\text{cat}} \left(\min^{-1} \right)^a$ | Acryl:β-A.a. ^b | $v_o \times 10^2$ (nmol (8f) •min ⁻¹) ^c |
|----|------------------------|--|---|---------------------------|--|
| 6 | | 250 (± 4) | 4.9 (± 0.1) | 99:1 | 56 (± 2) |
| 15 | | 130 (± 6) | 2.5 (± 0.1) | 91:9 | 22 (± 1) |
| 16 | O NH3 ⊕ | 341 (± 6) | 1.7 (± 0.3) | 100:0 | 1.0 (± 0.3) |
| 17 | ⊕NH ₃ O ⊕ O | 352 (± 9) | 0.7 (± 0.1) | 100:0 | 0.4 (>± 0.1) |

^a Acryl, acrylate derived from elimination of H/NH₂ from the amino donor; β -A.a., β -amino acid made from either **6**, **15**, or **17** via TcPAM catalysis.

^b Compound 14 was used as the amino group acceptor.

^c This ratio represents the proportion of acrylate to α -amino acid. Supplied arylacrylates **9–14** were the sole means of amino group exchange to produce (S)- α - and (R)- β -arylalanine. Standard deviations are in parentheses and were calculated from triplicate assays.

To simplify the kinetic evaluation, the rate of transfer of an amino group to 14 was considered identical in each reaction; thus, the different steady-state rates of production of8f by use of "sacrificial" substrates $\bf 6$ and $\bf 15-17$ were reflective of the NH $_2$ -MIO complex loading rate, e.g., 2.5-fold faster with 6 (0.56 \pm 0.02 nmol of 8f/min) than with 15 (0.22 \pm 0.01 nmol of 8f/min). This difference paralleled the 2-fold difference in catalytic efficiency $(k_{\rm cat}/K_{\rm M})$ between 6 (0.020 $\pm 0.001 \text{ min}^{-1} \mu\text{M}^{-1}$) and 15 $(0.010 \pm 0.001 \text{ min}^{-1} \mu\text{M}^{-1})$. By contrast, the catalytic efficiencies of tetralins 16 $(0.005 \pm 0.001 \text{ min}^{-1} \mu M^{-1})$ and 17 $(0.0020 \pm 0.0003 \text{ min}^{-1} \mu M^{-1})$ were only 4- and 10-fold lower, respectively, than that of 6, whereas the transamination rates differed 56- and 140fold, respectively (Table 3.3). Apparently, the catalytic efficiencies of TcPAM, with amino donors 6 and 15-17, trend with the transamination rate, yet the two kinetic parameters are not directly proportional. The identity of the 3,4-dihydronaphthalene-2-carboxylic acid (designated **16-Acr**) biosynthesized by TcPAM from both**16** and **17**, in the amino group transfer reactions, was compared to an authentic standard derived biosynthetically in a large-scale reaction that converted 16 to 16-Acr. NMR and mass spectrometry analysis verified the product as authentic 3,4-dihydronaphthalene-2-carboxylic acid.

3.4. Discussion

Overall, the intermolecular transamination reaction catalyzed by TcPAM required that the amino donor substrate yield an acrylate intermediate with a binding affinity for the active site lower than that of the acrylate serving as the amino acceptor. (S)-Styryl- α -alanine served as a suitable amino donor for probing the kinetic parameters of the transaminase reaction catalyzed by TcPAM in the presence of a series of arylacrylates, with varying enzyme binding affinities that served as amino group acceptor substrates and as inhibitors in a quasi-ping-pong exchange mechanism. These results suggested that the nearly exclusive intramolecular transfer process observed for TcPAM and its natural substrate³⁸ represented an extraordinary balance between both the retention of the cinnamate reaction intermediate and the migratory amino group in the active site. Moreover, the transamination reaction followed a course on which 6 and acrylates 9-14 engaged in a sequential ping-pong exchange in the active site. Because 9–14 competitively inhibited the catalysis of the conversion of 6 to 7 in the first step in which modified TcPAM (the NH₂-MIO complex) was produced, the transaminase mechanism accordingly deviated from true ping-pong (double-displacement) exchange. Generally, the substrate of the second step does not inhibit the first reaction step in a ping-pong mechanism. 95 Thus, strong inhibition of the first step in the TcPAM transaminase reaction by a tight binding acrylate (amino group acceptor) resulted in a slower than expected reaction flux to the α - and β -arylalanine products 8 as the amount of acrylate substrate was increased.

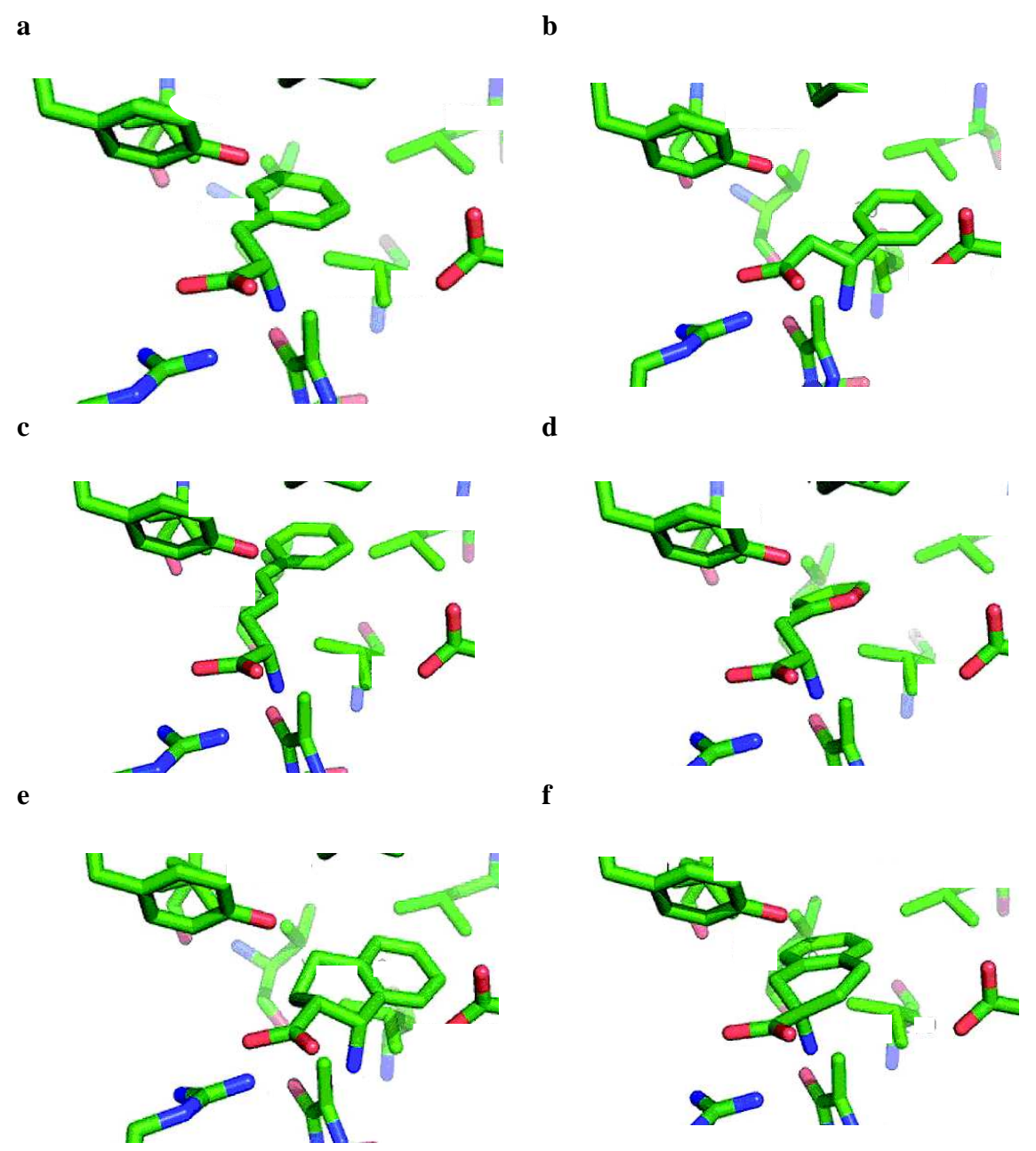


Figure 3.3. Modeled in the TcPAM active site are natural substrates (a) (S)-α-phenylalanine and (b) (R)-β-phenylalanine for reference, (c) (S)-styryl-α-alanine, (d) (S)-2'-furyl-α-alanine, (e) (3R)-3-aminotetralin-(2R)-2-carboxylate, and (f) (S)-2-aminotetralin-2-carboxylate. PyMOL (Schrödinger LLC, Cambridge, MA) was used for the substrate modeling by preserving the key interactions with the active site residues.

Interestingly, the TcPAM active site can apparently accommodate the bicyclic tetralin amino acids 16 and 17 in an orientation that produces the corresponding dihydronaphthalene derived from each. The structure of TcPAM in complex with cinnamate was determined in a previous report³⁸ and is used here to approximate the trajectory of each non-natural amino acid substrate used as an amino group donor (Figure 3.3). Key substrate docking interactions occur between the natural substrate phenylalanine and active site residues. The carboxylate and the aromatic ring of the substrate form a salt bridge with Arg325 and a hydrophobic contact with Leu104 of TcPAM, respectively. 38 The amino group of (S)-α-phenylalanine is held above and proximate to the methylidene carbon of the methylidene imidazolone (MIO) group by a hydrogen bond interaction between the amino group of the substrate and the hydroxyl of Tyr322 (not shown) in the active site (Figure 3.3a). The trajectory of the natural substrate phenylalanine essentially traces the carbon skeleton of the cocrystallized cinnamate scaffold, and the β-phenylalanine traces the carbon configuration of the presumed cinnamate rotamer needed to position C_{β} for the amino group rebound (**Figure 3.3b**).³⁸ TcPAM seemingly accommodates (S)-styryl-α-alanine (**Figure 3.3c**) and (S)-2'-furyl- α -alanine (**Figure 3.3d**) in a conformation similar to the trajectory of the modeled natural substrate (Figure 3.3a), and these substrates exhibited rates of amino group transfer higher than those of the amino tetralins. The furyl ring (Figure 3.3d) is oriented so that the heteroatom is pointed at Glu455 and toward the solvent-exposed entry point of the active site, where it could engage in hydrogen bonding. By contrast, the dimethylene bridge of (3R)-3-aminotetralin-(2R)-2-carboxylate (**Figure 3.3e**) causes the aromatic ring of the substrate to reside at a displaced angle compared to the β-phenylalanine congener model (**Figure 3.3b**); this displacement of the aromatic ring is more pronounced in the model for (S)-2-aminotetralin-2-carboxylate [the presumed productive enantiomer that is analogous to the (2S)-antipode of the

natural substrate] (**Figure 3.3f**). The distorted docking conformations of the latter likely contribute to their poor catalytic efficiencies ($k_{\rm caf}/K_{\rm M}$) in the transamination reaction catalyzed by $Tc{\rm PAM}$. In addition, on the basis of the structure of a $Tc{\rm PAM}$ -cinnamate complex, ³⁸ the dimethylene bridge likely prevented the tetralins from adopting an optimal conformation for binding to the active site and transferring their amino group. Further, the bridged **16** and **17** likely also, in part, precluded the reversible α/β -interchange via a two-bond rotation of the dihydronaphthalene intermediate, as proposed in previous accounts. ^{38, 57, 61}

3.5. Conclusion

TcPAM was employed as an amino acid:arylacrylate transaminase, and an interesting mechanistic property of the reaction was elucidated. The enzyme was originally characterized as principally producing its natural product (R)-β-phenylalanine from (S)-α-phenylalanine with nearly exclusive retention of the amino group and the carbon skeleton during the reaction.³⁸ A distinguishing feature of the TcPAM reaction was revealed in this study when (S)-styryl-α-alanine (S) was used as a substrate. The release of the ensuing T from TcPAM was apparently significantly faster than the release of the amino group from the enzyme. Thus, a significant proportion of TcPAM existed as the NH₂-MIO enzyme complex, and intermolecular transfer of the amino group to the exogenously supplied arylacrylates to produce α- and β-arylalanines was observed as the principal route of amino group transfer. In addition, it was demonstrated that under steady-state conditions, an appreciable amount of the amino group is lost nonproductively, likely as NH₃, from the NH₂-MIO complex to reset TcPAM for the next round of catalysis. This loss of the amino group was observed to occur prevalently when the exogenously supplied acrylate (amino group acceptor) bound the enzyme more weakly in the reaction mixture. With an

improved understanding of the mechanism of TcPAM and knowledge of how to employ surrogate substrates in examining cryptic aspects of the aminomutase chemistry and kinetics, it may become feasible to measure the rate at which the amino group is released from the enzyme complex.

In addition, bicyclic tetralin amino acids **16** (a bicyclic β -amino acid) and **17** (a bicyclic α -amino acid) were shown for the first time to function as surrogate substrates in the *TcPAM* reaction, or in any MIO-dependent enzyme-catalyzed reaction, to the best of our knowledge. The product pools derived from substrates **16** and **17** were comprised exclusively of the same corresponding acrylate (**16-Acr**). This suggested that a so far unknown impediment of the reaction stalled the progress of α - β isomerization, such as the ring fusion of the substrates preventing access to a productive rotamer of the dihydronaphthalene intermediate. Moreover, the amino acids produced during the transamination reaction were made concurrently with significant (2*E*,4*E*)-styrylacrylate (**7**) derived from **6** at >99% de.³⁸ Thus, *TcPAM* could be a tractable resource of conjugated dienic carbonyl derivatives such as **7** (and its analogues). Dienes of this type are typical structural subunits for the synthesis of natural products and useful as synthetic precursors.⁹⁶

4. ASSESSING THE DEAMINATION RATE OF NH₂-MIO ADDUCT BY BURST PHASE ANALYSIS

Reproduced with permission from [Wanninayake, U.; Walker, K. D., Assessing the deamination rate of a covalent aminomutase adduct by burst phase analysis. *Biochemistry* **2012**, 51, (26), 5226-5228] Copyright © 2012 American Chemical Society

4.1. Introduction

The subfamily of enzymes that includes aminomutases $^{38^{\circ}57^{\circ}64}$ and ammonia lyases 59 depends on the function of a 3,5-dihydro-5-methylidene-4*H*-imidazol-4-one (MIO) cofactor within the active site. The recently solved structures of a phenylalanine aminomutase from *Pantoea agglomerans* (PaPAM) 64 and a tyrosine aminomutase from *Streptomyces globisporus* (SgTAM) 69 support a mechanism where the amino group of the substrates attacks the MIO moiety (**Scheme** 4.1). The alkyl ammonium group is presumably removed by an elimination (E2-like; E2 = bimolecular, concerted elimination reaction) mechanism that is initiated by removal of the pro-(3S) proton from the substrate by a catalytic tyrosine residue. $^{38^{\circ}57^{\circ}64}$ For TcPAM, the resulting cinnamate intermediate is principally trapped in the active site for the entire isomerization reaction 38 and rotates 180° about the C_1 - C_{α} and C_{β} - C_{ipso} bonds. The amino group of the aminated-MIO attacks C_{β} and the pro-(3S) proton is recovered by C_{α} to complete the isomerization. In the TcPAM reaction, the original stereochemical configuration at both C_{α} and C_{β} is retained after the re-addition of the NH₂ and proton. In contrast, the bacterial isozyme

PaPAM and the related catalyst SgTAM invert the stereochemistry at the migration termini to make the corresponding β-amino acid product (cf. Chapter 2).^{61'}, 69

Scheme 4.1: Mechanism of MIO-Dependent Aminomutases

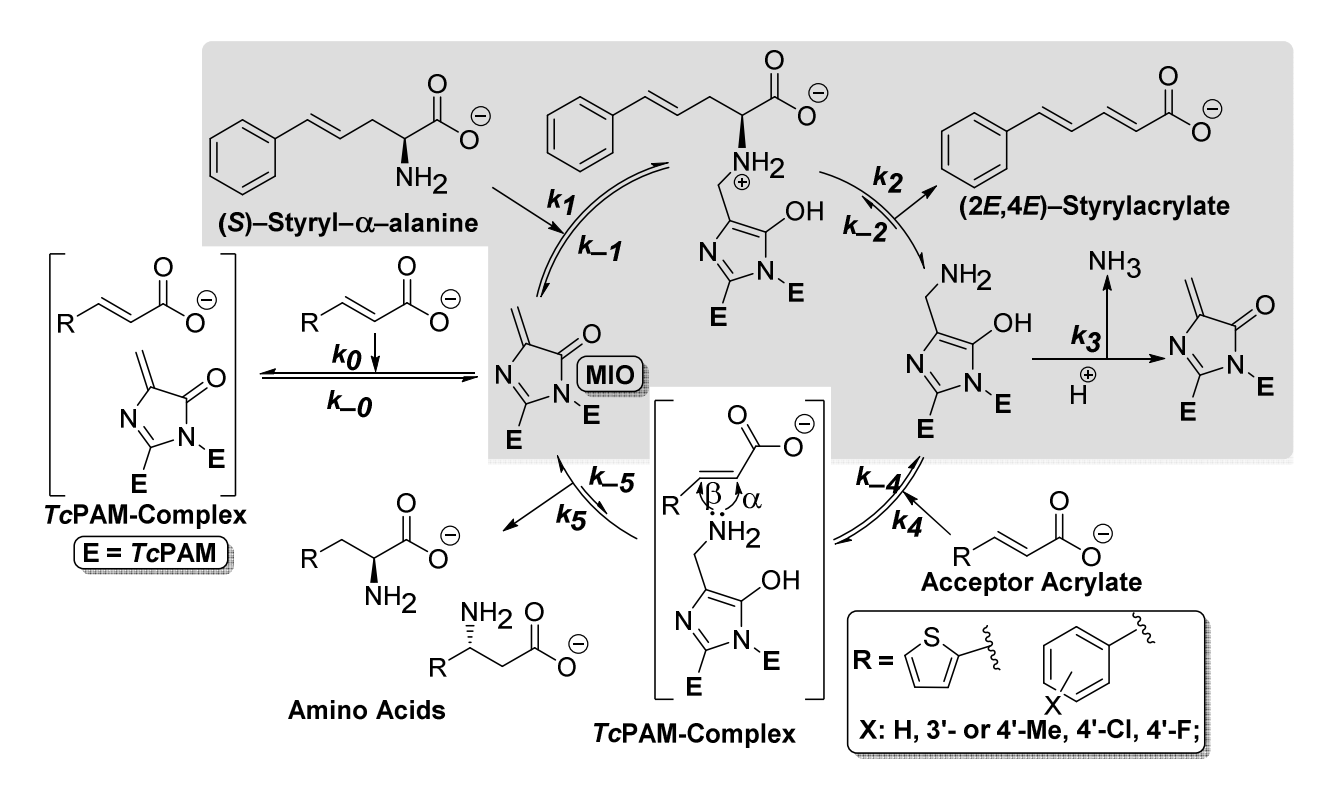
The TcPAM reaction was deemed predominantly intramolecular; the amino group and proton from α -phenylalanine rebound exclusively to the same carbon skeleton to make β -phenylalanine. Stable-isotope labeling studies revealed ~ 7% intermolecular amino group transfer from [^{15}N]- α -phenylalanine to [$^{2}H_{6}$]-cinnamate (Scheme 4.2a). 38 This observation suggested the cinnamate intermediate occasionally diffused from the active site while the ammonia–enzyme (NH₂–MIO; aminated 3,5-dihydro-5-methylidene-4*H*-imidazol-4-one) (cf. Scheme 4.1) adduct remained intact. Thus, the lifetime of the NH₂–MIO adduct was longer than the residence time of the

cinnamate complex in the active site. Reciprocally, under the same reaction conditions, PaPAM did not transfer any label from [^{15}N]- α -phenylalanine to [$^{2}H_{6}$]-cinnamate, 61 suggesting that the cinnamate remained in the active site longer than the lifetime of the NH_{2} -MIO. Another earlier study showed that during the SgTAM catalytic cycle, the transient amino group was transferred intermolecularly from 3'-chlorotyrosine to 4'-hydroxycinnamate (4'-HOCinn). This data suggested that the transient amino group remained attached to the enzyme during the course of the isomerization. This earlier study, however, did not evaluate an isotopically labeled-4'-HOCinn (an isotopomer of the natural pathway intermediate) to evaluate whether the amino group could transfer from α -tyrosine to 4'-HOCinn. Thus, it was unclear if the pathway intermediate, after elimination of NH_{3} from α -tyrosine, could occasionally exchange intermolecularly with an exogenous source of 4'-HOCinn already in solution. 62

An earlier study showed that TcPAM converted 99% of (S)-styryl- α -alanine to (2E,4E)-styrylacrylate (Scheme 4.2b) at 0.082 s⁻¹ steady state rate (k_{cat}) which is at the same order as the steady state rate of natural (S)- α - to (R)- β -phenylalanine isomerization (0.052 s^{-1}) . This suggested that during the conversion of styryl- α -alanine to styrylacrylate, the transient amino group likely remained as the NH₂-MIO adduct for the same duration as the α - to β -phenylalanine conversion. Therefore, deamination rate of the enzyme bound amino adduct should provide mechanistic details of the aminomutase reaction. This hypothesis was interrogated by a mixture of (S)-styryl- α -alanine (amino group donor) and an arylacrylate (amino group acceptor), both at steady state concentration. Acceptor substrates were selected, based on $K_{\rm P}$ to estimate the relative binding affinities compared to that of (2E,4E)-styrylacrylate. A model scheme for the transaminase reaction was proposed in order to quantify the deamination (Scheme 4.3).

Scheme 4.2: a) Intermolecular Amino Group Transfer from [15 N]- α -Phenylalanine to [2 H $_{6}$]-Cinnamate by TcPAM Catalysis. b) Predominantly Ammonia Lyase Behavior of TcPAM with (S)-styryl- α -alanine.

Scheme 4.3: Kinetic Model for Transaminase Reaction Catalyzed by TcPAM^a



^aShaded inset: Kinetic model to evaluate the burst kinetics of the deamination of (S)-styryl- α -alanine.

4.2. Experimental

4.2.1. Chemicals

(2E,4E)-styrylacrylate was acquired from Alfa Aesar (Ward Hill, MA), (S)- α -phenylalanine was purchased from Sigma-Aldrich, and (R)- β -phenylalanine was obtained from PepTech Corp. (Burlington, MA).

4.2.2. Enzyme Preparation

Codon-optimized cDNA from *Taxus canadensis* was previously ligated into expression vector pET28a(+), and the recombinant plasmid encoded an N-terminal His6 tag.⁷⁴ The *tcpam* clone was overexpressed in six 1 L cultures of *Escherichia coli* BL21(DE3) cells by induction with isopropyl β -D-thiogalactopyranoside. The overproduced protein was isolated from the bacteria and purified to 95% by Ni affinity chromatography to yield 5 mg of protein, as described previously (1). The purity of the enzyme was determined by the SDS-PAGE method. Routine assays for assessing enzyme function were conducted with (*S*)- α -styrylalanine at apparent saturation (1 mM) and *Tc*PAM (100 μ g, 1.3 nmol) in 50 mM phosphate buffer with 5% glycerol at pH 8.5 in 1 mL assays. The assays were analyzed by UV–visible spectroscopy (Beckmann DU 640, Beckmann Coulter, Brea, CA) with A_{340} monitoring of the sample to quantify the product (2*E*,4*E*)-styrylacrylate.

4.2.3. Quantification of Biosynthetic Styrylacrylate during Kinetic Progressions

The molar absorptivity constant ($\varepsilon_{340} = 4 \times 10^3 \, \mathrm{M}^{-1} \, \mathrm{ecm}^{-1}$, pH 8.5, 23 °C) for (2E,4E)-styrylacrylate was calculated from standard curve formed by UV-visible spectroscopy (Beckmann DU 640, Beckmann Coulter Brea, CA). The absorbance at A_{340} was measured for a series of concentrations of (2E,4E)-styrylacrylate (1-100 μ M) dissolved in 50 mM phosphate buffer (pH 8.5). A sample blank of 50 mM phosphate buffer was used to subtract the background absorbance. It should be noted, the 1 6 mM (S)-styryl- α -alanine substrate ($\lambda_{max} = 275 \, \mathrm{nm}$) does not have an absorbance signature at A_{340} . Beer's law was used to calculate the molar absorptivity constant, which was then used to convert the absorbance of styrylacrylate produced during the

stopped flow experiment to concentration. The formation of (2E,4E)-styrylacrylate was monitored at A_{340} ($\varepsilon_{340} = 4 \times 10^3$ M⁻¹ cm⁻¹, pH 8.5) with a stopped flow spectrometer (model SX.18MV-R, dead-time = 2 ms, 1 cm optical path, thermostatically controlled at 23 °C). Aliquots (125 μ L) of both TcPAM (5.5 μ M final concentration) and styryl- α -alanine (final concentrations between 50 and 750 μ M) (**Figure 4.1**) were separately mixed, and the absorbance was measured at 0.12 s intervals over 50 s.

4.3. Results

The TcPAM catalysis of the (S)-styryl- α -alanine ammonia lyase reaction shows a pre-steady burst at the initial progression of the reaction (Figure 4.1). The resulting absorbance data at each concentration at each time point were fit by nonlinear least-squares regression (**Eqn 4.1**) to obtain the burst amplitude (B) of the presteady-state and the velocity of the reaction at steady-state (A). is used generally to define the kinetic parameters when an enzyme-bound intermediate slowly dissociates to form the free enzyme. ⁹⁷ This equation was applied to calculate the rate constants and burst phase parameters of the TcPAM reaction.

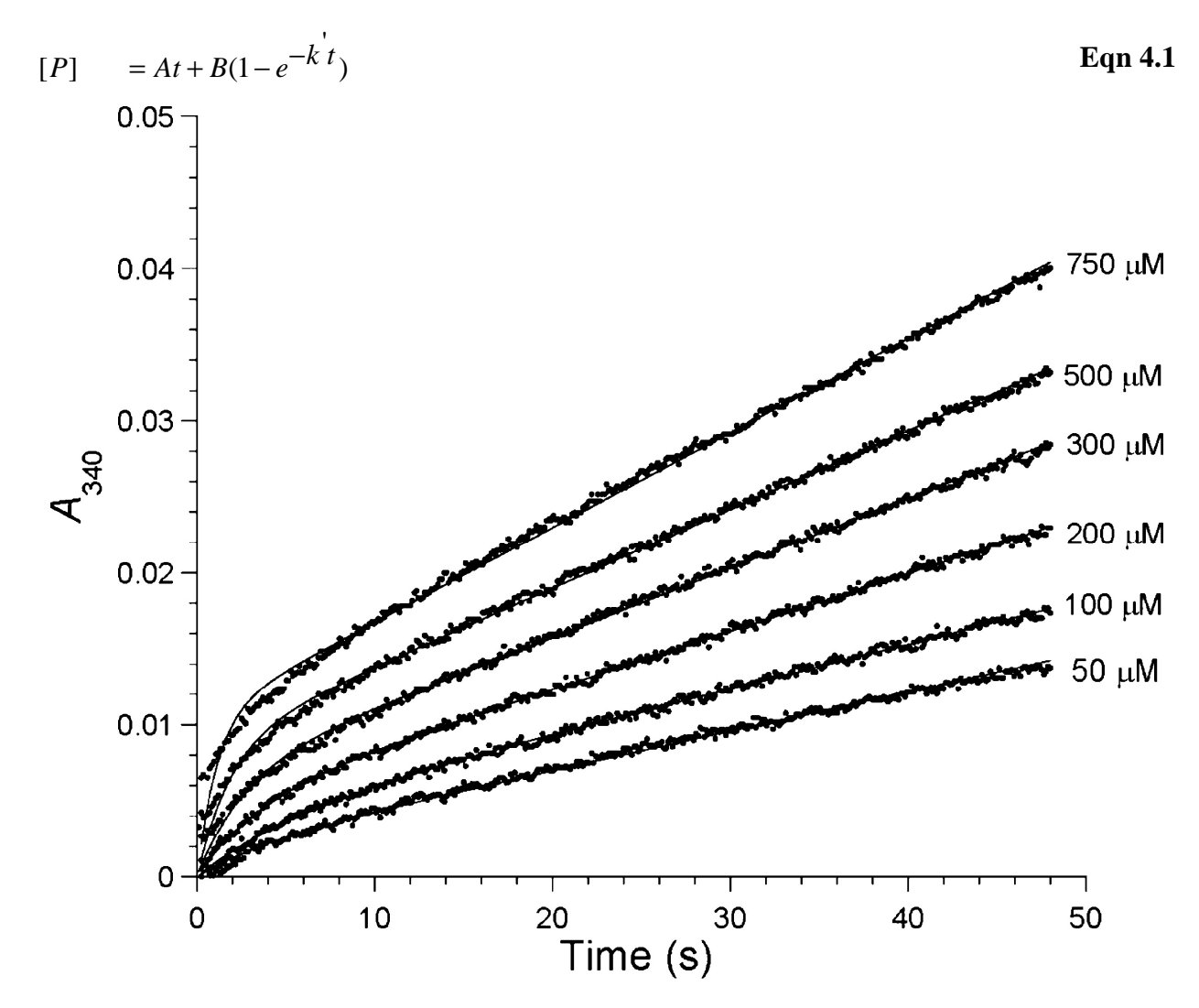


Figure 4.1. Evaluation of the kinetic model (Scheme 4.3, shaded inset) for TcPAM burst kinetics (Eqn 4.1) was used to globally fit experimental progress curves (Kaleidagraph 4.0) spanning six different (*S*)-styryl-α-alanine concentrations incubated with TcPAM (5.5 μM). Release of (2*E*,4*E*)-styrylacrylate was measured in a stopped-flow cell by A_{340} monitoring. Each time point is an average of three progression curves.

Where the terms are; [P]: product concentration; A: steady state velocity (Eqn 4.2); B: burst amplitude (Eqn 4.3); t: time; and k': apparent first order rate constant of the pre-steady-state.

$$A = \left(\frac{k_2 k_3}{k_2 + k_3}\right) \frac{[E]_0 [S]_0}{K_M^{app} + [S]_0}$$
 Eqn 4.2

$$B = [E]_0 \left(\frac{k_2}{k_2 + k_3}\right)^2 \left(\frac{[S]_0}{K_{\rm M}^{app} + [S]_0}\right)^2$$
 Eqn 4.3

Where the terms are $[E]_0$: total-enzyme concentration; $[S]_0$: initial substrate concentration; and the apparent $K_{\rm M}$ ($K_{\rm M}$ app) defined in Eqn 4.4 and the $k_{\rm cat}$ is defined in Eqn 4.6.

$$K_{\mathbf{M}}^{app} = K_{\mathbf{M}} \left(\frac{k_3}{k_2 + k_3} \right)$$
 Eqn 4.4

$$K_{M} = \left(\frac{k_{-1} + k_{2}}{k_{1}}\right)$$
 Eqn 4.5

$$k_{cat} = \frac{k_2 k_3}{k_2 + k_3}$$
 Eqn 4.6

The linear relationship with $[S]_o/A$ to $[S]_o$ was derived from Eqn 4.2 via a series of rearrangements and simplifications (Eqn 4.7, Eqn 4.8, & Eqn 4.9). The K_M^{app} of TcPAM for styryl- α -alanine was determined from the ratio of Intercept to the gradient of the linear regression fit of $[S]_o/A$ vs $[S]_o$ (Figure 4.2).

$$\frac{A}{[S]_0} = \left(\frac{k_2 k_3}{k_2 + k_3}\right) \frac{[E]_0}{K_{M}^{app} + [S]_0}$$
 Eqn 4.7

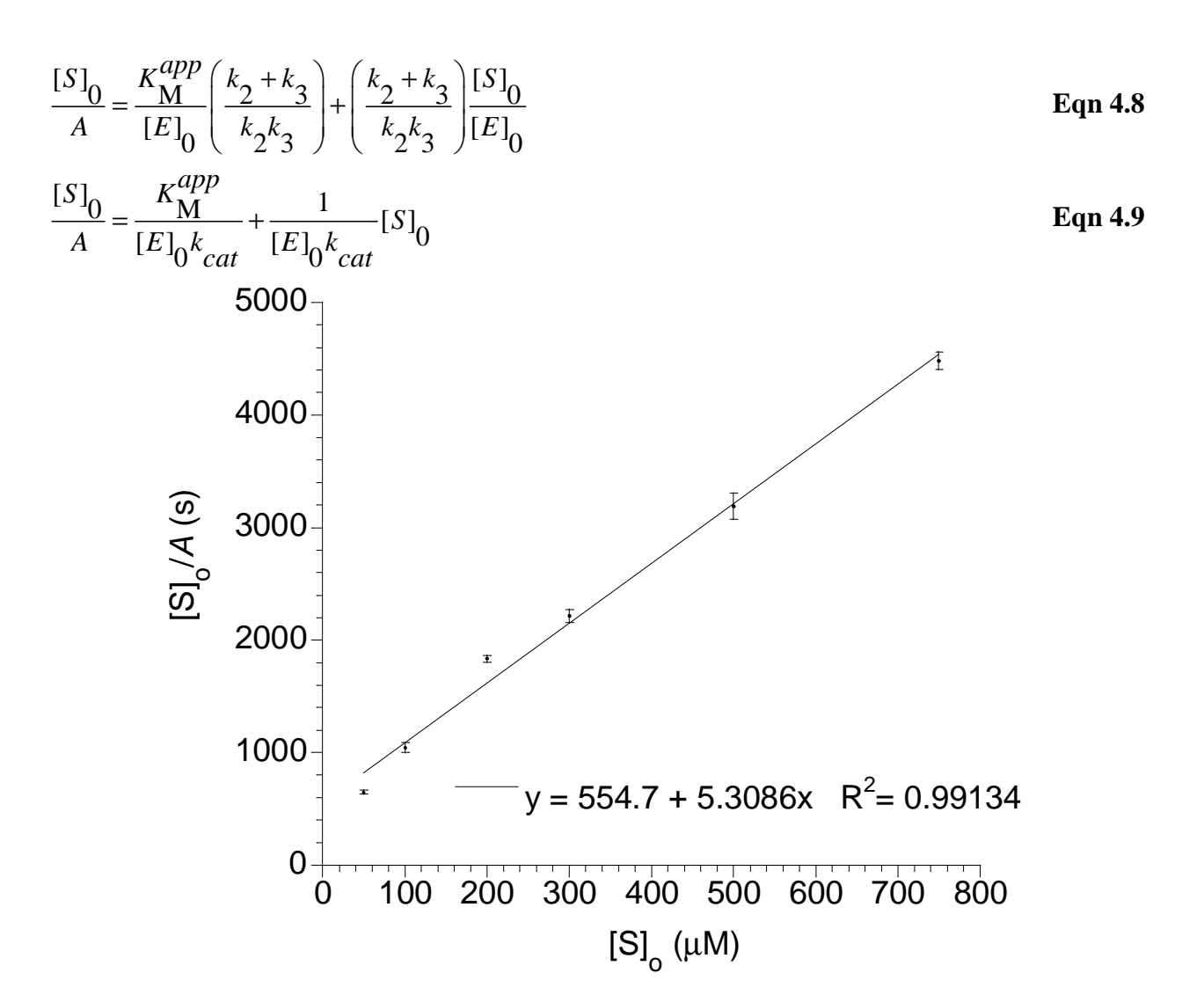


Figure 4.2. Hanes-Woolf analysis of the steady-state rates. The progress curves) were individually fit to the burst equation to evaluate the steady-state velocities (*A*), for each concentration of styryl- α-alanine, of the TcPAM burst kinetics. The average value for each data point *A* was used. The dependence $[S]_0/A$ on $[S]_0$ with S.D. for the triplicate measurements of *A*. Linear regression fit $([S]_0/A = 554.7 + 5.309[S]_0$; $R^2 = 0.9913$) to the data (solid line).

$$\frac{A^{2}}{B} = \frac{\left(\frac{k_{2}k_{3}}{k_{2} + k_{3}}\right)^{2} \left(\frac{[E]_{0}[S]_{0}}{K_{M}^{app} + [S]_{0}}\right)^{2}}{[E]_{0} \left(\frac{k_{2}}{k_{2} + k_{3}}\right)^{2} \left(\frac{[S]_{0}}{K_{M}^{app} + [S]_{0}}\right)^{2}}$$
Eqn 4.10

 $A^2 = B[E]_0 k_3^2$ Eqn 4.11

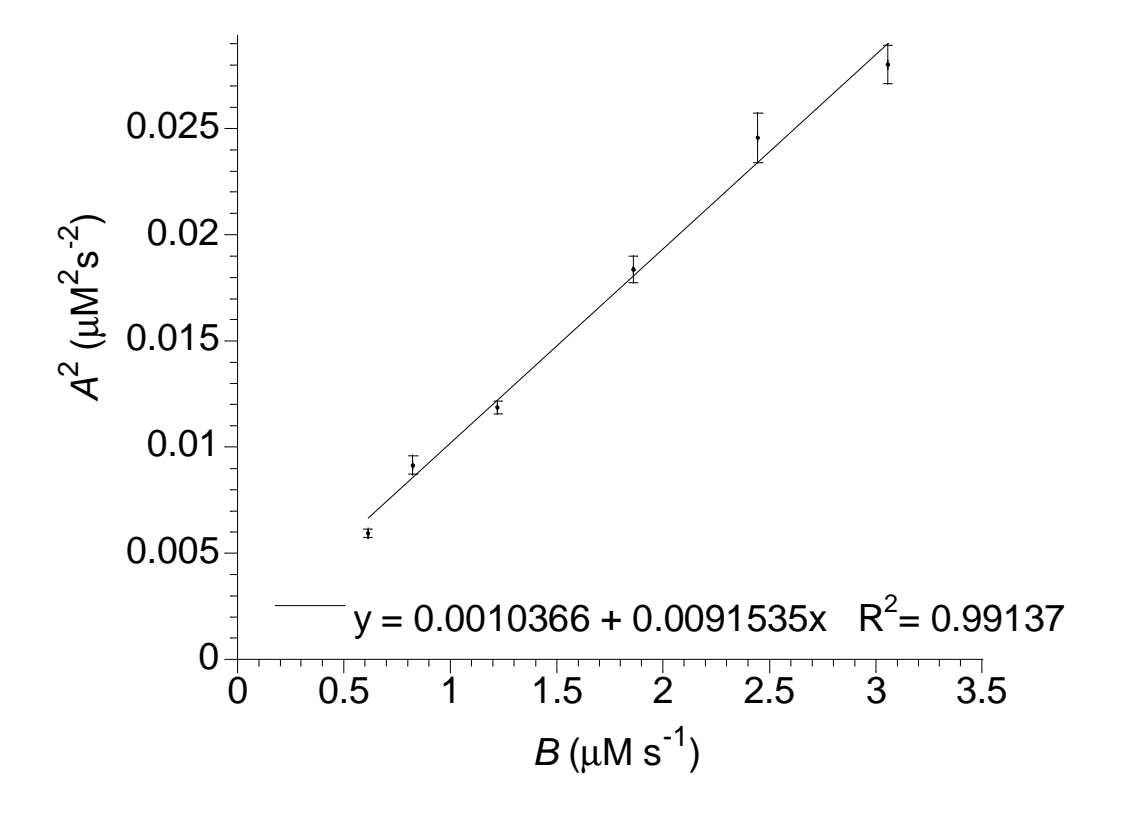


Figure 4.3: The progression curves were individually fit to the burst equation to evaluate the steady-state velocity A and the burst amplitude B for the TcPAM burst kinetics. The average value for each data point A was used. A^2 dependence on B with S.D. for the triplicate measurements. Linear regression fit ($A^2 = 0.001037 + 0.009153B$; $R^2 = 0.9914$) to the data (solid line).

Terms A^2 and B were simplified and then rearranged (Eqn 4.10) to define a linear relationship between A^2 and B at each substrate concentration (Eqn 4.11). Since $[E]_0$ was known, k_3 was thus calculated from the slope ($[E]_0k_3^2$) of the plot of A^2 against B (Figure 4.3). The steady state kinetic parameters $K_{\rm M}^{~app}$ (Eqn 4.4) and $k_{\rm cat}$ of $Tc{\rm PAM}$ for styryl- α -alanine were calculated from a Hanes-Woolf plot of $[S]_0/A$ against $[S]_0$ (Figure 4.2), where A was extracted from the steadystate formation of styrylacrylate (Figure 4.4. The progress curves were individually fit to the burst equation to evaluate the steady-state velocity A and the burst amplitude B for the TcPAM burst kinetics. The average value for each data point A was used. The dependence of A/B on $1/[S]_0$ with S.D. for the triplicate measurements. Linear regression fit (A/B = 0.049558 + $6.88821/[S]_0$; $R^2 = 0.97933$) to the data (solid line). **Figure 4.4**). Rate constant k_2 was calculated from k_{cat} that relates k_3 and k_2 (Eqn 4.6). A linear relationship between A/B and $1/[S]_0$ was established from Eqn 4.12 where $k_3(k_3 + k_2)/k_2$ is the intercept (Figure 4.4). The experimentally determined values for k_2 (0.19 \pm 0.01 s⁻¹) and k_3 (0.041 \pm 0.002 s⁻¹) were substituted into $k_3(k_3+k_2)/k_2$, and the resulting value $(0.050 \pm 0.002 \text{ s}^{-1})$ was comparable to the intercept (0.049) \pm 0.004 s⁻¹) from Eqn 4.12. Thus, the burst phase kinetic analysis of styryl- α -alanine deamination by TcPAM was considered reliable.

$$\frac{A}{B} = \frac{k_3(k_2 + k_3)}{k_2} + \frac{k_3(k_2 + k_3)K_M^{app}}{k_2} \frac{1}{[S]_0}$$
 Eqn 4.12

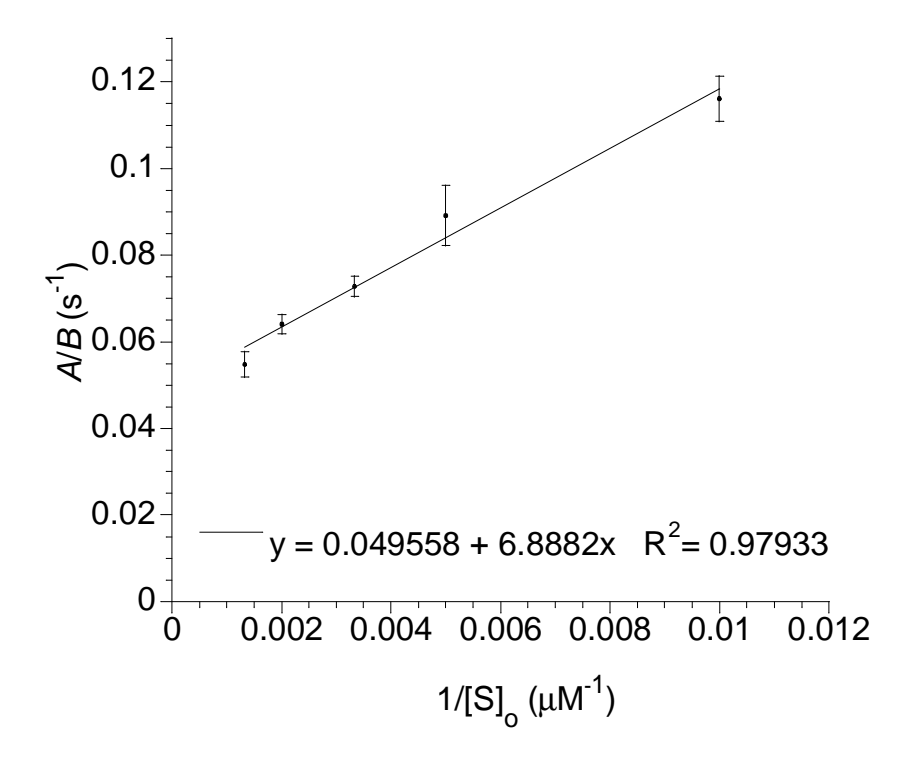


Figure 4.4. The progress curves were individually fit to the burst equation to evaluate the steady-state velocity A and the burst amplitude B for the TcPAM burst kinetics. The average value for each data point A was used. The dependence of A/B on $1/[S]_0$ with S.D. for the triplicate measurements. Linear regression fit $(A/B = 0.049558 + 6.88821/[S]_0$; $R^2 = 0.97933$) to the data (solid line).

Terms A^2 and B were simplified and then rearranged (Eqn 4.10) to define a linear relationship between A^2 and B at each substrate concentration (Eqn 4.11). Since $[E]_0$ was known, k_3 was thus calculated from the slope ($[E]_0k_3^2$) of the plot of A^2 against B (Figure 4.3). The steady state kinetic parameters $K_{\rm M}^{pp}$ (Eqn 4.4) and $k_{\rm cat}$ of $Tc{\rm PAM}$ for styryl- α -alanine were calculated from a Hanes-Woolf plot of $[S]_0/A$ against $[S]_0$ (Figure 4.2), where A was extracted from the steady-

state formation of styrylacrylate. Rate constant k_2 was calculated from $k_{\rm cat}$ that relates k_3 and k_2 (Eqn 4.6). A linear relationship between A/B and $1/[S]_{\rm o}$ was established from Eqn 4.12 where $k_3(k_3+k_2)/k_2$ is the intercept (Figure 4.4). The experimentally determined values for k_2 (0.19 \pm 0.01 s⁻¹) and k_3 (0.041 \pm 0.002 s⁻¹) were substituted into $k_3(k_3+k_2)/k_2$, and the resulting value (0.050 \pm 0.002 s⁻¹) was comparable to the intercept (0.049 \pm 0.004 s⁻¹) from Eqn 4.12. Thus, the burst phase kinetic analysis of styryl- α -alanine deamination by TcPAM was considered reliable.

4.4. Discussion

The $K_{\rm M}^{app}$ of $Tc{\rm PAM}$ for styryl- α -alanine was $105 \pm 10~\mu{\rm M}$ and the $k_{\rm cat}$ was $0.034 \pm 0.002~{\rm s}^{-1}$ at 23 °C (pH 8.5). These values were agreeable ($K_{\rm M}^{app} = 250~\mu{\rm M}$; $k_{\rm cat} = 0.082~{\rm s}^{-1}$) to those reported in an earlier study for the same reaction, at 31 °C. 35 The $K_{\rm M}$ (588 \pm 37 $\mu{\rm M}$) of $Tc{\rm PAM}$ was calculated from $K_{\rm M}^{app}$ (see Eqn 4.4 and Eqn 4.5) for styryl- α -alanine in the ammonia elimination reaction that produced styrylacrylate (Scheme 4.3, shaded inset). The burst amplitude (B) and steady-state velocity (A) was dependent on [S]_o. The rate constant ($k_3 = 0.041 \pm 0.002~{\rm s}^{-1}$) for the release of NH₃ (that reset $Tc{\rm PAM}$ for another catalytic cycle) was similar to $k_{\rm cat}$ (0.034 \pm 0.002 s⁻¹) for the conversion of styryl- α -alanine to styrylacrylate. In contrast, the calculated rate constant ($k_2 = 0.19 \pm 0.01~{\rm s}^{-1}$) for the release of styrylacrylate was 5-fold greater than $k_{\rm cat}$. Therefore, $k_{\rm cat}$ for the overall reaction was slowed 5-fold likely by the slower deamination rate of enzyme.

TcPAM normally deaminates α-phenylalanine in the first committed step, and the ensuing cinnamate complex, the protonated catalytic residue, and the NH₂-MIO adduct (see Scheme 4.1) are retained long enough to complete the intramolecular isomerization.³⁸ Under steady-state conditions, the $k_{cat}^{\alpha\beta}$ for this conversion was 0.014 ± 0.001 s⁻¹ at 23 °C, corresponding to a transit time (1/ $k_{cat}^{\alpha\beta}$) of 71 s. In addition, β-phenylalanine and cinnamate were produced at a 9:1 ratio. This kinetics data suggested that the transit time (1/ k_7 + 1/ k_9 + 1/ k_3) from the α-Phe-⁺NH₂-MIO-E complex to the release of NH₃, via the cinnamate-production pathway (Scheme 4.4), was ~9 times longer (639 s) than 1/ $k_{cat}^{\alpha\beta}$. Since 1/ k_3 (24 s) on this pathway is known, then (1/ k_7 + 1/ k_9), the estimated transit time to cinnamate (Scheme 4.4), was therefore 615 s. The latter transit time supported the notion that the dwell time of cinnamate in the active site is sufficient to preferentially promote the intramolecular amino group rebound pathway to β-phenylalanine.

Scheme 4.4: Kinetic Model for the Proposed Mechanism of the TcPAM-Catalyzed Conversion of α - to β -Phenylalanine

MIO-E
$$\xrightarrow{k_8}$$
 β -Phe $\xrightarrow{\oplus}$ γ -MIO-E $\xrightarrow{k_{-10}}$ γ -Phe γ -Phe

Cinn: (*E*)-Cinnamate; β -Phe: (*R*)- β -Phenylalanine

The efficiency of the amino group transfer from the NH₂-MIO adduct in the described exchange reaction was largely dependent on the binding affinity of the acceptor arylacrylate for TcPAM. The amino group transferred at nearly 100% efficiency to a tighter-binding acceptor, while the efficiency decreased exponentially for weaker-binding acceptors when the α - and β -amino acid mixtures were made.³⁵ This suggested that the transit time $(1/k_4 + 1/k_5)$ progressing from the amination of the acceptor to the release of the amino acids was significantly less than the transit time $(1/k_3)$ for the deamination of the NH₂-MIO adduct to the apo-MIO cofactor (Scheme 4.3). Reciprocally, for the weakest binding acceptor, the transit times were exchanged, where $(1/k_4 + 1/k_5) > (1/k_3)$, and now the deamination of the NH₂-MIO adduct predominated. To further understand why the amine transfer efficiency decreased with weaker binding acceptors in

the transamination reaction, and to infer the kinetics of the mechanistically similar MIO-dependent catalysts, the dissociation rate (k_3) of the NH₂-MIO adduct in TcPAM was calculated herein.

Since TcPAM forms a transient covalent NH_2 -MIO adduct in its interaction with amino acid substrates, a burst kinetic method was employed to establish the decay rate of the adduct. (S)-Styryl- α -alanine (Peptech Inc., Burlington, MA) was used as an adventitious substrate in the TcPAM-catalyzed reaction to show direct kinetic evidence of the accumulation of the purported (NH_2 -MIO)-modified enzyme. The burst phase of TcPAM was evident in assays when (S)-styryl- α -alanine was converted to chromophoric product (2E,4E)-styrylacrylate in a fast step (k_2), followed by slower release (k_3) of the second product NH_3 (Scheme 4.2, shaded inset). The slower NH_3 -release step led to the observed pre-steady state burst. In stopped-flow experiments, styrylacrylate was produced from styrylalanine initially along an exponential burst phase prior to reaching a steady-state progression. The burst phase parameters were then used to calculate the rate constants k_2 and k_3 (Scheme 4.3).

4.5. Conclusion

TcPAM undergoes finite inactivation during turnover of (S)-styryl- α -alanine to styrylacrylate, resulting in burst kinetics with the steady-state rate being a dynamic balance between the inactive modified enzyme (NH₂-MIO adduct) and reactivation by deamination of the adduct. To our knowledge there are no reports on the direct kinetic evaluation of this deamination for any MIO-dependent enzyme. Furthermore, above study provided kinetic data to indirectly obtain the dwelling time of cinnamic acid intermediate in the active site of TcPAM during the aminomutase

reaction. It will be in great interest to perform a similar study on PAL enzymes to understand the effect on deamination rate and cinnamic acid dwelling time to the PAM and PAL activity. In this study, the calculated deamination rate constant for the dissociation of the NH₂–MIO adduct contributes information to further understand the mechanism of the *Tc*PAM reaction.

5. A BACTERIAL TYROSINE AMINOMUTASE PROCEEDS THROUGH RETENTION OR INVERSION OF STEREOCHEMISTRY TO CATALYZE ITS ISOMERIZATION REACTION

Reproduced with permission from [Wanninayake, U.; Walker, K. D., A bacterial tyrosine aminomutase proceeds through retention or inversion of stereochemistry to catalyze its isomerization reaction. *J. Am. Chem. Soc.* **2013**, 135, (30), 11193-11204] Copyright © 2013 American Chemical Society

5.1. Introduction

β-Amino acids are emerging as an important class of compounds that are present in bioactive natural products, such as the antineoplastic pharmaceutical paclitaxel isolated from *Taxus* plants, 1,98 the aminopeptidase inhibitor bestatin obtained from *Streptomyces olivoreticuli*, 99 an antibacterial blasticidin S from *Streptomyces griseochromogenes*, 100 the antibiotic agent enediyne C-1027 from *Streptomyces globisporus*, 101 the anti-tuberculosis agent viomycin from *Streptomyces vinaceus*, 102 the antibiotic andrimid from *Pantoea agglomerans*, and cytotoxic agents chondramides A-D from *Chondromyces crocatus*. 5 In addition, single β-aryl-β-alanines show anti-epileptogenesis activity. 103 Other β-aryl-β-alanines have been used as building blocks toward the synthesis of complex bioactive molecules, including β-lactams, 104 β-peptides as mimics of α-peptide, 105 and antimicrobial compounds. 107

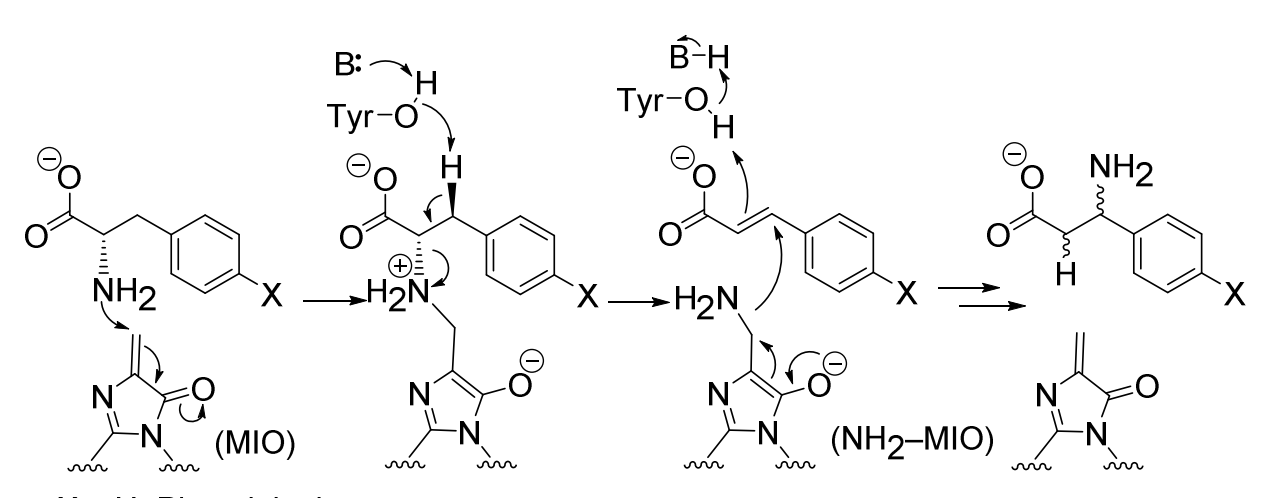
Several chiral synthetic strategies have been developed for variously substituted β -arylalanines that include tandem one-pot processes 108 and conjugate addition of homochiral lithium amides to α , β -unsaturated acceptors. 109 The Knoevenagel condensation of benzaldehyde and malonic acid in the presence of NH₄OAC produced a series of racemic β -arylalanines. 110 By contrast, there are only a few reports on the biocatalysis of asymmetric β -arylalanines from the corresponding readily available natural and nonnatural α -amino acids through aminomutase catalysis.

So far, five 3,5-dihydro-5-methylidene-4*H*-imidazol-4-one (MIO)-dependent aminomutases are known to isomerize either (*S*)- α -phenylalanine (EncP from *Streptomyces maritimus*, ⁶⁸ AdmH (*Pa*PAM) from *Pantoea agglomerans*, ⁶ ⁶¹ and *Tc*PAM from *Taxus* plants ⁴⁵ ⁶⁶) or (*S*)- α -tyrosine ((*S*)-1) (SgcC4 (*Sg*TAM) from *Streptomyces globisporus* ⁶⁹ ¹¹¹ and CmdF (*Cc*TAM) from *Chondromyces crocatus* ⁴⁶, further described herein) to their respective β -amino acids. Efforts to optimize the turnover of this family of aminomutases provide a potentially alternative means toward scalable biocatalytic production of novel enantiomerically pure β -amino acids as synthetic building blocks in medicinal chemistry. Earlier substrate specificity studies showed that *Tc*PAM can convert substituted aromatic and heteroaromatic α -alanines to the corresponding β -alanines. Apparently, since TAMs requires the 4'-hydroxyl group on the substrate for catalysis, their use to biosynthesize β -tyrosine analogues is limited. ⁴⁶ ¹¹¹

These aminomutases belong to a class I lyase-like family (comprised of ammonia lyases^{52, 112} and aminomutases^{6, 46, 63, 66}) where, mechanistically, the amino group of the arylalanine

substrate nucleophilically attacks the MIO to form an amino acid-MIO adduct. Removal of a β-proton via a tyrosine residue, and concommitant elimination of the NH₂-MIO adduct from the substrate produces an intermediary arylacrylate product. Interchange and rebound of the transient hydrogen and NH₂-MIO to the intermediate, and release of the β-amino acid complete the conversion (Scheme 5.1). Stereochemical evidence shows that these enzymes can be sorted by their enantioselectivity for the β-amino acid product; EncP, PaPAM and SgTAM make (S)-β-arylalanines, and CcTAM and TcPAM make (R)-β-arylalanines. Further, the properties of the MIO aminomutases segregate according to whether the cryptic stereochemistry at C_{α} and C_{β} of the product is inverted or retained. The different enantioselectivities of these isozymes is determined by the fate of the intermediate formed on distinct reaction pathways.

Scheme 5.1: General MIO-dependent Aminomutase Mechanism



X = H, Phenylalanine

X = OH, Tyrosine

MIO = 3,5-Dihydro-5-methylidene-4*H*-imidazol-4-one

For example, both PaPAM and SgTAM presumably bind their respective substrates and displace the NH_2 -MIO adduct and pro-(3S) hydrogen by anti-elimination. For both enzymes, the

NH₂-MIO and hydrogen interchange positions and rebound to the same face of the cinnamate intermediate from which they were removed to form the (S)-\beta-amino acids, with inversion of configuration at C_{α} and C_{β} . Therefore, the intermediate on this reaction sequence must reside as a single rotamer.^{61, 63} By contrast, for the isozyme TcPAM, the cinnamate intermediate is proposed to rotate 180° about the C_1 – C_{α} and C_{β} – C_{ipso} bonds. Then the labile NH $_2$ and pro-(3S) hydrogen exchange positions and reattach to the opposite face of the intermediate from which they were removed. This mechanism results in retention of configuration at C_{α} and C_{β} to form (R)- β phenylalanine. 38, 61, 66, 114

Scheme 5.2: The CcTAM Reaction on the Chondramides A-D Pathway

(S)-1 (R)-2Chondramides

A: $R_1 = OMe, R_2 = H$

B: $R_1 = OMe, R_2 = Cl$

 $C: R_1 = R_2 = H$

D: $R_1 = H$, $R_2 = C1$

Interestingly, the tyrosine aminomutases (TAMs) are less enantioselective than the PAMs. The former make both enantiomers of the β -tyrosine (2) at steady state and show significantly lower enantiomeric excess after reaching equilibrium, ⁴⁶ ¹¹⁵ while the PAM enzymes make product at >99% ee, even after reaching equilibrium, and racemization is not observed. ³⁸ ⁴⁵ ⁶¹ ¹¹⁴ It should be noted that earlier mutational studies on CcTAM (E399K) improved the enantioselectivity for (R)-2 from 69% to 97% ee. ⁴⁶ Despite this earlier study to correlate active site residues with the stereoselectivity of CcTAM, the basis for why the β -amino acid enantioselectivity was enhanced remained unexplored. In addition, the mode of attachment (i.e., retention or inversion of configuration) of the reciprocally migratory NH₂ group and the hydrogen at C_{α} and C_{β} during the reaction is unknown.

To understand and ultimately improve the substrate specificity profile, turnover rate, and enantioselectivity of CcTAM, its mechanisms must be fully understood. To this end, we add further mechanistic detail to CcTAM, which converts (S)-1 to (R)-2 on the biosynthetic pathway of the cytotoxic cyclodepsipeptide chondramides A-D in C. crocatus myxobacteria (Scheme 5.2).⁵ ⁴⁶ ¹¹⁶ The (R)-product stereochemistry catalyzed by CcTAM suggested that its stereochemical course is related to that catalyzed by TcPAM. Herein, we used deuterium-labeled isotopomers of α -tyrosine to evaluate the cryptic stereochemistry of the CcTAM mechanism and compare it to other aminomutases.

5.2. Experimental

5.2.1. Chemicals and Reagents

(*S*)-α-Tyrosine, 4'-hydroxycinnamic acid, unlabeled- and [α-²H]-4'-hydroxybenzaldehyde, hippuric acid, ethyl chloroformate, (*S*)-2-methylbutyric anhydride, acetic anhydride, pyridine, bicyclo[2.2.1]hepta-2,5-diene (norbornadiene), ²H₂ gas, (2*S*)-[3,3-²H₂]-α-tyrosine ((2*S*)-[3,3-²H₂]-1) and Dowex 50W (100-200 mesh, H⁺ form) ion exchange resin were purchased from Sigma Aldrich (St. Louis, MO). (*R*)-3-Amino-3-(4'-hydroxyphenyl)propanoic acid and (*S*)-3-amino-3-(4'-hydroxyphenyl)propanoic acid were purchased from Peptech Inc. (Bedford, MA). (*R*)-1,2-Bis(diphenylphosphino)propane ((*R*)-Prophos) was purchased from Alfa Aesar (Ward Hill, MA). Bicyclo[2.2.1]hepta-2,5-diene-rhodium(I) chloride dimer ([Rh(NBD)Cl]₂) and silver perchlorate were purchased from Strem Chemicals (Newburyport, MA). Hydrogen gas (99.995% purity) was obtained from Airgas Great Lakes (Independence, OH 44131).

5.2.2. Instrumentation

¹H-NMR (500 MHz), ²H-NMR (76.7 MHz) and ¹³C NMR (126 MHz) spectra were obtained on a Varian NMR-Spectrometer using standard acquisition parameters. X-ray crystallographic data were collected using a Bruker CCD (charge coupled device)–based diffractometer equipped with an Oxford Cryostream low-temperature apparatus operating at 173 K. The biosynthetic products were quantified and analyzed by gas chromatography/electron-impact mass spectrometry (GC/EIMS): GC (model 6800N, Agilent, Santa Clara, CA) was coupled to a mass analyzer (model 5973 *inert*, Agilent, Santa Clara, CA) in ion scan mode from 50-400 atomic mass units. The GC conditions were as follows: column temperature was held at 200 °C for 1

min and then increased linearly at 20 °C/min to 250 °C with a 1-min hold. Splitless injection was selected, and helium was used as the carrier gas.

5.2.3. Subcloning, Expression, and Purification of CcTAM

The cctam cDNA was codon-optimized by GenScript (Piscataway, NJ 08854) in the pUC57 vector. The clone was ligated into the pET-28a(+) vector between the NdeI/BamHI cloning sites. Recombinant plasmids were used to transform Escherichia coli BL21(DE3) cells, which were grown in 1 L Luria–Bertani medium supplemented with kanamycin (50 µg/mL). Overexpression of CcTAM was induced by the addition of isopropyl- β -D-thiogalactopyranoside (100 μ M) to the medium, and the cells were grown at 16 °C for 16 h. The cells were then harvested by centrifugation, and the resulting pellet was resuspended in buffer (50 mL of 50 mM sodium phosphate containing 5% (v/v) glycerol, 300 mM NaCl, and 10 mM imidazole, pH 8.0). The cells were lysed by sonication, and the cellular debris and light membranes were removed by centrifugation. The crude, functionally soluble aminomutase was purified by nickel nitrilotriacetic acid (Ni-NTA) affinity chromatography according to the protocol described by the manufacturer (Qiagen, Valencia, CA). Fractions that eluted from the column, containing active CcTAM (62 kDa) in 250 mM imidazole, were combined. The buffer was exchanged with 50 mM sodium phosphate (pH 8.0) containing 5% (v/v) glycerol through several concentration/dilution cycles, using a Centriprep centrifugal filter (30,000 MWCO, Millipore). The purity of the concentrated CcTAM (15 mg/mL in 4 mL, estimated by the Bradford method) was >95% by SDS-PAGE with Coomassie Blue staining.

5.2.4. Assessing the Activity and Stereochemistry of the CcTAM Reaction

(S)-1 (1 mM) was incubated with CcTAM (0.1 mg) at 31 °C in 50 mM phosphate buffer (1 mL, pH 8.5) for 1 h. The assay mixtures were treated in twice (5 min each time) with pyridine (0.6 mmol) and ethyl chloroformate (0.5 mmol). This step, containing excess ethyl chloroformate, caused partial ethyl esterification. Afterwards, the reaction was acidified to pH 2 (6M HCl), and the 4'-O,2-N- and 4'-O,3-N-di(ethoxycarbonyl) derivative of α- and β-tyrosine, respectively, were extracted into ether and treated with a slight excess of diazomethane. The resulting sample contained a mixture of ethyl (~20 mol%) and methyl (80 mol%) esters. 4'-Hydroxycinnamic acid by-product was converted to its 4'-O-ethoxycarbonyl-(E)-coumaric acid ethyl (10 mol%) and methyl (90 mol%) esters under these conditions. The methyl esters of the α-tyrosine derivative and the 4'-O-ethoxycarbonyl-(E)-coumaric acid, and the ethyl ester of the β-tyrosine derivative were analyzed by GC/EIMS.

To confirm the stereochemistry of the β -isomer product, ⁴⁶ another sample of *Cc*TAM (0.1 mg) was incubated at 31 °C with (*S*)-1 (1 mM) in phosphate buffer (1 mL, pH 8.5) for 1 h. To this solution were added pyridine (50 μ L, 0.64 mmol) and (*S*)-2-methylbutyric anhydride (10 μ L, 0.05 mmol), and the mixture was stirred vigorously for 5 min. Another batch of pyridine (0.64 mmol) and (*S*)-2-methylbutyric anhydride (0.05 mmol) was added, and the reaction was stirred for 5 min. The solution was acidified to pH 2 (6M HCl) and extracted with diethyl ether (3 × 2 mL). The ether fractions were combined and dried. The resulting residue was dissolved in diethyl ether (100 μ L) and the solution was titrated with a dilute solution of diazomethane dissolved in diethyl ether until the yellow color persisted. These samples were analyzed by GC/EIMS and compared to the retention time and mass fragmentation of authentic standards (Figure A 38-40)

5.2.5. Synthesis of Authentic α - (1) and β -Tyrosine (2) and (E)-4-Hydroxycinnamic Acid Derivatives

To (S)- α -, (R)- β -tyrosine or (E)-4'-hydroxycinnamic acid (0.1 mmol of each) dissolved in 50 mM phosphate buffer (1 mL, pH 8.5) were added pyridine (200 µL, 2.4 mmol) and ethyl chloroformate (200 µL, 1.6 mmol). The reactions were stirred for 5 min and treated with another batch of pyridine and ethyl chloroformate (both at 200 µL) for 5 min with stirring. The ethanolic mixtures caused partial ethyl esterification. Each mixture was acidified to pH 2 (6M HCl), and extracted into diethyl ether $(3 \times 2 \text{ mL})$. The ether fractions were combined, dried under vacuum, and the residue was dissolved in methanol (100 µL). To this solution was added a dilute diazomethane solution dissolved in diethyl ether, until the yellow color persisted. This procedure resulted in a mixture of ethyl and methyl esters for each sample, as described earlier.

5.2.5.1. 4'-O-Ethoxycarbonyl-(E)-coumaric Acid Methyl Ester (i.e., 4'-O-Ethylcarboxy-(E)-4'-Hydroxycinnamic Acid Methyl Ester)

The coumarate ester was recrystallized from ethanol and isolated at 80% yield (20 mg). Exact mass [M + H]⁺ observed 251.0890 & calculated 251.0919 for [C₁₃H₁₅O₅]⁺. ¹H NMR (500 MHz, CDCl₃) δ : 7.68 (d, J = 16.1 Hz, 1 H), 7.55 (d, J = 8.3 Hz, 2 H), 7.22 (d, J = 8.3 Hz, 1 H), 6.41 (d, J = 16.1 Hz, 1 H), 4.34 (q, J = 7.3 Hz, 2 H), 3.82 (s, 3 H), 1.41 (t, J = 7.3 Hz, 3 H). ¹³C NMR (126 MHz, CDCl₃) δ : 167.2 (C(O)OCH₃), 153.2 (OC(O)O), 152.4 (C4'), 143.6 (C $_{\beta}$), 132.2 (C1'), 129.2 (C2'), 121.6 (C3'), 118.1 (C $_{\alpha}$), 65.1 (OC(O)OCH₂CH₃), 51.7 (C(O)OCH₃), 14.2 (OC(O)OCH₂CH₃). (Figure A 6-Figure A 8 for GC/EIMS fragmentation dataand NMR Spectra)

5.2.5.2. The 4'-O,2-N-Di(ethoxycarbonyl)-α-tyrosine Methyl Ester.

A mixture of ethyl (10 mol%) and methyl (90 mol%) esters of 4'-O,2-N-di(ethoxycarbonyl)-αtyrosine was obtained at 74% yield (25 mg). The methyl ester of the α-tyrosine derivative was used in the GC/EIMS analyses of labeled and unlabeled α-tyrosine substrates. Therefore, the mixed ester sample, dissolved in chloroform (500 µL), was loaded onto a preparative silica gel TLC plate and eluted with 90:10 hexane:ethyl acetate. Authentic 4-O,2-N-di(ethoxycarbonyl)-αtyrosine methyl ester was isolated ($R_f = 0.65$) at 67% yield (22.5 mg). Exact mass [M + H + Pyridine]⁺ observed 419.1781 & calculated 419.1818 for $[C_{21}H_{27}N_2O_7]^+$. ¹H NMR (500 MHz, CDCl₂) δ : 7.21 - 6.98 (m, 4 H), 5.10 (d, J = 7.3 Hz, 1 H), 4.67 - 4.55 (m, 1 H), 4.28 (q, J = 7.1Hz, 2 H), 4.08 (q, J = 6.7 Hz, 2 H), 3.69 (s, 3 H), 3.10 (dd, J = 6.1, 14.0 Hz, 1 H), 3.05 (dd, J =6.1, 14.0 Hz, 1 H), 1.36 (t, J = 7.0 Hz, 3 H), 1.20 (t, J = 6.7 Hz, 3 H). ¹³C NMR (126 MHz, CDCl₂) δ: 171.9 (<u>C</u>(O)OCH₂), 155.8 (OC(O)NH), 153.5 (OC(O)O), 150.2 (C4'), 133.6 (C1'), 130.3 (C2'), 121.0 (C3'), 64.8 (CH₂CH₂OC(O)O), 61.2 (CH₂CH₂OC(O)NH), 54.5 (C(O)OCH₂), 52.3 (C₀), 37.6 (C_B), 14.4 (<u>C</u>H₃CH₂OC(O)O), 14.1 (<u>C</u>H₃CH₂OC(O)NH). (See Figure A10-12 for GC/EIMS fragmentation data and NMR spectra). 4'-O,2-N-Di(ethoxycarbonyl)-α-tyrosine Ethyl Ester. The corresponding ethyl ester was isolated ($R_f = 0.50$) from the TLC plate at 7% yield (2.5 mg). Exact mass [M + H + Pyridine] observed 433.1933 & calculated 433.1974 for $[C_{22}H_{20}N_2O_7]^+$. ¹H NMR (500 MHz, CDCl₃) δ : 7.17 (d, J = 8.6 Hz, 2 H), 7.14 – 7.11 (m, J = 8.6Hz, 2 H), 5.14 (d, J = 7.8 Hz, 1 H), 4.63 (dd, J = 5.6, 13.4 Hz, 1 H), 4.33 (q, J = 7.1 Hz, 2 H), $4.17 \text{ (q, } J = 7.2 \text{ Hz, } 2 \text{ H), } 4.12 \text{ (q, } J = 7.1 \text{ Hz, } 2 \text{ H), } 3.11 \text{ (d, } J = 5.1 \text{ Hz, } 2 \text{ H), } 1.40 \text{ (t, } J = 7.1 \text{ Hz, } 2 \text{ H$ 3 H), 1.25 (t, J = 7.3 Hz, 3 H), 1.24 (t, J = 7.2 Hz, 3 H). ¹³C NMR (126 MHz, CHCl₃) δ : 171.7

 $(\underline{C}(O)OCH_3)$, 156.1 (OC(O)NH), 153.8 (OC(O)O), 150.4 (C4'), 133.9 (C1'), 130.6 (C2'), 121.3 (C3'), 65.1 (CH₃CH₂OC(O)O), 61.8 (CH₃CH₂OC(O)), 61.4 (CH₃CH₂OC(O)NH), 54.9 (C₀), 38.0 (C_{\beta}), 14.7 (\overline{C}H₃CH₂OC(O)O), 14.4 (\overline{C}H₃CH₂OC(O)), 14.3 (\overline{C}H₃CH₂OC(O)NH). (See Figure A 12-14 for NMR spectra)

5.2.5.3. 4'-O,3-N-Di(ethoxycarbonyl)- β -tyrosine Ethyl Ester

A mixture of ethyl (33 mol%) and methyl (67 mol%) esters of 4'-O,3-N-di(ethoxycarbonyl)-βtyrosine was isolated ($R_f = 0.38$) at 68% yield (24 mg). The *ethyl* ester of the β -tyrosine derivative was used in the GC/EIMS analyses of labeled and unlabeled biosynthetic β-tyrosines. Thus, authentic ethyl ester was purified by silica gel TLC (90:10 hexane:ethyl acetate). 4'-0,2-N-Di(ethoxycarbonyl)-β-tyrosine ethyl ester was isolated at 23% yield (8 mg). Exact mass [M + H + Pyridine]⁺ observed 433.1922 & calculated 433.1974 for $[C_{22}H_{29}N_2O_7]^+$. ¹H NMR (500 MHz, CDCl₂) δ : 7.30 (d, J = 8.8 Hz, 2 H), 7.12 (d, J = 8.8 Hz, 2 H), 5.67 (d, J = 6.8 Hz, 1 H), 5.12 (br. s., 1 H), 4.28 (q, J = 7.3 Hz, 2 H), 4.08 (q, J = 6.8 Hz, 2 H), 4.05 (q, J = 7.0 Hz, 2 H), 2.91 - 2.69(m, 2 H), 1.36 (t, J = 7.1 Hz, 3 H), 1.20 (t, J = 6.8 Hz, 3 H), 1.14 (t, J = 7.3 Hz, 3 H). (See Supporting Information Figures S17 – S19 for NMR spectra and GC/EIMS fragmentation data). ¹³C NMR (126 MHz, CDCl₂) δ: 170.7 (<u>C</u>(O)OCH₂CH₂), 155.8 (OC(O)NH), 153.5 (OC(O)O), 150.3 (C4'), 138.8 (C1'), 127.4 (C2'), 121.3 (C3'), 64.8 (CH₂CH₂OC(O)O)), 61.0 $(CH_2CH_2OC(O)), 60.7 (CH_2CH_2OC(O)NH), 51.0 (C_B), 40.6 (C_g), 14.5 (CH_2CH_2OC(O)O), 14.1 (CH_2CH_2OC(O)O), 1$ (CH3CH2OC(O)), 14.0 (CH3CH2OC(O)NH). (Figure A 15-18 for GC/EIMS fragmentation data and NMR spectra). 4'-0,3-N-Di(ethoxycarbonyl)- β -tyrosine Methyl Ester was isolated ($R_{\rm f}$ = 0.54) at 46% yield (16 mg). Exact mass [M + H + Pyridine] observed 419.1770 & calculated 419.1818 for $[C_{21}H_{27}N_2O_7]^{+}$. ¹H NMR (500 MHz, CDCl₃) δ : 7.29 (d, J = 8.5 Hz, 2 H), 7.12 (d, J = 8.5 Hz, 1 H), 5.66 (br. s., 1 H), 5.17 - 5.07 (m, 1 H), 4.28 (q, J = 6.9 Hz, 2 H), 4.08 (q, J = 7.3 Hz, 2 H), 3.60 (s, 3 H), 2.90 - 2.73 (m, 2 H), 1.36 (t, J = 7.3 Hz, 3 H), 1.20 (t, J = 7.0 Hz, 3 H). ¹³C NMR (126 MHz, CD₃COCD₃) δ : 170.7 (\underline{C} (O)OCH₃), 155.9 (OC(O)NH), 153.4 (OC(O)O), 150.5 (C4'), 140.3 (C1'), 128.4 (C2'), 121.7 (C3'), 65.0 (CH₃CH₂OC(O)O), 64.4 (CH₃CH₂OC(O)NH), 60.0 (C(O)OCH₃), 51.0 (C_{β}), 40.2 (C_{α}), 14.1 (\underline{C} H₃CH₂OC(O)O), 13.6 (\underline{C} H₃CH₂OC(O)NH). (See Figure A 18-20 for NMR spectra).

5.2.6. Synthesis of [Rh(NBD)₂]ClO₄ Complex.

The $[Rh(NBD)_2]CIO_4$ complex was synthesized according to a described process. ¹¹⁷⁻¹¹⁸ Briefly, a mixture of dimeric $[Rh(NBD)Cl]_2$ (0.46 g, 1 mmol) and norbornadiene (0.19 g, 2 mmol) dissolved in CH_2Cl_2 (15 mL) was added to silver perchlorate (0.42 g, 2 mmol) under N_2 , and stirred for 1 h. The suspension was filtered to remove the white precipitate, and the filtrate was diluted with dry THF (15 mL). The sample was concentrated under vacuum until the orange needles of $[Rh(NBD)_2]ClO_4$ appeared. The crystals were collected, washed with ice-cold, dry THF, and dried under vacuum to obtain 0.65 g (85% isolated yield) of rust brown crystals. ¹H NMR (500 MHz, CDCl₂) δ : 5.20 (q, J = 2.0 Hz, 4 H), 4.13 (br s, 2 H), 1.51 (t, J = 1.6 Hz, 2 H).

5.2.7. Synthesis of $[Rh(NBD)((R)-Prophos)]ClO_4$ Complex.

The Rh-Prophos catalyst was prepared by an established procedure. ¹¹⁷ ¹¹⁸ To the orange-red solution of [Rh(NBD)₂]ClO₄ (0.54 g, 1.4 mmol) and (*R*)-Prophos (0.57 g, 1.4 mmol) dissolved in

a mixture of dry CH_2Cl_2 and THF (5 mL of each) was added hexane (5 mL) dropwise under N_2 . The solution stood, undisturbed at room temperature for 5 h, and then at 5 °C for 16 h. Orangered crystals were collected by vacuum filtration and washed with ice-cold, dry THF and then with hexane. The crystals were dried under N_2 to obtain 0.8 g (80% isolated yield) of the Rhcatalyst. 1H NMR (500 MHz, $CDCl_3$) δ : 7.79 - 7.73 (m, 2 H), 7.72 - 7.67 (m, 3 H), 7.65 - 7.61 (m, 2 H), 7.61 - 7.58 (m, 6 H), 7.58 - 7.55 (m, 6 H), 7.47 - 7.41 (m, 2 H), 7.35 - 7.29 (m, 2 H), 5.42 (br. s., 2 H), 5.33 (br. s., 1 H), 5.31 (s, 1 H), 4.87 (br s, 1 H), 4.28 (br s, 1 H), 4.16 (br s, 1 H), 3.84 - 3.67 (m, 1 H), 2.71 - 2.59 (m, 2 H), 2.57 (d, J = 2.2 Hz, 1 H), 2.04 (td, J = 7.4, 12.9 Hz, 1 H), 1.88 - 1.84 (m, 1 H), 1.84 - 1.76 (m, 2 H), 1.20 (dd, J = 6.5, 12.3 Hz, 4 H). ^{13}C NMR (126 MHz, DMSO-d₆) δ : 143.1, 135.1, 135.1, 134.8, 134.5, 134.1, 133.9, 132.8, 132.7, 132.0, 131.9, 131.7, 131.1, 131.0, 130.9, 130.1, 129.3, 129.3, 128.9, 128.8, 128.8, 128.6, 128.5, 128.2, 127.8, 125.9, 125.5, 67.0, 63.4, 48.2, 25.1, 14.8, 14.6.

5.2.8. Synthesis of [²H]-Labeled (2S)-1 Isotopomers

5.2.8.1. Synthesis of (Z)-2-Benzamido-3-(4'-hydroxyphenyl)acrylic Acid

According to a described procedure, 119 a mixture of 4-hydroxybenzaldehyde (1.9 g, 12.5 mmol), K_2HPO_4 (2.2 g, 12.5 mmol), and acetic anhydride (3.8 mL, 40 mmol) was stirred and heated at 80 °C under N_2 for 5 min. To the mixture was added hippuric acid (2.3 g, 12.5 mmol) in one lot, and the reaction was stirred at 80 °C for 2 h. Yellow crystals were collected by vacuum filtration and washed with water to obtain an oxazolone intermediate (3.1 g, 81% yield) that was used without further purification. To the oxazolone (3.07 g, 10 mmol) was added 2% NaOH in 70% aqueous ethanol (100 mL), and the suspension was refluxed for 12 h. The reaction

mixture was cooled to room temperature, diluted with distilled water (~50 mL) and titrated with 12 M HCl until precipitation of the product ceased. The mixture was vacuum filtered, washed with distilled water, dried, and recrystallized from ethanol:water (70:30, v/v) to obtain 3 g (85% yield) of the desired product. 1 H NMR (500 MHz, DMSO-d₆) δ : 12.49 (br s, 1 H), 9.91 (s, 1 H), 9.77 (s, 1 H), 7.99 (d, J = 7.1 Hz, 2 H), 7.59 (t, J = 7.3 Hz, 1 H), 7.54 (dd, J = 3.4, 8.8 Hz, 3 H), 7.51 (d, J = 7.3 Hz, 1 H), 6.77 (d, J = 8.7 Hz, 2 H, 13 C NMR (126 MHz, DMSO-d₆) δ : 166.6, 165.9, 158.8, 134.0, 133.7, 131.9, 131.8, 128.5, 128.3, 127.7, 127.5, 124.6, 124.0, 115.5, 115.4. (See Figure A 20 for crystallographic data).

5.2.8.2. Synthesis of (Z)-2-Benzamido-[3-²H]-3-(4'-hydroxyphenyl)acrylic Acid

The [3- 2 H]-acrylic acid isotopomer was synthesized analogously to the unlabeled isomer (above), except [α - 2 H]-4'-Hydroxybenzaldehyde (0.62 g, 5 mmol) was used. Acetic anhydride (1.6 mL, 17 mmol), K $_2$ HPO $_4$ (0.9 g, 5 mmol), and hippuric acid (0.9 g, 5 mmol) were varied to make the intermediate oxazolone (1.26 g, 82 % yield). The oxazolone (1.23 g, 4 mmol) was saponified under reflux with ethanolic NaOH as before. The mixture was diluted with distilled water (25 ml), and the product was precipitated by the adding 12 M HCl at room temperature. The suspension was worked up and the product was recrystallized as described previously to obtain 1 g (88% yield) of product. 1 H NMR (500 MHz, DMSO-d $_6$) δ : 12.49 (s, 1 H), 9.91 (s, 1 H), 9.77 (s, 1 H), 7.99 (d, J = 7.1 Hz, 1 H), 7.60 (t, J = 7.3 Hz, 1 H), 7.56 - 7.48 (m, 4 H), 6.77 (d, J = 8.8 Hz, 1 H). 13 C NMR (126 MHz, DMSO-d $_6$) δ : 166.6, 165.9, 158.8, 133.8, 131.9, 131.8, 131.6, 128.5, 128.4, 127.7, 127.5, 124.6, 123.9, 115.6, 115.4. (See Figure A 20 for crystallographic data).

5.2.8.3. Synthesis of (2S,3S)- $[2,3-^2H_2]$ - and (2S,3R)- $[3-^2H]$ -1

The following procedure is based on previously described methods. 117, 118, 120 (Z)-2- $Benzamido-[3-{}^2\!H]-3-(4'-hydroxyphenyl) \ acrylic \ acid \ (1\ g,\ 3.5\ mmol) \ and \ 10\ mg \ of$ $[Rh(NBD)((R)-Prophos)]ClO_4$ were dissolved in dry THF (25 mL) in a Parr reactor. The reactor was successively evacuated and filled with H₂ gas and kept under H₂ gas (2.0 bar) for 16 h. The solvent was evaporated, followed by azeotropic removal of residual THF with methanol. To the resultant yellow residue dissolved in methanol (15 mL) was added dry Dowex 50 W (100-200 mesh) cation exchange resin (1.5 g). The mixture was stirred until a clear solution was obtained, and then filtered. The retained resin was washed with warm methanol. All methanol filtrates were combined and dried under vacuum to obtain the crude N-benzoyl-(2S,3R)-[3-2H]-tyrosine (0.9 g). The product was then refluxed with 40% HBr (aqueous) (10 mL) for 3 h. The mixture was cooled to room temperature, and the benzoic acid crystals were removed by filtration. The filtrate was washed with diethyl ether $(3 \times 20 \text{ mL})$ to remove residual benzoic acid. The aqueous layer was lyophilized, and the crude product was dissolved in 0.2 M NaOH (10 mL) and acidified with acetic acid to yield crystals after 1h at 0 °C. The product was isolated by vacuum filtration and the retentate was washed with ice cold water to yield (2S,3R)-[3-2H]-1 as its zwitterionic amino acid (0.41 g, 70% yield).

(2S,3S)- $[2,3^{-2}H_2]$ - $\mathbf{1}$ was synthesized by a procedure analogous to that described for the synthesis of (2S,3R)- $[3^{-2}H]$ - $\mathbf{1}$ with the following exceptions. (*Z*)-2-Benzamido-3-(4'-hydroxyphenyl)acrylic acid was used instead of the unlabeled isotopomer, and D_2 gas was used

in place of H_2 gas for the reduction step to obtain (2S,3S)- $[2,3-^2H_2]$ - $\mathbf{1}$ as the zwitterionic amino acid (038 g, 65% yield).

5.2.9. Characterization of (2S,3S)- $[2,3-{}^{2}H_{2}]$ - and (2S,3R)- $[3-{}^{2}H]$ -1

(2S,3S)- $[2,3-^2H_2]$ - and (2S,3R)- $[3-^2H]$ -**1** (1 µmol of each) were separately derivatized to their 4'-O,2-N-di(ethoxycarbonyl) derivatives in water (1 mL) with ethyl chloroformate (50 µL, 0.5 mmol) and pyridine (50 µL, 0.6 mmol), and the samples were acidified to pH 2 (6M HCl) and extracted into diethyl ether (1 mL). After treatment of the ethanolic extract with diazomethane, the derivatives were isolated as a mixture of ethyl (10 mol%) and methyl (90 mol%) esters, as described before. The methyl esterified amino acid derivative was analyzed by GC/EIMS. The $[^2H]$ -labeled fragment ions originating from the identically derivatized (2S)- $[3,3-^2H_2]$ -**1** were used to interpret the structures of various ions. The relative ratio of diagnostic $[^2H]$ -labeled ions was compared to that of identical fragment ions of the unlabeled (S)-1 derivative to calculate the deuterium enrichment of labeled isotopomers: (2S,3S)- $[2,3-^2H_2]$ -**1** and (2S,3R)- $[3-^2H]$ -**1** (Table A 1, and Figure A 28-31).

The coupling constants (J) for the geminal protons (H_A and H_B) against H_X observed by 1H NMR for authentic (S)-1 in D_2O were $J_{AX} = 5.0$ Hz at δ 3.23 (H_A) and $J_{BX} = 7.8$ Hz at δ 3.08. 121 In a previous study, the preferred conformation of (S)-1 in water was established by NMR using stereospecifically deuterium isotopomers of 1 to correlate chemical shift and the magnitude of coupling constants with the conformation of the prochiral hydrogens. 122 These earlier findings put the dihedral angle between the carboxy group and the aromatic ring at 180° . In this

conformation, H_A and H_X were separated by ~ 60°, and H_B and H_X by 180°. Using this earlier data along with the magnitude of the *J*-values¹²² observed for (*S*)-1, we assigned H_A as pro-(3*S*) and H_B as pro-(3*R*). This data was used to assign the absolute stereochemistry at C_β of the synthetic (2*S*,3*S*)-[2,3- 2 H₂]- and (2*S*,3*R*)-[3- 2 H]-1.

Authentic (*S*)-**1** (10 mg) was dissolved in D₂O (1 mL), and transferred to a 5 mm diameter NMR tube, and analyzed by 1 H NMR [(500 MHz, D₂O, 32 scans, 25 °C) δ : 7.23 (d, J = 8.5 Hz, 2 H), 6.93 (d, J = 8.5 Hz, 2 H), 3.97 (dd, J = 5.1, 7.8 Hz, 1 H), 3.23 (dd, J = 5.0, 14.7 Hz, 1 H), 3.08 (dd, J = 7.8, 14.7 Hz, 1 H)]. (2*S*,3*S*)-[2,3- 2 H₂]- and (2*S*,3*R*)-[3- 2 H]-**1** (10 mg of each) were separately dissolved in D₂O (and H₂O) and analyzed by 1 H NMR (and 2 H NMR). (2*S*,3*S*)-[2,3- 2 H₂]-**1**: 1 H NMR (500 MHz, D₂O, 32 scans, 25 °C) δ : 7.23 (d, J = 8.5 Hz, 2 H), 6.93 (d, J = 8.5 Hz, 2 H), 3.07 (s, 1 H). 2 H NMR (77 MHz ,H₂O, 512 scans, 25 °C) δ : 7.23 (d, J = 8.3 Hz, 2 H), 6.93 (d, J = 8.8 Hz, 2 H), 3.97 (d, J = 4.9 Hz, 1 H), 3.22 (d, J = 4.9 Hz, 1 H). 2 H NMR (77 MHz, H₂O, 512 scans, 25 °C) δ : 3.07 (bs, 1 H)

5.2.10. Synthesis of Authentic 4'-O,3-N-Di((S)-2-methylbutanoyl) Methyl Esters of (R)- and (S)-2

To a sample of (R)-and (S)-2 (0.5 μ mol of each) dissolved in 50 mM phosphate buffer (1 mL) were added pyridine (50 μ L, 0.6 mmol) and (S)-2-methylbutyric anhydride (10 μ L, 5 μ mol) at 0 °C. The reactions were stirred for 5 min and treated with another batch of pyridine (50 μ L) and (S)-2-methylbutyric anhydride (10 μ L) and stirred for 5 min. The mixtures were each acidified

(pH 2 with 6 M HCl) and extracted with diethyl ether (3 \times 2 mL). The ether fractions were combined, dried under vacuum, and the residue was dissolved in methanol (100 μ L). To this solution was added a dilute diazomethane solution dissolved in diethyl ether, until the yellow color persisted. The resultant 4'-O,3-N-di((S)-2-methylbutanoyl)- β -tyrosine methyl ester diastereoisomers were analyzed by GC/EIMS; their retention times and fragment ions are noted in Figure A 38-40

5.2.11. Assessing the Stereospecificity of the C_{β} -Hydrogen Abstraction Catalyzed by CcTAM

(2*S*,3*S*)-[2,3- 2 H₂]- and (2*S*,3*R*)-[3- 2 H]-**1** (each at 1 mM) were separately incubated with *Cc*TAM (0.1 mg) at 31 °C in 50 mM phosphate buffer (1 mL, pH 8.5) for 1 h. The tyrosine isomers were derivatized *in situ* with ethyl chloroformate (50 μL, 0.5 mmol) and pyridine (50 μL, 0.6 mmol) to their 4'- O N-di(ethoxycarbonyl) derivatives. The samples were acidified to pH 2 (6M HCl) and extracted into diethyl ether (1 mL). After treatment of the extract with excess diazomethane, the amino acid derivatives were isolated as a mixture of ethyl and methyl esters and analyzed by GC/EIMS, as before. Diagnostic fragment ions from the ethyl ester derivative of the biosynthetic β-**2** were analyzed to determine the regiochemistry of the deuterium atoms.

5.2.12. Assessing the Stereospecificity of the Hydrogen Rebound at C_{α} Catalyzed by CcTAM

(2S)- $[3,3-{}^{2}H_{2}]$ -**1** (5 mM) was incubated with CcTAM (0.8 mg) at 31 °C in 50 mM phosphate buffer (40 mL, pH 8.5) for 36 h. The incubation mixture was lyophilized, and the remaining residue was dissolved in methanol (7 mL) for ${}^{2}H$ -NMR analysis or CD₃OD (7 mL) for ${}^{1}H$ -NMR

analysis. As a control sample, authentic unlabeled (R)-2 (2 mM) in 50 mM phosphate buffer (40 mL, pH 8.5) was lyophilized, and the remaining residue was dissolved in CD₃OD (7 mL) for ¹H-NMR analysis. The magnitude of the coupling constants of the ABX spin system observed in the ¹H NMR for authentic unlabeled (R)-2 in CD₃OD was used to assign the chemical shifts of the protons at the prochiral center of 2. This data was then used to assign the absolute stereochemistry at C_{α} of the biosynthetic [²H]-2.

5.2.13. Assessing the Intramolecular Proton Transfer Step of the CcTAM Reaction

(2*S*)-[3,3- 2 H₂]-**1** (1 mM) was incubated with *Cc*TAM (0.1 mg) at 31 °C in 50 mM phosphate buffer (10 mL, pH 8.5). Aliquots (1 mL) were withdrawn from the reaction mixture at 10 min, then at 2, 4, 7, 12, 22, 33 and 45 h. The samples were derivatized *in situ* with ethyl chloroformate (50 μL, 0.5 mmol) and pyridine (50 μL, 0.6 mmol) to their 4'-O,N-di((ethoxycarbonyl)) derivatives, acidified to pH 2 (6M HCl), and extracted into diethyl ether (1 mL). After treatment of the ethanolic extract with diazomethane, the amino acid derivatives were isolated as a mixture of ethyl and methyl esters. During the derivatization, 4'-hydroxycinnamate was converted to its 4'-O-(ethoxycarbonyl)-(*E*)-coumaric acid as an ethyl and methyl ester mixture. The methyl esters of the α-tyrosine and (*E*)-coumaric acid derivatives and the ethyl ester of the β-tyrosine derivative were analyzed by GC/EIMS (see Figure A 44-46) for representative diagnostic fragment ions observed for the derivatized biosynthetic **2** and 4'-hydroxycinnamate in this time course study). GC/EIMS was used in selected-ion mode to calculate the ion abundance ratio of $[^{2}$ H₁](M)⁺ (m/z 354) and $[^{2}$ H₂](M)⁺ (m/z 355) for the derivatives of the biosynthetic deuterium labeled **2**. This ratio informed on the D \rightarrow H exchange during the reaction. The ion abundance of

 $[^{2}\text{H}_{2}](M)^{+}$ (m/z 355) was corrected by subtracting the abundance of the naturally occurring ^{13}C isotopomer (i.e., the $[^{2}\text{H}_{1}](M+1)^{+}$ (m/z 355) of the molecular ion $[^{2}\text{H}_{1}](M)^{+}$ (m/z 354)) of the singly deuterium-labeled derivative.

5.2.14. Assessing the Effect of pH on CcTAM Stereoselectivity

(S)-1 (1 mM) was incubated with CcTAM (0.1 mg) separately at pHs 7, 8, and 9 (6 mL of each) in 50 mM phosphate buffer at 31 °C. Aliquots (1 mL) were withdrawn at 1, 2.5, 5, 11, and 25 h. The amino acids were derivatized *in situ* with (S)-2-methylbutyric anhydride to form the 4'-O,3-N-di((S)-2-methylbutanoyl)-2 and methyl esterified with diazomethane and analyzed by GC/EIMS. The sum of ion abundances for fragment ions m/z 278 [M – methyl butyl]⁺ (90% of base peak) and m/z 194 [M – (2 × methyl butyl) + H]⁺ (base peak) for each enantiomer was compared to calculate the product ratio of (R)- and (S)-2 in the sample.

5.2.15. Synthesis of (R)-2 Methyl Ester

In brief, to (*R*)-2 (18.1 mg, 0.1 mmol) dissolved in methanol (1 mL, 25 mmol) was added trimethylsilyl chloride (25 μ L, 0.2 mmol). ¹²³ The suspension was stirred for 16 h and the methanol was evaporated *in vacuo* to obtain the (19.5 mg, quantitative yield). ¹H NMR (500 MHz, CD₃OD) δ : 7.29 (d, 8.5 Hz, 2 H), 6.85 (d, 8.5 Hz, 2 H), 4.63 (dd, J = 6.3, 7.8 Hz, 1 H), 3.69 (s, 3 H), 3.09 (dd, J = 7.8, 17.0 Hz, 1 H), 2.98 (dd, J = 6.3, 17.0 Hz, 1 H).

5.3. Results

5.3.1. CcTAM Activity and Stereochemistry

*Cc*TAM was expressed from the pET-28a(+) vector in *Escherichia coli* (BL21), and then *Cc*TAM and (*S*)-1 were incubated. The amino acids and hydroxycinnamate were derivatized and analyzed by GC/EIMS to show that product 2 (90 mol %) and by-product 4'-hydroxycinnamate (10 mol %) were formed (Figure A 40 and Figure A 41). The biosynthetic β-tyrosine was also derivatized with a chiral auxiliary that indicated a mixture containing (*R*)-2 and (*S*)-2 at an 85:15 ratio (See Figure A 38 and Figure A 39). This product distribution was consistent with that shown in an earlier study.⁴⁶

5.3.2. Assignment of the Prochiral Hydrogens of (R)-2 by ¹H-NMR

The 1 H-NMR of authentic unlabeled (R)-2 showed signals at δ 4.41 (dd, J = 4.4, 10.1 Hz, C_{β} -H), 2.73 (dd, J = 10.1, 16.6 Hz, C_{α} -H), 2.61 (dd, J = 4.4, 16.7 Hz, C_{α} -H) in CD₃OD solvent (Figure 5.1). According to the Karplus equation for 1 H NMR, 124 3 3 3 3 3 4 5

spin-coupled with C_{β} -H (designated as the X spin) were identified by their distinct *J*-values [AX ($^3J_{\rm AX}$ = 10.1 Hz, $\phi \approx 180^\circ$) and BX ($^3J_{\rm BX}$ = 4.4 Hz, $\phi \approx 60^\circ$)] (Figure 5.4).

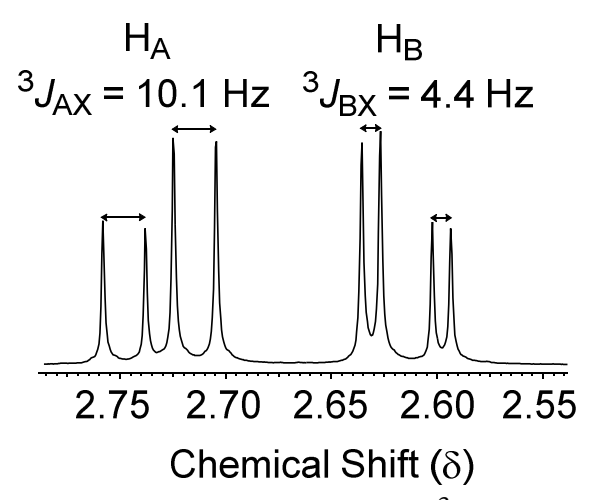


Figure 5.1. Partial ¹H-NMR profile of unlabeled 2 and the ³*J* coupling constants for the ABX spin system of (R)-2.

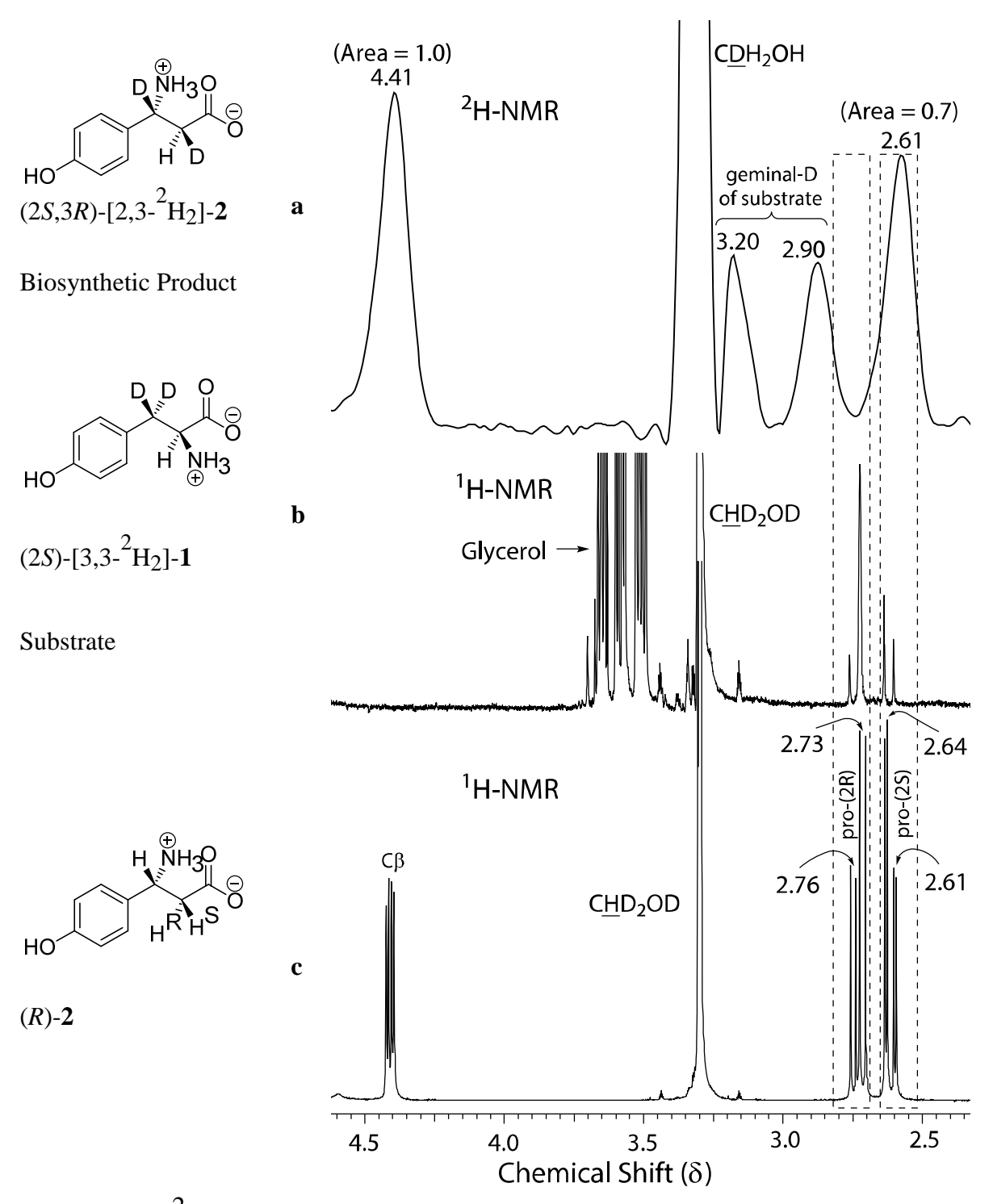


Figure 5.2. a) ²H-NMR (after solvent exchange into CH₃OH); the relative area of the peaks at δ 4.41 and 2.61 are shown and b) ¹H-NMR (after solvent exchange into CD₃OD) of a mixture

Figure 5.2 (cont'd).

containing the remaining substrate (2S)- $[3,3-{}^2H_2]$ -1 and the biosynthetic (2S,3R)- $[2,3-{}^2H_2]$ -2 after a CcTAM-catalyzed reaction.c) 1H -NMR (in CD₃OD) of authentic (R)-2. The signals for the prochiral protons of authentic (R)-2 are aligned (boxes) with signals for the deuterium labeled product in the biosynthetic sample.

5.3.3. Using NMR to Assess the Mechanism of the Hydrogen Transfer at ${\bf C}_{\alpha}$ in the ${\it Cc}$ TAM Reaction

The ${}^2\text{H-NMR}$ chemical shifts of the propanoid side chain deuteriums at C_{α} and C_{β} of $[{}^2\text{H}_2]$ -2 biosynthesized from (2S)-[3,3- ${}^2\text{H}_2]$ -1 by *Cc*TAM were at δ 2.61 (relative peak area = 0.7) and 4.41 (relative peak area = 1.0), respectively (Figure 5.2a). The deuterium signals were compared to the ${}^1\text{H-NMR}$ chemical shifts of the prochiral hydrogens of authentic (*R*)-2 (Figure 5.2a and Figure 5.2c) to assign the absolute stereochemistry of the $[{}^2\text{H}]$ -labeled biosynthetic sample.

The ¹H-NMR signal at δ 2.73 (singlet) produced by the biosynthetic [²H]-labeled (*R*)-2 (Figure 5.2b) coincided with the chemical shift of the *pro*-(2*R*) proton of authentic (*R*)-2 (Figure 5.2c). Two nearby doublets were also observed at δ 2.75 (d, J = 16.8 Hz, 1 H) and 2.63 (d, J = 16.8 Hz, 1 H) with a peak area that was ~30% of the singlet at δ 2.73 (Figure 5.2b). These resonances corresponded to a [²H]-labeled isotopomer of 2 containing two geminal hydrogens at C_{α} creating an AB-coupled spin system.

5.3.4. Assessing the Mode of the Amino Group Attachment at C_{β} by CcTAM.

5.3.4.1. Synthesis of (2S,3S)- $[2,3-{}^2H_2]$ - and (2S,3R)- $[3-{}^2H]$ -(S)-1

The mode of the amino group transfer to C_B during the isomerization reaction catalyzed by CcTAM was assessed. (2S,3S)- $[2,3^{-2}H_2]$ - and (2S,3R)- $[3^{-2}H]$ -1 were synthesized by [3-²H]-labeled stereospecific reduction of unlabeled and (Z)-2-benzamido-3-(4'hydroxyphenyl)acrylic acid using a chiral [Rh((R)-Prophos)(NBD)]ClO4 catalyst with deuterium or hydrogen gas, according to an earlier procedure. 117 The [2H]-labeled isotopomers of 1 were treated with a chiral auxiliary (S)-2-methylbutyric anhydride and titrated with diazomethane to make the 4'-O,3-N-di((S)-2-methylbutanoyl)- α -tyrosine methyl ester derivatives. The retention times and mass spectrometry fragmentation of the synthesized [2H]-labeled (S)-1 derivatives observed by GC/EIMS analysis were identical to those of an identically derivatized sample of authentic (S)-1.

5.3.5. Analysis of 2 Made by CcTAM Catalysis from (2S,3S)- $[2,3-^2H_2]$ - and (2S,3R)- $[3-^2H]$ -

CcTAM was incubated separately with (2S,3S)- $[2,3-{}^{2}H_{2}]$ - and (2S,3R)- $[3-{}^{2}H]$ -1. Afterwards, the reaction was basified, and the amino acids were derivatized to their 4'-O,3-N-di(ethoxycarbonyl) derivatives, acidified, extracted from the aqueous reaction buffer, and reacted with diazomethane to make the methyl esters. Interestingly, during the basification step of the derivatization procedure, ethanol by-product from the excess ethyl chloroformate caused partial ethyl esterification of the amino acids (10-30 mol% compared to the methyl esters).

Table 5.1. EI-MS Fragmentation of 4'-O,3-N-Di((ethoxycarbonyl)) Ethyl Ester Derivatives of Labeled and [2 H]-Labeled Biosynthesized Isotopomers of 2

| 1) CcTAM 2) Ethyl chloroformate/pyridine 3) pH < 2 4) Extract with diethyl ether (3 ×) 5) CH ₂ N ₂ m/z 353 | | | |
|--|---|--|---|
| Isotopomers of Substrate 1 | Fragment ion F1: Cleavage at bond a | Fragment ion F2: Cleavage at bond b | Fragment ion F3: Cleavage at bonds b and c; H-transfer ^g to O |
| HO NH ₃ | $\begin{bmatrix} NHO \\ O \\ O \end{bmatrix}^+$ | Ο Ο ΝΗ Ο βΗ | O NH HO HO |
| a (2S)-unlabeled | m/z 280 | m/z 266 | m/z 194 |
| H D O NH ₃ | NHO O DD(H) m/z 282 (m/z 281 D→H | O NH | O NH HO H |
| b $(2S,3S)$ - $[2,3-^2H_2]$ | exchange) | m/z 266 | m/z 194 |
| D H O O O O O O O O O O O O O O O O O O | NHO + | O NH O D | O NH HO D |
| c $(2S,3R)$ - $[3-^2H]$ | m/z 281 | m/z 267 | m/z 195 |
| D D O O O O O O O O O O O O O O O O O O | NHO D H | O NH O D | HO O NH D |
| d (2S)-[3,3- ² H ₂] | <i>m/z</i> 282 (<i>m/z</i> 281 D→H exchange) | m/z 267 | m/z 195 |

^gD-transfer was negligible compared to H-transfer based on analysis of mass spectrometry fragments

The mass spectrum of the *methyl* ester derivatives of the β -isomers yielded ions of diagnostic labeled fragments that were perturbed by overlapping satellite fragment ions. Therefore, the ethyl esters of the β -isomers were separated by GC, and the fates of the deuteriums on the β -amino acids, originating from the substrate, were evaluated by the identity of diagnostic fragment ions made in the mass spectrometer (Figure A 41, Figure A 42, and Figure A 43 for fragment ions). The molecular ion [M+] (m/z 353) of the 4'-O,3-N-di(ethoxycarbonyl) ethyl ester derivative of unlabeled (R)-2 fragmented into diagnostic ions F1A, F2A, and F3A (m/z 280, 266, and 194, respectively) (Table 1A). The corresponding fragment ions of the derivatized β-amino acid biosynthesized by CcTAM from (2S,3S)- $[2,3-{}^{2}H_{2}]$ -1 were **F1B**, **F2B**, and **F3B** (m/z) 282, 266, and 194, respectively, Table 1b). Fragment ions **F2B** (m/z) 266 and **F3B** (m/z) 194 are identical to those of the unlabeled derivatized product (Table 1a), indicating that deuterium was not at C_{β} of the biosynthetic 2. Further, the fragment ion F1B (m/z 282, Table 1b) corresponding to the intact phenylpropanoid was shifted by two mass units above the similar fragment ion of the unlabeled isotopomer. These data indicate that both deuteriums are at C_{α} of the biosynthetic product derived from (2S,3S)- $[2,3-{}^{2}H_{2}]$ -1. Notably, the mass spectrum of the biosynthetic product 2 made from (2S,3S)- $[2,3-{}^{2}H_{2}]$ -1 showed a molecular ion $([{}^{2}H_{2}](M)+, m/z = 355)$ and ion m/z = 354([2H₁](M)+), one mass unit lower (Table 1b), indicating 36% deuterium was lost from the product compared to the substrate. This deuterium-to-hydrogen (D→H) exchange during the CcTAM isomerization of (2S,3S)-[2,3-2H₂]-1 was also supported by the ratio of diagnostic fragment ion F1B (m/z 282) (Table 1b) and its [F1B – 1] partner (m/z 281), showing 32% deuterium loss. Conversely, when (2S,3R)-[3-2H]-1 was used as the substrate with CcTAM, the resulting derivatized [2 H]-labeled 2 yielded fragment ion F1C (m/z 281) that was shifted one

mass unit over its unlabeled counterpart (Table 1c), indicating retention of one deuterium in the propanoid side chain. Fragment ions **F2C** (m/z 267) and **F3C** (m/z 195) (Table 1c) were also one mass unit higher than the corresponding fragments derived from the unlabeled product. The latter clarified that the deuterium at C_{β} of the substrate remained at this position after the CcTAM isomerization reaction to **2**.

5.3.6. Assessing the D \rightarrow H Exchange Rate during CcTAM Catalysis

(2S)- $[3,3-{}^{2}H_{2}]$ -1 was incubated with CcTAM in a time course experiment to assess the extent of the D \rightarrow H exchange during the isomerization (Table 1d). The β -amino acids isolated at designated time intervals were derivatized to their 4'-0,3-N-di(ethoxycarbonyl) ethyl esters and analyzed by GC/EIMS, as before. Tracking the molecular ion $[^{2}H_{2}](M)+(m/z 355)$ and its $[^{2}H_{1}](M)$ + partner (m/z 354) showed that the deuterium enrichment decreased from 85% at 10 min to 60% after 12 h, under steady state reaction conditions. After 45 h, the reaction reached equilibrium (70% conversion of substrate to products 4'-hydroxycinnamate and 2, and the D > H exchange stabilized at 30% deuterium retention (see Table 1d, Figure A 43, Figure A 44, Figure A 45). Moreover, the relative abundances of fragment ions **F2D** (m/z 267) and **F3D** (m/z 195)(Table 1d) (both one mass unit above their unlabeled counterparts) from the derivatized biosynthetic product 2, at each time point, confirmed that a deuterium remained at C_{β} . Thus, one of the geminal deuteriums of (2S)-[3,3- 2 H₂]-1 was 100% retained at C_{β} of the product, while the migratory deuterium was partially exchanged with hydrogen. This deuterium loss during the reaction was supported by the parallel decrease in the ratio between ion F1D (m/z 282) (a fragment containing two deuteriums, one at C_{α} (exchangeable during catalysis), the other at C_{β} (100% retained)) and ion [**F1D** – 1] (m/z 281) (a fragment containing one deuterium at C_{β}) in the same spectrum (Table 1d and see Figure A 43 as reference).

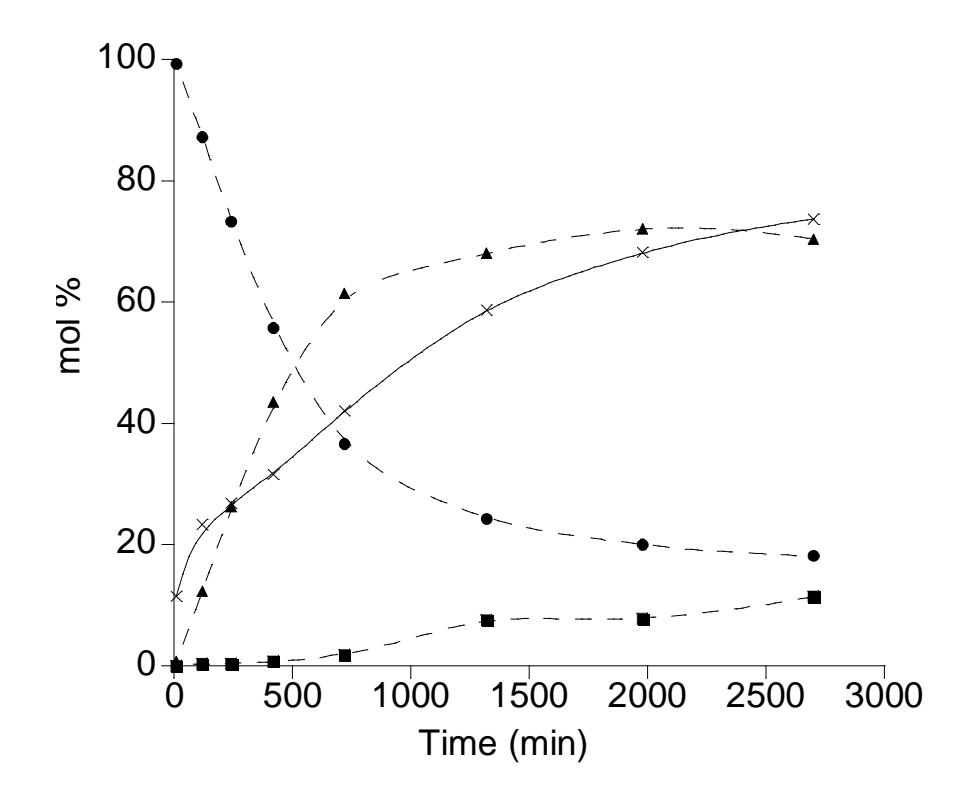


Figure 5.3. Plotted are the D \rightarrow H exchange (×) and (2*S*)-[3,3- 2 H₂]-1 (•), [2,3- 2 H₂]-2 (\blacktriangle), and [3- 2 H]-4'-hydroxycinnamic acid (\blacksquare) (as mol %) during the *Cc*TAM conversion of (2*S*)-[3,3- 2 H₂]-1 to labeled 2.

5.3.7. Re-evaluation of the Stereoisomeric Product Distribution Catalyzed by CcTAM

A previous study on CcTAM reported that the enzyme stereoselectivity was 69% ee for (R)-2 at pH 8.8.46 The earlier study however also showed that (S)-2 was produced at <5 mol% for the duration of the steady state (0 to 4 h) of the reaction containing CcTAM (10-50 μ g), but increased significantly as the reaction entered equilibrium. This interesting perturbation in the production of (R)- and (S)-2 at equilibrium prompted us to re-evaluate this reaction phenomenon.

Here, GC/EIMS was used to separate the diastereoisomeric 4'-O,3-N-di((S)-2-methylbutanoyl)- β -tyrosine methyl ester derivatives of enantiomers of **2** produced by CcTAM at steady state. Even after 1% conversion of the substrate, after 5 min, CcTAM (50 μ g) was already producing an enantiomeric mixture containing 80% ee of (R)-**2** from 1 mM of substrate. The mixture approached 85:15 R:S (i.e., 70% ee of (R)-**2**) at a steady state rate just before reaching equilibrium at 120 min (Figure 5.5). The steady state production of (S)-**2** (from 5 mol% to 15 mol%) over 2 h starkly contrasted the <5 mol% production of (S)-**2** prior to reaching equilibrium over 4 h, as reported earlier.⁴⁶

5.3.8. pH Effect on the Stereoselectivity of the Reaction Catalyzed by CcTAM

The CcTAM reaction was incubated with (S)-1 separately at different pH values. After the conversion of (S)-1 to 2 reached 13, 35, and 56% at each pH, the amount of the (S)-isomer (the minor antipode) relative to the total amount of 2 was calculated. The rate of the reaction was similar at pHs 8 and 9, yet half as fast at pH 7. After the conversion of substrate to product reached ~13% in each assay, the samples incubated at pHs 7, 8, and 9 contained 10.8%, 13.0%, and 16.7% (S)-2, respectively, relative to the (R)-antipode (Figure 5.6). At higher percentages of conversion, the proportion of (S)-2 continued to increase, and the trend of increasing production of (S)-2 with higher pHs was also maintained (Figure 5.6).

5.4. Discussion

5.4.1. Retention of Configuration at the Migration Termini during the CcTAM Reaction.

5.4.1.1. Amino Group Migration

The stereochemistry of the major biosynthetic product **2** made by CcTAM was confirmed herein as (3R); this was consistent with the assignment made in an earlier report. ⁴⁶ The synthesis of stereospecifically deuterium labeled isotopomers (2S,3S)- $[2,3-{}^2H_2]$ - and (2S,3R)- $[3-{}^2H]$ -**1** made it possible to assess the mode of attachment of the amino group at C_β during the isomerization reaction catalyzed by CcTAM. GC/EIMS profiles of derivatized isotopomers of **2** showed diagnostic fragment ions that informed on the location of the deuteriums. Fragment ions **F2B** and **F3B** (Table 2b) revealed that the C_β deuterium of the (2S,3S)- $[2,3-{}^2H_2]$ -**1** substrate was replaced by the amino group en route to **2** (Table 1).

Fragment ion **F1B** revealed that the deuterium migrated reciprocally to C_{α} (Table 2b), thus confirming that CcTAM migrated the pro-(3S) hydrogen from C_{β} to C_{α} . Further, fragments ions **F2C** and **F3C** of the derivatized [2 H]-labeled product (Table 2c) showed complementary that the C_{β} deuterium of the (2S,3R)-[3- 2 H]-substrate was retained at its original position. Coupled with the known (R)-2 stereochemistry made in the aminomutase reaction, the deuterium remaining at C_{β} confirmed that CcTAM uses a retention-of-configuration mechanism at the amino migration terminus.

5.4.1.2. Hydrogen Migration Stereochemistry

The transient C_{β} -deuterium of (2S,3S)- $[2,3^{-2}H_2]$ - $\mathbf{1}$ migrates from C_{β} to C_{α} as the amino group moves reciprocally from C_{α} to C_{β} . The stereochemical mode of attachment of the deuterium to C_{α} was assessed by ${}^{1}H^{-}$ and ${}^{2}H^{-}$ NMR analyses of the zwitterion of the product dissolved in methanol. The magnitude of the difference between the AX and BX coupling constants $(\Delta^{3}J \approx 6 \, \mathrm{Hz})$ of (R)- $\mathbf{2}$ was measure and compared to the experimentally calculated $\Delta^{3}J$ (~7 Hz) for the vicinal protons of the cyclohexane structure. ${}^{125^{\circ}}$ 126 These similar $\Delta^{3}J$ magnitudes calculated for these two structures suggested that the propionate hydrogens of (R)- $\mathbf{2}$ are conformationally restricted as they are in cyclohexane. It can be imagined that a monodentate interaction between the ammonium cation and carboxylate anion of the (R)- $\mathbf{2}$ zwitterion forms a pseudo-staggered six-membered ring to account for the magnitude of the observed $\Delta^{3}J$ (Figure 5.4).

Ho
$$pro-(2S)$$
 $pro-(2R)$ $pro-(2R)$

Figure 5.4. Intramolecular salt-bridge between the ammonium ion and carboxylate group of (*R*)-2 in methanol. Dihedral angles (ϕ_1 and ϕ_2) between H_A and H_X and between H_B and H_X , respectively, in the pseudo six-membered ring formed by 2 are shown in Newman Projection.

To support the proposed restricted rotamer conformation, the carboxylate group of (R)-2 was methyl esterified to disrupt the ionic ammonium/carboxylate ionic interaction. In acyclic systems, the conformational preference of hydrogens in an ABX spin system is commonly lower than in a restricted conformer. As an example, ${}^3J_{(AX)}$ (7.8 Hz) and ${}^3J_{(BX)}$ (6.3 Hz) coupling constants ($\Delta^3J_{(AX)-(BX)}=1.5$ Hz) of the (R)-2 methyl ester were nearly identical in CD₃OD. This observation suggested that H_A and H_B in the (R)-2 methyl ester was conformationally more equivalent with respect to H_X due to greater rotational freedom about the C_α - C_β bond. This likely resulted from removal of the *intramolecular* ionic interaction of underivatized (R)-2 (see Figure 5.4).

The proposed six-membered ring conformation of (R)-2 places the side chain hydrogens of the amino acid in defined axial and equatorial positions by restricted rotation about the C_{α} - C_{β} bond (Figure 5.4). In addition, the carboxylate and aromatic ring of (R)-2 are considered to be positioned *anti*, according to a described lowest energy rotamer of 1. 122 Therefore, based on the 1 H-NMR chemical shifts and coupling constants, H_{A} was definitively assigned as pro-(2R) and H_{B} as pro-(2S) (see Figure 5.1). These chemical shift assignments were used as reference in 1 H- and 2 H-NMR analyses of the deuterium-labeled biosynthetic samples. CcTAM shuttled one deuterium of (2S)-[3,3- 2 H₂]-1 from C_{β} and attached it to C_{α} with retention-of-configuration, placing the deuterium in the formal pro-(2S) position of (R)-2.

Previous stereochemical studies showed that a related MIO-dependent phenylalanine aminomutase from Taxus plants (TcPAM) exchanges the position of the NH_2 and hydrogen migration partners of (S)- α -phenylalanine with retention of configuration at the terminal

carbons.⁵ Thus, the CcTAM and TcPAM reactions are likely mechanistically similar,⁶⁶ where both remove NH₂ and H from their substrates to form an acrylate intermediate. Apparently, these enzymes can rotate their intermediates 180° about the C_1 - C_{α} and C_{β} - C_{ipso} bonds prior to the rebound of NH₂ and H to retain the stereochemistry in the corresponding β -products.³⁸

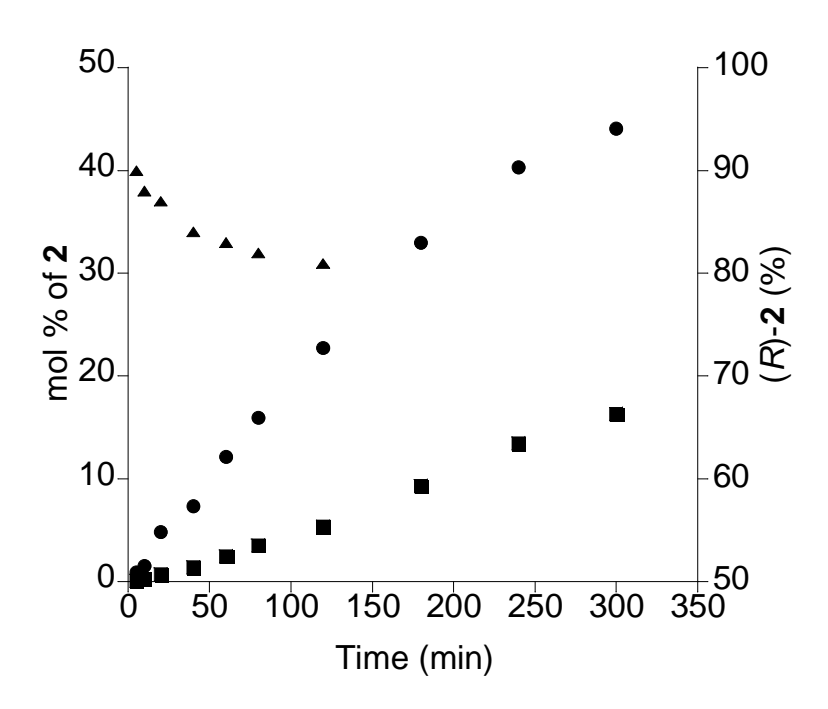


Figure 5.5. Analysis of the diastereomeric mixture of products catalyzed by CcTAM. Plotted are mol % of (R)-2 (\bullet) and (S)-2 (\blacksquare) relative to amount of (S)-1 added. The amount of (R)-2 (as %) (\blacktriangle) relative to the total amount of (R)- and (S)-2 made at steady state. (Average of duplicate assays is plotted).

It is important to note that (R)-2 produced by CcTAM decreased from 90% to 80% (while (S)-2 increased accordingly) during the steady state phase of the reaction from 5 to 120 min (Figure 5.5). The isotope enrichment in fragment ion clusters of the biosynthetic $[^2H]$ -2 (Table 1) in the mass spectrometer did not indicate that the (S)-isomer was labeled regionselectively different from (R)-2. In addition, 2H -NMR analysis of the labeled mixture of 2 indicated isochronous signals for

the deuteriums at C_{α} of both enantiomers of **2** present in the reaction mixture. Therefore, the biosynthetic [2 H]-(S)-**2** was labeled as the enantiomer of (R)- β -isomer. In contrast to the retention of configuration mechanism to access (R)-**2**, CcTAM must use an inversion-of-configuration process to obtain the (S)-isomer (Scheme 5.3)

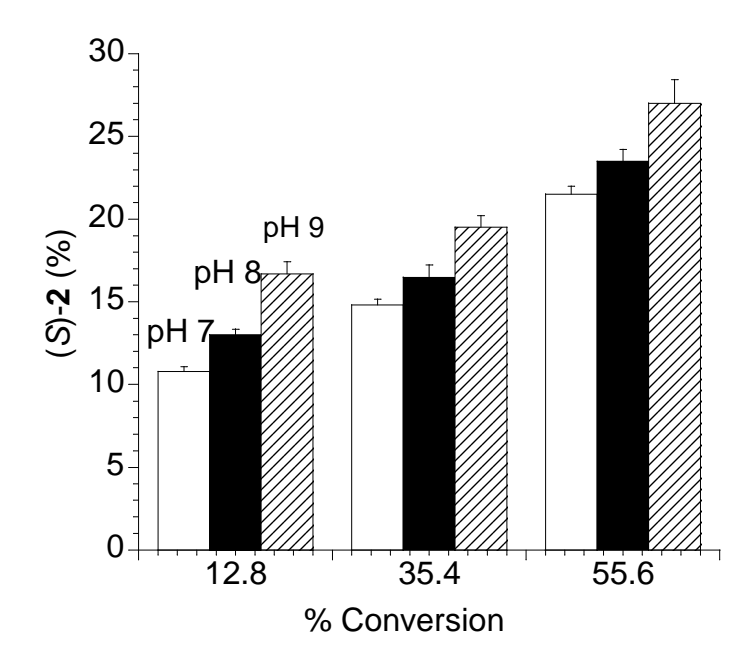


Figure 5.6. (*S*)-**2** (as % of total **2**) measured after substrate (*S*)-**1** was depleted by 13%, 35%, and 56% at pHs 7, 8, and 9 while incubated with *Cc*TAM.

5.4.2. Hydrogen Exchange during Migration

(2S)-[3,3- 2 H₂]-1 was incubated with *Cc*TAM in a time course study to track the D \rightarrow H exchange rate of the migratory *pro-(3S)* deuterium during the isomerization reaction. The deuterium enrichment in the [2 H]-2 decreased from 85% at 5 min to 30% after 10 h as the reaction reached equilibrium. This level of D \rightarrow H exchange was also observed for the (R)- β -phenylalanine product made in a similar reaction catalyzed by the plant *Tc*PAM with (2S)-[3,3-

²H₂]-α-phenylalanine as the substrate.⁶⁶ However, no deuterium exchange was observed in the reaction catalyzed by an isozyme from the bacteria *Pantoea agglomerans* (*Pa*PAM) with (2*S*)-[3,3-²H₂]-α-phenylalanine substrate.⁶¹ Structural data showed that the *Pa*PAM active site is slightly smaller and more ordered than *Tc*PAM.³⁸ ¹¹⁴ Thus, bulk water likely can access the active site of *Tc*PAM better than that of *Pa*PAM. While the *Cc*TAM structure is not yet solved, it can be imagined that its active site, like that of *Tc*PAM, allows access by bulk water to account for the observed proton exchange during catalysis.

The D H exchange rate progressively increases as the reaction progresses under steady state conditions. A monoprotic Tyr52 residue, also reported for other MIO aminomutases (and located on a flexible loop structure)^{38, 69, 114} presumably, serves as the general base in the CcTAM reaction. In this case, after deuterium abstraction from the (2S)- $[3,3-{}^{2}H_{2}]$ -1, the D \rightarrow H exchange on the catalytic Tyr52 should theoretically remain constant if all of the conditions stayed the same for the duration of the reaction; however, this is not the case. One notion to explain the observed increase in deuterium washout uses ureases as a model. Ureases are known to change the pH of the enzyme-microenvironment upon release of ammonia from urea. 127, 128 Likewise, each of the known MIO-dependent arylalanine aminomutases catalyzes an ammonia lyase reaction that releases ammonia and produces an arylacrylate as a by-product (see Figure A 45). 38° ⁴⁶ ⁶¹ ¹¹⁵ Thus, the microenvironment of CcTAM, containing increasing amounts of ammonia, might increase the pH and influence the proton exchange rates during catalysis. It is conceivable that as the microenvironment ultimately reaches equilibrium with bulk water, the D>H exchange becomes zero order as the reaction reaches equilibrium (see Figure A 45). To assess

this, *Cc*TAM was separated from the (2*S*)-[3,3-²H₂]-**1** substrate and biosynthesized products after a 24-h time course study. The isolated enzyme was re-incubated with more (2*S*)-[3,3-²H₂]-**1**, and the change in the deuterium washout rate was the same as observed before (see Figure A 45). Thus, the factors affecting the deuterium exchange were reversible, and the microenvironment was reset to its initial conditions.

5.4.3. Diastereomeric Product Ratio Catalyzed by CcTAM

Thus far, the MIO-dependent aminomutases can be categorized according to their stereoselectivity. SgTAM and PaPAM catalysis stereoselectively produce (S)- β -arylalanines. 6 61 It can be imagined that these aminomutases follow a similar stereochemical course during removal and rebounding of the transient hydrogen and NH_2 groups.

Scheme 5.3: Inversion and Retention of Configuration Pathways Catalyzed by CcTAM^a

^a(*Path* a) Retention and (*Path* b) inversion-of-configuration at C_{α} and C_{β} after exchange and reattachment of the *pro*-(3*S*) proton (H[†]) and the NH₂ of the (*S*)-1 substrate to make (*R*)-2 and (*S*)-2, respectively by *Cc*TAM catalysis.

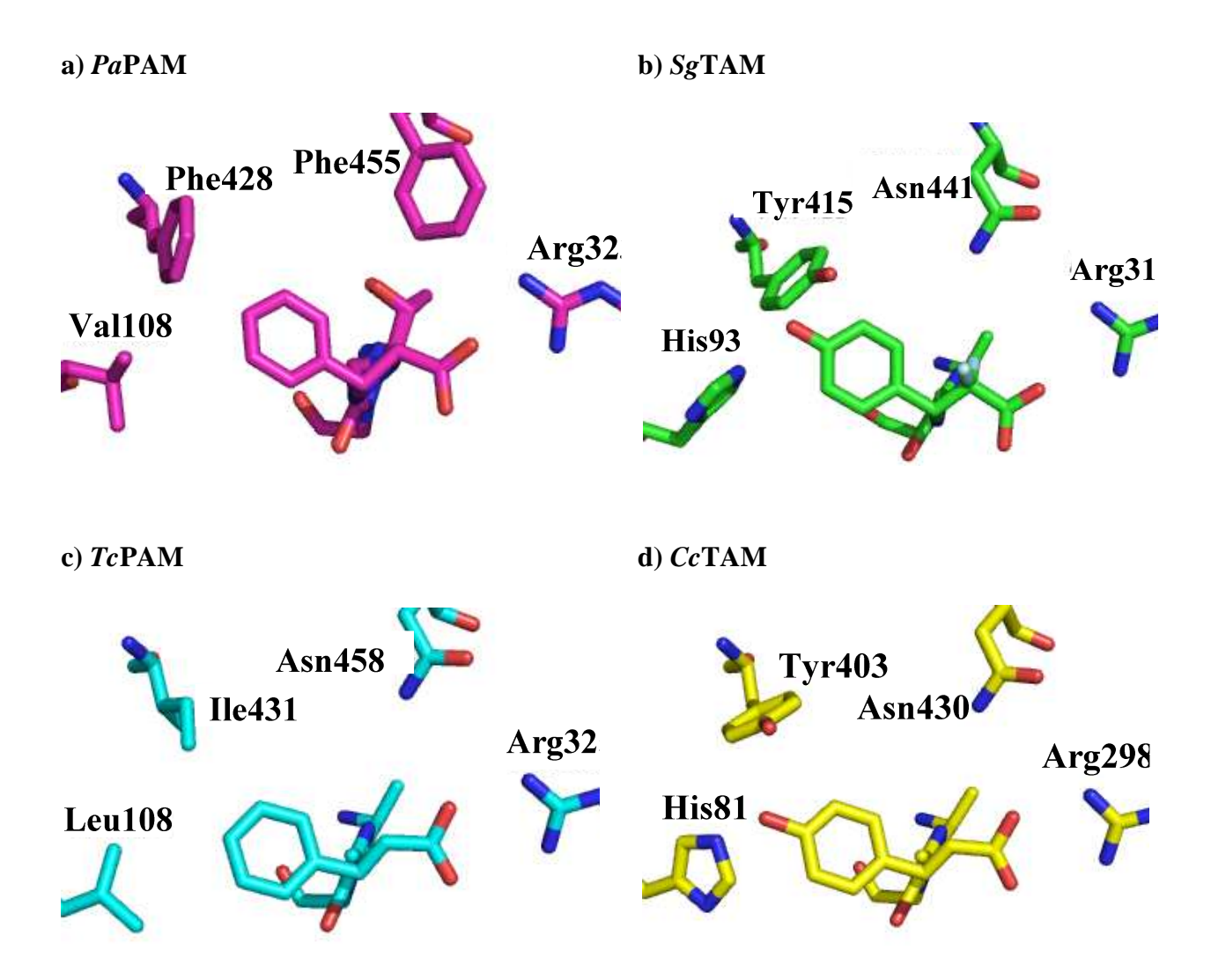


Figure 5.7. Comparison of the *Tc*PAM, *Pa*PAM, and *Sg*TAM active site structures co-crystallized with phenylpropanoid adducts or complexes and the *Cc*TAM active site with 4'-hydroxycinnamate was modeled on the *Tc*PAM crystal structure (PDB# 3NZ4). The orientation of phenylpropanoid (center of each diagram) relative to the Arg residue (at right of each diagram) is shown. Also shown are key non-catalytic residues involved in binding and positioning the substrate; the catalytic tyrosine residue is above the plane in each drawing and is not shown.

The crystal structures of a phenylalanine aminomutase (PaPAM) (Figure 5.7a) and a tyrosine aminomutase (SgTAM) (Figure 5.7b) show that the trajectories of the phenylalanine and tyrosine substrates, respectively, are nearly identical. However, these aminomutases use distinct enzyme/substrate interactions to orient their substrates. SgTAM apparently uses residues His93 and Tyr415 to form a hydrogen bond network with the 4'-OH of the tyrosine substrate and place the carboxylate in a monodentate salt bridge interaction with Arg311.¹²⁹ By contrast, these H-bond interactions are absent in PaPAM, which has hydrophobic residues Val108 and Phe428 positioned analogously to His93 and Tyr415, respectively, of SgTAM. Instead, PaPAM uses the steric bulk of Phe455 to force the phenylalanine substrate into a monodentate salt bridge interaction with Arg323. This steric interaction aligns phenylalanine in PaPAM at a similar orientation as the enzyme/substrate pairing in SgTAM. It was postulated that after elimination of the hydrogen and NH₂ from the PaPAM substrate, the distinct angle somehow prevents rotation of the cinnamate intermediate. In this way, the hydrogen and NH_2 can rebound to the same face of the intermediate from which they were removed. The similar substrate docking conformations and trajectories of PaPAM and SgTAM likely, in part, define their identical (3S)-product stereoselectivity. By analogy, CcTAM (described herein) and TcPAM from Taxus plants both make β-amino acid product with (3R)-stereochemistry; 5, 45, 46 thus, these aminomutases likely progress through similar stereochemical profiles. Earlier structural analyses showed that TcPAM has Asn458 positioned in contrast to the sterically larger Phe455 of isozyme PaPAM. The smaller Asn of TcPAM enables the carboxylate of the transient cinnamate intermediate to engage in a bidentate salt bridge with Arg325 (Figure 5.7c). In addition, the aryl portion of cinnamate sits in hydrophobic pocket that is, in part, comprised of residues Leu108, and Ile431, which also help aligns the reaction intermediate in $TcPAM \sim 15^{\circ}$ different from that of phenylalanine about

the C_{β} -axis in the $PaPAM^{114}$ (Figure 5.7a). The altered angle presumably allows the TcPAM intermediate to rotate 180° and retain the configuration at the chiral and prochiral centers of the (R)- β -phenylalanine product. CcTAM probably also proceeds through an identical process to obtain (R)-2.

The CcTAM structure has not yet been solved. However, its reaction stereochemistry (retention of configuration at both C_{α} and C_{β} in the major reaction product) is identical to that of TcPAM. This suggested that the two enzymes have common active site architecture and likely position their reaction intermediates similarly. Thus, CcTAM was modeled on TcPAM (PDB# 3NZ4) (30% sequence similarity). Placing the 4'-hydroxycinnamate in an orientation identical to that of cinnamate in TcPAM shows the hydroxyaryl portion of the former interacts with His81 and Tyr403 residues of CcTAM (Figure 5.7d). The plausible hydrogen bonding between CcTAM and the 4'-hydroxyaryl of the substrate likely helps align the substrate with Arg298 to form a bidentate salt bridge interaction (Figure 5.7d), similar to the interaction in TcPAM.

As mentioned, a significant difference between the aminomutase isozymes is the TAMs use His and Tyr residues in the aromatic pocket to help bind and orient the tyrosine substrate through hydrogen bonding. The PAMs, instead, use hydrophobic residues in the aromatic pocket and likely, other not yet fully understood factors to direct the substrate binding orientation and stereoselectivity. It is feasible that hydrogen bonding with the phenol of the substrate, in part, governs the stereoselectivity of the TAMs and enables the minor antipodal product to form through a new reaction route. As mentioned previously, each MIO-dependent arylalanine aminomutases catalyzes an ammonia lyase reaction, releasing ammonia and an arylacrylate as by-products (see Figure A 45). ^{38,46,61,115} We posited earlier that the observed D→H exchange for

the CcTAM reaction was likely influenced by the increased pH of the microenvironment caused by ammonia-release (Figure A 45). Variation in bulk and local pH is known generally to disturb hydrogen bonding networks within an enzyme active site. $^{130^{\circ}132}$ In the TAM enzymes, the perturbation of the local pH could also affect the H-bonding network within the active site. Alteration of the hydrogen bonding network in the 4'-hydroxyaryl binding pocket of the TAM enzymes could potentially change the enantioselectivity, since this region likely contributes significantly to the substrate docking conformation. Therefore, in this study, the buffered pH of a CcTAM reaction was adjusted to 9 and below to assess whether this would change the % ee of the product.

A lower % conversion of (*S*)-1 to 2 correlated with a higher % ee of (*R*)-2 for each pH tested. Also, at higher pHs, the relative proportion of (*S*)-2 made by *Cc*TAM increased compared to (*R*)-2. *Cc*TAM consistently produced more (*S*)-2 enantiomer at higher pHs, regardless of the amount of (*S*)-1 converted to 2 (Figure 5.6). As we proposed earlier, (*S*)-2 is made via a conformer of a 4'-hydroxycinnamate intermediate that receives the NH₂ group and hydrogen (dwelling temporarily on the enzyme) on the same face they were removed from (*S*)-1. (*R*)-2 is provided via a rotamer of the initially formed conformer of 4'-hydroxycinnamate. Therefore, since the production of (*S*)-2 increases with higher pH, these conditions can be imagined to restrict the rotation of the 4'-hydroxycinnamate intermediate within the *Cc*TAM active site by possibly altering the substrate binding angle or by strengthening the hydrogen bond network with the 4'-OH of the substrate. Increases in pH are known to partition the phenol groups of active site tyrosines to the phenolates and thereby shorten hydrogen bond distances interacting with these oxyanions. ¹³¹ However, the mechanism through which the pH exactly affects the product stereochemistry of *Cc*TAM remains unclear and will require further inquiry.

5.5. Conclusion

In summary, the synthesis of stereospecifically [2 H]-labeled **1** enabled us to provide evidence to support that CcTAM catalyzes its isomerization reaction along a path similar to that of TcPAM from a plant. That is, both likely overcome a torsional barrier to access two pivotal rotameric intermediates. CcTAM converts one rotamer to (R)-2 as the major product through retention of configuration. This pathway competes with a route involving a second rotamer, producing (S)-2 as the minor enantiomer through inversion of configuration. TcPAM uses only one rotamer to advance to a single enantiomer, (R)-phenylalanine.

Thus, this study potentially starts to shed light on how CcTAM catalysis uses the 4'-hydroxyl group to orient the substrate in the active site. In addition, this investigation provides a basis to probe the driving force that rotates the branch point intermediate in CcTAM to produce two enantiomers.

APPENDIX

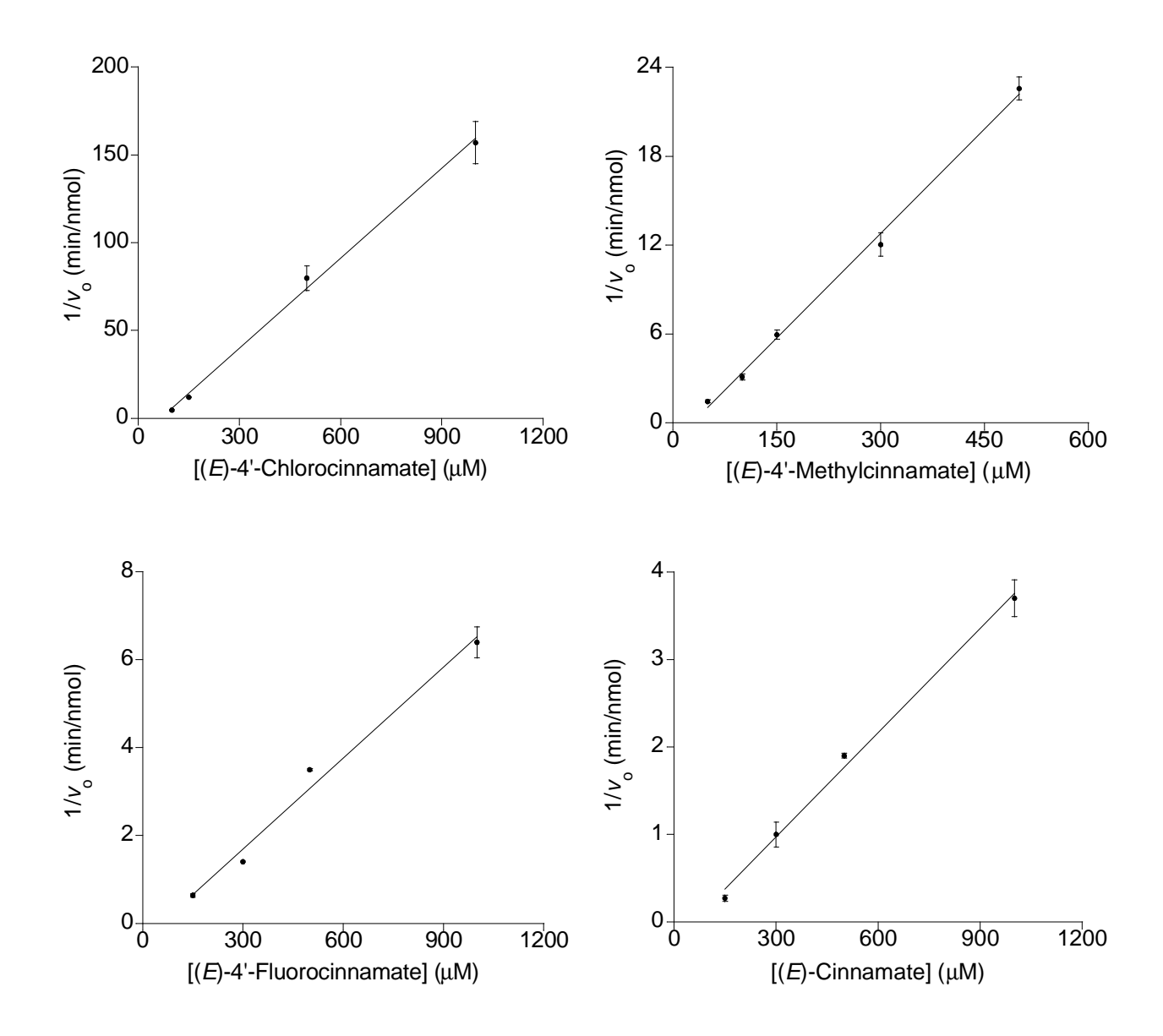
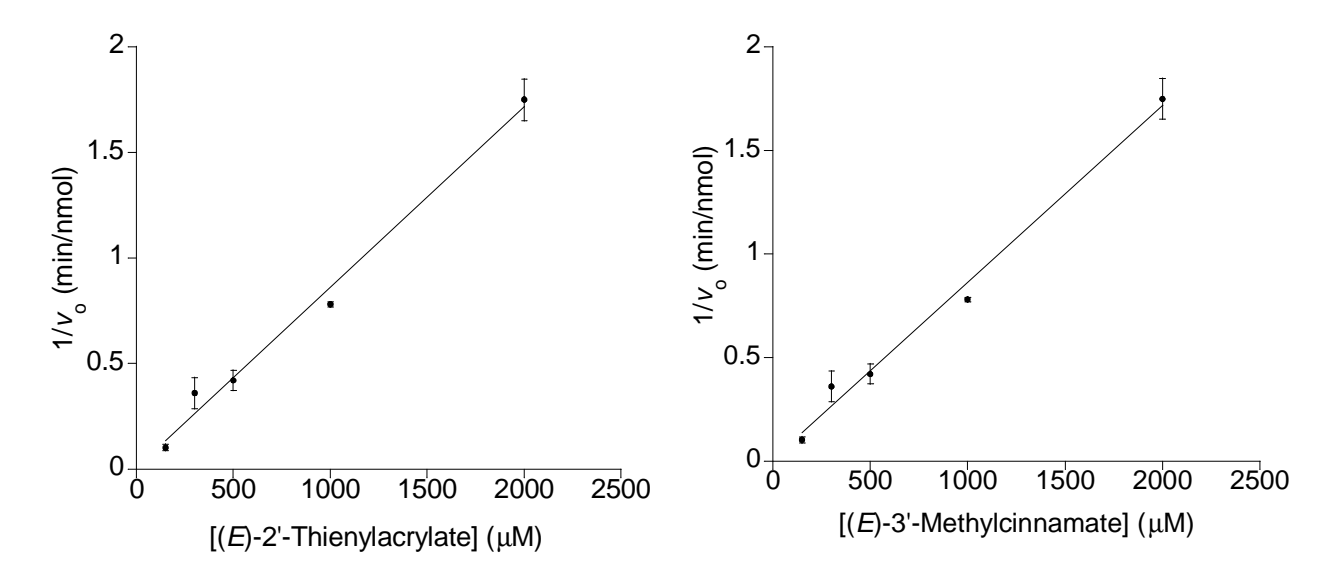


Figure A 1. The linear relationship between the reciprocal of the steady-state rate $(1/v_0)$ and the concentrations of competitive inhibitors ([I]₀ in eq. 4 above): Top Left) *trans*-4'-Chloro- (9), Top Right) *trans*-4'-Methyl- (10), Middle Left) *trans*-4'-Fluorocinnamate (11), Middle Right) *trans*-Cinnamate (12).

Figure A1 (cont'd).



The linear relationship between the reciprocal of the steady-state rate $(1/v_0)$ and the concentrations of competitive inhibitors ([I]₀ in eq. 4 above): Bottom Left) *trans*-2'-Thienylacrylate (13), and Bottom Right) *trans*-3'-Methylcinnamate (14) (each at 50, 100, 150, 300, 500, 1000, 2000 μ M) are shown. The inhibitors were co-incubated with *Tc*PAM and (*S*)-styryl- α -alanine (6), in triplicate. The production of (2*E*,4*E*)-Styrylacrylate (7) was monitored. The standard deviation for each calculated slope ($K_{\rm I}$) was approximately \pm 6% of the mean.

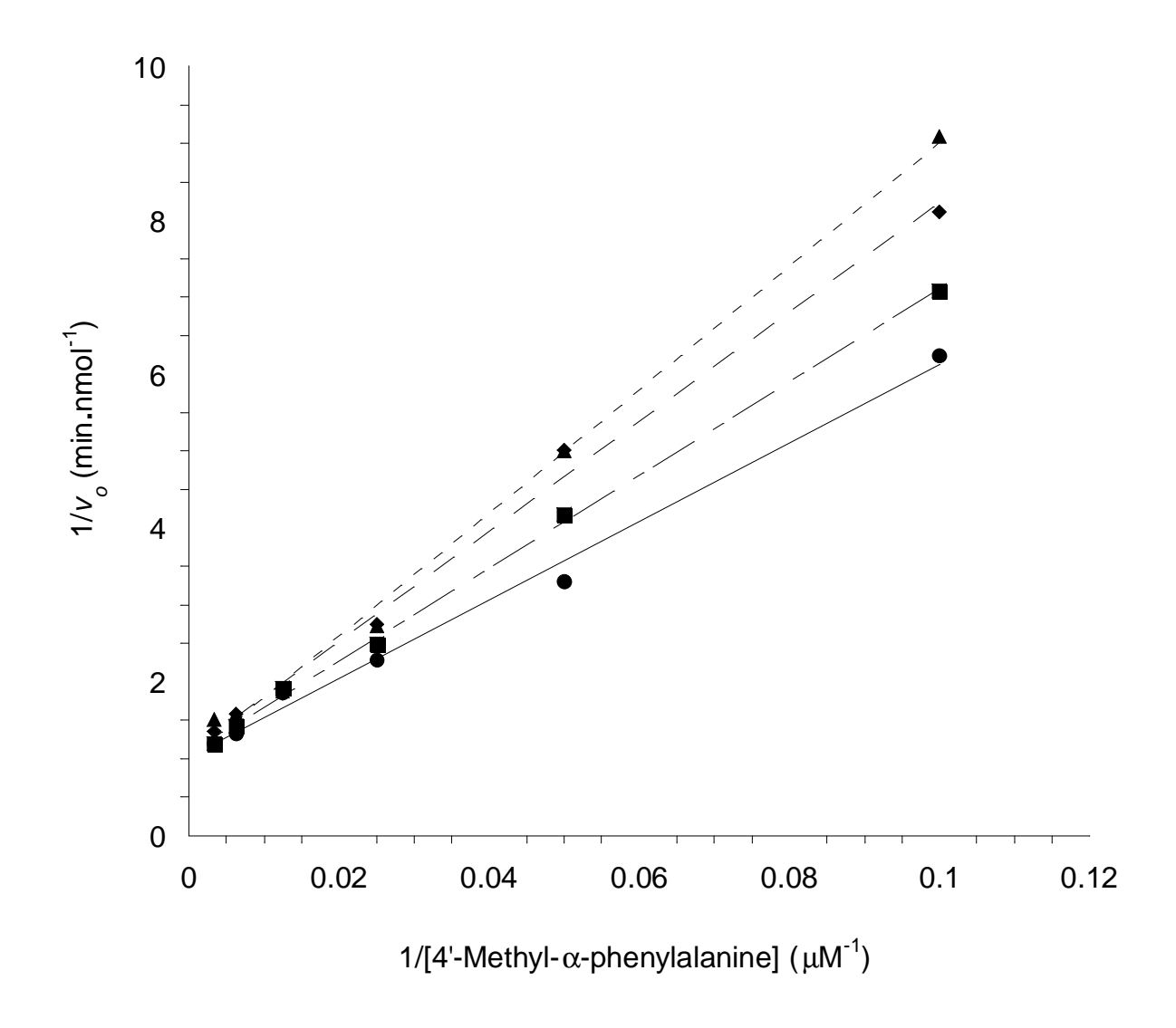


Figure A 2. Double Reciprocal Plots of the Rate of Conversion of 8b/α to 8b/β and Concentration of Substrate (*S*)-4'-Methyl-α-phenylalanine (8b/α) in TcPAM Reactions Containing (2E,4E)-Styrylacrylate (7) at 0 (\bullet), 50 (\blacksquare), 100 (\bullet), 200 (\blacktriangle) μM to Assess the $K_{\rm I}$ of 7.

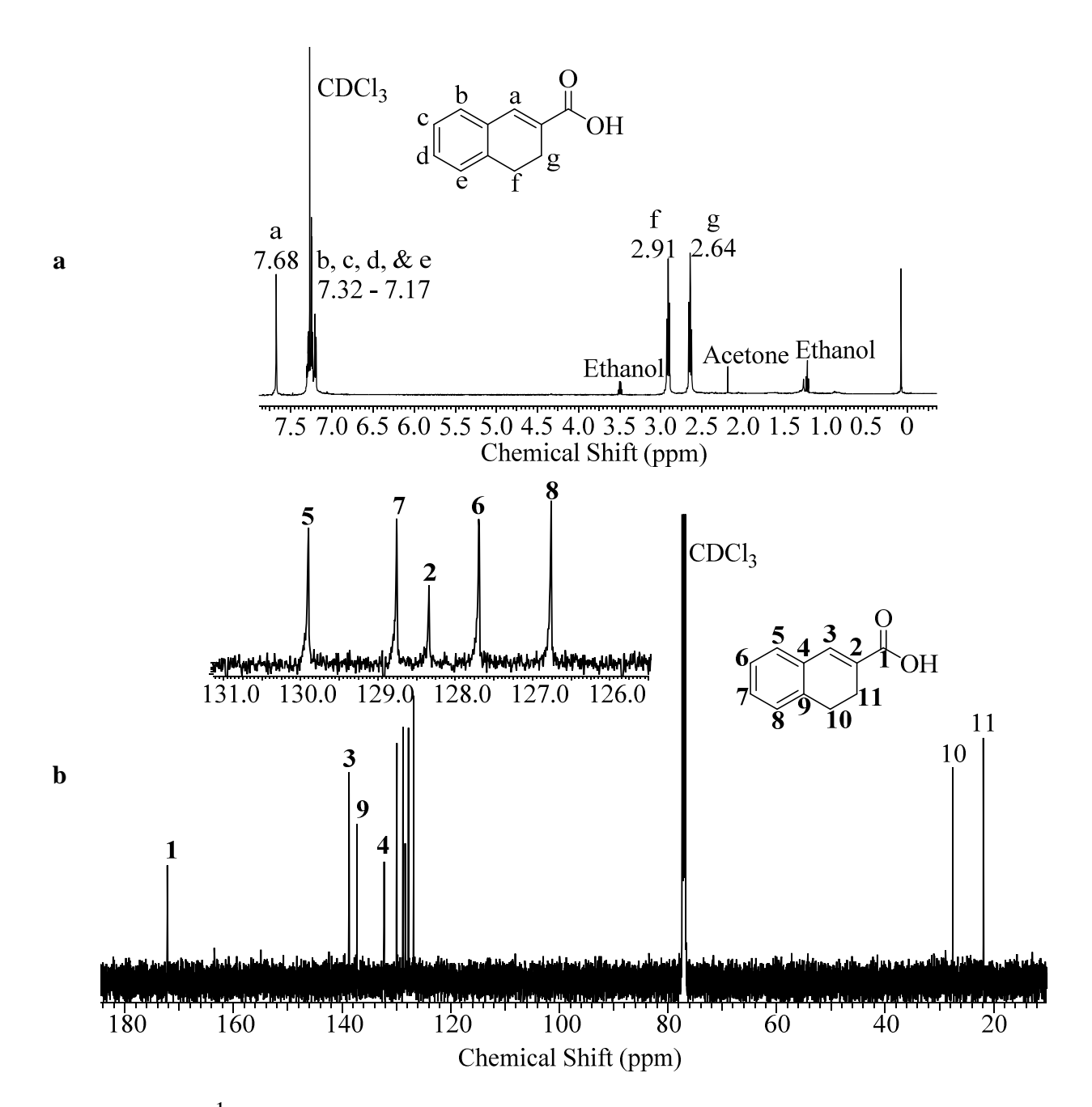


Figure A 3. a) ¹H-NMR spectrum ((500 MHz, CDCl₃) δ : 7.68 (s, 1 H), 7.32 - 7.17 (m, 4 H), 2.91 (t, J = 8.4 Hz, 2 H), 2.64 (dt, J = 1.5, 8.5 Hz, 2 H))of and the **b**) ¹³C-NMR spectrum ((126 MHz, CDCl₃) δ : 172.2, 138.7, 137.2, 132.3, 129.9, 128.8, 128.4, 127.7, 126.8, 27.5, 21.9) of **16**-Acr

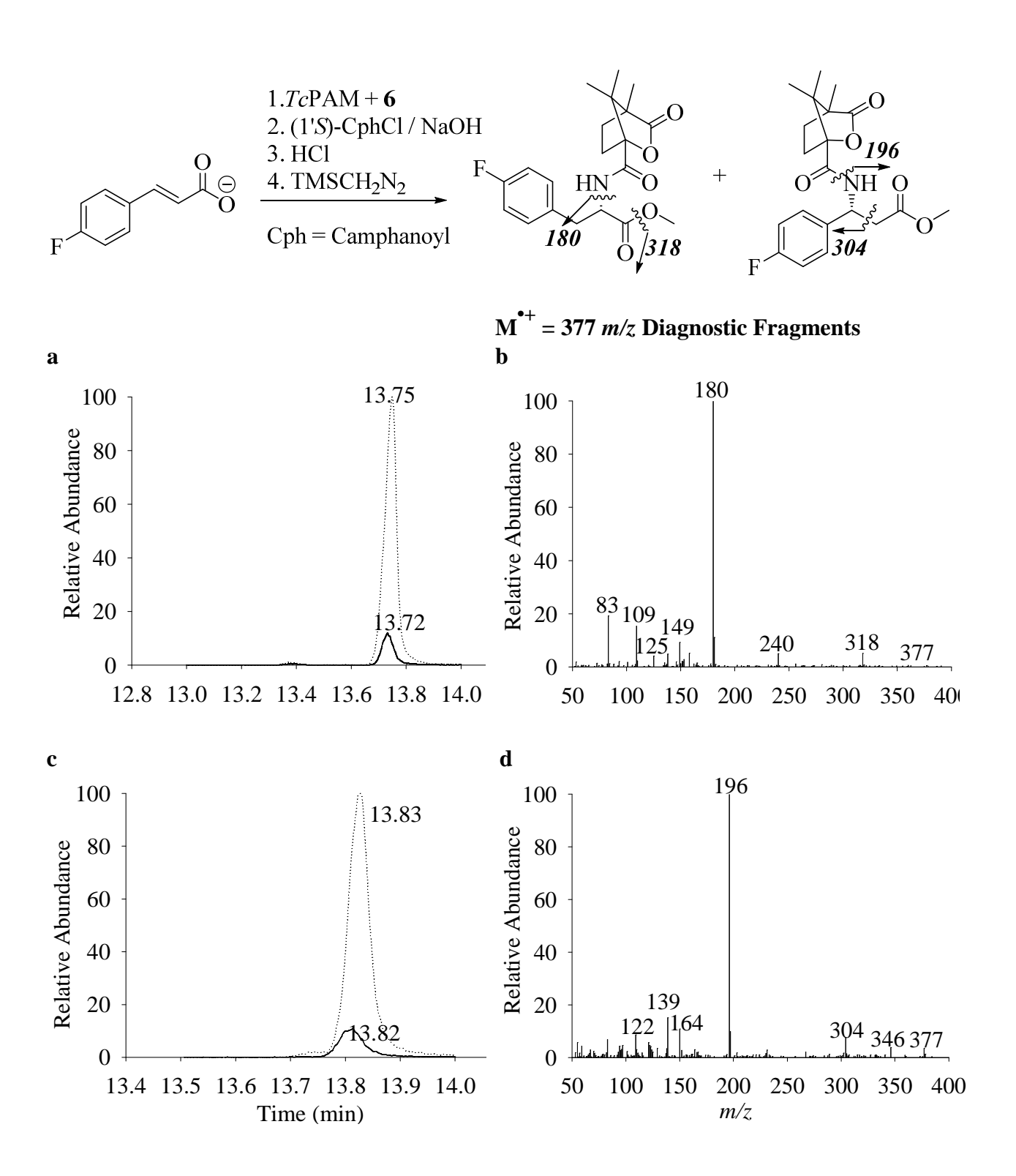


Figure A 4. Overlay of gas chromatography profiles of; a) N-[(1'S)-camphanoyl] methyl esters

Figure A 4 (cont'd).

of (2S)- α -4'-fluorophenylalanine (13.72 min) derived from intermolecular amino group transfer by TcPAM catalysis (solid line) and of the N-[(1'S)-camphanoyl] methyl ester of (2S)- α -4'-fluorophenylalanine (13.75 min) (dashed line); b) N-[(1'S)-camphanoyl] methyl ester of (3R)- β -4'-fluorophenylalanine (13.82 min) derived from intermolecular amino group transfer catalysis of TcPAM (solid line) and of the N-[(1'S)-camphanoyl] methyl ester of (3R)- β -4'-fluorophenylalanine (13.83 min) (dashed line). The mass spectrometry profile of c) N-[(1'S)- of (2S)- α -4'-fluorophenylalanine (13.72 min), and d) N-[(1'S)-camphanoyl] methyl ester of (3R)- β -4'-fluorophenylalanine (13.82 min) and derived from intermolecular amino group transfer catalysis of TcPAM.

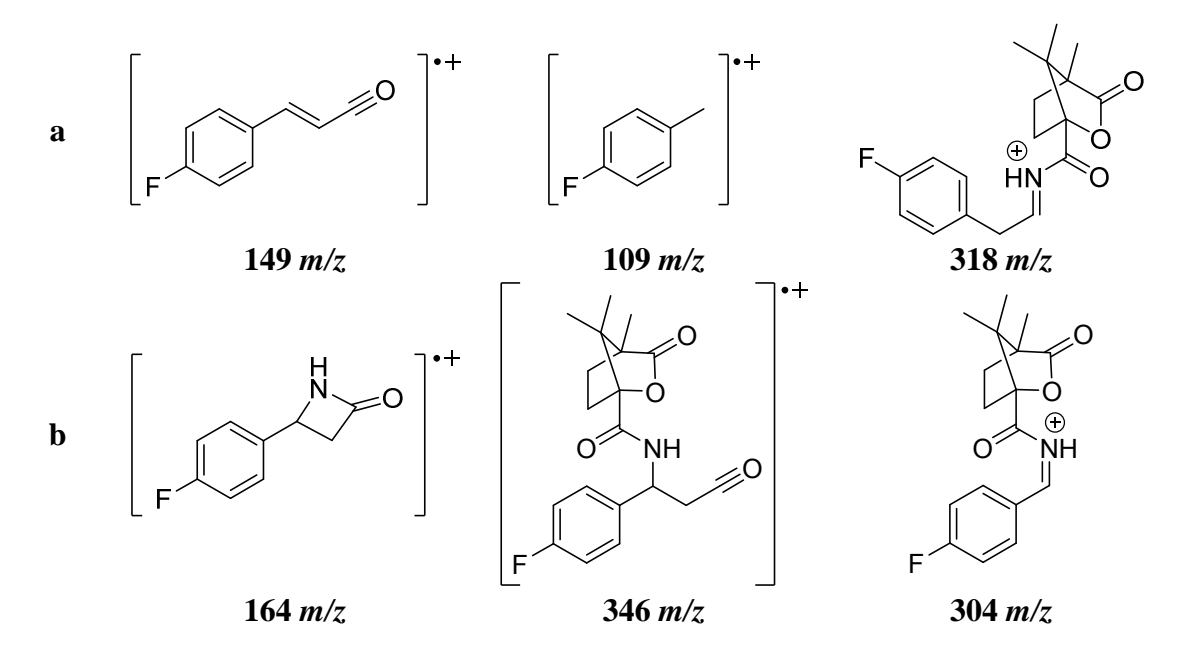


Figure A 5. GC EI/MS fragments of a) N-[(1'S)-camphanoyl] methyl ester of (2S)- α -4'-fluorophenylalanine and b) N-[(1'S)-camphanoyl] methyl ester of (3R)- β -4'-fluorophenylalanine

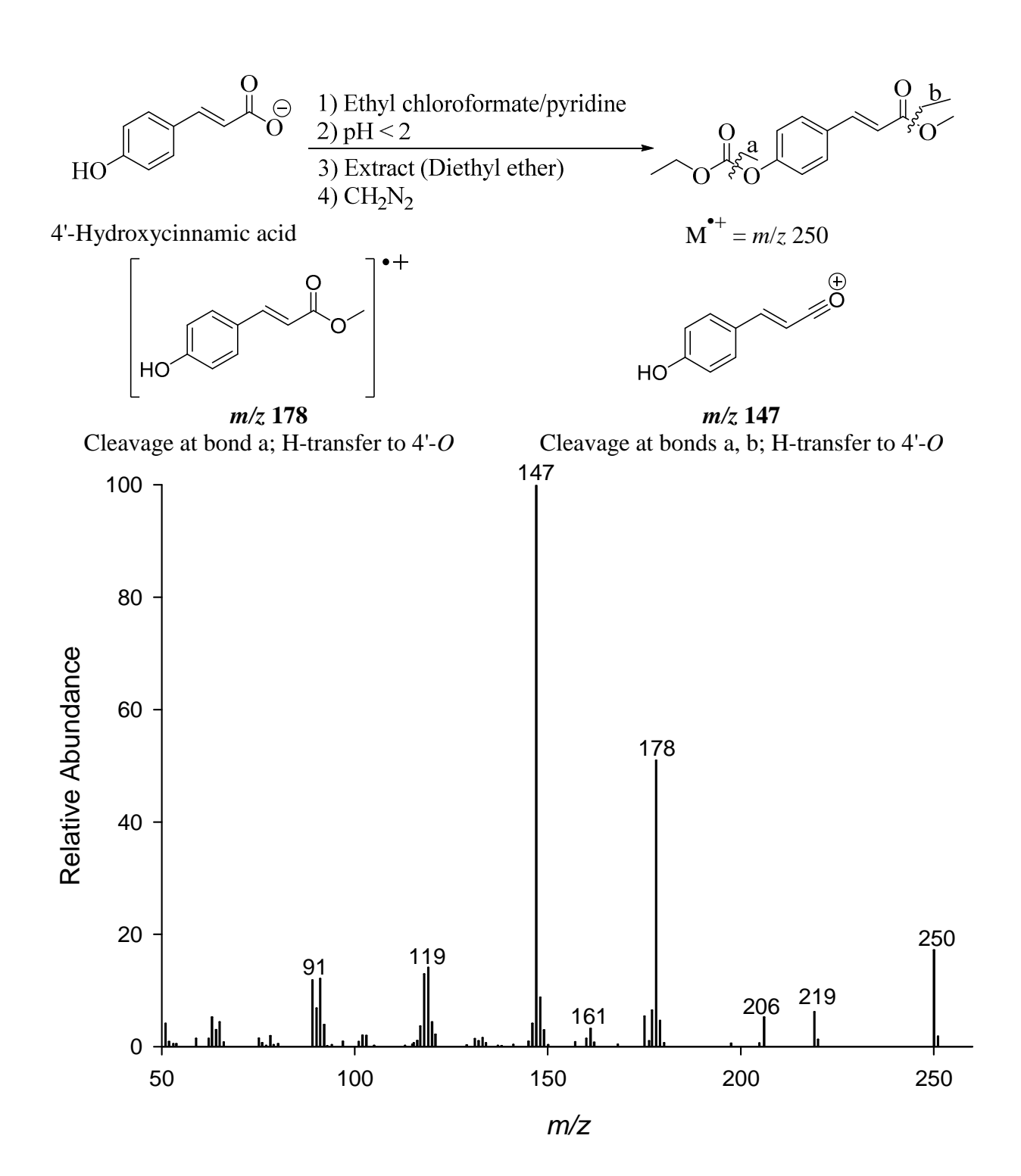


Figure A 6. EI-MS fragmentation of 4'-*O*-(ethoxycarbonyl) methyl ester derivative of authentic 4'-hydroxycinnamic acid. Diagnostic fragment ions are m/z 178 and 147.

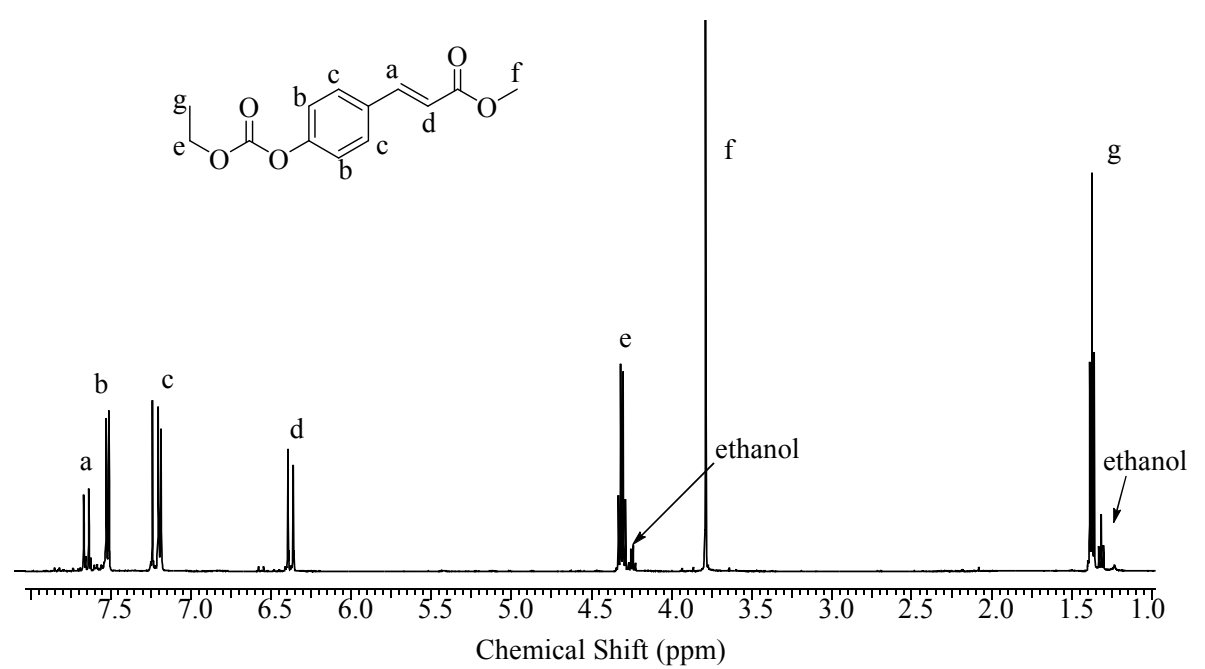


Figure A 7. a) ¹H NMR of 4'-*O*-(ethoxycarbonyl) methyl ester of 4'-hydroxycinnamic acid ¹H NMR (500 MHz, CDCl₃) δ: 7.68 (d, J = 16.1 Hz, 1 H), 7.55 (d, J = 8.3 Hz, 2 H), 7.22 (d, J = 8.3 Hz, 1 H), 6.41 (d, J = 16.1 Hz, 1 H), 6.41 (d, J = 16.1 Hz, 1 H), 4.34 (q, J = 7.3 Hz, 2 H), 3.82 (s, 3 H), 1.41 (t, J = 7.3 Hz, 3 H)

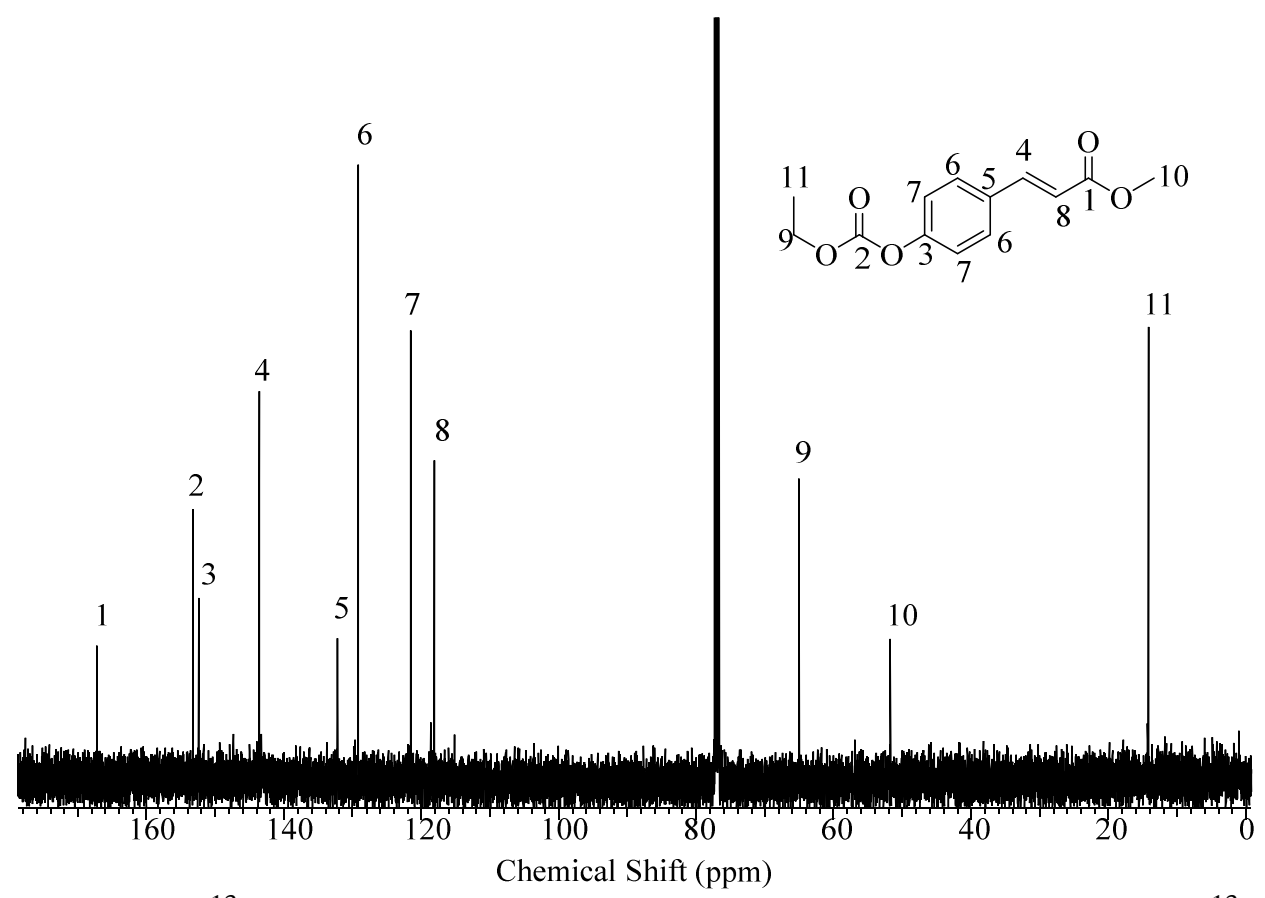


Figure A 8. a) ¹³C NMR of 4'-*O*-(ethoxycarbonyl) methyl ester of 4'-hydroxycinnamic acid ¹³C NMR (126 MHz, CDCl₃) δ: 167.2, 153.2, 152.4, 143.6, 132.2, 129.2, 121.6, 118.1, 65.1, 51.7, 14.2

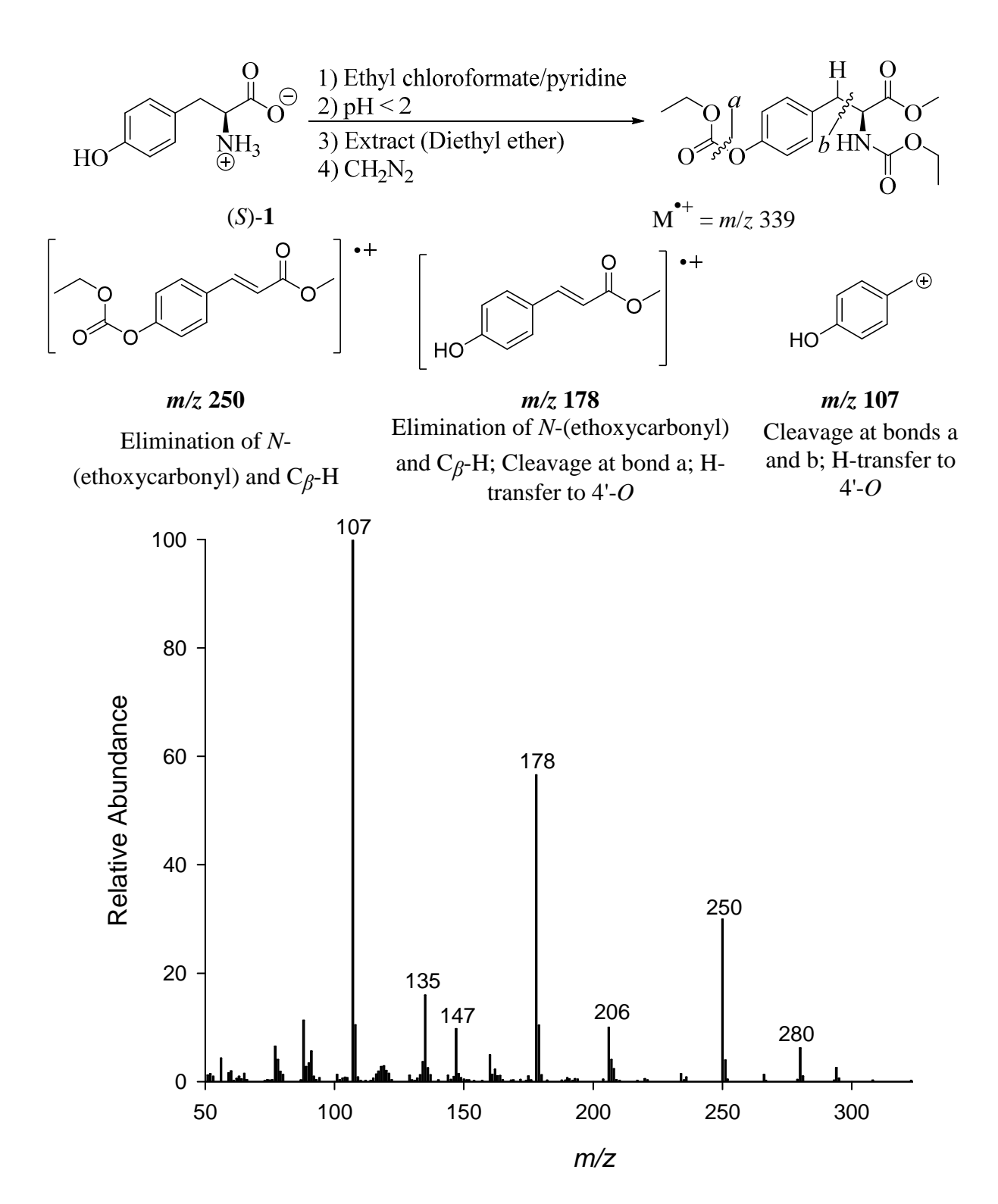


Figure A 9. EI-MS fragmentation of 4'-*O*,3-*N*-di(ethoxycarbonyl) methyl ester derivatives of unlabeled (*S*)-1. Diagnostic fragment ions are m/z 250, 178, and 107.

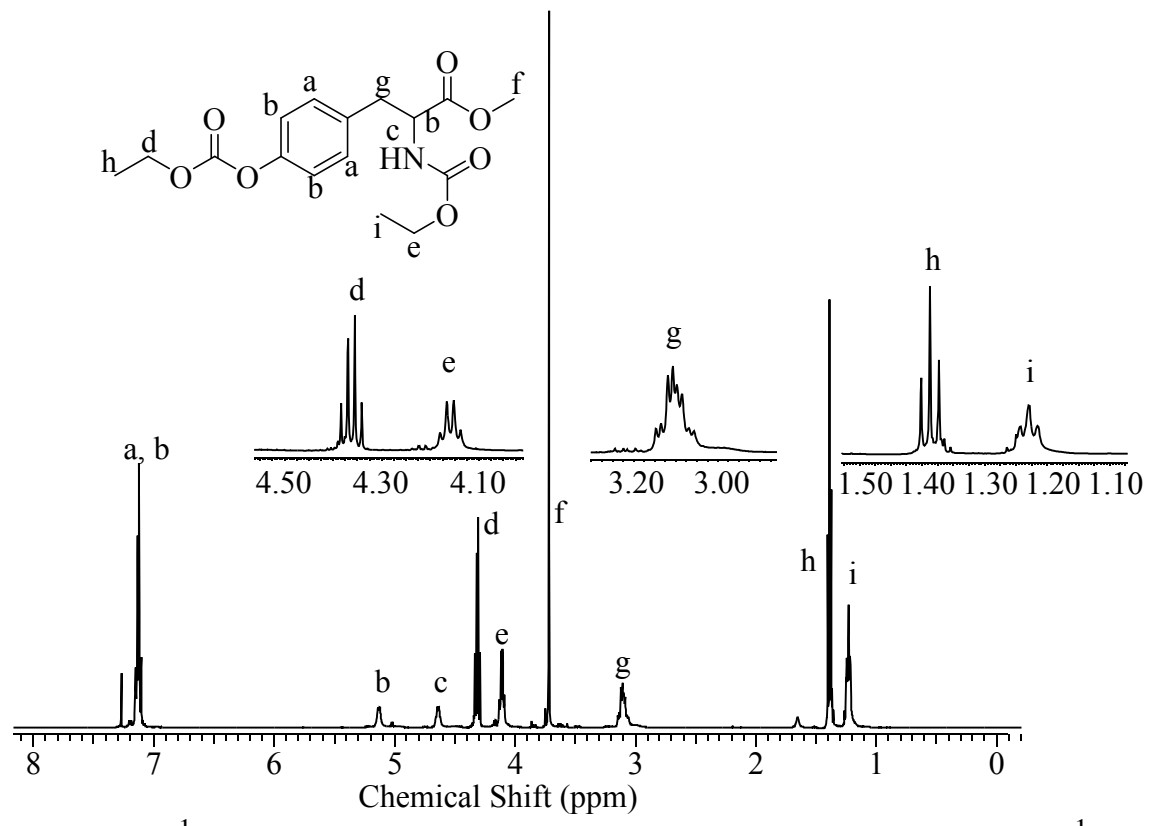


Figure A 10. a) ¹H NMR of 4'-*O*,2-*N*-di(ethoxycarbonyl) methyl ester of α-tyrosine. ¹H NMR (500 MHz, CDCl3) $\delta = 7.21 - 6.98$ (m, 4 H), 5.10 (d, J = 7.3 Hz, 1 H), 4.67 - 4.55 (m, 1 H), 4.28 (q, J = 7.1 Hz, 2 H), 4.08 (q, J = 6.7 Hz, 2 H), 3.69 (s, 3 H), 3.10 (dd, J = 6.1, 14.0 Hz, 1 H), 3.05 (dd, J = 6.1, 14.0 Hz, 1 H), 1.36 (t, J = 7.0 Hz, 3 H), 1.20 (t, J = 6.7 Hz, 3 H).

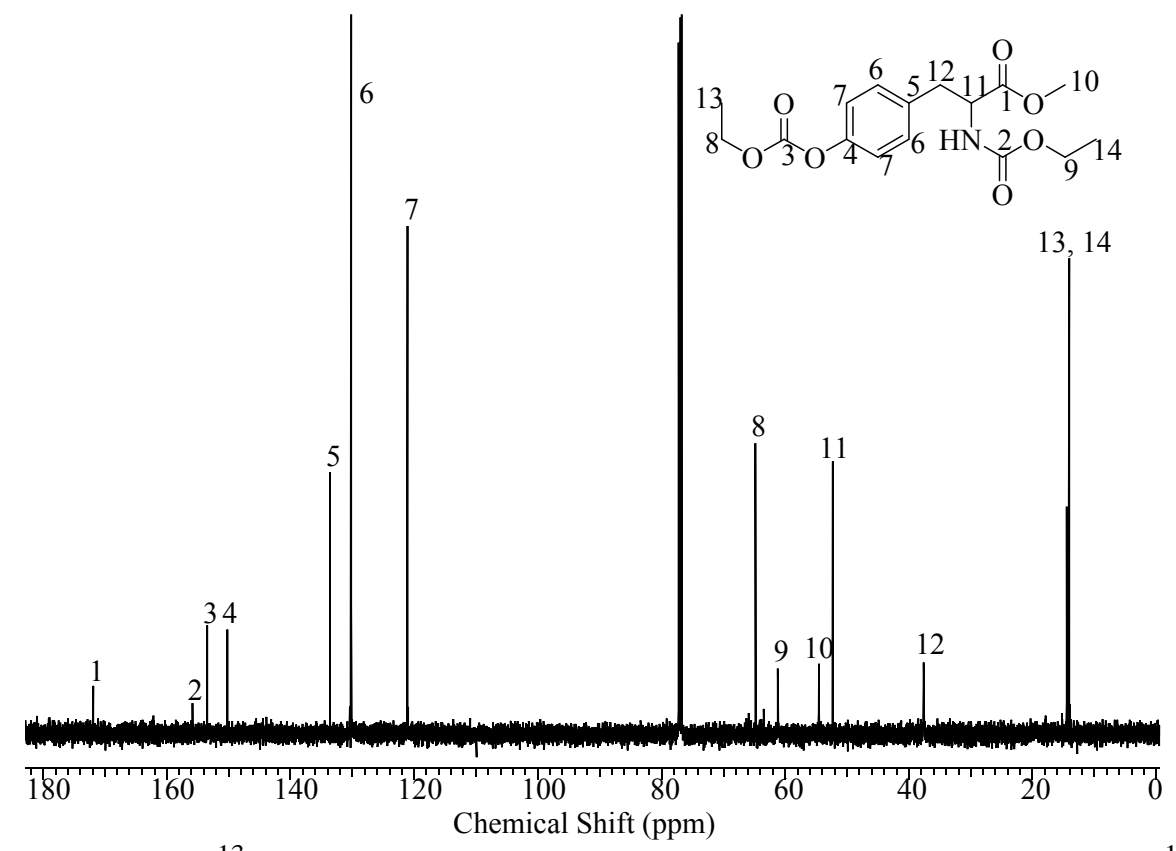


Figure A 11. a) 13 C NMR of 4'-*O*,2-*N*-di(ethoxycarbonyl) methyl ester of α-tyrosine. 13 C NMR (126 MHz, CDCl3) δ = 171.9, 155.8, 153.5, 150.2, 133.6, 130.3, 121.0, 64.8, 61.2, 54.5, 52.3, 37.6, 14.4, 14.1

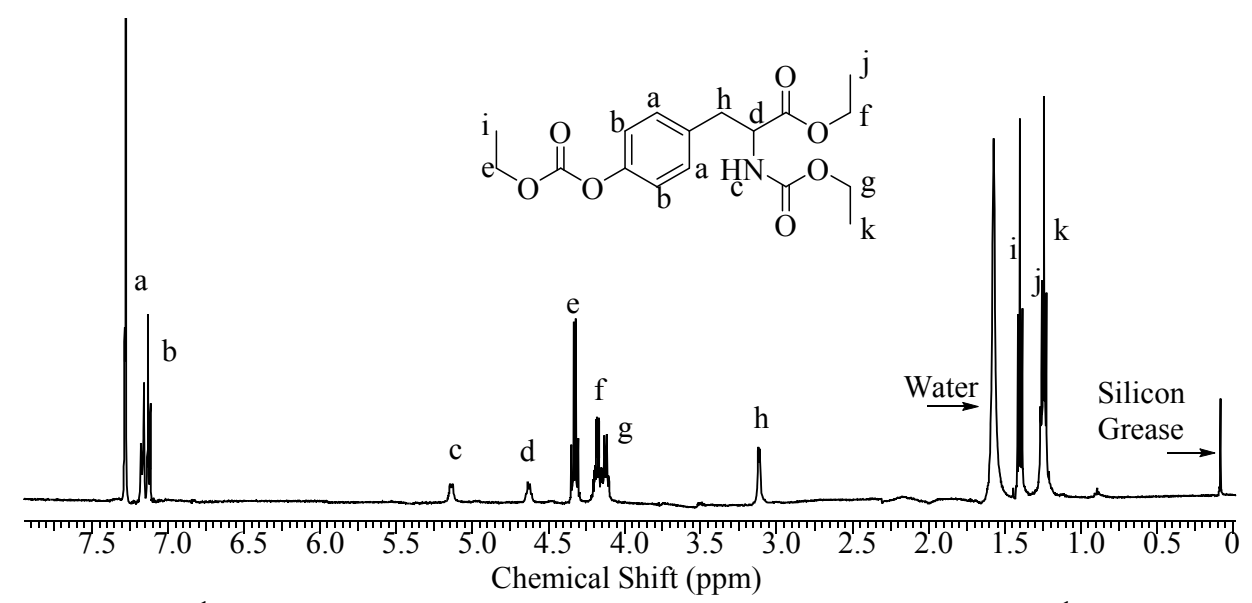


Figure A 12. ¹H NMR of 4'-*O*,2-*N*-di(ethoxycarbonyl) ethyl ester of α-tyrosine. ¹H NMR (500 MHz, CDCl3) δ = 7.17 (d, J = 8.6 Hz, 2 H), 7.14 - 7.11 (m, J = 8.6 Hz, 2 H), 5.14 (d, J = 7.8 Hz, 1 H), 4.63 (dd, J = 5.6, 13.4 Hz, 1 H), 4.33 (q, J = 7.1 Hz, 2 H), 4.17 (q, J = 7.2 Hz, 2 H), 4.12 (q, J = 7.1 Hz, 2 H), 3.11 (d, J = 5.1 Hz, 2 H), 1.40 (t, J = 7.1 Hz, 3 H), 1.25 (t, J = 7.3 Hz, 3 H), 1.24 (t, J = 7.2 Hz, 3 H)

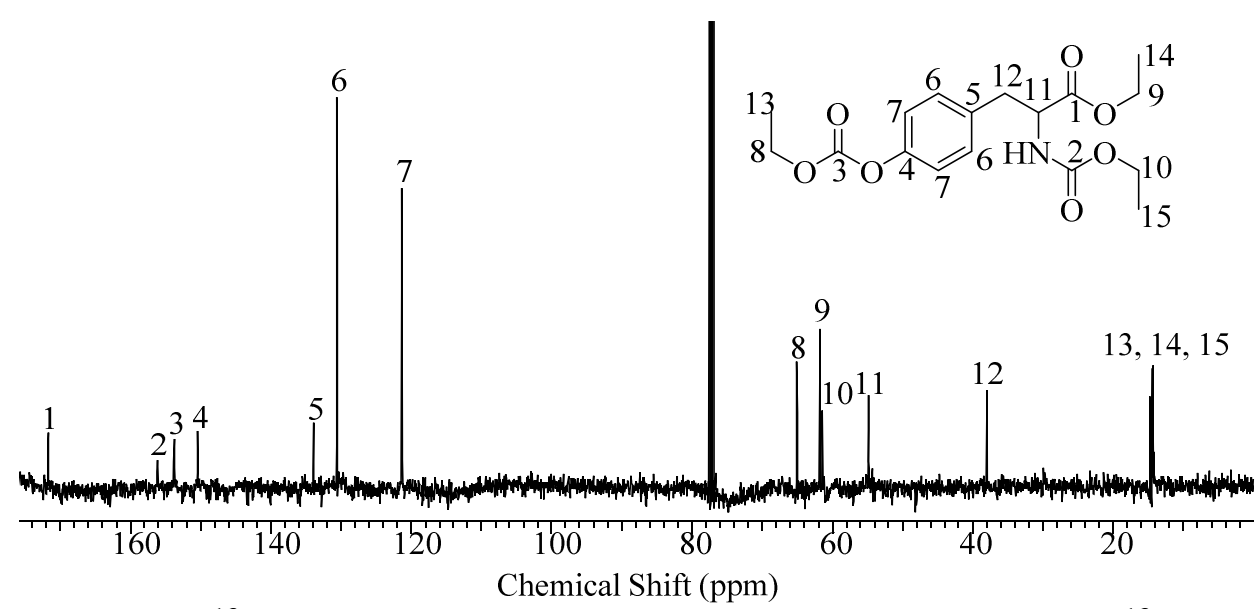


Figure A 13. ¹³C NMR of 4'-*O*,2-*N*-di(ethoxycarbonyl) ethyl ester of α-tyrosine. ¹³C NMR (126 MHz, CHCl₃) δ: 171.7, 156.1, 153.8, 150.4, 133.9, 130.6, 121.3, 65.1, 61.8, 61.4, 54.9, 38.0, 14.7, 14.4, 14.3

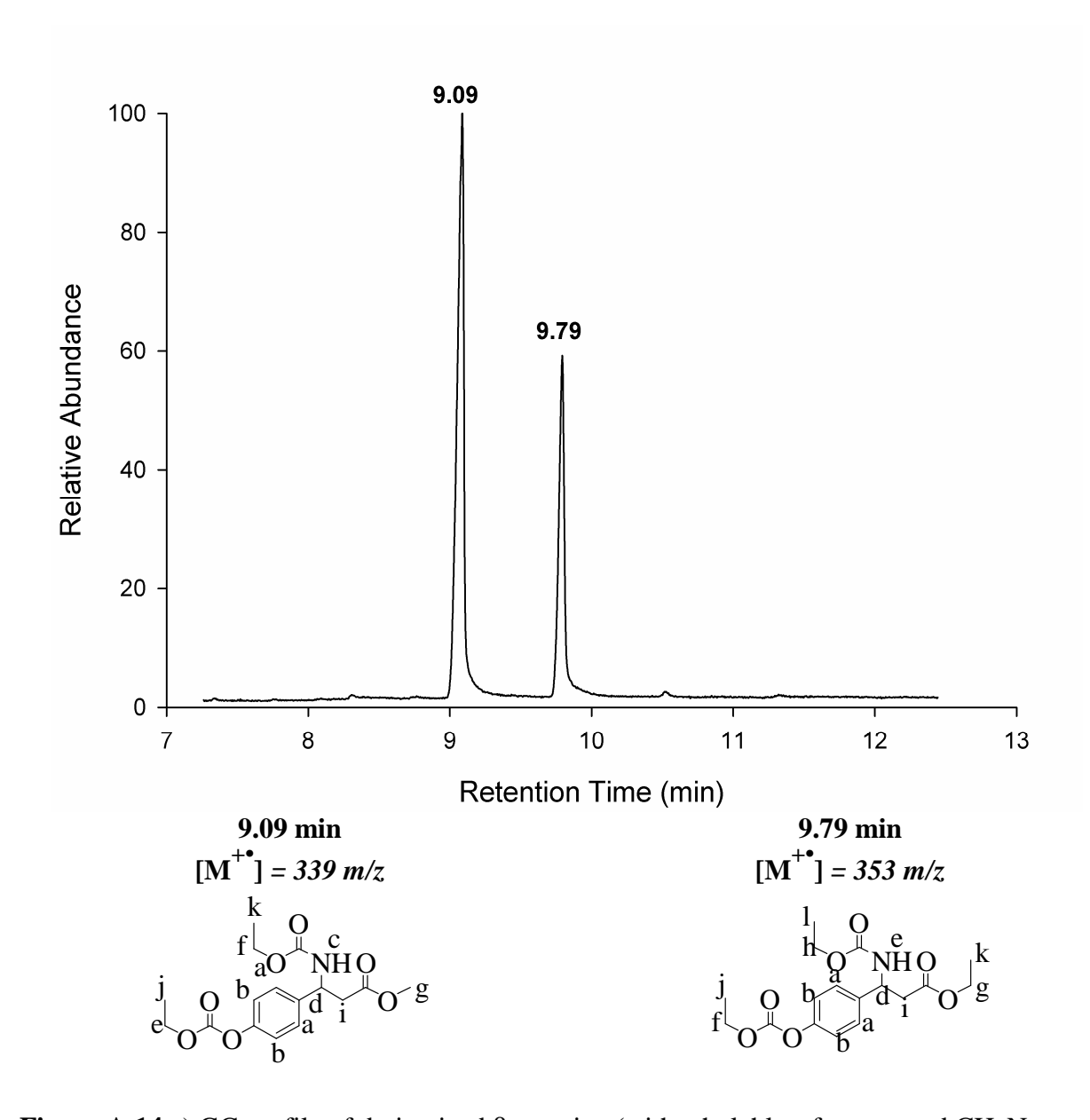
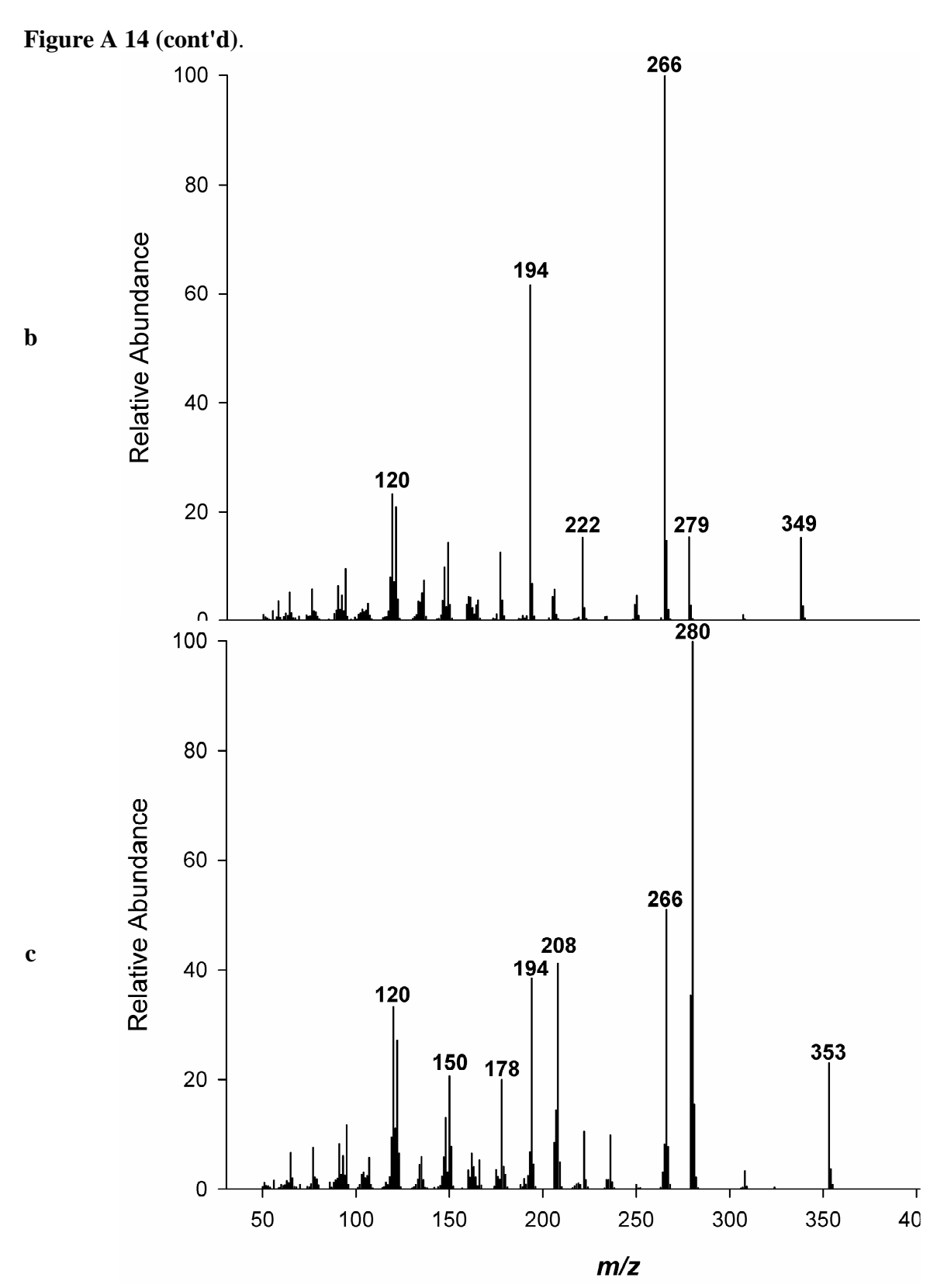


Figure A 14 a) GC profile of derivatized β -tyrosine (with ethylchloroformate and CH_2N_2



b) MS profiles of peak at 9.09 min retention time and c) of peak at 9.79 min retention time.

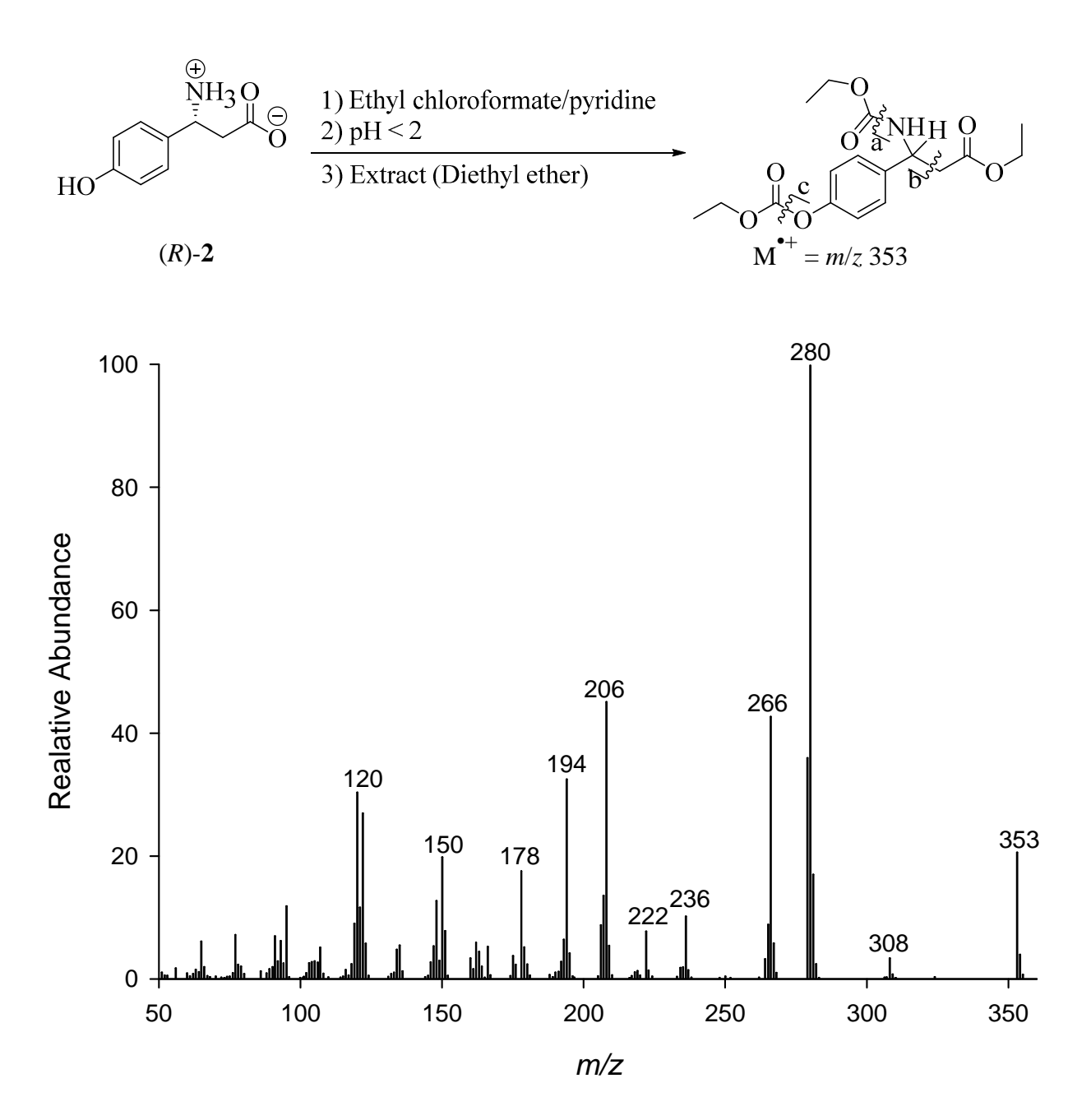


Figure A 15. EI-MS fragmentation of 4'-*O*,3-*N*-di(ethoxycarbonyl) ethyl ester derivatives of authentic (*R*)-2. Diagnostic fragment ions are m/z 280, 266, and 194.

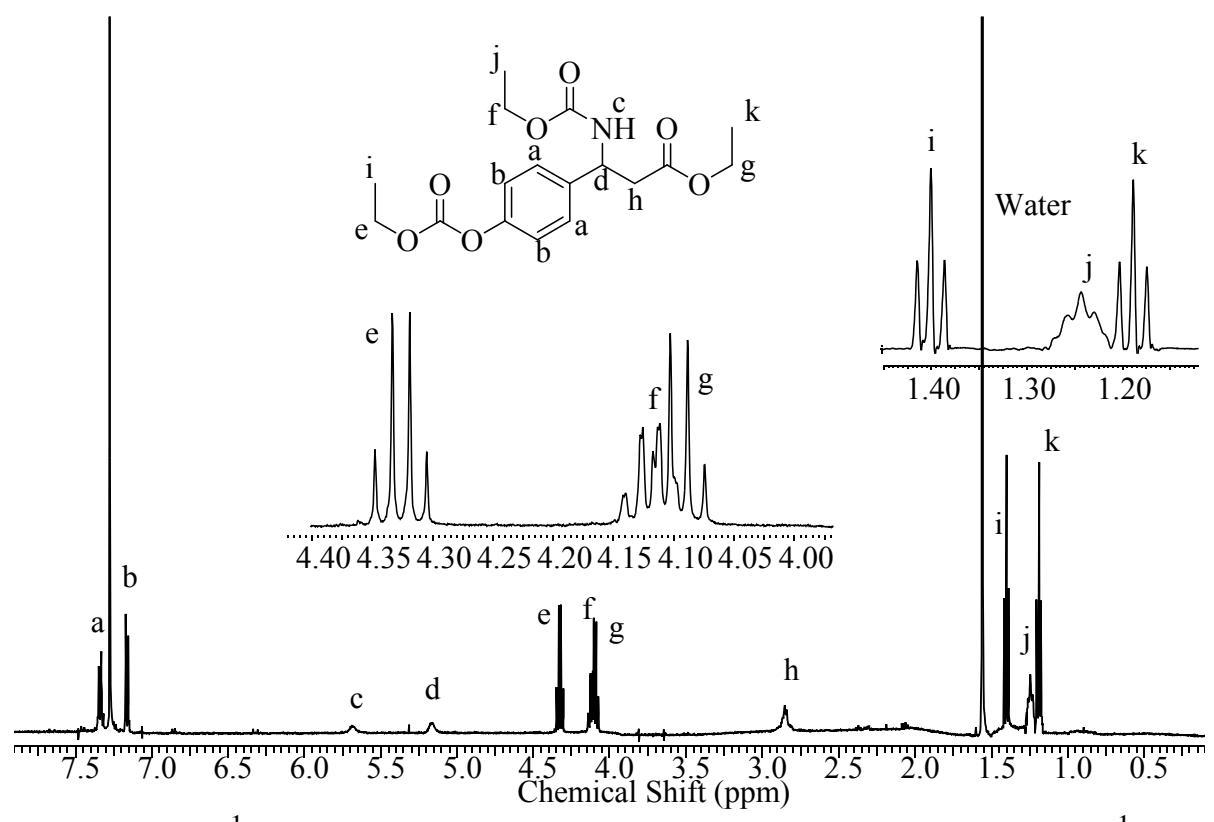


Figure A 16. a) ¹H NMR of 4'-*O*,3-*N*-di(ethoxycarbonyl) ethyl ester of β-tyrosine. ¹H NMR (500 MHz, CDCl₃) δ: 7.34 (d, J = 8.5 Hz, 2 H), 7.16 (d, J = 8.8 Hz, 2 H), 4.33 (q, J = 7.3 Hz, 2 H), 4.12 (q, J = 7.1 Hz, 2 H), 4.09 (q, J = 7.3 Hz, 2 H), 2.92 - 2.78 (m, 2 H), 1.40 (t, J = 7.3 Hz, 3 H), 1.24 (t, J = 7.2 Hz, 3 H), 1.19 (t, J = 7.3 Hz, 3 H)

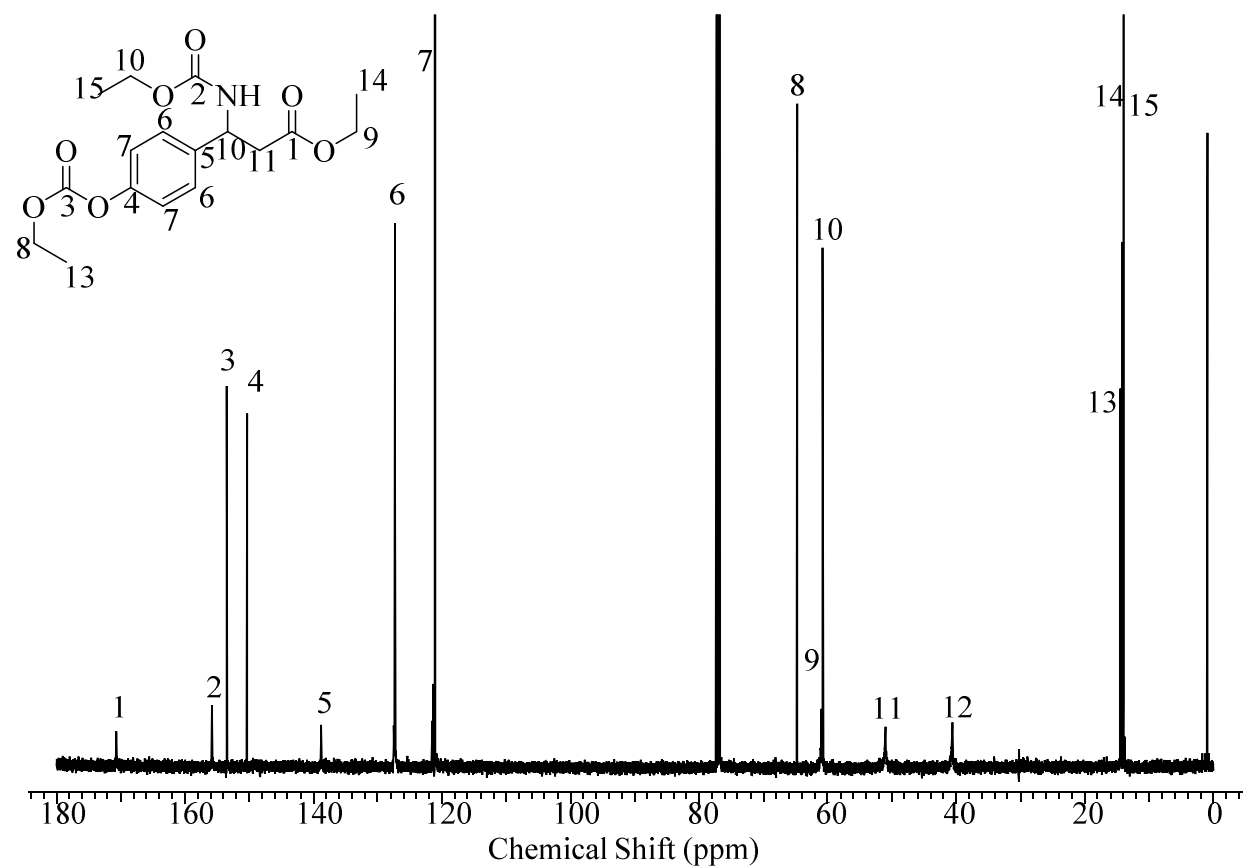


Figure A 17. a) ¹³C NMR of 4'-*O*, 3-*N*-di(ethoxycarbonyl) ethyl ester of β-tyrosine. ¹³C NMR (126 MHz, CDCl₃) δ: 170.7, 155.8, 153.5, 150.3, 138.8, 127.4, 121.3, 64.8, 61.0, 60.7, 51.0, 40.6, 14.5, 14.1, 14.0

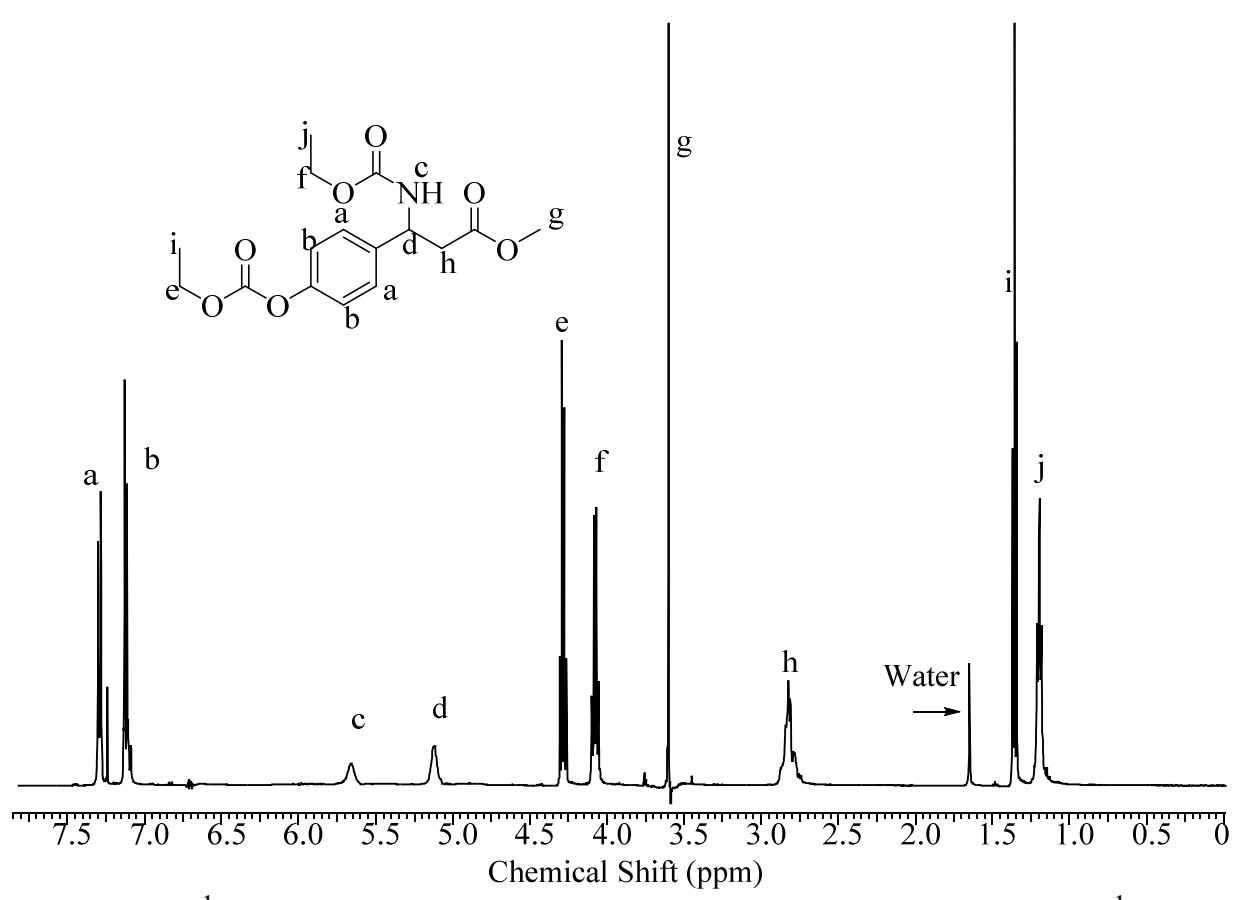


Figure A 18. ¹H NMR of 4'-*O*,3-*N*-di(ethoxycarbonyl) methyl ester of β-tyrosine. ¹H NMR (500 MHz, CDCl₃) δ = 7.29 (d, J = 8.5 Hz, 2 H), 7.12 (d, J = 8.5 Hz, 1 H), 5.66 (br. s., 1 H), 5.17 - 5.07 (m, 1 H), 4.28 (q, J = 6.9 Hz, 2 H), 4.08 (q, J = 7.3 Hz, 2 H), 3.60 (s, 3 H), 2.90 - 2.73 (m, 2 H), 1.36 (t, J = 7.3 Hz, 3 H), 1.20 (t, J = 7.0 Hz, 3 H)

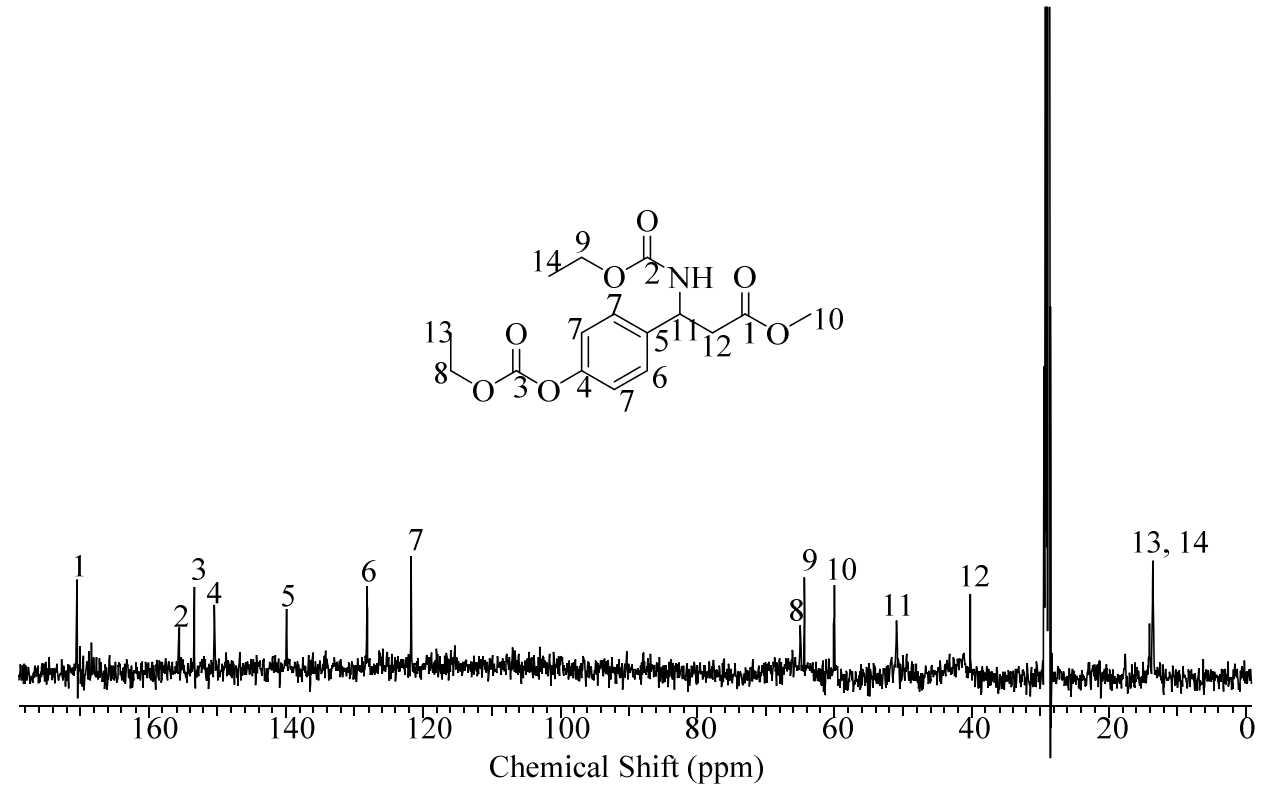


Figure A 19. ¹³C NMR of 4'-*O*,3-*N*-di(ethoxycarbonyl) methyl ester of β-tyrosine. ¹³C NMR (126 MHz, CD₃COCD₃) δ: 170.7, 155.9, 153.4, 150.5, 140.3, 128.4, 121.7, 65.0, 64.4, 60.0, 51.0, 40.2, 14.1, 13.6

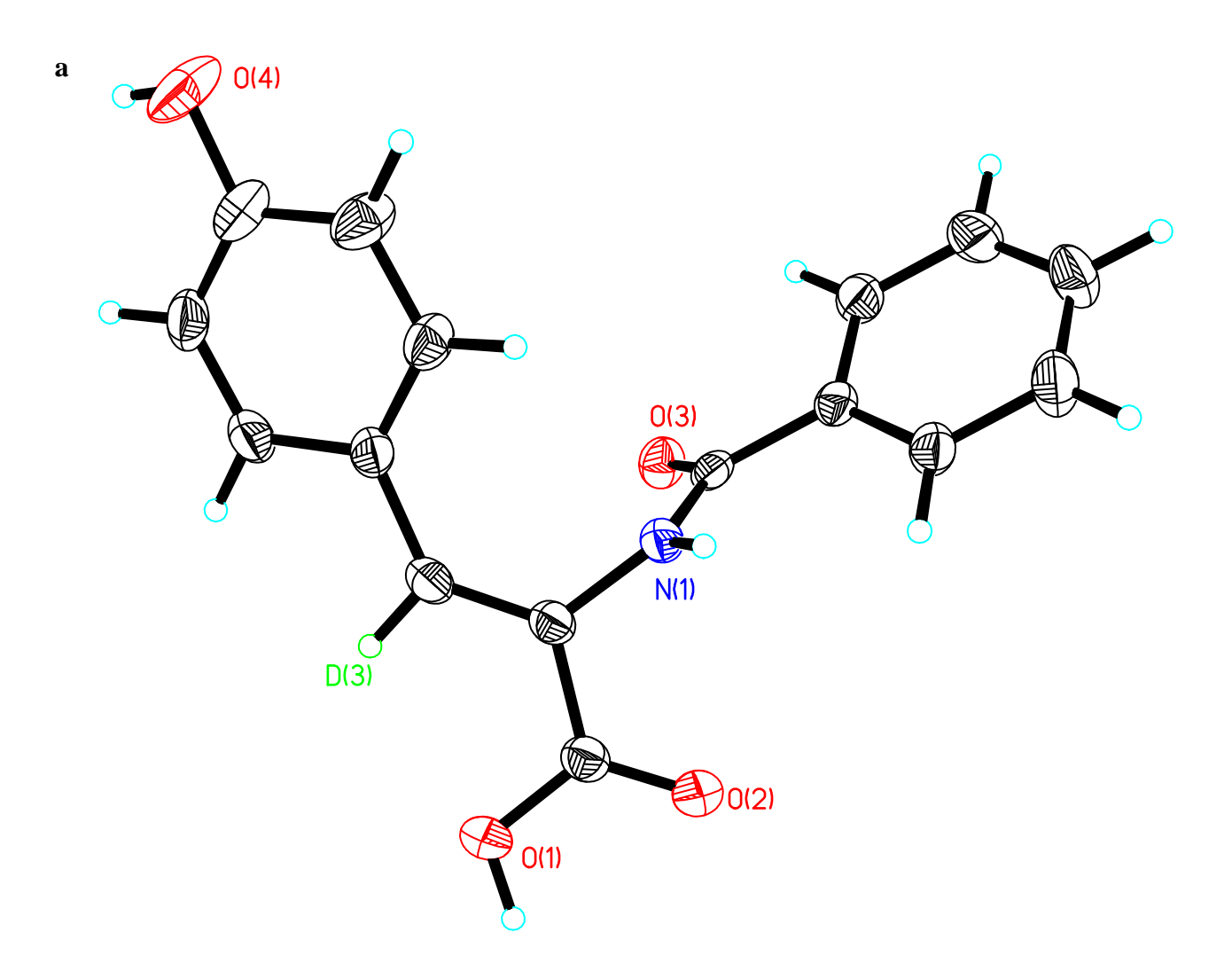
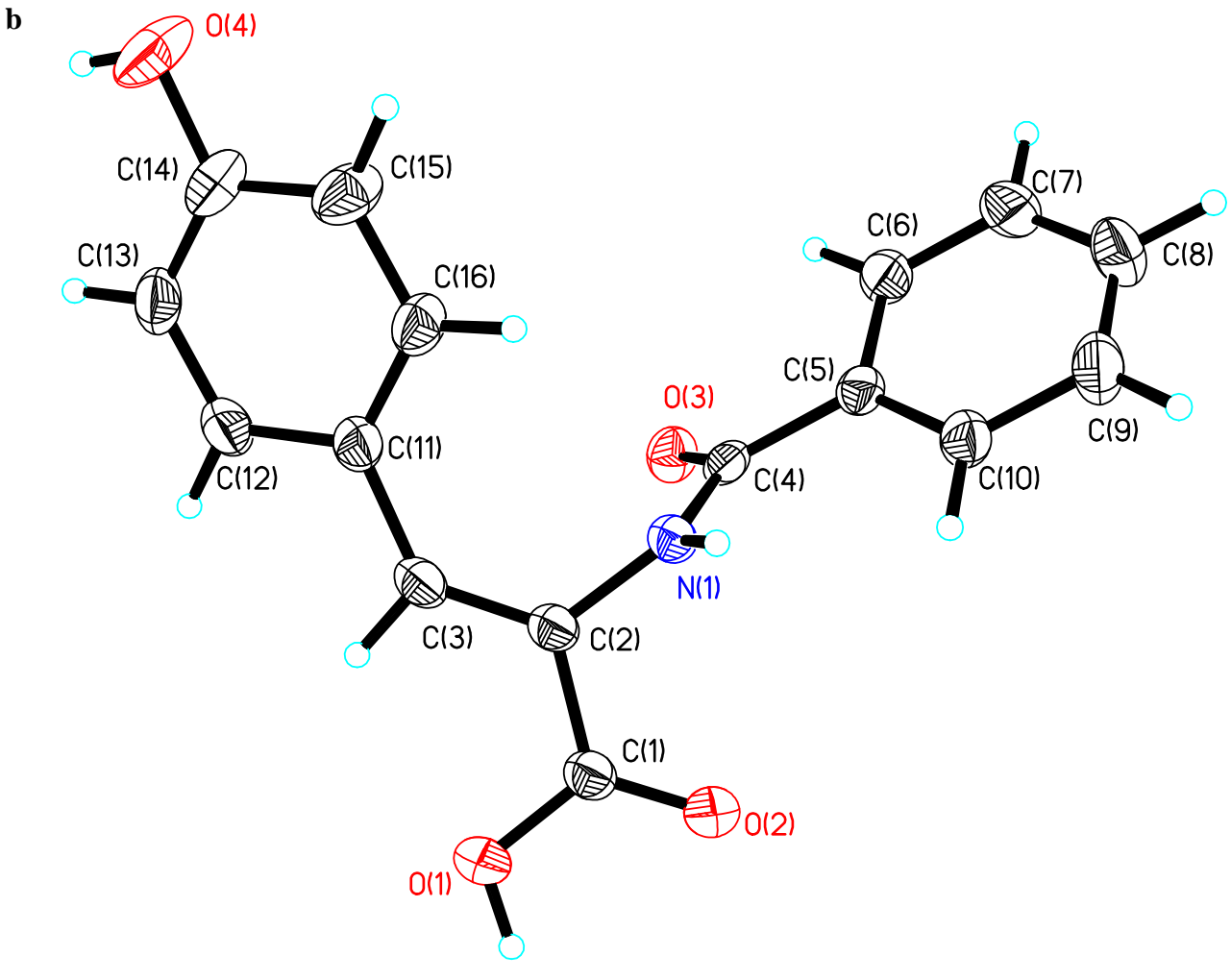


Figure A 20. Crystal structure of a) (*Z*)-2-benzamido-[3-²H]-3-(4'-hydroxyphenyl) acrylic acid and Color coding: Carbon (black), Hydrogen (Cyan), Deuterium (green) Oxygen (red), and Nitrogen (blue),





Crystal structure of b) (*Z*)-2-benzamido-3-(4'-hydroxyphenyl) acrylic acid. Color coding: Carbon (black), Hydrogen (Cyan), Deuterium (green) Oxygen (red), and Nitrogen (blue),

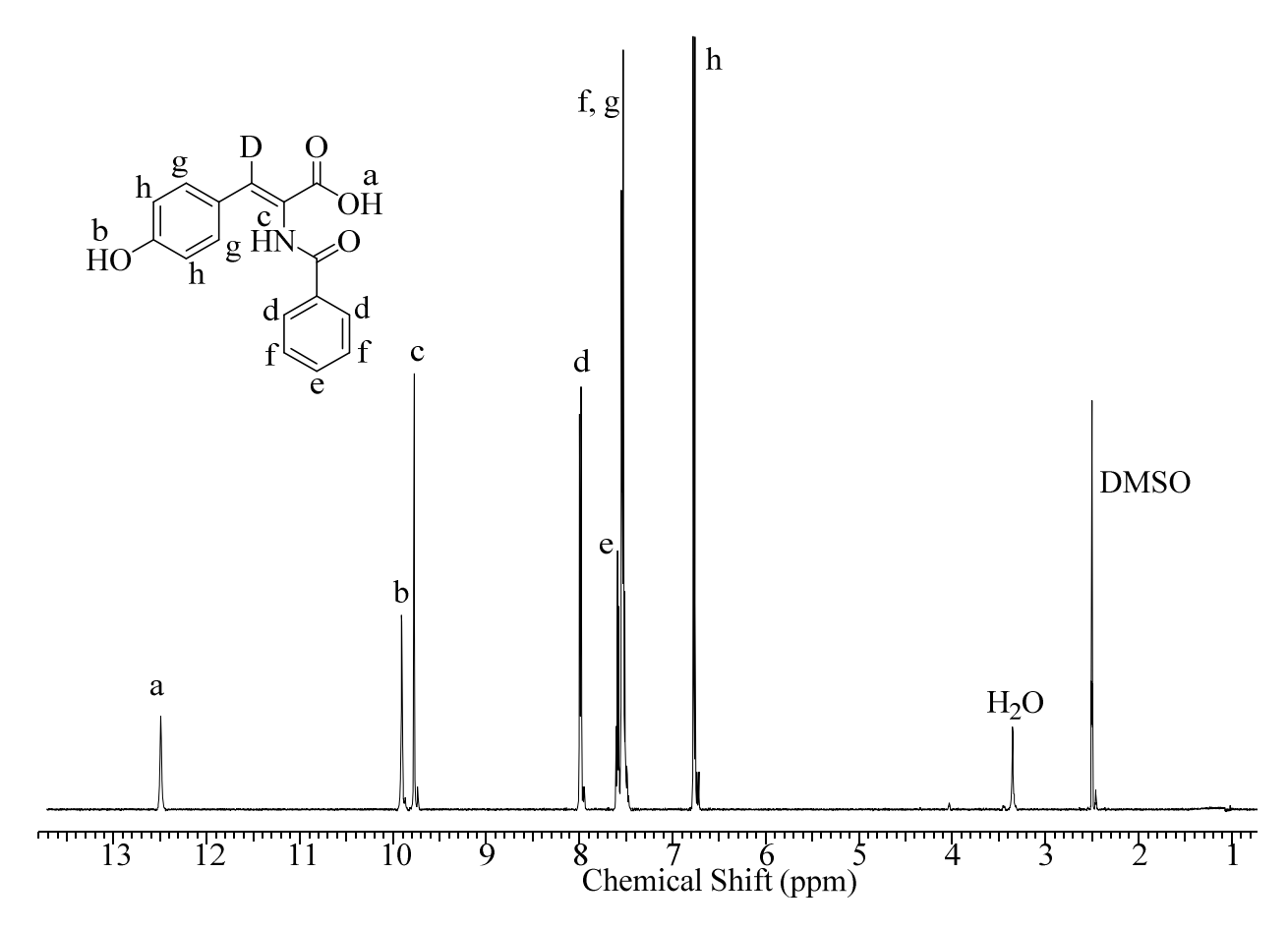


Figure A 21. ¹H NMR spectrum of (*Z*)-2-Benzamido-[3-²H]-3-(4'-hydroxyphenyl)acrylic Acid. ¹H NMR (500 MHz, DMSO-d₆) δ: 12.49 (br. s., 1 H), 9.91 (s, 1 H), 9.77 (s, 1 H), 7.99 (d, J = 7.1 Hz, 2 H), 7.59 (t, J = 7.6 Hz, 1 H), 7.56 - 7.49 (m, 4 H), 6.77 (d, J = 8.3 Hz, 2 H)

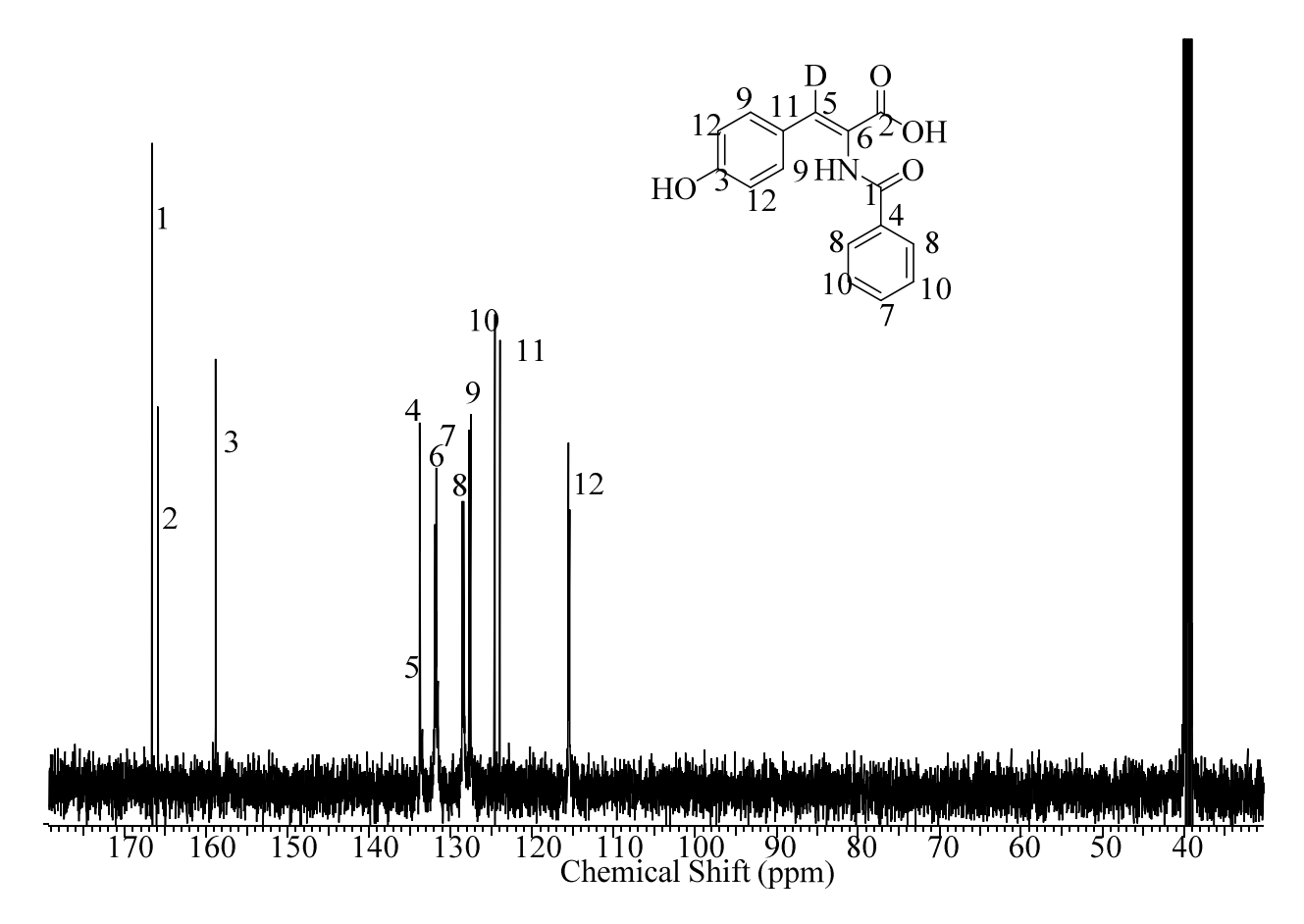


Figure A 22. ¹³C NMR spectrum of (*Z*)-2-Benzamido-[3-²H]-3-(4'-hydroxyphenyl)acrylic Acid. ¹³C NMR (126 MHz, DMSO-d₆) δ: 166.6, 165.9, 158.8, 133.7, 133.4, 131.9, 131.8, 128.5, 128.3, 127.7, 127.5, 124.6, 123.9, 115.5, 115.4

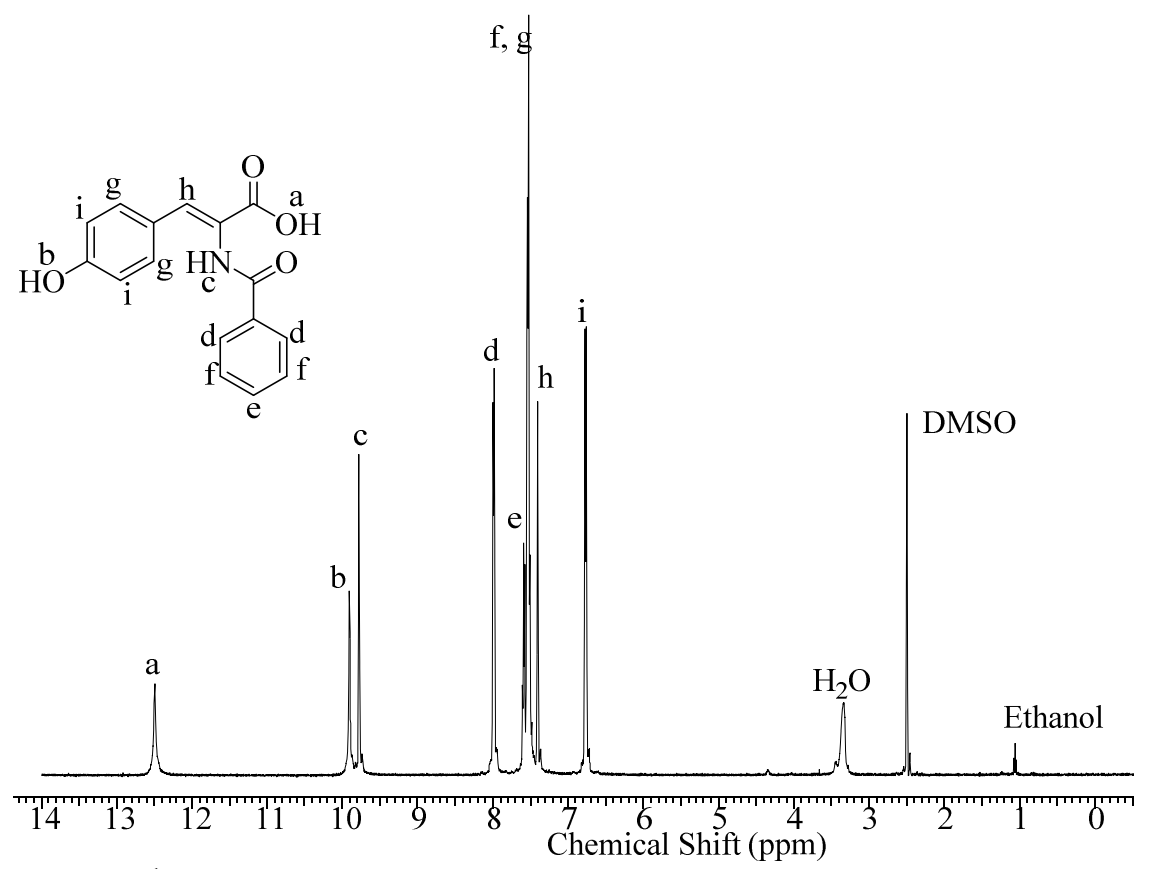


Figure A 23. ¹H NMR spectrum of (*Z*)-2-Benzamido-3-(4'-hydroxyphenyl)acrylic Acid. ¹H NMR (500 MHz, DMSO-d₆) δ : 12.49 (br. s., 1 H), 9.91 (br. s., 1 H), 9.82 - 9.72 (m, 1 H), 7.99 (d, J = 7.3 Hz, 2 H), 7.59 (t, J = 7.1 Hz, 1 H), 7.56 - 7.47 (m, 4 H), 7.41 (s, 1 H), 6.77 (d, J = 8.3 Hz, 2 H)

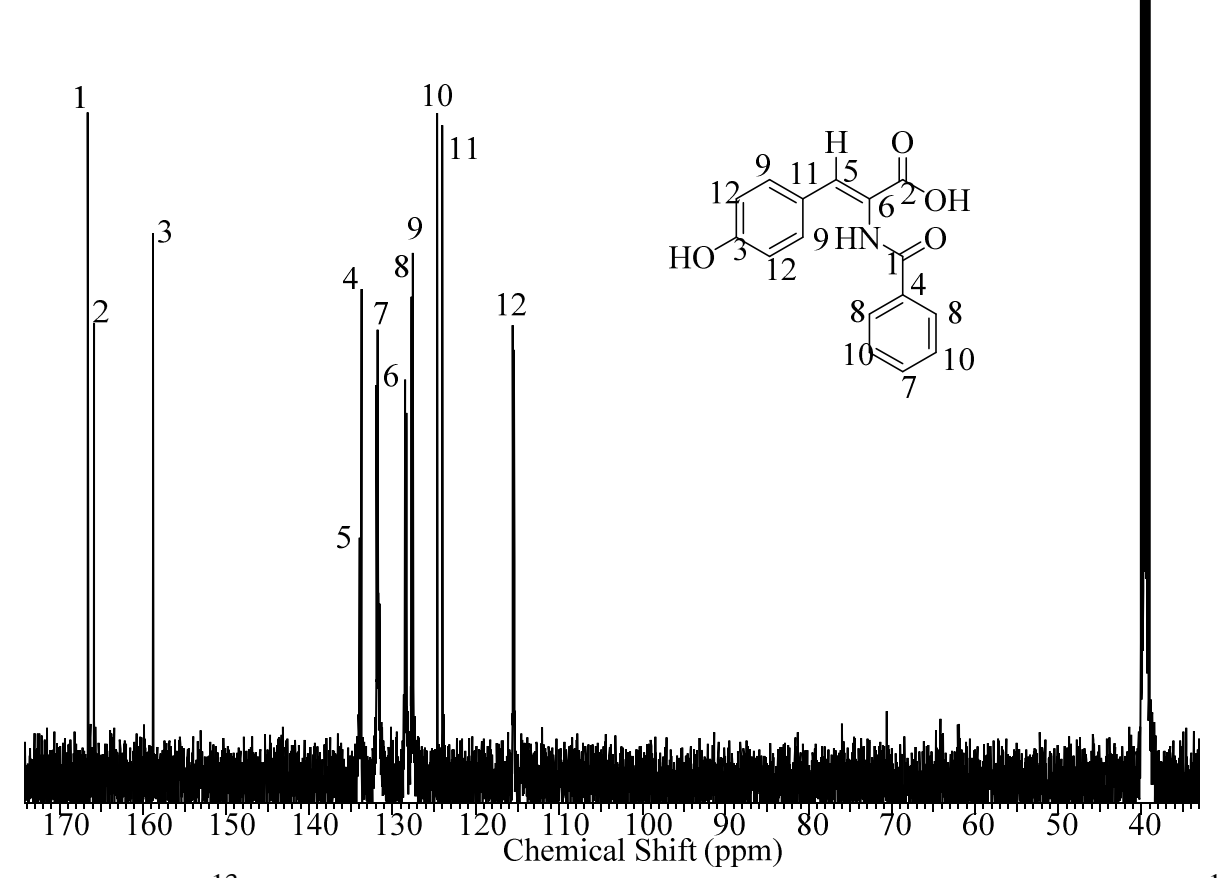


Figure A 24. ¹³C NMR spectrum of (*Z*)-2-Benzamido-3-(4'-hydroxyphenyl)acrylic Acid. ¹³C NMR (126 MHz, DMSO-d₆) δ: 166.6, 165.9, 158.8, 134.0, 133.8, 131.9, 131.8, 128.5, 128.4, 127.7, 127.5, 124.6, 124.0, 115.5, 115.4

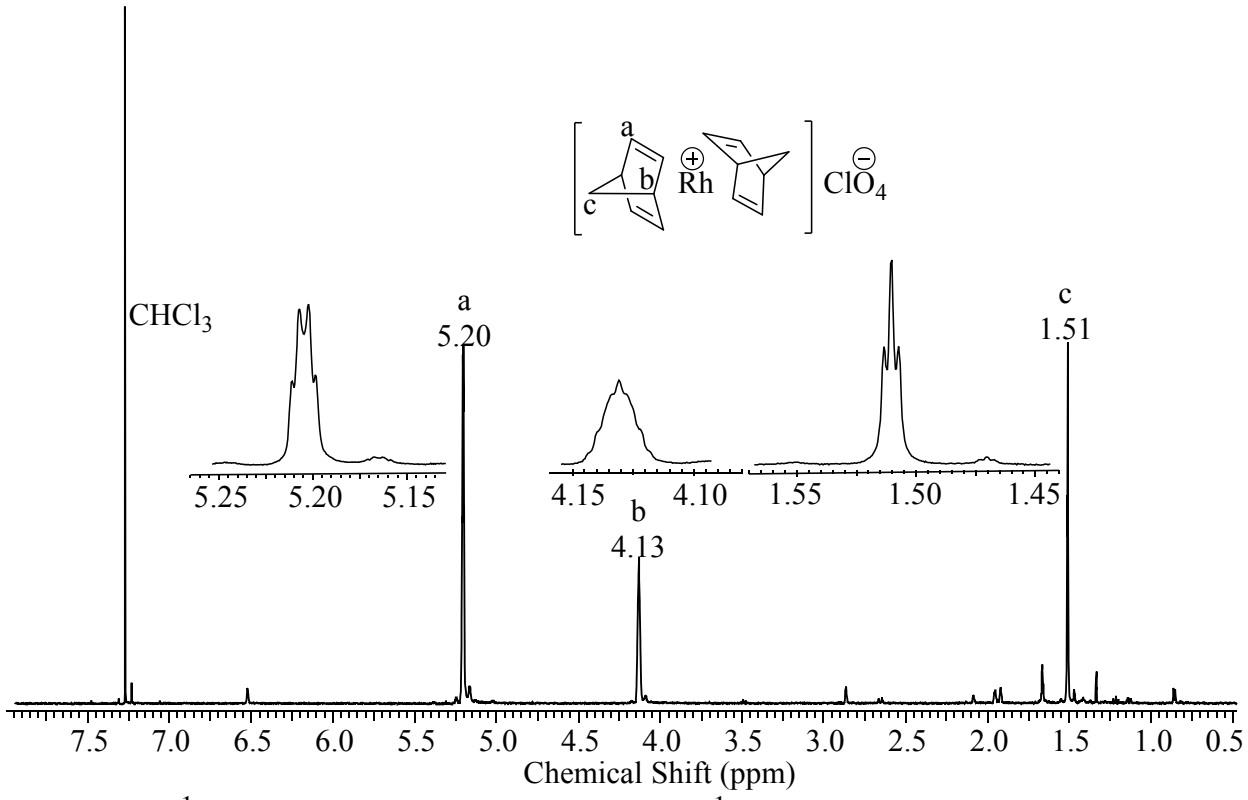


Figure A 25. ¹H NMR spectrum of [Rh(NBD)₂]ClO₄. ¹H NMR (500 MHz, CDCl₃) δ: 5.20 (q, J = 2.2 Hz, 8 H), 4.15 - 4.11 (m, 4 H), 1.51 (t, J = 1.6 Hz, 4 H)

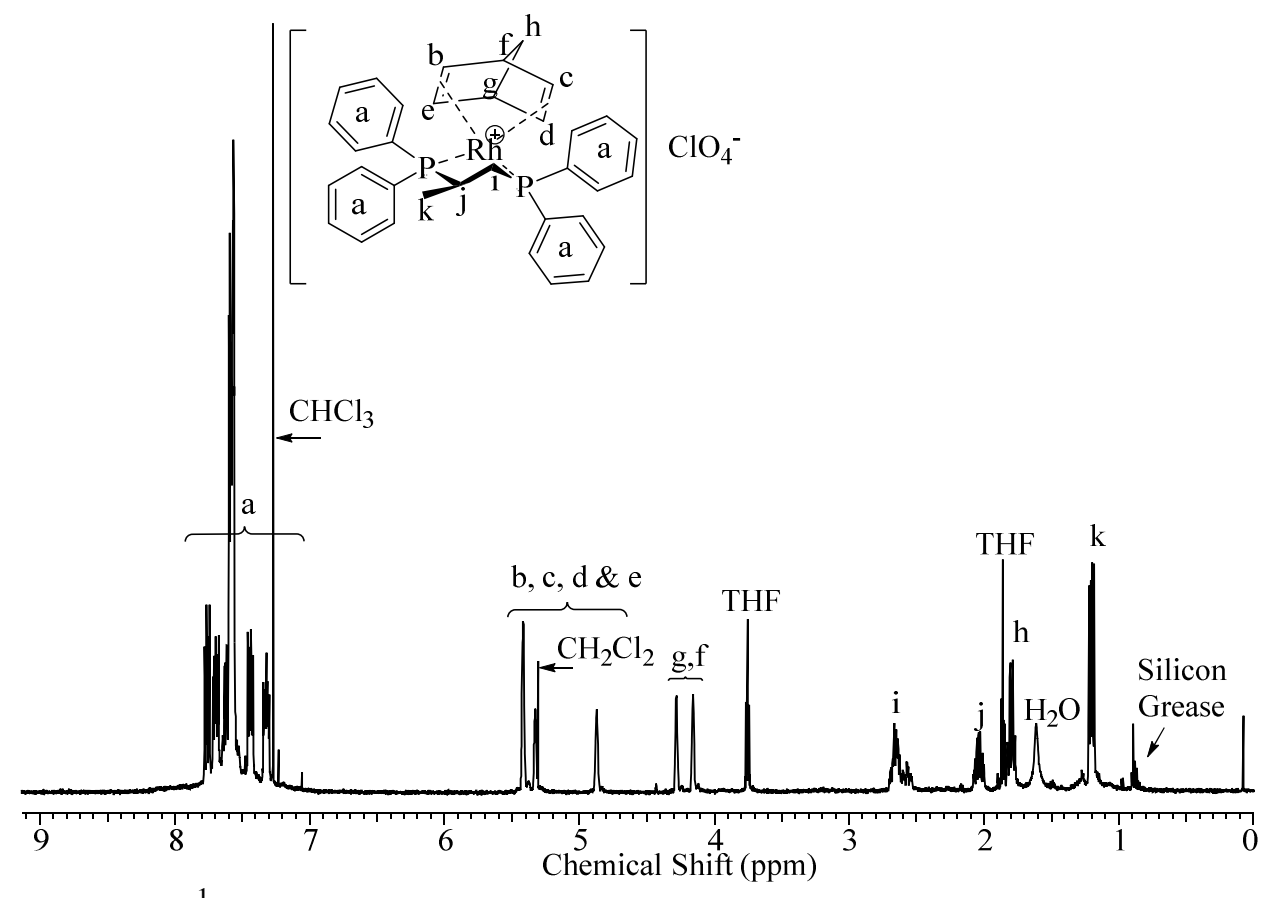


Figure A 26. ¹H NMR spectrum of [Rh(NBD)(R)-Prophos]ClO₄•0.5 CH₂Cl₂. Trace amounts of THF, H₂O, and silicon grease are present as impurities. ¹H NMR (500 MHz, CDCl₃) δ = 7.79 - 7.73 (m, 2 H), 7.72 - 7.67 (m, 3 H), 7.65 - 7.61 (m, 2 H), 7.61 - 7.58 (m, 6 H), 7.58 - 7.55 (m, 6 H), 7.47 - 7.41 (m, 2 H), 7.35 - 7.29 (m, 2 H), 5.42 (br. s., 2 H), 5.31 (s, 1 H), 4.87 (br. s., 1 H), 4.28 (br. s., 1 H), 4.16 (br. s., 1 H), 2.71 - 2.59 (m, 2 H), 2.04 (td, J = 7.4, 12.5 Hz, 1 H), 1.84 - 1.76 (m, 2 H), 1.21 (dd, J = 6.5, 12.5 Hz, 3 H)

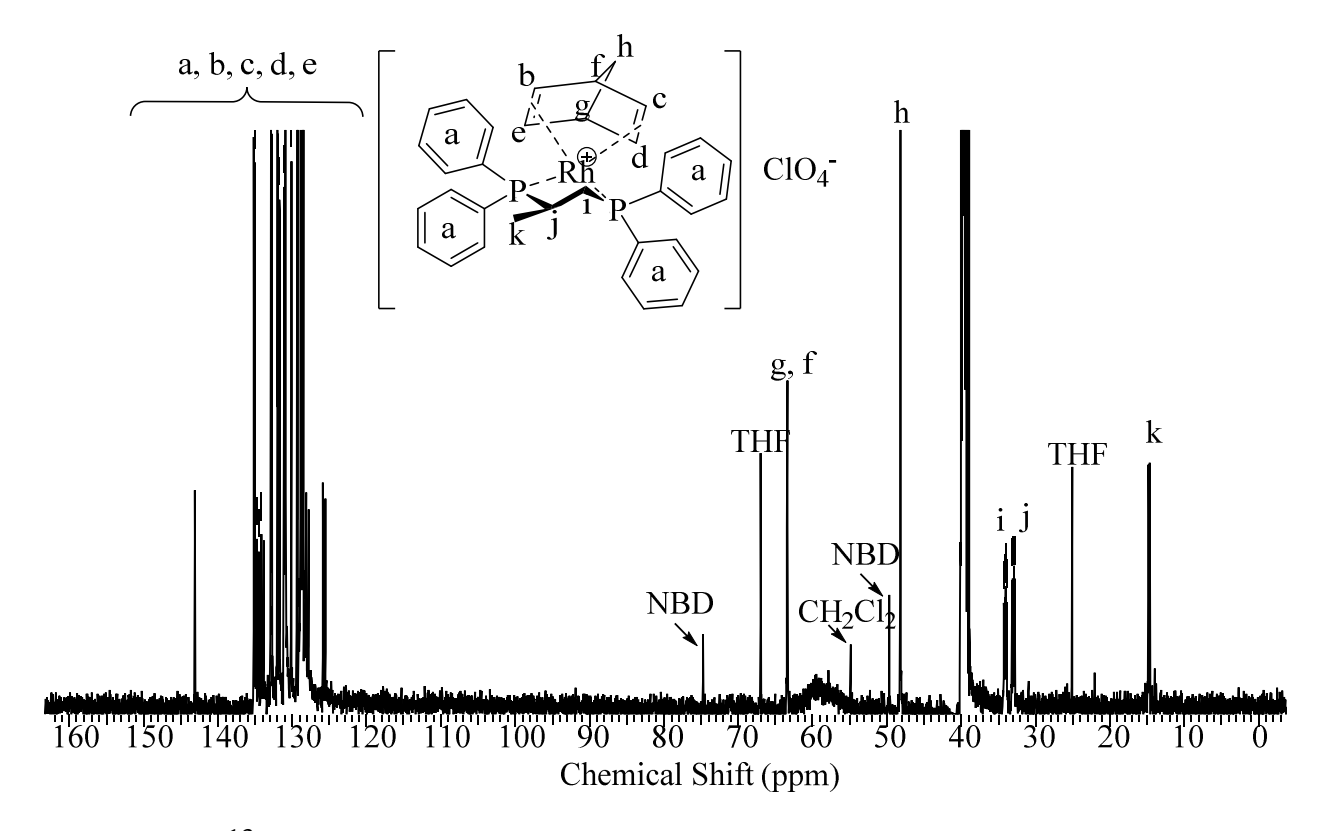


Figure A 27. 13 C NMR spectrum of [Rh(NBD)(R)-Prophos]ClO₄•0.5 CH₂Cl₂. Trace amounts of THF, is present as impurities. 13 C NMR (126 MHz, DMSO-d₆) δ = 143.1, 135.1, 135.1, 134.8, 134.5, 134.1, 133.9, 132.8, 132.7, 132.0, 131.9, 131.7, 131.1, 131.0, 130.9, 130.1, 129.3, 129.3, 128.9, 128.8, 128.8, 128.6, 128.5, 128.2, 127.8, 125.9, 125.5, 63.4, 48.2, 34.2, 33.0, 14.7

Table A 1. EI-MS Fragment Ions of 4'-0,2-N-Di(ethoxycarbonyl) Methyl Ester Derivatives of Authentic and Synthesized Isotopomers of (S)-1.

m/z 339

| Isotopomers of Substrate 1 | Fragment ion F4: Cleavage at Bond <i>e</i> | Ion abundance ratio ^a [F4] ⁺ :[F4 ⁺ - 1] ⁺ :[F4 - 2] ⁺ | D atom |
|---|---|---|--------|
| HO NH ₃ | H H H H H H H | 100:0:0 | 0 |
| a (2S)-unlabeled | m/z 280 | 280:279:278 | |
| H D O O O NH ₃ | | 93:5:2 | 98 |
| b $(2S,3S)$ - $[2,3^2H_2]$ | m/z 282 | 282:281:280 | |
| D H O O O O NH NH3 | D H HN O | 98:2:0 | 99 |
| c $(2S,3R)$ - $[3-^2H]$ | m/z 281 | 281:280:279 | |
| D D O O O O O O O O O O O O O O O O O O | | 93:5:2 | 98 |
| d $(2S)$ - $[3,3-^2H_2]$ | m/z 282 | 282:281:280 | |

^aRatio of ion abundances of m/z [**F4**] ⁺:[**F4** - 1] ⁺:[**F4** - 2] ⁺ for entries **b**, **c**, and **d** (where

 $[\mathbf{F4}]^+ = [\mathbf{M}^+ - 59]$ is calculated to determine deuterium enrichment).

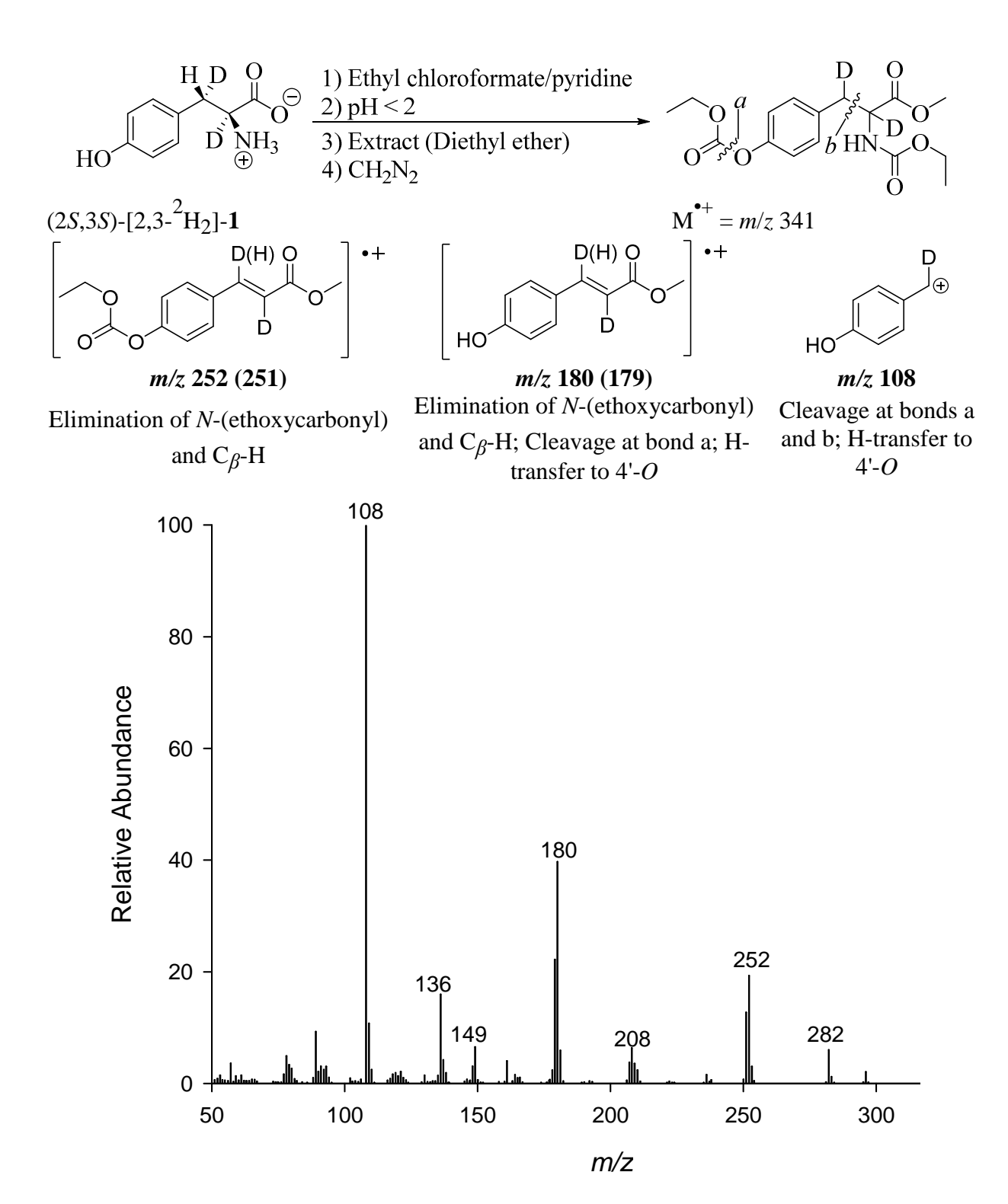


Figure A 28. EI-MS fragmentation of 4'-O,2-N-di(ethoxycarbonyl) methyl ester derivatives of (2S,3S)-[2,3- 2 H₂]-1. Diagnostic fragment ions are m/z 252, 180, and 108.

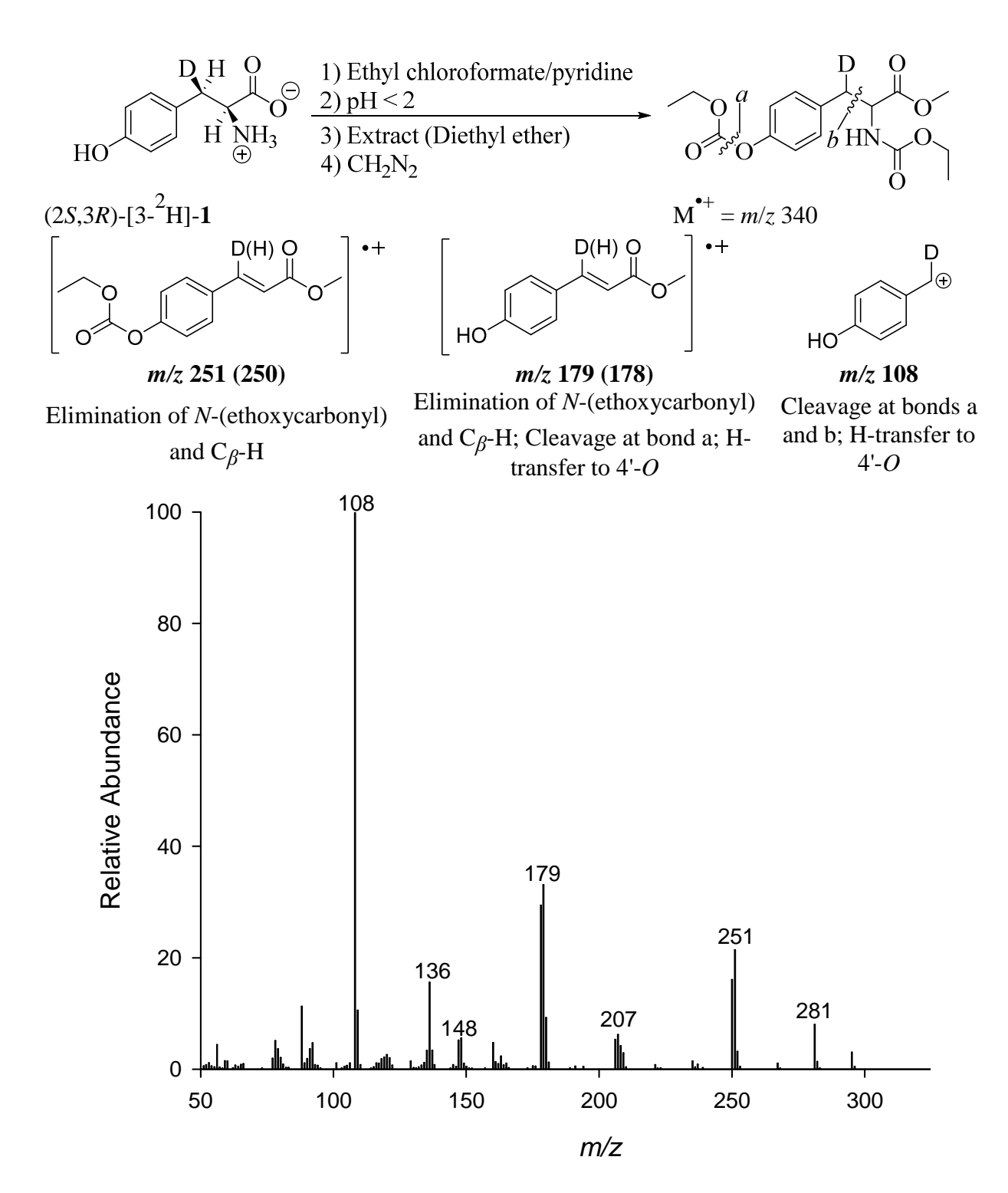


Figure A 29. EI-MS fragmentation of 4'-O,2-N-di(ethoxycarbonyl) methyl ester derivatives of (2S,3R)- $[3^2H]$ -1. Diagnostic fragment ions are m/z 251, 179, and 108.

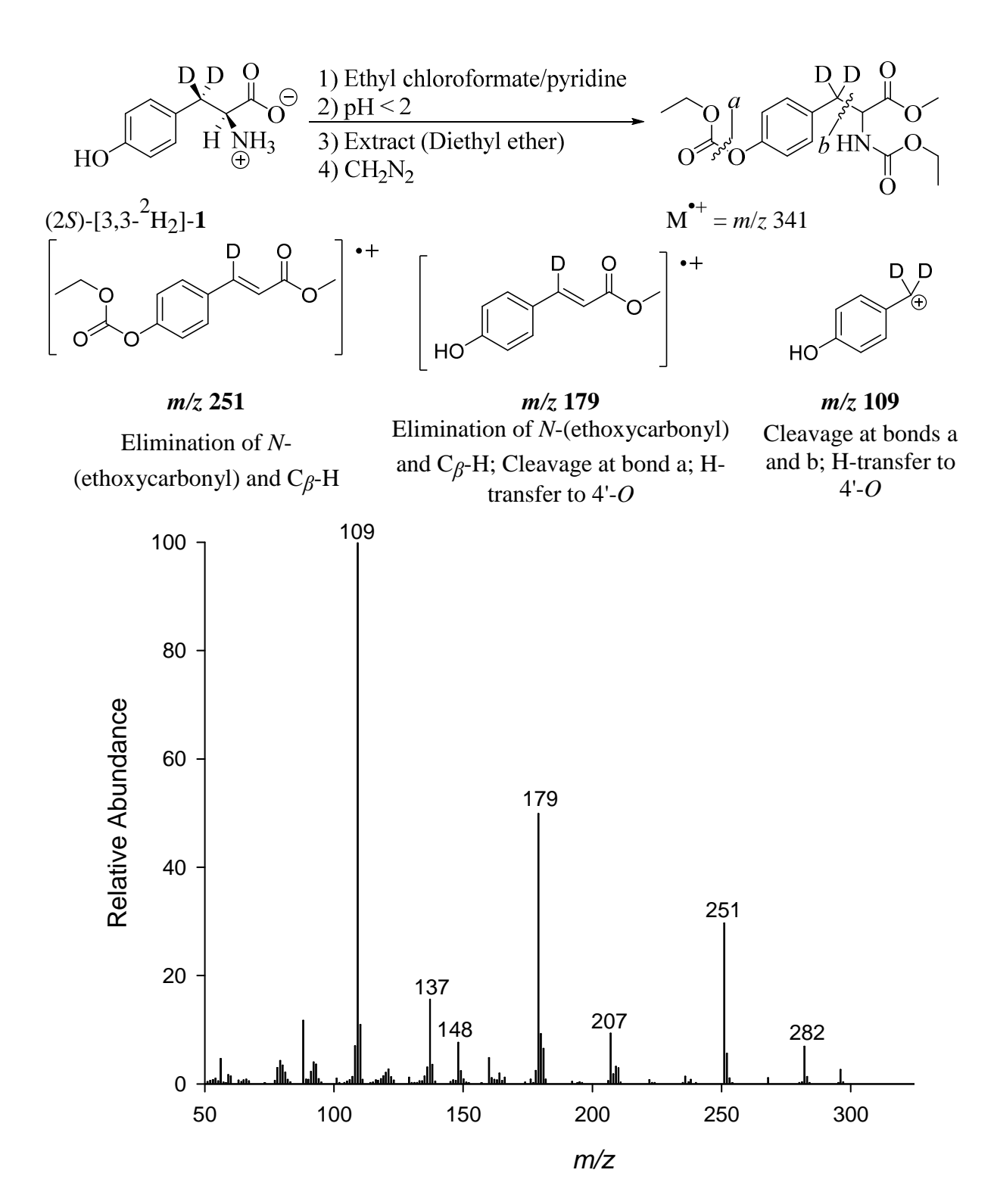


Figure A 30. EI-MS fragmentation of 4'-O,2-N-di(ethoxycarbonyl) methyl ester derivatives of (2S)-[3,3- 2 H₂]-1. Diagnostic fragment ions are m/z 251, 179, and 109.

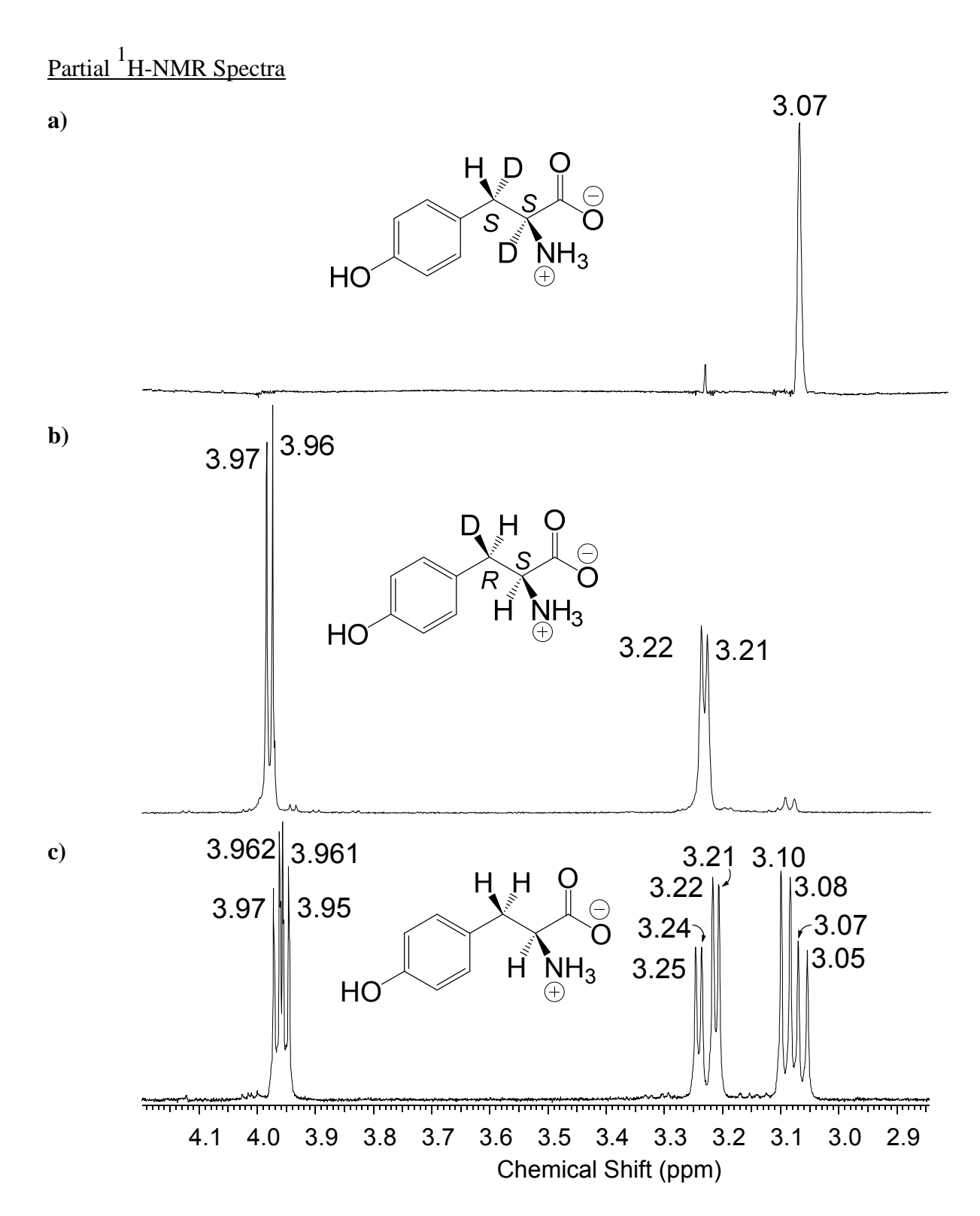
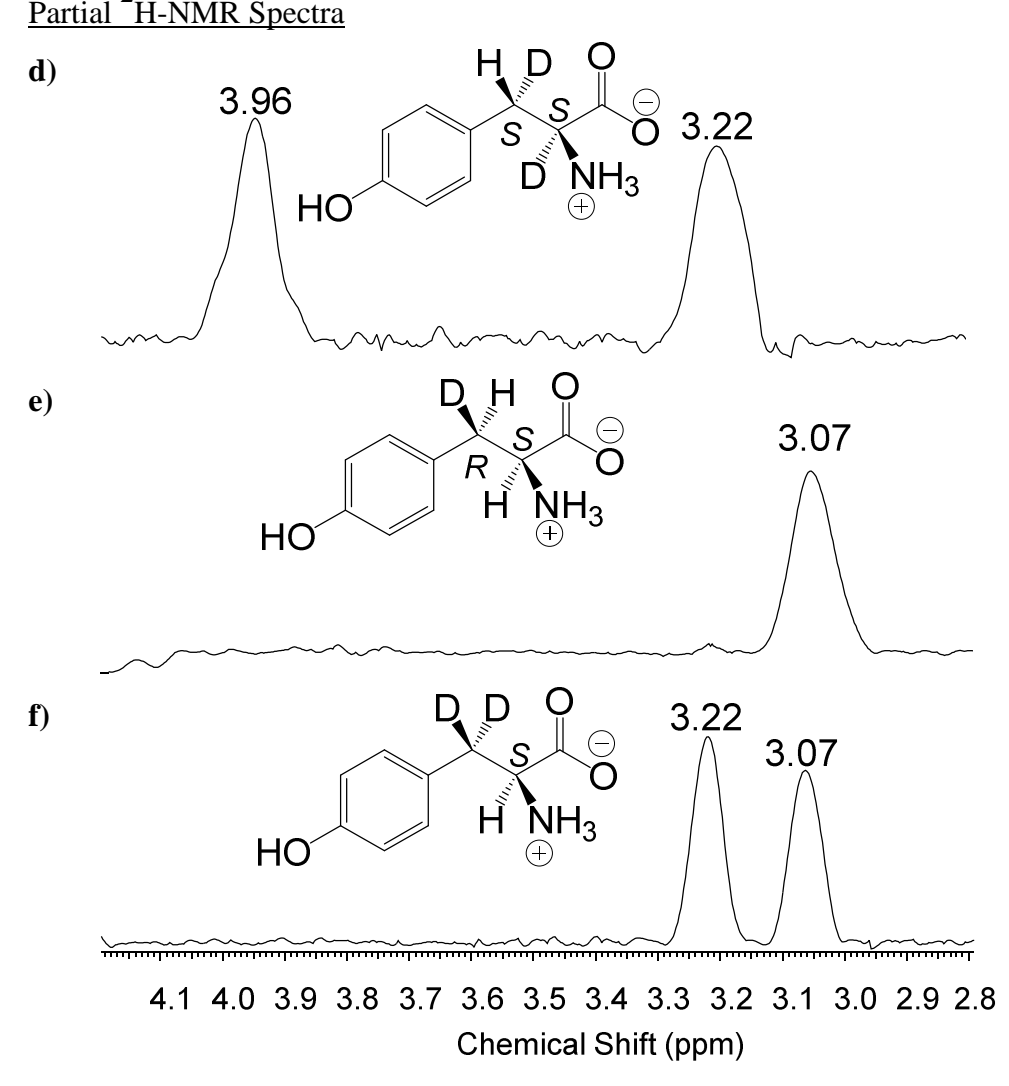


Figure A 31. Partial NMR spectra of isotopomers of (S)-1.

Figure A 31 (cont'd).

Partial ²H-NMR Spectra



Partial NMR spectra of isotopomers of (S)-1.

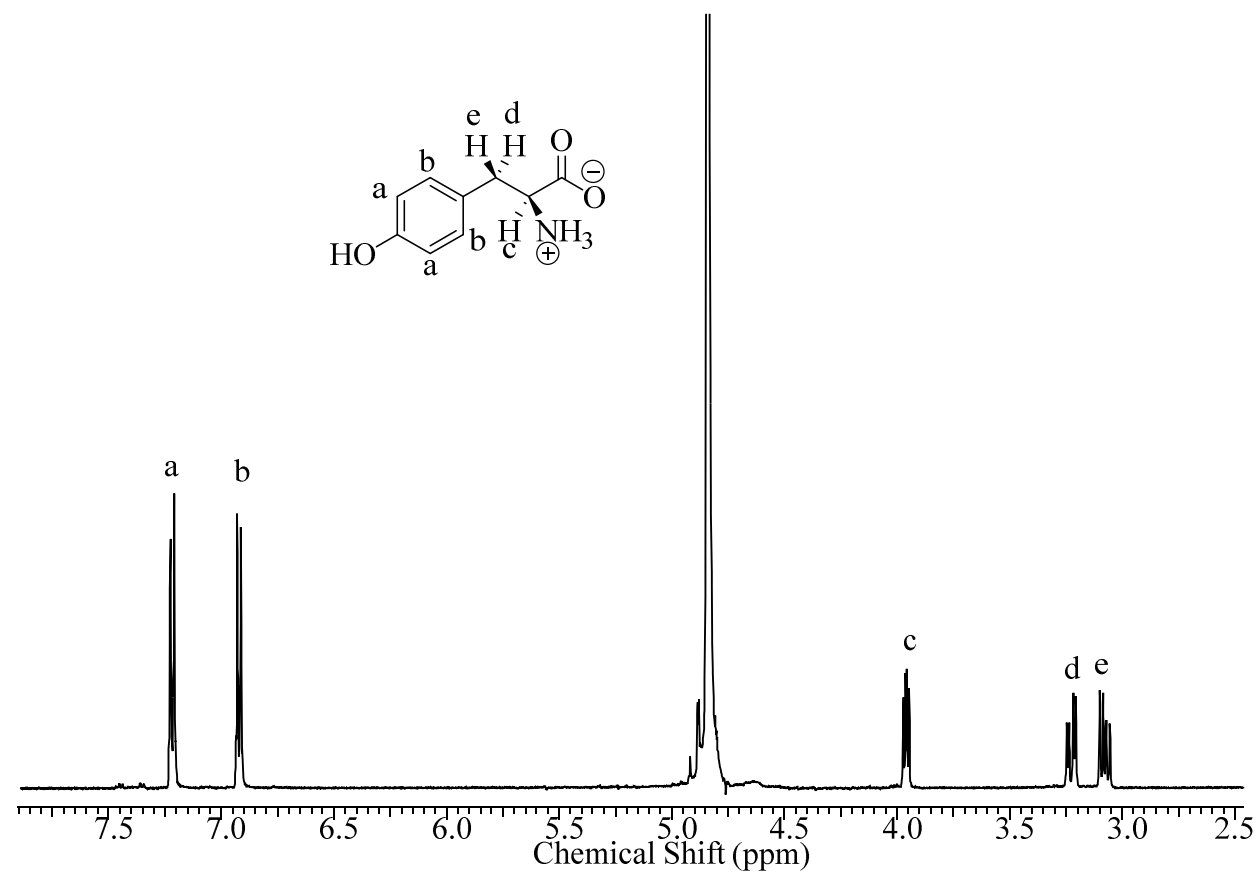


Figure A 32. ¹H NMR spectrum of α-tyrosine. ¹H NMR (500 MHz, D₂O) δ: 7.22 (d, J = 8.5 Hz, 2 H), 6.92 (d, J = 8.5 Hz, 2 H), 3.96 (dd, J = 5.1, 7.8 Hz, 1 H), 3.23 (dd, J = 5.0, 14.8 Hz, 1 H), 3.08 (dd, J = 7.8, 14.6 Hz, 1 H)

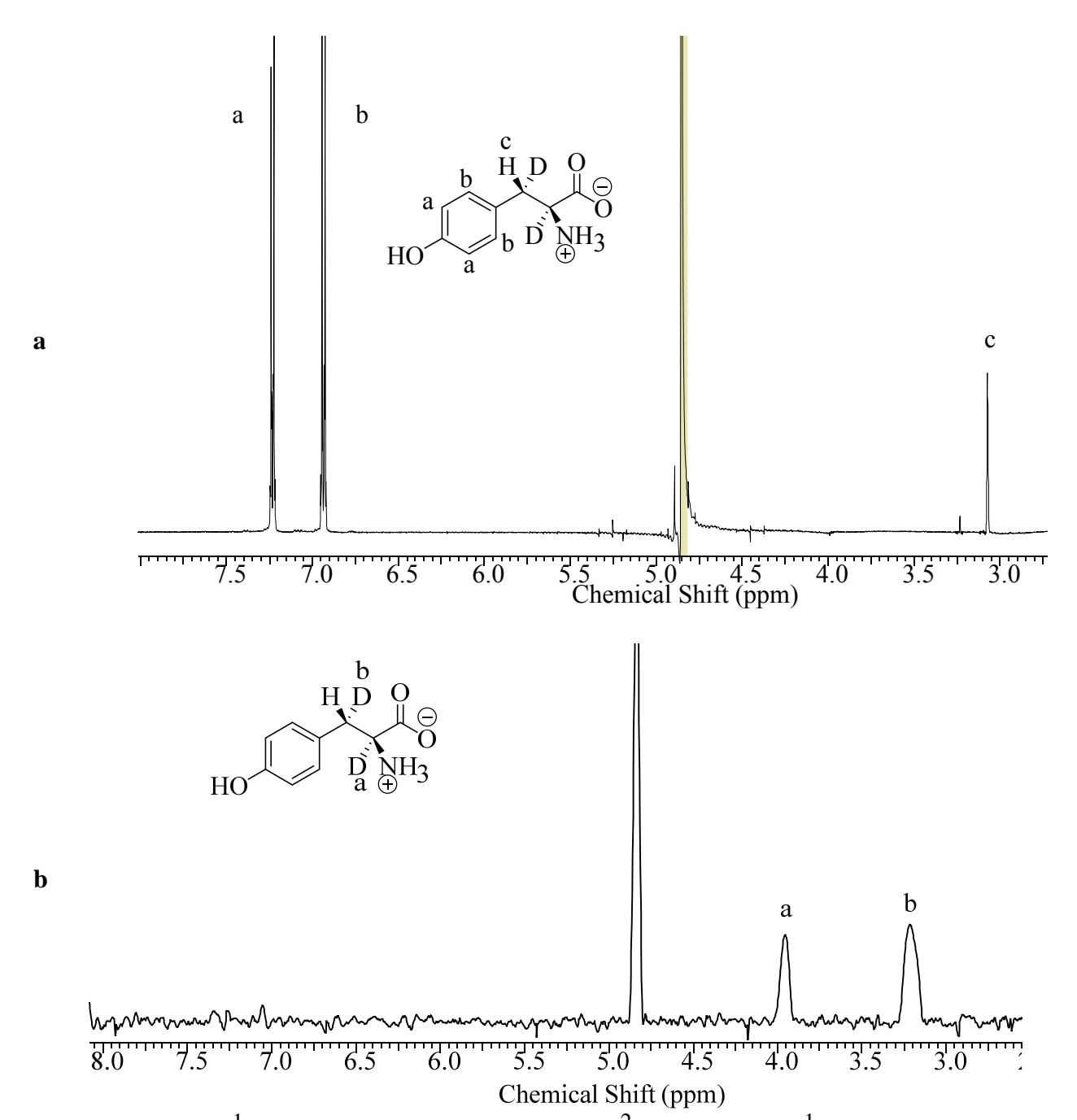


Figure A 33. a) ¹H NMR spectrum of (2S,3S)-[2,3-²H₂]-α-tyrosine. ¹H NMR (500 MHz, D₂O) δ: 7.22 (d, J = 8.5 Hz, 2 H), 6.92 (d, J = 8.5 Hz, 2 H), 3.08 (s, 1 H). b) ²H NMR spectrum of (2S,3S)-[2,3-²H₂]-α-tyrosine. ²H NMR (77 MHz, H₂O) δ: 3.97 (bs, 1 ²H) 3.22 (bs, 1 ²H).

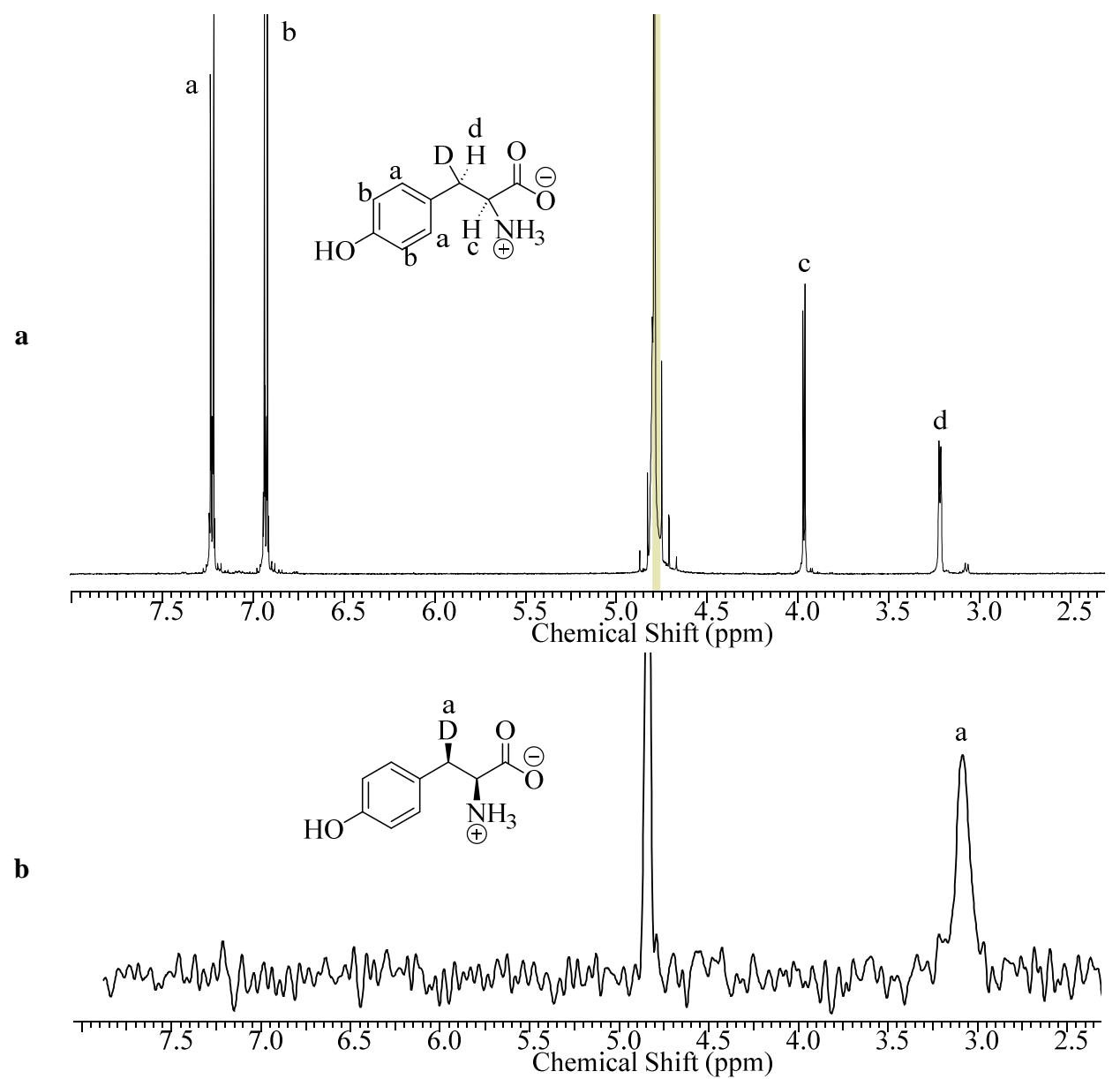


Figure A 34. a) ¹H NMR spectrum of (2S,3R)-[3-²H]-α-tyrosine. ¹H NMR (500 MHz, D₂O) δ: 7.22 (d, J = 8.5 Hz, 2 H), 6.92 (d, J = 8.5 Hz, 2 H), 3.97 (d, J = 5.0 Hz, 1 H), 3.22 (d, J = 5.0 Hz, 1 H) b) ²H NMR spectrum of (2S,3R)-[3-²H]-α-tyrosine. ²H NMR (77 MHz, H₂O) δ: 3.08 (bs, 1 ²H).

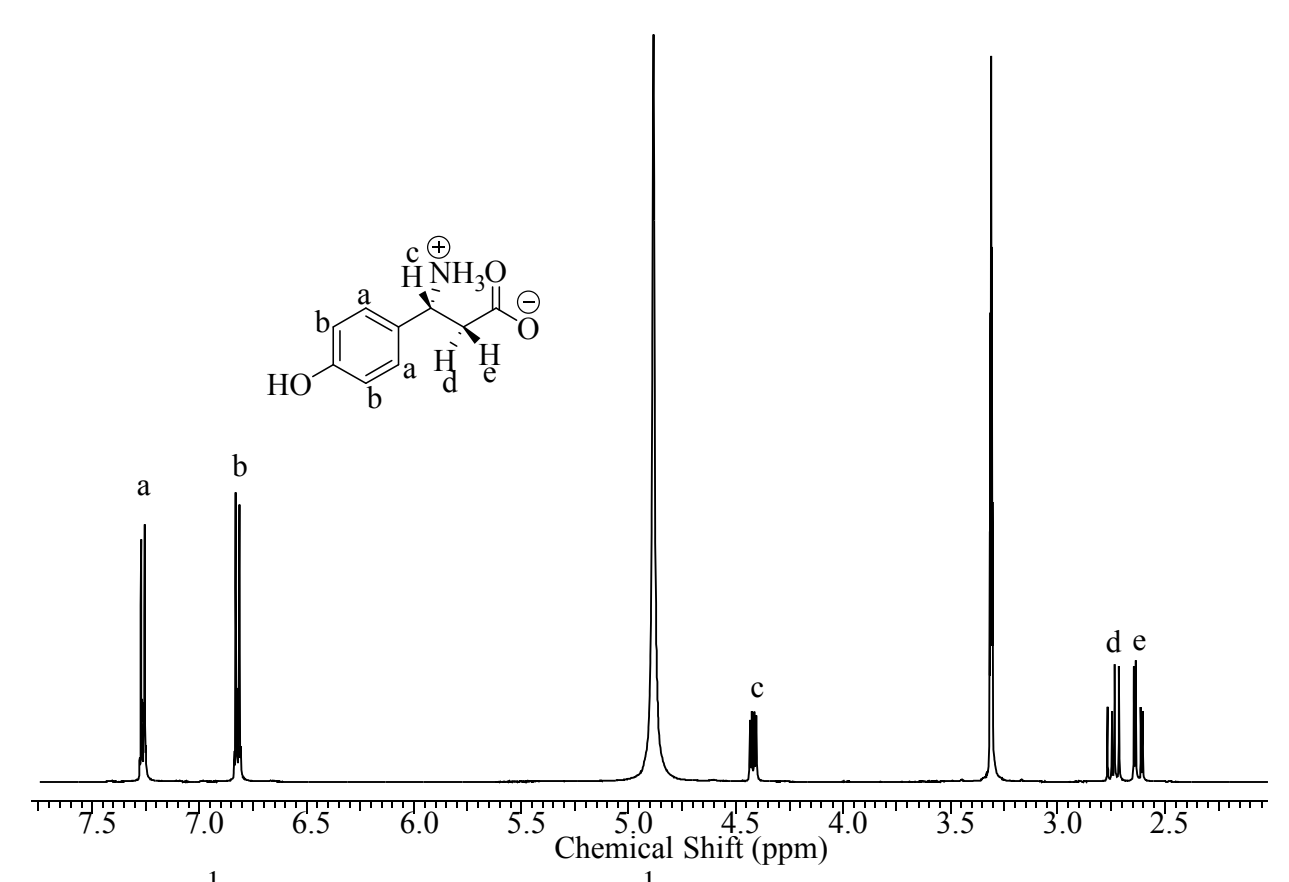


Figure A 35. ¹H NMR spectrum of β-tyrosine. ¹H NMR (500 MHz, CD₃OD) δ: 7.25 (d, J = 8.8 Hz, 2 H), 6.81 (d, J = 8.8 Hz, 2 H), 4.41 (dd, J = 4.2, 10.0 Hz, 1 H), 2.73 (dd, J = 10.0, 16.6 Hz, 1 H), 2.61 (dd, J = 4.2, 16.6 Hz, 1 H)

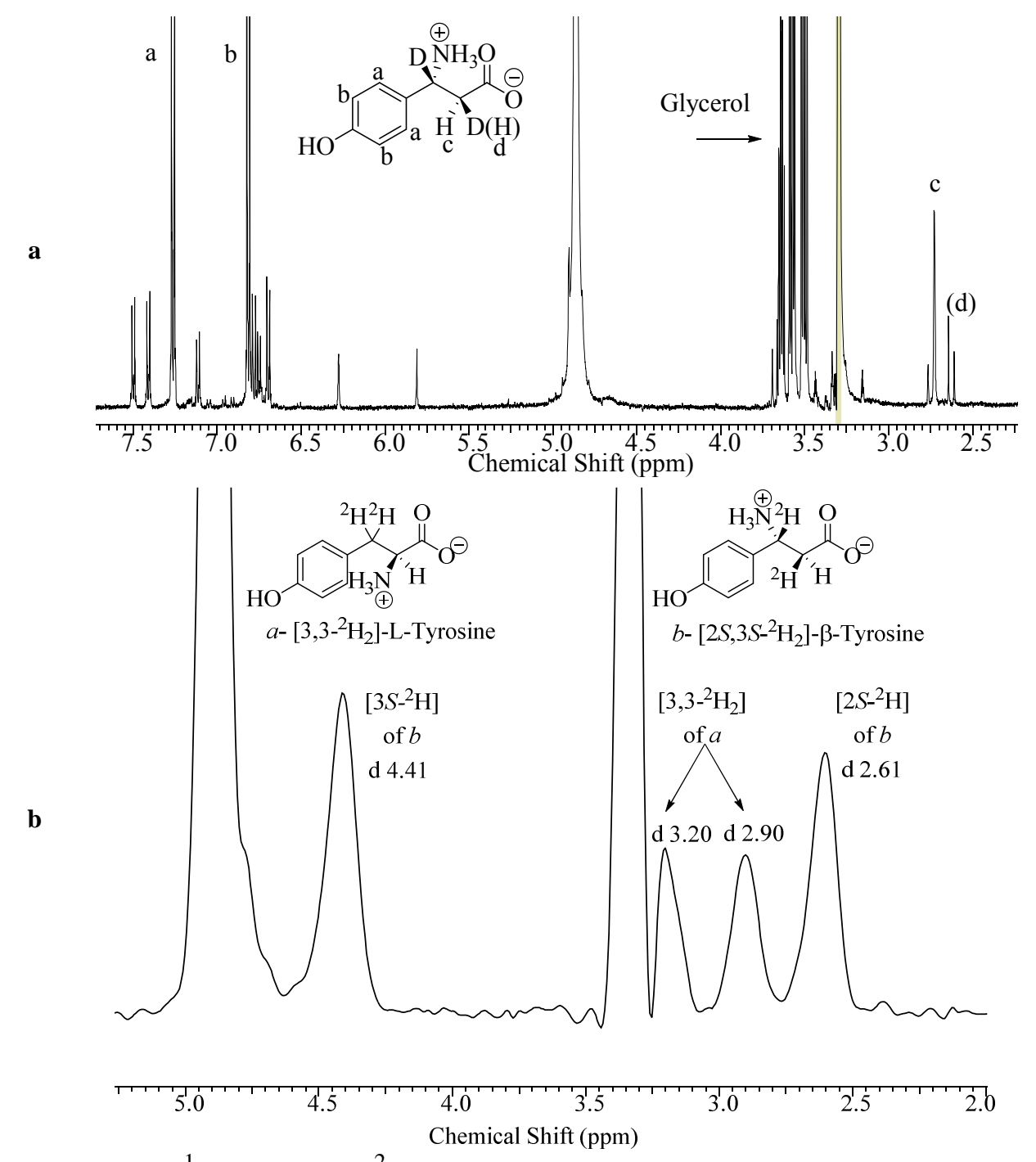


Figure A 36. a) 1 H NMR and b) 2 H NMR spectra of the reaction mixture of biosynthesized products catalyzed by CcTAM from (2S)-[3,3- 2 H₂]- α -tyrosine.

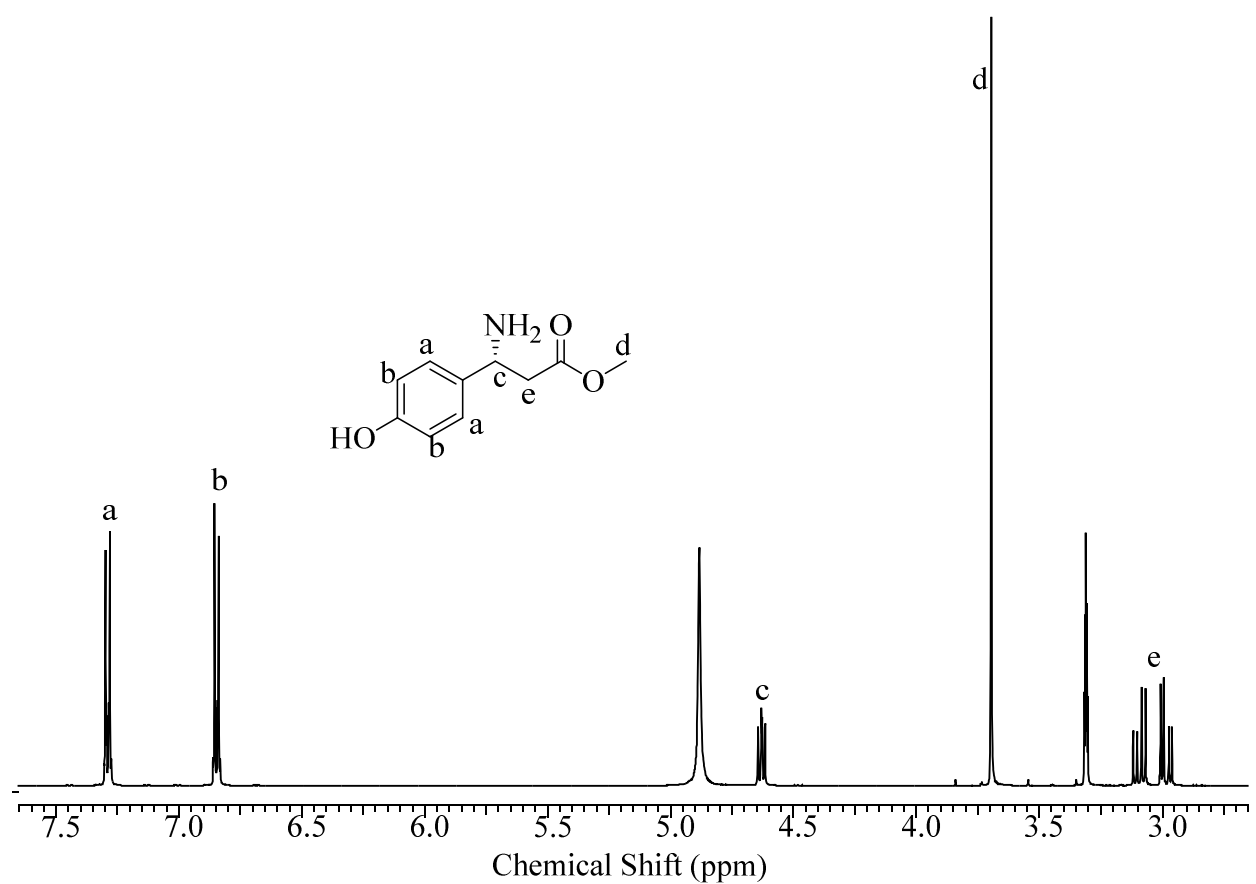


Figure A 37. ¹H NMR spectrum of β-tyrosine methyl ester. ¹H NMR (500 MHz, CD₃OD) δ: 7.29 (td, J = 2.2, 8.5 Hz, 2 H), 6.85 (td, J = 2.2, 8.5 Hz, 2 H), 4.63 (dd, J = 6.3, 7.8 Hz, 1 H), 3.09 (dd, J = 7.8, 16.6 Hz, 1 H), 2.98 (dd, J = 6.3, 16.7 Hz, 1 H)

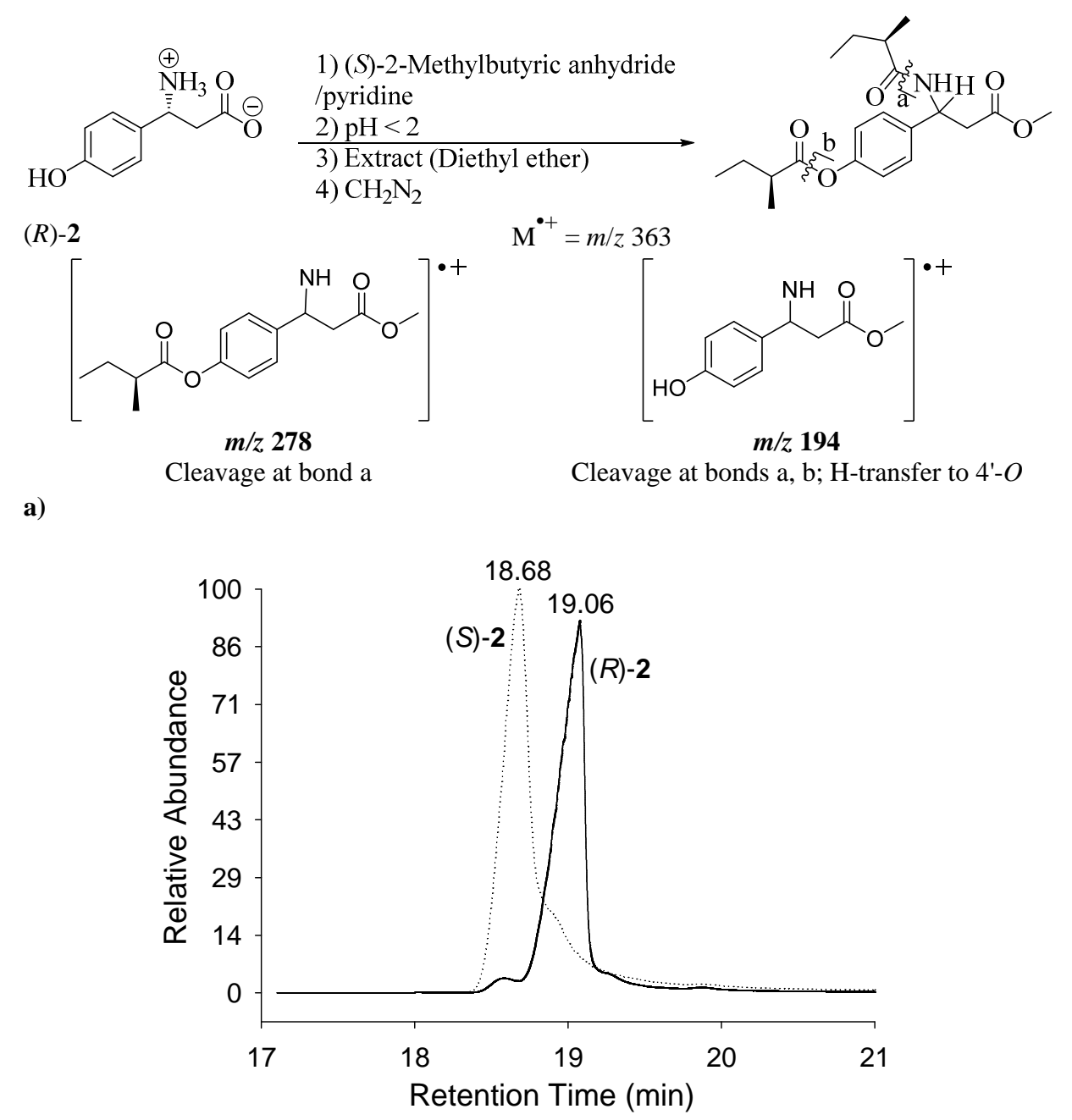
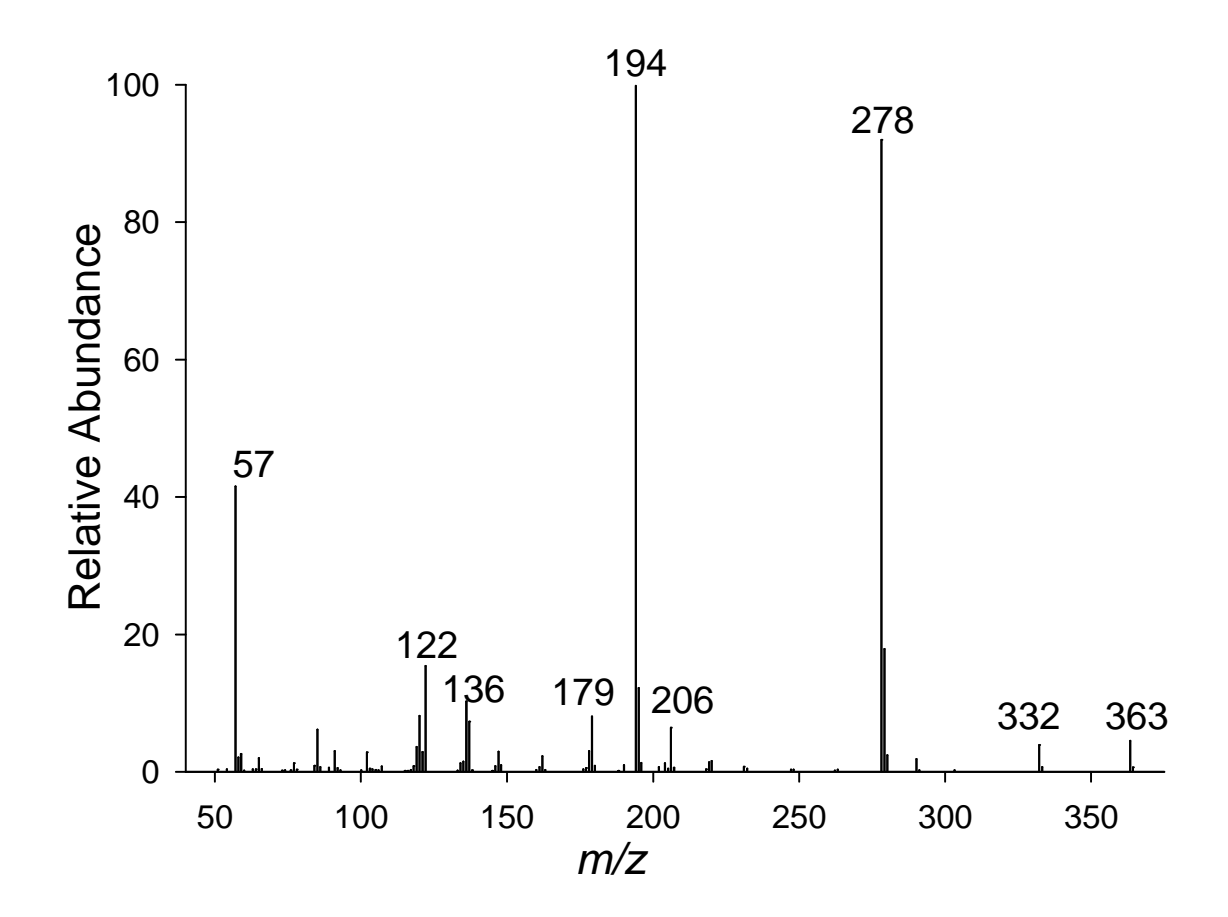


Figure A 38. GC trace of 4'-O,3-N-di((S)-2-methylbutanoyl) methyl ester derivatives of authentic (S)-2 (18.68 min) and (R)-2 (19.06 min) (a). EI-MS fragmentation of 4'-O,3-N-di((S)-2-methylbutanoyl) methyl ester derivatives of authentic (R)-2. Diagnostic fragment ions are m/z 278 and 194.

Figure A 38 (cont'd). b)



(b). EI-MS fragmentation of 4'-O,3-N-di((S)-2-methylbutanoyl) methyl ester derivative of authentic (S)-2 was virtually identical.

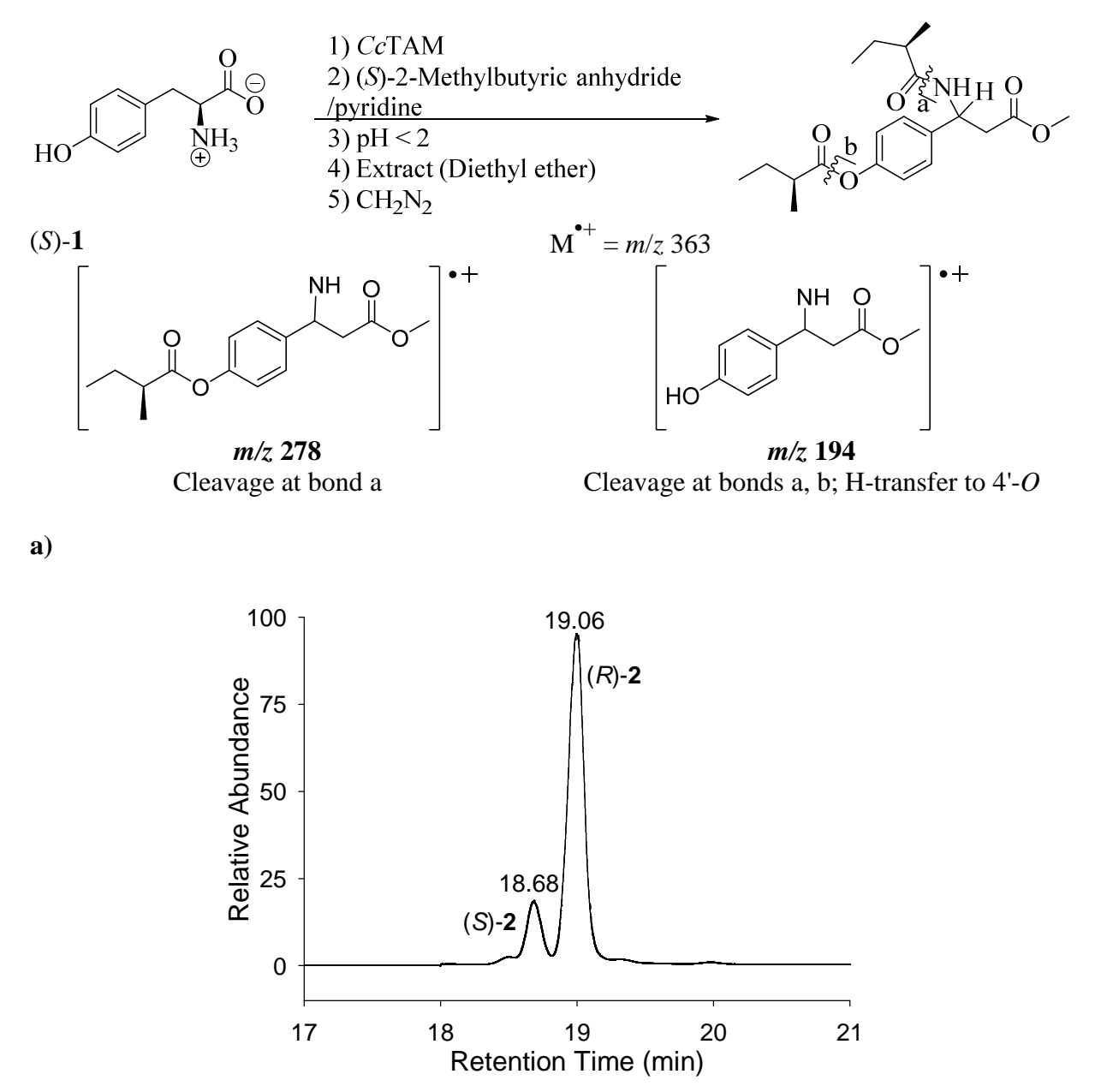


Figure A 39. GC trace of 4'-O,3-N-di((S)-2-methylbutanoyl) methyl ester derivatives of (S)-2 (18.68 min) and (R)-2 (19.06 min) (a) and EI-MS fragmentation of 4'-O,3-N-di((S)-2-methylbutanoyl) methyl ester derivatives of (R)-2 biosynthesized by CcTAM from unlabeled (S)-1.

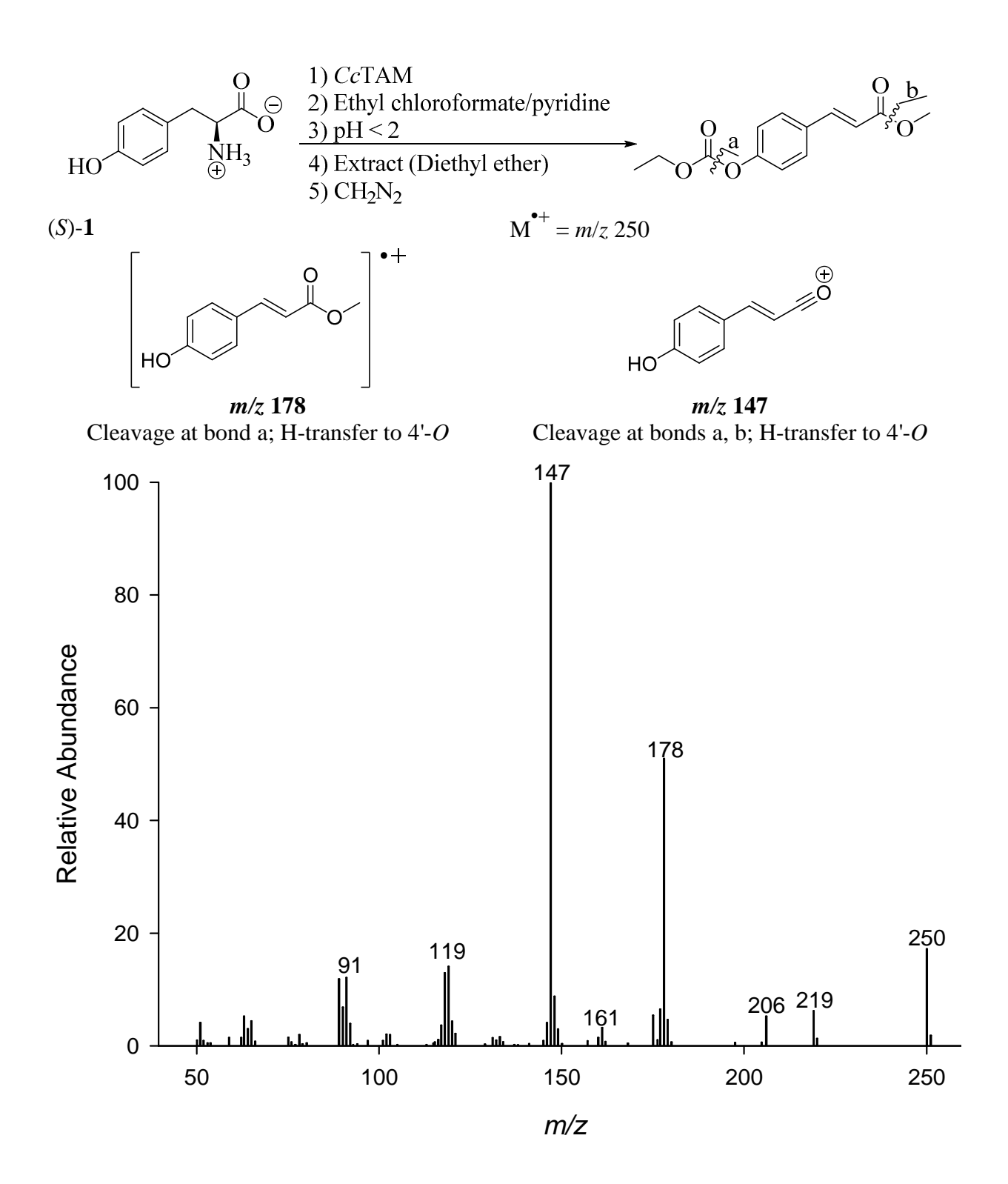
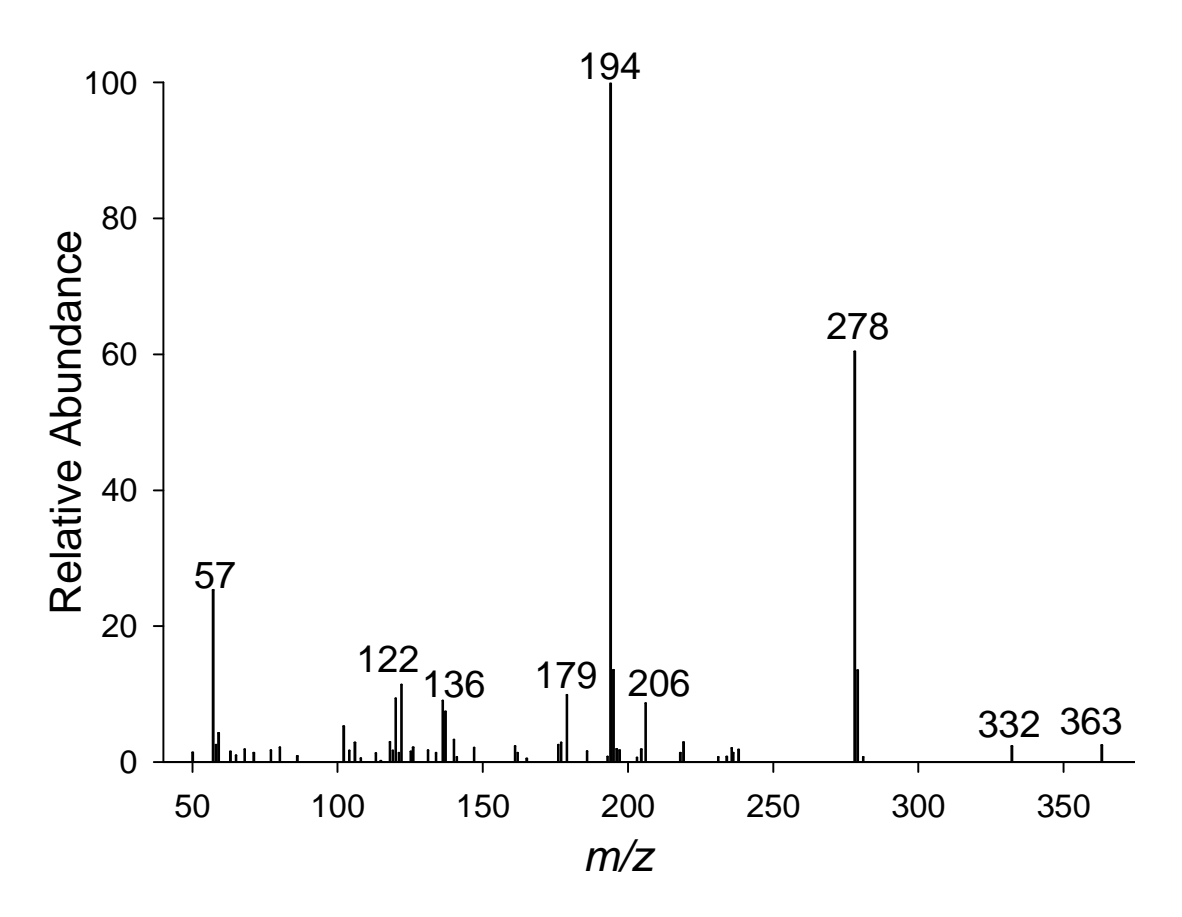


Figure A 40. EI-MS fragmentation of 4'-*O*-(ethoxycarbonyl) methyl ester derivative of 4'-hydroxycinnamic acid biosynthesized by *Cc*TAM from unlabeled (*S*)-1.

Figure A 40 (cont'd). b)



Diagnostic fragment ions are m/z 178 and 147. (b). Diagnostic fragment ions are m/z 278 and 194). EI-MS fragmentation of 4'-O,3-N-di((S)-2-methylbutanoyl) methyl ester derivatives of (S)-2 biosynthesized by CcTAM from unlabeled (S)-1 was virtually identical.

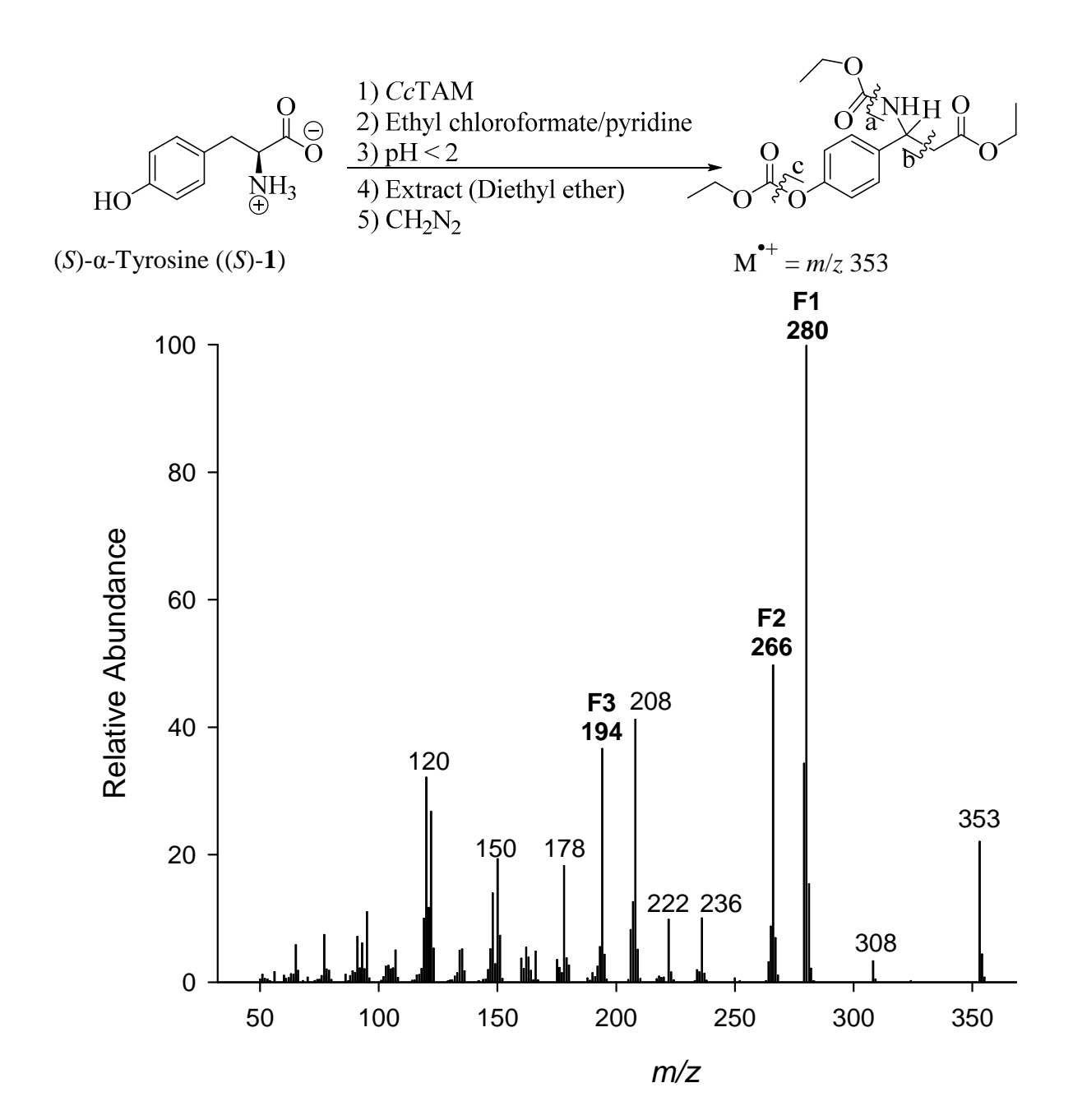


Figure A 41. EI-MS fragmentation of 4'-*O*,3-*N*-di(ethoxycarbonyl) ethyl ester derivatives of 2 biosynthesized by *Cc*TAM from unlabeled (*S*)-1. Diagnostic fragment ions F1, F2, and F3 (m/z 280, 266, and 194) are highlighted.

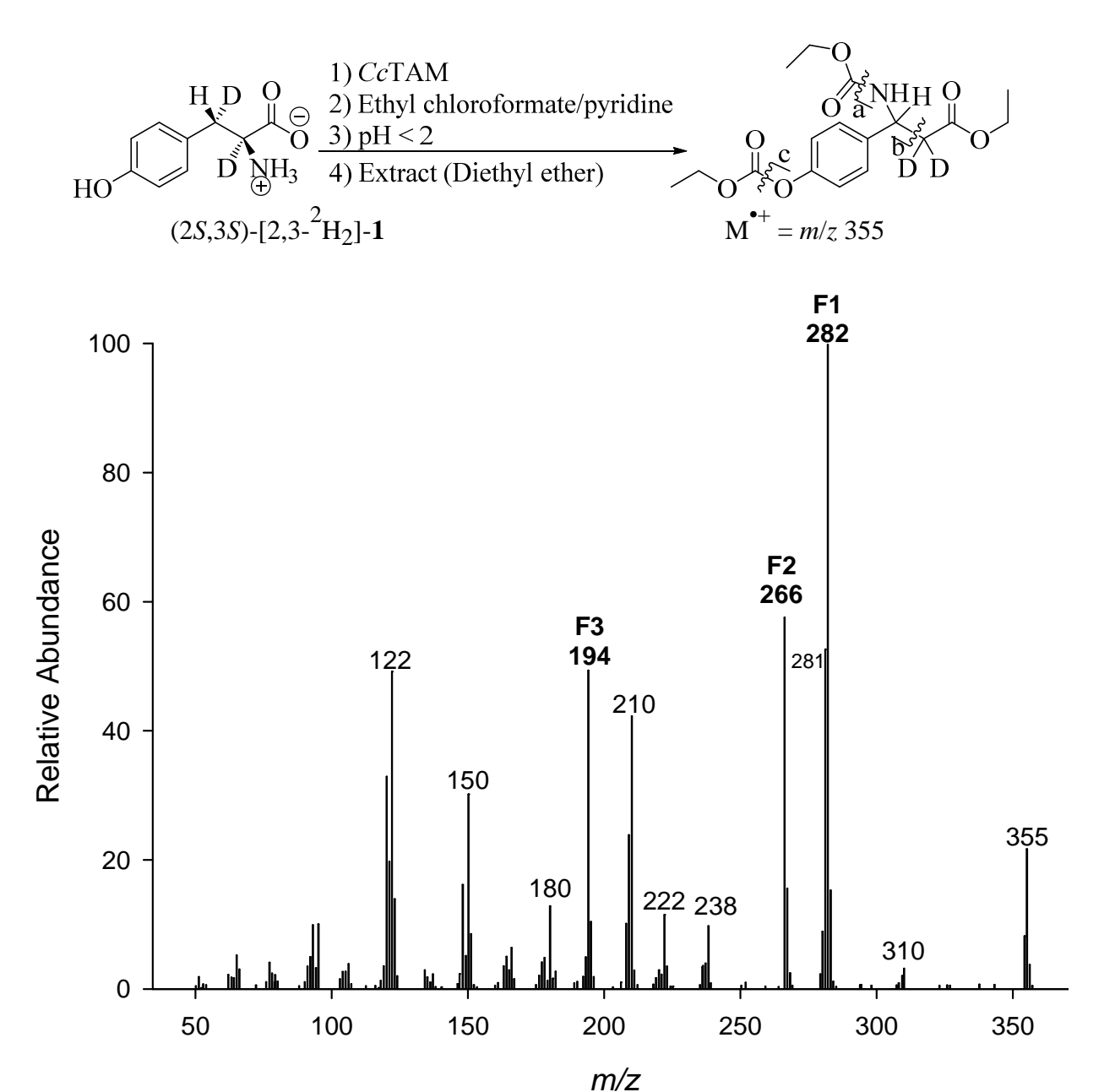


Figure A 42. EI-MS fragmentation of 4'-*O*,3-*N*-di(ethoxycarbonyl) ethyl ester derivatives of isotopomers of 2 biosynthesized by *Cc*TAM from (2*S*,3*S*)-[2,3-²H₂]-1. Diagnostic fragment ions F1, F2, and F3 (m/z 282, 266, and 194) are highlighted.

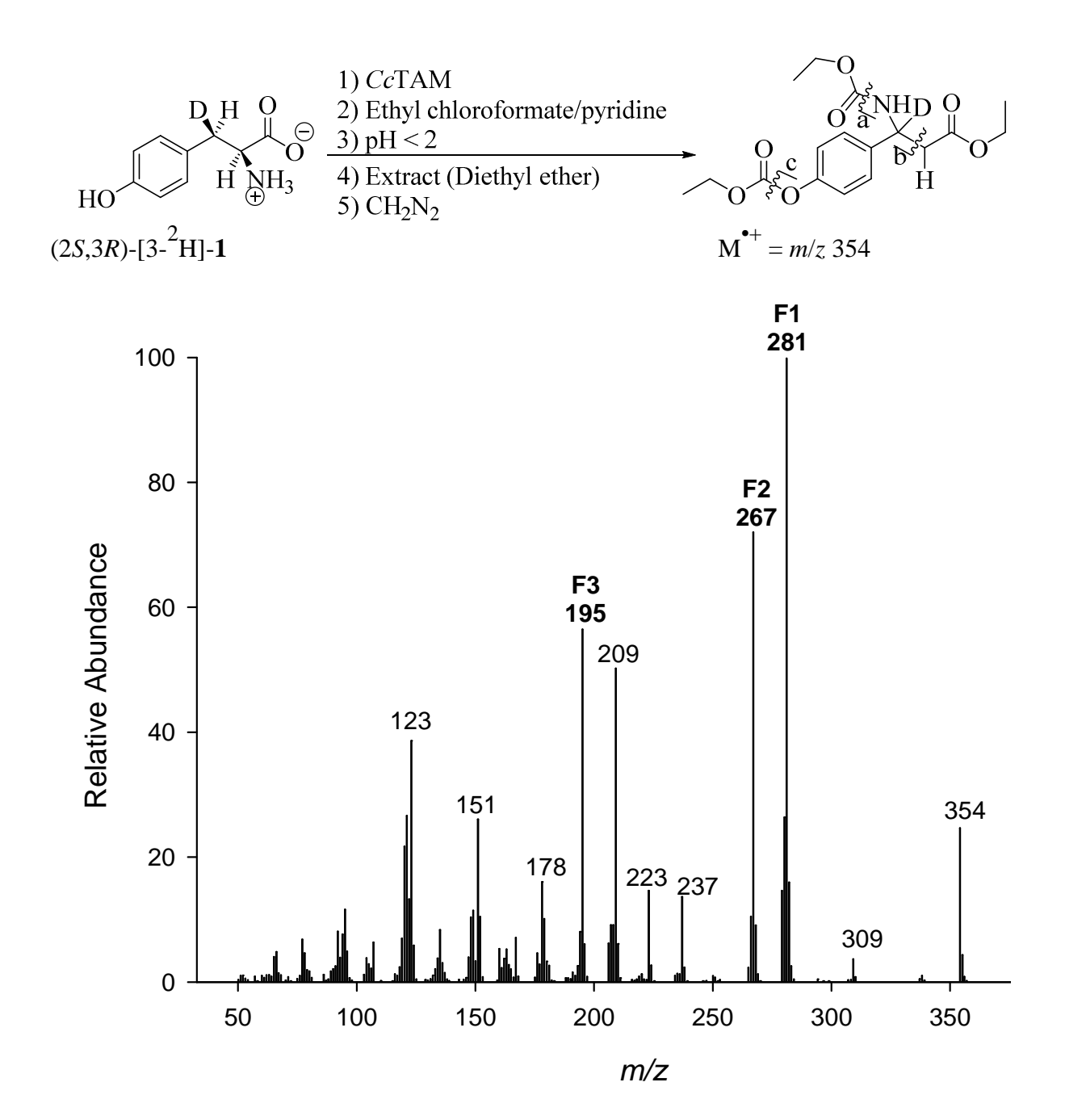


Figure A 43. EI-MS fragmentation of 4'-O,3-N-di(ethoxycarbonyl) ethyl ester derivatives of isotopomers of 2 biosynthesized by CcTAM from (2S,3R)-[3- 2 H]-1. Diagnostic fragment ions F1, F2, and F3 (m/z 281, 267, and 195) are highlighted.

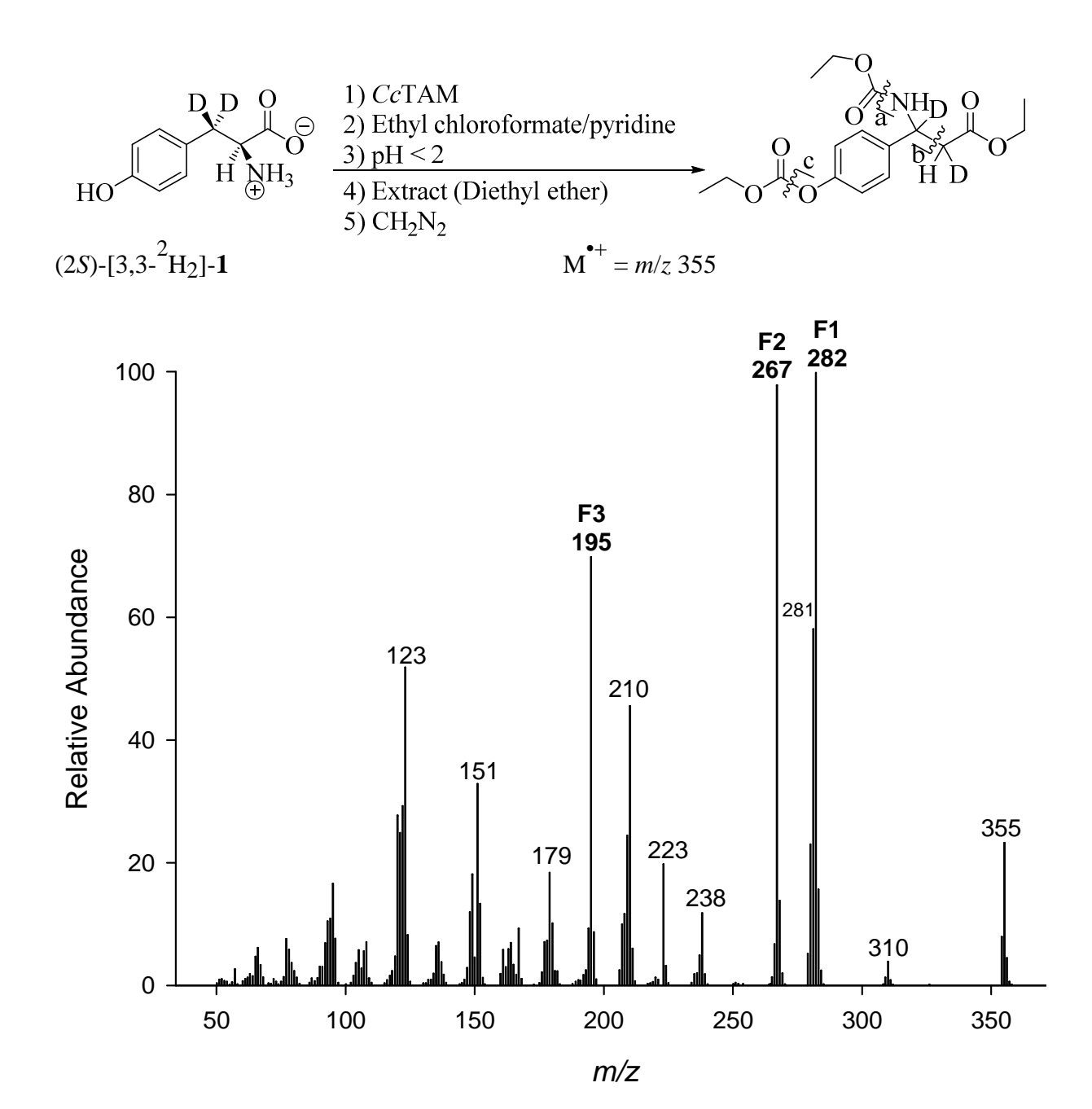


Figure A 44. EI-MS fragmentation of 4'-*O*,3-*N*-di(ethoxycarbonyl) ethyl ester derivatives of isotopomers of 2 biosynthesized by *Cc*TAM from (2*S*)-[3,3-²H₂]-1. Diagnostic fragment ions F1, F2, and F3 (m/z 282, 267, and 195) are highlighted.

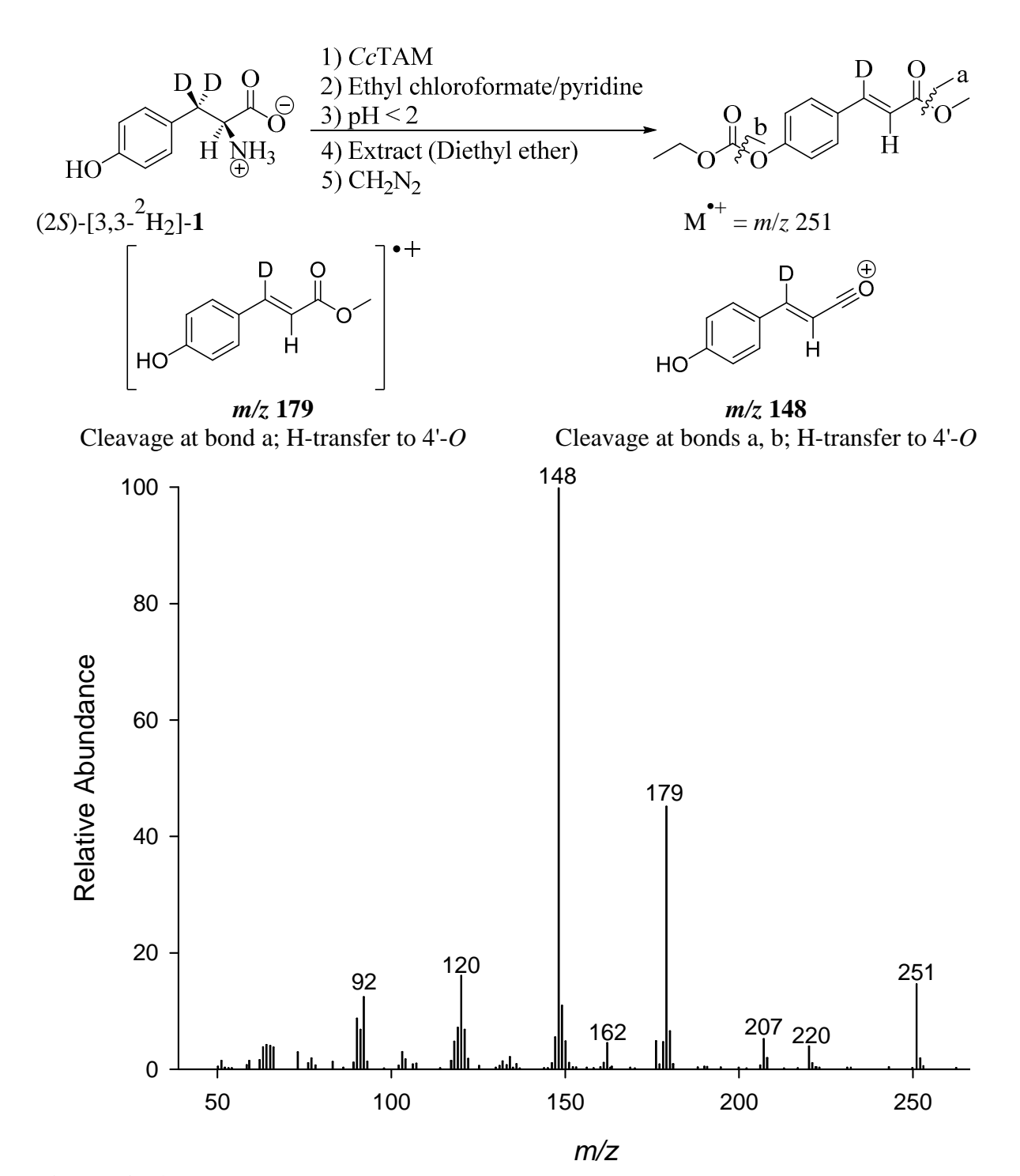


Figure A 45. EI-MS fragmentation of 4'-O-(ethoxycarbonyl) methyl ester derivative of biosynthesized [3- 2 H]-4'-hydroxycinnamic acid biosynthesized by CcTAM from (2S)-[3,3- 2 H₂]-1. Diagnostic fragment ions are m/z 179 and 148.

REFERENCES

REFERENCES

- 1. Garcion, E.; Lamprecht, A.; Heurtault, B.; Paillard, A.; Aubert-Pouessel, A.; Denizot, B.; Menei, P.; Benoit, J. P., A new generation of anticancer, drug-loaded, colloidal vectors reverses multidrug resistance in glioma and reduces tumor progression in rats. *Mol. Cancer Ther.* **2006**, *5*, (7), 1710-1722.
- 2. von Nussbaum, F.; Spiteller, P.; Rüth, M.; Steglich, W.; Wanner, G.; Gamblin, B.; Stievano, L.; Wagner, F. E., An iron(III)—catechol complex as a mushroom pigment. *Angew. Chem., Int. Ed. Engl.* **1998,** 37, (23), 3292-3295.
- 3. Crews, P.; Manes, L. V.; Boehler, M., Jasplakinolide, a cyclodepsipeptide from the marine sponge, *Jaspis sp. Tetrahedron Lett.* **1986**, 27, (25), 2797-2800.
- 4. Christenson, S. D.; Liu, W.; Toney, M. D.; Shen, B., A novel 4-methylideneimidazole-5-one containing tyrosine aminomutase in enediyne antitumor antibiotic C-1027 biosynthesis. *J. Am. Chem. Soc.* **2003**, 125, (20), 6062-6063.
- 5. Rachid, S.; Krug, D.; Weissman, K. J.; Müller, R., Biosynthesis of (*R*)-β-tyrosine and its incorporation into the highly cytotoxic chondramides produced by *Chondromyces crocatus*. *J. Biol. Chem.* **2007**, 282, (30), 21810-21817.
- 6. Magarvey, N. A.; Fortin, P. D.; Thomas, P. M.; Kelleher, N. L.; Walsh, C. T., Gatekeeping versus promiscuity in the early stages of the andrimid biosynthetic assembly line. *ACS Chem. Biol.* **2008**, 3, (9), 542-554.
- 7. Benaglia, M.; Cinquini, M.; Cozzi, F., The *S*-thioester enolate/imine iondensation: a shortcut to β-lactams. *Eur. J. Org. Chem.* **2000**, 2000, (4), 563-572.
- 8. Fueloep, F.; Martinek, T. A.; Toth, G. K., Application of alicyclic β-amino acids in peptide chemistry. *Chem. Soc. Rev.* **2006**, 35, (4), 323-334.
- 9. Disney, M. D.; Hook, D. F.; Namoto, K.; Seeberger, P. H.; Seebach, D., *N*-Linked glycosylated β-peptides are resistant to degradation by glycoamidase A. *Chem. Biodiversity* **2005**, 2, (12), 1624-1634.
- 10. Wu, Y.-D.; Han, W.; Wang, D.-P.; Gao, Y.; Zhao, Y.-L., Theoretical analysis of secondary structures of β-peptides. *Acc. Chem. Res.* **2008**, 41, (10), 1418-1427.
- 11. Seebach, D.; Beck, A. K.; Bierbaum, D. J., The world of β- and γ-peptides comprised of homologated proteinogenic amino acids and other components. *Chem. Biodiversity* **2004**, 1, (8), 1111-1239.

- 12. Duursma, A.; Minnaard, A. J.; Feringa, B. L., Highly enantioselective conjugate addition of dialkylzinc reagents to acyclic nitroalkenes: A catalytic route to β^2 -amino acids, aldehydes, and alcohols. *J. Am. Chem. Soc.* **2003**, 125, (13), 3700-3701.
- 13. Peña, D.; Minnaard, A. J.; de Vries, J. G.; Feringa, B. L., Highly enantioselective rhodium-catalyzed hydrogenation of β-dehydroamino acid derivatives using monodentate phosphoramidites. *J. Am. Chem. Soc.* **2002**, 124, (49), 14552-14553.
- 14. Abele, S.; Seebach, D., Preparation of achiral and of enantiopure geminally disubstituted β-amino acids for β-peptide synthesis. *Eur. J. Org. Chem.* **2000**, 2000, (1), 1-15.
- 15. Liu, M.; Sibi, M. P., Recent advances in the stereoselective synthesis of β-amino acids. *Tetrahedron* **2002**, 58, (40), 7991-8035.
- 16. Cardillo, G.; Tomasini, C., Asymmetric synthesis of β-amino acids and α-substituted β-amino acids. *Chem. Soc. Rev.* **1996,** 25, (2), 117-128.
- 17. Podlech, J.; Seebach, D., The Arndt–Eistert reaction in peptide chemistry: A facile access to homopeptides. *Angew. Chem., Int. Ed. Engl.* **1995,** 34, (4), 471-472.
- 18. Jefford, C. W.; McNulty, J.; Lu, Z.-H.; Wang, J. B., The enantioselective synthesis of β-amino acids, their α-hydroxy derivatives, and the N-terminal components of bestatin and microginin. *Helv. Chim. Acta* **1996,** 79, (4), 1203-1216.
- 19. Lakner, F. J.; Chu, K. S.; Negrete, G. R.; Konopelski, J. P., Enantiomerically pure β-amino acids from 2-*tert*-butyl-1-carbomethoxy-2,3-dihydro-4(1*H*)-pyrimidinone: (*R*)-3-amino-3-(*p*-methoxyphenyl)propionic acid. *Org. Synth.* **1996,** 73, 201-209.
- 20. Sibi, M. P.; Deshpande, P. K., A new methodology for the synthesis of β-amino acids. *J. Chem. Soc., Perkin Trans. I* **2000,** 0, (9), 1461-1466.
- 21. Fitzi, R.; Seebach, D., Resolution and use in α-amino acid synthesis of imidazolidinone glycine derivatives. *Tetrahedron* **1988**, 44, (17), 5277-5292.
- d'Angelo, J.; Desmaële, D.; Dumas, F.; Guingant, A., The asymmetric Michael addition reactions using chiral imines. *Tetrahedron: Asymmetry* **1992,** 3, (4), 459-505.
- 23. Zhu, G.; Chen, Z.; Zhang, X., Highly efficient asymmetric synthesis of β-amino acid derivatives via rhodium-catalyzed hydrogenation of β-(acylamino)acrylates. *J. Org. Chem.* **1999**, 64, (18), 6907-6910.
- 24. Cimarelli, C.; Palmieri, G., Stereoselective reduction of enantiopure β-enamino esters by hydride: A convenient synthesis of both enantiopure β-amino esters. *J. Org. Chem.* **1996**, 61, (16), 5557-5563.
- 25. Li, G.; Chang, H.-T.; Sharpless, K. B., Catalytic asymmetric aminohydroxylation (AA) of olefins. *Angew. Chem., Int. Ed. Engl.* **1996,** 35, (4), 451-454.

- 26. Palomo, C.; Aizpurua, J. M.; Ganboa, I.; Oiarbide, M., β-Lactams as versatile intermediates in α- and β-amino acid synthesis. *Synlett* **2001**, 2001, (12), 1813-1826.
- Weiner, B.; Poelarends, G. J.; Janssen, D. B.; Feringa, B. L., Biocatalytic enantioselective synthesis of *N*-substituted aspartic acids by aspartate ammonia lyase. *Chem. Eur. J.* **2008**, 14, (32), 10094-10100.
- 28. Kim, J.; Kyung, D.; Yun, H.; Cho, B.-K.; Seo, J.-H.; Cha, M.; Kim, B.-G., Cloning and characterization of a novel β-transaminase from *Mesorhizobium sp.* strain LUK: A new biocatalyst for the synthesis of enantiomerically pure β-amino acids. *Appl. Environ. Microbiol.* **2007**, 73, (6), 1772-1782.
- 29. Wohlgemuth, R., Asymmetric biocatalysis with microbial enzymes and cells. *Curr. Opin. Chem. Biol.* **2010**, 13, (3), 283-292.
- 30. Turner, N. J., Deracemisation methods. Curr. Opin. Chem. Biol. 2010, 14, (2), 115-121.
- 31. van Rantwijk, F.; Sheldon, R. A., Enantioselective acylation of chiral amines catalysed by serine hydrolases. *Tetrahedron* **2004**, 60, (3), 501-519.
- 32. Gotor-Fernández, V.; Busto, E.; Gotor, V., *Candida antarctica* lipase B: An ideal biocatalyst for the preparation of nitrogenated organic compounds. *Adv. Synth. Catal.* **2006,** 348, (7-8), 797-812.
- 33. Altenbuchner, J.; Siemann-Herzberg, M.; Syldatk, C., Hydantoinases and related enzymes as biocatalysts for the synthesis of unnatural chiral amino acids. *Curr. Opin. Biotechnol.* **2001**, 12, (6), 559-563.
- 34. Köhler, V.; Bailey, K. R.; Znabet, A.; Raftery, J.; Helliwell, M.; Turner, N. J., Enantioselective biocatalytic oxidative desymmetrization of substituted pyrrolidines. *Angew. Chem., Int. Ed. Engl.* **2010,** 49, (12), 2182-2184.
- 35. Wanninayake, U.; DePorre, Y.; Ondari, M.; Walker, K. D., (*S*)-Styryl-α-alanine used to probe the intermolecular mechanism of an intramolecular MIO-aminomutase. *Biochemistry* **2011**, 50, (46), 10082-10090.
- 36. Koszelewski, D.; Tauber, K.; Faber, K.; Kroutil, W., ω-Transaminases for the synthesis of non-racemic α-chiral primary amines. *Trends Biotechnol.* **2010**, 28, (6), 324-332.
- 37. Walker, K. D.; Floss, H. G., Detection of a phenylalanine aminomutase in cell-free extracts of *Taxus brevifolia* and preliminary characterization of its reaction. *J. Am. Chem. Soc.* **1998**, 120, (21), 5333-5334.
- 38. Feng, L.; Wanninayake, U.; Strom, S.; Geiger, J.; Walker, K. D., Mechanistic, mutational, and structural evaluation of a *Taxus* phenylalanine aminomutase. *Biochemistry* **2011**, 50, (14), 2919-2930.

- 39. Klettke, K. L.; Sanyal, S.; Mutatu, W.; Walker, K. D., β-Styryl- and β-aryl-β-alanine products of phenylalanine aminomutase catalysis. *J. Am. Chem. Soc.* **2007**, 129, (22), 6988-6989.
- 40. Szymanski, W.; Wu, B.; Weiner, B.; de Wildeman, S.; Feringa, B. L.; Janssen, D. B., Phenylalanine aminomutase-catalyzed addition of ammonia to substituted cinnamic acids: A route to enantiopure α- and β-amino acids. *J. Org. Chem.* **2009**, 74, (23), 9152-9157.
- 41. Wu, B.; Szymański, W.; Wybenga, G. G.; Heberling, M. M.; Bartsch, S.; de Wildeman, S.; Poelarends, G. J.; Feringa, B. L.; Dijkstra, B. W.; Janssen, D. B., Mechanism-inspired engineering of phenylalanine aminomutase for enhanced β-regioselective asymmetric amination of cinnamates. *Angew. Chem., Int. Ed. Engl* **2012**, 51, (2), 482-486.
- 42. Ratnayake, N. D.; Walker, K. D., *Arch. Biochem. Biophys* **2013,** In preparation.
- 43. Gloge, A.; Zon, J.; Kovari, A.; Poppe, L.; Retey, J., Phenylalanine ammonia-lyase: The use of its broad substrate specificity for mechanistic investigations and biocatalysis synthesis of L-arylalanines. *Chem. Eur. J.* **2000**, 6, (18), 3386-3390.
- 44. Takaç, S.; Akay, B.; Özdamar, T. H., Bioconversion of *trans*-cinnamic acid to L-phenylalanine by L-phenylalanine ammonia-lyase of *Rhodotorula glutinis*: Parameters and kinetics. *Enzyme Microb. Technol.* **1995**, 17, (5), 445-452.
- 45. Walker, K. D.; Klettke, K.; Akiyama, T.; Croteau, R., Cloning, heterologous expression, and characterization of a phenylalanine aminomutase involved in Taxol biosynthesis. *J. Biol. Chem.* **2004**, 279, (52), 53947-53954.
- 46. Krug, D.; Müller, R., Discovery of additional members of the tyrosine aminomutase enzyme family and the mutational analysis of CmdF. *ChemBioChem* **2009**, 10, (4), 741-750.
- 47. MacDonald, M. J.; D'Cunha, G. B., A modern view of phenylalanine ammonia lyase. *Biochem. Cell Biol.* **2007**, 85, (3), 273-282.
- 48. Kyndt, J. A.; Meyer, T. E.; Cusanovich, M. A.; Van Beeumen, J. J., Characterization of a bacterial tyrosine ammonia lyase, a biosynthetic enzyme for the photoactive yellow protein. *FEBS Lett.* **2002**, 512, 240-244.
- 49. Baedeker, M.; Schulz, G. E., Structures of two histidine ammonia-lyase modifications and implications for the catalytic mechanism. *Eur. J. Biochem.* **2002**, 269, (6), 1790-1797.
- 50. Schwede, T. F.; Rétey, J.; Schulz, G. E., Crystal structure of histidine ammonia lyase revealing a novel polypeptide modification as the catalytic electrophile. *Biochemistry* **1999**, 38, (17), 5355-5361.

- 51. Wickner, R. B., Dehydroalanine in histidine ammonia lyase. *J. Biol. Chem.* **1969**, 244, (23), 6550-6552.
- 52. Röther, D.; Poppe, L.; Viergutz, S.; Langer, B.; Retey, J., Characterization of the active site of histidine ammonia-lyase from *Pseudomonas putida*. *Eur. J. Biochem.* **2001**, 268, (23), 6011-6019.
- 53. Tsien, R. Y., The green fluorescent protein. Annu. Rev. Biochem. 1998, 67, (1), 509-544.
- 54. Cooke, H. A.; Bruner, S. D., Probing the active site of MIO-dependent aminomutases, key catalysts in the biosynthesis of β -amino acids incorporated in secondary metabolites. *Biopolymers* **2010**, 93, (9), 802-810.
- 55. Hanson, K. R.; Havir, E. A., L-Phenylalanine ammonia-lyase: Evidence that the prosthetic group contains a dehydroalanyl residue and mechanism of action. *Arch. Biochem. Biophys.* **1970**, 141, (1), 1-17.
- 56. Calabrese, J. C.; Jordan, D. B.; Boodhoo, A.; Sariaslani, S.; Vannelli, T., Crystal structure of phenylalanine ammonia lyase: Multiple helix dipoles implicated in catalysis. *Biochemistry* **2004**, 43, (36), 11403-11416.
- 57. Christianson, C. V.; Montavon, T. J.; Festin, G. M.; Cooke, H. A.; Shen, B.; Bruner, S. D., The mechanism of MIO-based aminomutases in β-amino acid biosynthesis. *J. Am. Chem. Soc.* **2007**, 129, (51), 15744-15755.
- 58. Schuster, B.; Rétey, J., The mechanism of action of phenylalanine ammonia lyase: The role of prosthetic dehydroalanine. *Proc. Natl. Acad. Sci. U. S. A.* **1995,** 92, (18), 8433-8437.
- 59. Poppe, L.; Rétey, J., Friedel-Crafts-type mechanism for the enzymatic elimination of ammonia from histidine and phenylalanine. *Angew. Chem., Int. Ed. Engl.* **2005**, 44, (24), 3668-3688.
- 60. Bartsch, S.; Bornscheuer, U. T., A single residue influences the reaction mechanism of ammonia lyases and mutases. *Angew. Chem., Int. Ed. Engl.* **2009,** 48, (18), 3362-3365.
- 61. Ratnayake, N. D.; Wanninayake, U.; Geiger, J. H.; Walker, K. D., Stereochemistry and mechanism of a microbial phenylalanine aminomutase. *J. Am. Chem. Soc.* **2011**, 133, (22), 8531-8533.
- 62. Christenson, S. D.; Wu, W.; Spies, M. A.; Shen, B.; Toney, M. D., Kinetic analysis of the 4-methylideneimidazole-5-one-containing tyrosine aminomutase in enediyne antitumor antibiotic C-1027 biosynthesis. *Biochemistry* **2003**, 42, (43), 12708-12718.
- 63. Montavon, T. J.; Christianson, C. V.; Festin, G. M.; Shen, B.; Bruner, S. D., Design and characterization of mechanism-based inhibitors for the tyrosine aminomutase *SgTAM*. *Bioorg. Med. Chem. Lett.* **2008**, 18, (10), 3099-3102.

- 64. Strom, S.; Wanninayake, U.; Ratnayake, N. D.; Walker, K. D.; Geiger, J. H., Insights into the mechanistic pathway of the *Pantoea agglomerans* phenylalanine aminomutase. *Angew. Chem., Int. Ed. Engl.* **2012,** 51, 11-17.
- 65. Wanninayake, U.; Walker, K. D., Assessing the deamination rate of a covalent aminomutase adduct by burst phase analysis. *Biochemistry* **2012**, 51, (26), 5226-5228.
- 66. Mutatu, W.; Klettke, K. L.; Foster, C.; Walker, K. D., Unusual mechanism for an aminomutase rearrangement: Retention of configuration at the migration termini. *Biochemistry* **2007**, 46, (34), 9785-9794.
- 67. Wanninayake, U.; Walker, K. D., A bacterial tyrosine aminomutase proceeds through retention or inversion of stereochemistry to catalyze its isomerization reaction. *J. Am. Chem. Soc.* **2013**, 135, (30), 11193-11204.
- 68. Chesters, C.; Wilding, M.; Goodall, M.; Micklefield, J., Thermal bifunctionality of bacterial phenylalanine aminomutase and ammonia lyase enzymes. *Angew. Chem., Int. Ed. Engl.* **2012,** 51, (18), 4344-8.
- 69. Christianson, C. V.; Montavon, T. J.; Van Lanen, S. G.; Shen, B.; Bruner, S. D., The structure of L-tyrosine 2,3-aminomutase from the C-1027 enediyne antitumor antibiotic biosynthetic pathway. *Biochemistry* **2007**, 46, (24), 7205-7214.
- 70. Louie, G. V.; Bowman, M. E.; Moffitt, M. C.; Baiga, T. J.; Moore, B. S.; Noel, J. P., Structural determinants and modulation of substrate specificity in phenylalanine-tyrosine ammonia-lyases. *Chem. Biol.* **2006**, 13, (12), 1327-1338.
- 71. Ritter, H.; Schulz, G. E., Structural basis for the entrance into the phenylpropanoid metabolism catalyzed by phenylalanine ammonia-lyase. *Plant Cell* **2004**, 16, (12), 3426-3436.
- 72. Wu, B.; Szymanski, W.; Wietzes, P.; de, W. S.; Poelarends, G. J.; Feringa, B. L.; Janssen, D. B., Enzymatic synthesis of enantiopure α- and β-amino acids by phenylalanine aminomutase-catalysed amination of cinnamic acid derivatives. *ChemBioChem* **2009**, 10, (2), 338-344.
- 73. Ege, M.; Wanner, K. T., Synthesis of β-amino acids based on oxidative cleavage of dihydropyridone derivatives. *Org. Lett.* **2004**, 6, (20), 3553-3556.
- 74. Cox, B. M.; Bilsborrow, J. B.; Walker, K. D., Enhanced conversion of racemic α-arylalanines to (*R*)-β-arylalanines by coupled racemase/aminomutase catalysis. *J. Org. Chem.* **2009**, 74, (18), 6953-6959.
- 75. O'Maille, P. E.; Tsai, M. D.; Greenhagen, B. T.; Chappell, J.; Noel, J. P., Gene library synthesis by structure-based combinatorial protein engineering. In *Protein Engineering*, Elsevier Academic Press Inc: San Diego, 2004; Vol. 388, pp 75-91.

- 76. Dunkley, K. D.; Callaway, T. R.; Chalova, V. I.; Anderson, R. C.; Kundinger, M. M.; Dunkley, C. S.; Nisbet, D. J.; Ricke, S. C., Growth and genetic responses of *Salmonella typhimurium* to, pH-shifts in an anaerobic continuous culture. *Anaerobe* **2008**, 14, (1), 35-42.
- 77. Turner, N. J., Ammonia lyases and aminomutases as biocatalysts for the synthesis of α-amino and β-amino acids. *Curr. Opin. Chem. Biol.* **2011,** 15, (2), 234-240.
- 78. Moffitt, M. C.; Louie, G. V.; Bowman, M. E.; Pence, J.; Noel, J. P.; Moore, B. S., Discovery of two cyanobacterial phenylalanine ammonia lyases: Kinetic and structural characterization. *Biochemistry* **2007**, 46, (4), 1004-1012.
- 79. Poppe, L.; Pilbak, S.; Paizs, C.; Retey, J., Mechanistic aspects and biocatalytic implications of the MIO-containing ammonia-lyase/aminomutase family. *Stud. Univ. Babes-Bolyai, Chem.* **2008,** 53, (2), 15-19.
- 80. Sawada, S.; Kumagai, H.; Yamada, H.; Hill, R. K.; Mugibayashi, Y.; Ogata, K., Stereochemistry of ammonia elimination from L-tyrosine with L-phenylalanine ammonia-lyase. *Biochim. Biophys. Acta, Enzymol.* **1973,** 315, (1), 204-7.
- 81. Hanson, K. R.; Havir, E. A., L-Phenylalanine ammonia-lyase. Evidence that the prosthetic group contains a dehydroalanyl residue and mechanism of action. *Arch. Biochem. Biophys.* **1970**, 141, (1), 1-17.
- 82. Ellis, B. E.; Zenk, M. H.; Kirby, G. W.; Michael, J.; Floss, H. G., Steric course of the tyrosine ammonia-lyase reaction. *Phytochemistry* **1973**, 12, (5), 1057-8.
- 83. Thompson, J. D.; Gibson, T. J.; Higgins, D. G., Multiple sequence alignment using ClustalW and ClustalX. In *Curr Protoc Bioinformatics*, 2008/09/17 ed.; 2002; Vol. Chapter 2, p Unit 2 3.
- 84. Kvicala, J.; Hrabal, R.; Czernek, J.; Bartosova, I.; Paleta, O.; Pelter, A., Low-temperature F¹⁹ NMR spectroscopy of 1-fluoro-1-lithioethenes stability, shifts and unexpected coupling constants. *J. Fluorine Chem.* **2002**, 113, (2), 211-218.
- 85. Sayers, E. W.; Barrett, T.; Benson, D. A.; Bryant, S. H.; Canese, K.; Chetvernin, V.; Church, D. M.; DiCuccio, M.; Edgar, R.; Federhen, S.; Feolo, M.; Geer, L. Y.; Helmberg, W.; Kapustin, Y.; Landsman, D.; Lipman, D. J.; Madden, T. L.; Maglott, D. R.; Miller, V.; Mizrachi, I.; Ostell, J.; Pruitt, K. D.; Schuler, G. D.; Sequeira, E.; Sherry, S. T.; Shumway, M.; Sirotkin, K.; Souvorov, A.; Starchenko, G.; Tatusova, T. A.; Wagner, L.; Yaschenko, E.; Ye, J., Database resources of the national center for biotechnology information. *Nucleic Acids Res.* **2009**, 37, (suppl 1), D5-D15.
- 86. Xiang, L.; Moore, B. S., Inactivation, complementation, and heterologous expression of EncP, a novel bacterial phenylalanine ammonia-lyase gene. *J. Biol. Chem.* **2002**, 277, (36), 32505-32509.

- 87. Xiang, L.; Moore, B. S., Biochemical characterization of a *Prokaryotic* phenylalanine ammonia lyase. *J. Bacteriol.* **2005**, 187, (12), 4286-4289.
- 88. Grecu, T., Masters of philosophy thesis, University of Manchester (UK) **2010**.
- 89. Oclarit, J. M.; Okada, H.; Ohta, S.; Kaminura, K.; Yamaoka, Y.; Iizuka, T.; Miyashiro, S.; Ikegami, S., Anti-*Bacillus* substance in the marine sponge, *Hyatella* species, produced by an associated *Vibrio* species *Bacterium*. *Microbios* **1994**, 78, (314), 7-16.
- 90. Koksal, M.; Jin, Y.; Coates, R. M.; Croteau, R.; Christianson, D. W., Axadiene synthase structure and evolution of modular architecture in terpene biosynthesis. *Nature* **2011**, 469, (7328), 116-120.
- 91. Jennewein, S.; Wildung, M. R.; Chau, M.; Walker, K.; Croteau, R., Random sequencing of an induced *Taxus* cell cDNA library for identification of clones involved in taxol biosynthesis. *Proc. Natl. Acad. Sci. U. S. A.* **2004**, 101, (24), 9149-9154.
- 92. Creighton, T. E., *Proteins. Structure and molecular principles*. 2nd ed.; Freeman: NewYork, 1984; p 515 pp.
- 93. Wu, B.; Szymanski, W.; Wijma, H. J.; Crismaru, C. G.; de Wildeman, S.; Poelarends, G. J.; Feringa, B. L.; Janssen, D. B., Engineering of an enantioselective tyrosine aminomutase by mutation of a single active site residue in phenylalanine aminomutase. *Chem. Commun. (Cambridge, U. K.)* **2010**, 46, (43), 8157-8159.
- 94. Takaç, S.; Akay, B.; Özdamar, T. H., Bioconversion of *trans*-cinnamic acid to L-phenylalanine by L-phenylalanine ammonia-lyase of *Rhodotorula glutinis*: Parameters and kinetics. *Enzyme Microb. Technol.* **1995**, 17, (5), 445-452.
- 95. Fersht, A., Enzyme structure and mechanism. *W.H Freeman and Company* **1985**, second ed., (Chapter 4), 128-147.
- 96. Lipshutz, B. H.; Ghorai, S.; Bošković, Ž. V., Tandem olefin metathesis-elimination reactions. A new route to doubly unsaturated carbonyl derivatives. *Tetrahedron* **2008**, 64, (29), 6949-6954.
- 97. Gutfreund, H.; Sturtevant, J. M., Mechanism of the reaction of chymotrypsin with *p*-nitrophenyl acetate. *Biochem. J.* **1956**, 63, (4), 656-661.
- 98. Ahn, H. J.; Kim, Y. S.; Kim, J.-U.; Han, S. M.; Shin, J. W.; Yang, H. O., Mechanism of taxol-induced apoptosis in human Skov3 ovarian carcinoma cells. *J. Cell. Biochem.* **2004**, 91, (5), 1043-1052.
- 99. Belyaev, N. A.; Kolesanova, E. F.; Kelesheva, L. F.; Rotanova, T. V.; Panchenko, L. F., Effect of the aminopeptidase inhibitor bestatin on rat-brain enkephalin levels. *Bull. Exp. Biol. Med.* **1990**, 110, (11), 1483-1485.

- 100. Prabhakaran, P. C.; Woo, N. T.; Yorgey, P. S.; Gould, S. J., Biosynthesis of blasticidin S from L-α-arginine. Stereochemistry in the arginine-2,3-aminomutase reaction. *J. Am. Chem. Soc.* **1988**, 110, (17), 5785-5791.
- 101. Liu, W.; Christenson, S. D.; Standage, S.; Shen, B., Biosynthesis of the enediyne antitumor antibiotic C-1027. *Science* **2002**, 297, (5584), 1170-1173.
- 102. Yin, X. H.; O'Hare, T.; Gould, S. J.; Zabriskie, T. M., Identification and cloning of genes encoding viomycin biosynthesis from *Streptomyces vinaceus* and evidence for involvement of a rare oxygenase. *Gene* **2003**, 312, 215-224.
- 103. Weaver, D. F.; Tan, C. Y. K.; Kim, S. T.; Kong, X.; Wei, L.; Carran, J. R. Antiepileptogenic agents. WO 2002073208, March 13, 2002.
- 104. Georg, G. I., *The Organic Chemistry of \beta-Lactams*. Wiley-VCH, New York, N. Y.: 1993; p 381 pp.
- 105. Gademann, K.; Kimmerlin, T.; Hoyer, D.; Seebach, D., Peptide folding induces high and selective affinity of a linear and small b-peptide to the human somatostatin receptor 4. *J. Med. Chem.* **2001**, 44, (15), 2460-2468.
- 106. Sonti, R.; Gopi, H. N.; Muddegowda, U.; Ragothama, S.; Balaram, P., A Designed Three-Stranded β-Sheet in an α/β Hybrid Peptide. *Chem. Eur. J.* **2013**, 19, (19), 5955-65.
- 107. Murray, J. K.; Farooqi, B.; Sadowsky, J. D.; Scalf, M.; Freund, W. A.; Smith, L. M.; Chen, J.; Gellman, S. H., Efficient synthesis of a β-peptide combinatorial library with microwave irradiation. *J. Am. Chem. Soc.* **2005**, 127, (38), 13271-13280.
- 108. Ibrahem, I.; Rios, R.; Vesely, J.; Zhao, G.-L.; Cordova, A., Catalytic enantioselective 5-hydroxyisoxazolidine synthesis: an asymmetric entry to β-amino acids. *Synthesis* **2008**, (Copyright (C) 2013 American Chemical Society (ACS). All Rights Reserved.), 1153-1157.
- 109. Davies, S. G.; Mulvaney, A. W.; Russell, A. J.; Smith, A. D., Parallel synthesis of homochiral β-amino acids. *Tetrahedron: Asymmetry* **2007**, 18, (13), 1554-1566.
- 110. Tan, C. Y. K.; Weaver, D. F., A one-pot synthesis of 3-amino-3-arylpropionic acids. *Tetrahedron* **2002**, 58, (37), 7449-7461.
- 111. Christianson, C. V.; Montavon, T. J.; Festin, G. M.; Cooke, H. A.; Shen, B.; Bruner, S. D., The mechanism of MIO-based aminomutases in β-amino acid biosynthesis. *J. Am. Chem. Soc.* **2007**, 129, (51), 15744-15745.
- 112. Asano, Y.; Kato, Y.; Levy, C.; Baker, P.; Rice, D., Structure and function of amino acid ammonia-lyases. *Biocatal. Biotransform.* **2004**, 22, (2), 131-138.
- 113. Rettig, M.; Sigrist, A.; Rétey, J., Mimicking the reaction of phenylalanine ammonia lyase by a synthetic model. *Helv. Chim. Acta* **2000**, 83, (9), 2246-2265.

- 114. Strom, S.; Wanninayake, U.; Ratnayake, N. D.; Walker, K. D.; Geiger, J. H., Insights into the Mechanistic Pathway of the Pantoea agglomerans Phenylalanine Aminomutase. *Angew. Chem. Int. Ed.* **2012**, 51, 11-17.
- 115. Christenson, S. D.; Wu, W.; Spies, M. A.; Shen, B.; Toney, M. D., Kinetic Analysis of the 4-Methylideneimidazole-5-one-Containing Tyrosine Aminomutase in Enediyne Antitumor Antibiotic C-1027 Biosynthesisâ€*Biochemistry* **2003**, 42, (43), 12708-12718.
- 116. Sasse, F.; Kunze, B.; Gronewold, T. M. A.; Reichenbach, H., The chondramides: Cytostatic agents from *Myxobacteria* acting on the actin cytoskeleton. *Journal of the National Cancer Institute* **1998**, 90, (20), 1559-1563.
- 117. Fryzuk, M. D.; Bosnich, B., Asymmetric synthesis. An asymmetric homogeneous hydrogenation catalyst which breeds its own chirality. *J. Am. Chem. Soc.* **1978**, 100, (17), 5491-5494.
- 118. Fryzuk, M. D.; Bosnich, B., Asymmetric synthesis. Production of optically active amino acids by catalytic hydrogenation. *J. Am. Chem. Soc.* **1977**, 99, (19), 6262-6267.
- 119. Cleary, T.; Brice, J.; Kennedy, N.; Chavez, F., One-pot process to Z-α-benzoylamino-acrylic acid methyl esters via potassium phosphate-catalyzed Erlenmeyer reaction. *Tetrahedron Lett.* **2010**, 51, (4), 625-628.
- 120. Kirby, G. W.; Michael, J., Stereoselective β-labelling of aromatic amino-acids with deuterium and tritium. *J. Chem. Soc.*, *Perkin Trans. 1* **1973**, 0, (0), 115-120.
- 121. Jin, M.; Fischbach, M. A.; Clardy, J., A biosynthetic gene cluster for the acetyl-CoA carboxylase inhibitor andrimid. *J. Am. Chem. Soc.* **2006**, 128, (33), 10660-10661.
- 122. Oba, M.; Ueno, R.; Fukuoka, M.; Kainosho, M.; Nishiyama, K., Synthesis of L-threo-and L-erythro-[1-13C, 2,3-2H2]amino acids: novel probes for conformational analysis of peptide side chains. *J. Chem. Soc., Perkin Trans. 1* **1995,** 0, (12), 1603-1609.
- 123. Li, J.; Sha, Y., A convenient synthesis of amino acid methyl esters. *Molecules* **2008**, 13, (5), 1111-9.
- 124. Lambert, J. B.; Shurvell, H. F.; Lightner, D.; Cooks, R. G., *Organic Structural Spectroscopy*. 1st ed.; Prentice Hall: New Jersey, 1998; p 568.
- 125. Jensen, F. R.; Bushweller, C. H., Separation of conformers: Axial and equatorial isomers of chlorocyclohexane and trideuteriomethoxycyclohexane. *J. Am. Chem. Soc.* **1969**, 91, (12), 3223-3225.
- 126. Garbisch, E. W.; Griffith, M. G., Proton couplings in cyclohexane. *J. Am. Chem. Soc.* **1968**, 90, (23), 6543-6544.

- 127. Kumar, S.; Dwevedi, A.; Kayastha, A. M., Immobilization of soybean (Glycine max) urease on alginate and chitosan beads showing improved stability: Analytical applications. *J. Mol. Catal. B: Enzym.* **2009**, 58, (1-4), 138-145.
- 128. Stingl, K.; Uhlemann, E. M.; Schmid, R.; Altendorf, K.; Bakker, E. P., Energetics of Helicobacter pylori and its implications for the mechanism of urease-dependent acid tolerance at pH 1. *J. Bacteriol.* **2002**, 184, (11), 3053-3060.
- 129. Cooke, H. A.; Bruner, S. D., Probing the active site of MIO-dependent aminomutases, key catalysts in the biosynthesis of β -amino acids incorporated in secondary metabolites. *Biopolymers* **2010**, 93, (9), 802-810.
- 130. Katz, B. A.; Elrod, K.; Verner, E.; Mackman, R. L.; Luong, C.; Shrader, W. D.; Sendzik, M.; Spencer, J. R.; Sprengeler, P. A.; Kolesnikov, A.; Tai, V. W. F.; Hui, H. C.; Guy Breitenbucher, J.; Allen, D.; Janc, J. W., Elaborate Manifold of Short Hydrogen Bond Arrays Mediating Binding of Active Site-directed Serine Protease Inhibitors. *J. Mol. Biol.* **2003**, 329, (1), 93-120.
- 131. Hanoian, P.; Sigala, P. A.; Herschlag, D.; Hammes-Schiffer, S., Hydrogen Bonding in the Active Site of Ketosteroid Isomerase: Electronic Inductive Effects and Hydrogen Bond Coupling. *Biochemistry* **2010**, 49, (48), 10339-10348.
- 132. Lyubimov, A. Y.; Lario, P. I.; Moustafa, I.; Vrielink, A., Atomic resolution crystallography reveals how changes in pH shape the protein microenvironment. *Nat. Chem. Biol.* **2006**, 2, (5), 259-264.